A GEOCHEMICAL STUDY OF DIAMONDS, DIAMOND INCLUSION MINERALS AND OTHER MANTLE MINERALS FROM THE KLIPSPRINGER KIMBERLITES, SOUTH AFRICA

KALLE WESTERLUND

Thesis submitted in fulfilment of the requirements
for the degree of Master of Science

University of Cape Town
February, 2000

DECLARATION

I hereby declare that the work presented in this thesis is my own, except where otherwise stated in the text.

Karl Johan Westerlund
February, 2000

Signed by candidate

Signature removed

ACKNOWLEDGEMENTS

First of all, many thanks to my supervisor John Gurney for giving me the opportunity to study some beautiful diamonds and for "pushing" me forward when energy and inspiration was lacking. Thanks also to my co-supervisor Steve Richardson especially for being a great source of inspiration in the isotope work.

I am grateful to Chris Jennings and Southernera Resources Ltd. for providing diamonds for what turned out to be a very interesting project. Many people at the Southernera Klipspringer mine made my visits a shear pleasure and they facilitated an otherwise difficult task of getting away with diamonds from a diamond mine. Thanks especially to the mine manager David Gadd-Claxton and to all the guys in the recovery and the security.

Many people have contributed to the present study with their invaluable practical and theoretical knowledge.
At the Carnegie Institution of Washington Rick Carlson, Steve Shirey, Mary Horan and Tim Mock helped with the Rhenium-Osmium analyses. Erik Hauri and Jianhua Wang fine-tuned the ion-probe for sulfur isotope analyses and Nabil Boctar made his laboratory available for sulfide preparation. Chris Haddidiakos and Dave George introduced me to their Jeol Superprobe.
At the University of Cape Town Dick Rickard kept the electron microprobe together. Dane Gerneke and Miranda Waldron at the Electrone Microscope Unit assisted in obtaining catodoluminescence images of the diamonds and Shireen Govender assisted in the radiogenic isotope laboratory.
Ingrid Chinn first taught me how to tune in the eyes to find inclusions in diamonds and assisted with the initial FTIR analyses. Fanus Viljoen at the AARL let me on to their FTIR equipment and helped with the analyses. Judith Milledge provided both valuable thoughts and soft-ware for interpreting the FTIR data.
To all of you, I am deeply grateful. I feel privileged to have had the opportunity to work with experts in many different analytical methods. I have learnt a lot!

Baz, Claire and Stewart! Without your chatter (decreasing volume in mentioned order), this thesis would have been finished a long time ago. But I forgive you. I had a really great time and it was a pleasure to share office you. Petrus, thanks for giving me access to your "mafic" data-base.

Finally, to my family Torsten, Lena, Åsa, Anna, Ola, L-O, Ebba, Elsa and Lova: Thank you for staying close to me even though I spend most of the time at the "back-side" of the earth.

ABSTRACT

The Klipspringer kimberlites occur in the north-eastern part of the Kaapvaal craton which is poorly represented in kimberlite and mantle studies. The kimberlites have been dated at 148±4 Ma and the current study presents the geochemical characteristics of their diamonds, diamond inclusion minerals and mantle macrocrysts/bimineralic nodules.

The Klipspringer lithosphere is dominated by eclogite and lherzolite with harzburgite and dunite present to a lesser extent. Group I eclogite which shows affinity to diamondiferous eclogite is more common than Group II eclogite. The eclogites display a range in equilibration temperatures of 960-1090 °C and a fairly "cool" geotherm of 37-39 mW/m^2 has been inferred. The lherzolites display a range in equilibration temperatures of 890-1070 °C and they originate from depths corresponding to pressures of 35-60 kbars. Garnet megacrysts are unusually poor in Ti (TiO_2=0.2-0.5) at fairly high Cr (Cr_2O_3 up to ~ 3 wt.%) and Mg-numbers (up to ~ 90) and they may represent an early garnet phase in a fractionating megacryst parental magma.

34 diamonds investigated for silicate/oxide inclusions are eclogitic/grospyditic, 3 are harzburgitic and 2 are websteritic. Three compositionally diverse eclogitic/grospyditic inclusion groups are present: A grospydite paragenesis (garnet: 12.6-22.5 wt.% CaO, 5.44-12.0 wt.% MgO; clinopyroxene: 16.2-19.2 wt.% Al_2O_3), a rutile-kyanite eclogite paragenesis (garnet: 3.17-13.4 wt.% CaO, 8.78-19.1 wt.% MgO) and a "Fe-rich" eclogite paragenesis (garnet: 8.92-14.8 wt.% CaO, 16.4-21.2 wt.% FeO). Each paragenesis internally displays magmatic fractionation compositional trends while a direct petrogenetic relationship between any of the groups is precluded. Hypothetical bulk rock compositions re-calculated from diamond inclusion compositions mirror the ranges of these elements observed in modern mid-ocean ridge crustal cumulates. Further, the bulk-rock compositions suggest that the inferred cumulate protoliths were related through magmatic fractionation. The grospydite clinopyroxene inclusions carry 2-18 mole% pseudojadeite. The pseudojadeite content is determined by the amount of fractionation of a partial melt of an anorthosite-type protolith. Fe-Mg partitioning between garnet and clinopyroxene inclusions indicate formation temperatures of 1152-1233 °C and 1200-1278 °C at 50 kbars and 60 kbars respectively. This suggests that the diamonds formed during thermal perturbation of the mantle which is consistent with the "small-scale" chemical disequilibrium displayed by multiple inclusions from individual diamonds.

While the peridotitic and websteritic diamonds are deficient in N, the bulk of the diamonds are "regular" type I diamonds with 500-1300 ppm N. Two main N aggregation diamond groups which represent two different diamond formation events are present: A Low-T group and a High-T group with time-averaged mantle residence temperatures (at 2.5 Ga mantle residence) of 1075-1090 °C and 1150-1180 °C respectively. A higher H content in the former diamonds correlates with a comparatively lower platelet peak evolution. The High-T diamonds are commonly brown-pink in colour and they frequently display lamination lines which indicate that they were plastically deformed. Some diamonds have High-T type cores and Low-T type rims and each one of the three eclogitic/grospyditic diamond parageneses is represented in both the N aggregation groups. This shows that the High-T diamonds and Low-T diamonds were spatially related in the mantle, that the former predate the latter and that the inclusions in the Low-T diamonds acquired their compositions from the host rock of the High-T diamonds. Cathodoluminescence images of Low-T diamond plates reveal a poorly developed internal octahedral structure and alternating zones of luminescent (type I) and non-luminescent (type II) diamond. The zones correlate with elevated and depleted levels of hydrogen. These characteristics suggest formation in an open environment from fluids highly supersaturated in C.

Sulfide diamond inclusions are much more common than silicate inclusions. 42 sulfide bearing diamonds all carry low-Ni (< 5 wt.% NiO) eclogitic sulfides. The sulfides display similar mineralogy (po±pen±cp) and a narrow range in $\delta^{34}S$ of –1.8 to +2.4 which is similar to the chondritic $\delta^{34}S$. Re/Os ratios of sulfides from Low-T diamonds are indicative of a basaltic source. Re-Os systematics of the sulfides give an age of 2.5±0.3 Ga and an initial $^{187}Os/^{188}Os$ of 0.19±0.09 which is compatible with a basaltic source which had an elevated Re/Os ratio compared to the primitive mantle for a maximum of ~200 Ma but it also overlaps with the primitive mantle.

Multiple silicate inclusions from individual High-T diamonds display compositional trends which are concordant with the magmatic fractionation trends displayed by other inclusions. This may be suggestive of an igneous origin for the High-T diamonds. The Low-T diamonds are proposed to have formed during the break-up of the Vaalbara supercontinent at ~ 2.7 Ga at approximately the time of formation of the Ventersdorp lavas and a major re-activation of the Thabazimbi-Murchinson Lineament (TML). The TML may have acted as a path-way for sub-lithospheric S and C saturated fluids which carried the C, N and H for the

diamonds and the S, Os and the bulk of the Fe and Ni for the sulfide inclusions. This event likely raised the local geotherm and the Low-T diamonds formed during a thermal perturbation of the mantle as indicated by the elevated temperature of formation recorded by their silicate inclusions. The silicate inclusions in the Low-T diamonds do not display evolved compositions compared to the silicate inclusions in the High-T diamonds as would be expected if the former formed from a partial melt of the High-T diamond host-rock. Rather, the Low-T diamonds formed from re-crystallisation of minerals in the eclogitic/grospyditic protoliths. The heating event with shear-stress induced from the reactivation of the TML may have caused the plastic deformation of the High-T diamonds. The similarity in time-averaged mantle residence temperatures for the Low-T diamonds and the temperature of the deep lithosphere at ~ 150 Ma implies that a "cool" mantle existed already at the Archaean/Proterozoic boundary and that thermal relaxation back to a steady-state geotherm followed shortly after diamond formation.

The high diamond grade of the kimberlites confirms that dykes may be economically viable diamond deposits. The present study shows the importance of targeting large-scale tectonic structures in diamond exploration as well as the importance of prospecting for eclogitic diamonds locally.

TABLE OF CONTENTS

1. INTRODUCTION

1.1 Diamonds and the cratonic lithosphere

Since Richardson et al. (1984) obtained mid-Archaean ages for syngenetic garnet diamond inclusions from late Cretaceous kimberlites, it has been generally accepted that most diamonds are exotic rather than cognate with respect to their kimberlite or lamproite host. Except for rare occurrences of asthenospheric diamonds (see Chapter 7 for references), the primary environments for diamond formation and residence are the different lithologies of the cratonic lithosphere. Since diamonds are stable only at pressures in excess of ~ 50 kbars (Kennedy and Kennedy, 1976) at geothermal conditions found in cratons, mid-Archaean diamonds indicate the existence of an ancient lithosphere. Recently, Re-Os ages of both peridotites and eclogites originating from the deep lithosphere have confirmed that a lithosphere substantially thicker than the Proterozoic lithosphere was present beneath the Kaapvaal craton already in the Archaean (Carlson et al., 1999; Menzies et al., 1998).

Geothermobarometry on mantle xenoliths hosted by late Cretaceous kimberlites is indicative of a petrological and thermal boundary between the lithosphere and the asthenosphere at a depth of ~ 170-190 km (Boyd and Gurney, 1986). The lithosphere was probably fairly cool already in the Archaean as suggested by equilibration temperatures for presumed Archaean peridotitic diamond inclusions which commonly are between 900 °C and 1100 °C (Boyd et al., 1985), similar to those of late Cretaceous peridotite xenoliths (Finnerty and Boyd, 1984). Pressures and temperatures of equilibration for these late Cretaceous xenoliths correspond well to a present-day conductive thermal profile for the Kaapvaal lithosphere based on a surface heat flow of ~ 40 mW/m^2 (e.g. Pollack and Chapman, 1977; Jones, in press).

Conductive model geotherms for the Kaapvaal craton terminate against adiabatic temperatures at depths of ~ 250-400 km depending on the preferred model (Jones, in press) which is suggestive of a considerably deeper thermal base of the lithosphere compared to indications from mantle xenoliths. This is supported by seismic data which indicates the existence of a cool and stable lithosphere with conductive heat transfer down to at least 200 km (James et al., 1997) and perhaps down to 400 km (Jordan, 1978).

Studies of mineral inclusions in diamond have recognised two predominant parageneses which are mineralogically and chemically akin to peridotite and eclogite

respectively (see Section 7.1.2) which are the main constituent rock types of the cratonic lithosphere. Most ages for syngenetic diamond mineral inclusions obtained through studies of radiogenic isotopes range between ~ 1 Ga and ~3.5 Ga (see Chapter 7 for references). Amongst other things this demonstrates that the inclusions were prevented from equilibrating chemically with the surrounding environment by the chemically inert diamond host. Thus, the diamonds and their mineral inclusions may provide information about ancient geochemical environments in the mantle and processes of diamond formation.

Elevated calculated temperatures of equilibration in several diamond inclusion studies have suggested that some peridotitic and eclogitic diamonds have formed during thermal perturbation of the lithosphere (Griffin et al., 1988, 1992, 1993; Sobolev et al., 1997). Further, integrated studies of cathodoluminescence images, nitrogen aggregation state and mineral inclusions of diamonds are suggestive of diamond growth in response to decreasing temperature following a heating event (Bulanova and Milledge, 1995; Taylor and Milledge, 1995; Taylor et al., 1995). However, the source material and mechanism of formation of diamonds and their inclusions has been the subject of much debate and generally accepted models have yet to emerge. Different proposed ideas for the formation of peridotitic and eclogitic diamonds are presented separately below.

1.1.1 Theories of peridotitic diamond formation

Peridotitic diamonds can be sub-divided into harzburgitic and lherzolitic diamonds of which the former are more abundant on a world-wide scale (Meyer, 1987; Gurney, 1989). Calcium depleted harzburgite may represent the residue after komatiitic melt extraction during the Archaean (Boyd and Gurney, 1982) and has often been suggested as a protolith for harzburgitic diamonds (e.g. Gurney et al., 1985). A sub-solidus metamorphic or metasomatic origin for harzburgitic diamonds was first suggested by Boyd and Finnerty (1980) based on derived diamond inclusion equilibration temperatures that were lower than the C-H-O solidus of ultramafic rocks. Based on trace element compositions of sub-calcic harzburgitic diamond inclusion garnets, both Shimizu and Richardson (1987) and Stachel and Harris (1997) preclude that the garnets formed in chemical equilibrium with any known silicate or carbonate magma. The former authors advocate sub-solidus metasomatism of residual harzburgite that predated diamond formation to account for the concurrent depletion in magmaphile elements and enrichment in LREE and elevated Cr contents of the garnet inclusions. In contrast, Stachel and Harris (1997) do not distinguish between the

LREE enrichment and the diamond formation event. They suggest that the peridotitic solidus is lowered by the introduction of a CH_4-enriched melt or fluid with diamonds precipitating from low volume partial melts through oxidation of CH_4.

In contrast to studies mentioned above, Schulze (1986) proposed subducted, Ca depleted serpentinite as a protolith for both harzburgitic and less common lherzolitic diamonds, the latter being formed if some diopside "survived" the serpentinization. This was questioned by Kesson and Ringwood (1989) mainly on the basis that Cr/(Cr+Al) ratios of serpentinite are too low (due to comparatively high Al contents) to be compatible with this ratio in peridotitic diamond inclusions. Similar to Shimizu and Richardson (1987), the authors proposed a refractory harzburgite (or dunite) as a protolith for harzburgitic diamonds. However, contrary to the mentioned studies they argue for an igneous origin of harzburgitic diamonds from hydrous partial melts from subducted oceanic crust which carried dissolved carbonate and ascended into overlying refractory peridotite. The melts would have evolved towards equilibrium through precipitation of crystalline phases and hybridisation with peridotitic minerals with diamond formation through reduction of carbonate rather than oxidation of CH_4. Kesson and Ringwood (1987) argue that precipitation of garnets from the resultant hybrid fluid could account for the LREE enrichment observed by Shimizu and Richardson (1987).

Haggerty (1986) emphasised the lithosphere-asthenosphere boundary as a region of not only contrasting densities and temperatures but also contrasting redox conditions and shows that both oxidation of CH_4 and reduction of CO_2 entering the lithosphere may readily occur. He suggests that carbon precipitates through gaseous cracking at the lithosphere-asthenosphere boundary with concurrent vapour fractionation of O-H. Alternatively, comparatively incompatible carbon is relegated to a refractory residue during partial melting of the mantle and dissociation of CH_4 or CO_2. Contrary to most ideas presented above, Haggerty (1986) proposed a solid-state metamorphic growth in a closed environment for harzburgitic diamonds. It must here be emphasised that neither Haggerty (1986) nor Schulze (1986) debates the intriguing trace element chemistry displayed by harzburgitic diamond inclusions.

Stachel and Harris (1997) also showed that contrary to the case of harzburgitic diamond inclusions, REE patterns for lherzolitic inclusions are compatible with equilibrium crystallisation with a kimberlite/lamproite or a carbonatite magma. An igneous origin for lherzolitic diamonds has also been suggested on the basis of elevated diamond inclusion equilibration temperatures compared to the C-H-O peridotite solidus (Griffin et al., 1992).

1.1.2 Theories of eclogitic diamond formation

Equilibration temperatures for non-touching eclogitic diamond inclusions are generally higher than those of peridotitic inclusions and range up to ~ 1400-1500 °C (e.g. Sobolev et al., 1983; Griffin et al., 1988). While melt experiments on eclogites at pressures in excess of 50 kbars are absent, many of the derived temperatures are above the C-H-O solidus of harzburgite at 50 kbars (~ 1300 °C; Wyllie, 1989) and almost all are higher than the C-H-O solidus of lherzolite at 50 kbars (~ 1100 °C; Wyllie, 1987). This may be indicative of an igneous origin for eclogitic diamonds as previously suggested (e.g. Boyd and Gurney, 1986).

Haggerty (1986) proposed that eclogite from the upper part of the lithosphere gets concentrated at the base of the lithosphere due to gravitational sinking and at temperatures exceeding the Fe-Ni-Cu monosulfide solution fluidus of 1100 °C (Craig and Kullerud, 1969), an immiscible sulfide fluid would form. A presumed large concentration of sulfides in the lithosphere may have maintained a relatively reduced environment required for diamonds to form and the preferred partition of carbon into a sulfide fluid would yield carbon saturation and diamond precipitation. In this way, Haggerty (1986) suggests that diamonds nucleate and initially grow in a sulfide fluid with subsequent continued solid-state metamorphic growth.

The Haggerty (1986) model conflicts with an increasing amount of evidence for an origin of eclogites through underplating onto the lithosphere of subducted oceanic crust. The chemical composition and highly fractionated oxygen isotopes of eclogites may indicate that they represent metamorphic fragments of oceanic lithosphere and/or oceanic crust (perhaps hydrothermally altered) with or without associated sediments (e.g. Helmstaedt and Doig, 1975; Jagoutz et al., 1984; MacGregor and Manton, 1986; Jacob et al., 1994). Alternatively, subducted oceanic crust may be remelted (Hofmann and White, 1982; Ringwood, 1982) or melt incongruently (Ireland et al., 1994; Rudnick, 1995) and be subsequently underplated onto the lithosphere. Based on major and trace element compositions, an origin of eclogite from subducted Archaean island-arc type basalts has been suggested (Jacob and Foley, 1998).

As summarised in a review by Kirkley et al. (1991), many eclogitic diamonds are depleted in ^{13}C suggestive of an input from organic carbon. An organic source has also been proposed from the observed concurrent depletion in ^{13}C and enrichment in ^{15}N in diamonds from unknown and eclogitic parageneses (Boyd and Pillinger, 1994; van Heerden

et al., 1995). Large positive and negative fractionation of sulphur isotopes from diamond inclusion sulfides may also be indicative of an organic source and perhaps even hydrothermally altered mid-ocean ridge basalt (Eldridge et al., 1991). Although Cartigny et al. (1998a, 1998b) suggest that high temperature fractionation of carbon and nitrogen isotopes can occur in the mantle, stable isotope data for diamonds and diamond inclusions to a large extent support an origin of eclogites from subducted material.

Kesson and Ringwood (1989) argue for an igneous origin of eclogitic diamonds in a subducting oceanic crust at depths between 150 and 400 km. The authors propose that water from dehydration of serpentinite in the subducted lithosphere ascends into the overlying crust and initiates melting of eclogite. The diamonds would crystallise in incipient partial melts in a closed-system crystal-fluid fractionation process which would explain the slightly more fertile chemical composition of eclogitic diamond inclusions compared to their xenolith counterparts as observed by Sobolev et al. (1983). Further, Kesson and Ringwood (1989) suggest that this process could account for the wide range in temperatures recorded for Orapa diamond inclusions and the concurrent decrease in Mg number and Cr_2O_3 and increase in Na_2O with falling temperature (Gurney et al., 1984a). Kesson and Ringwood (1989) reported that no fluids can coexist with eclogite at commonly reported equilibration temperatures for eclogitic inclusions. The diamonds and their inclusions more likely precipitate from a melt.

Griffin et al. (1988) reported on extremely high concentrations of Pb, U, Rb, and K in eclogitic garnet and clinopyroxene diamond inclusions. Contrary to ideas presented above, the authors proposed that eclogitic diamonds precipitate during an open-system fluid-flux through an eclogite protolith (as previously suggested by Gurney et al., 1984a) to account for the enrichment in the aforementioned elements particularly in the clinopyroxene. Deines and Harris (1995) also invoke introduction of fluids into a protolith and proposed that diamonds form from reaction between CO_2 and CH_4 with C and H_2O as the end products. The released water would lower the solidus and induce melting of the host rock. In this way, elements like C, S, N and H may dominantly be derived from the fluid while silica compatible elements may be derived from the wall-rock.

1.2 Background and aims of the study

From the above, it is apparent that further studies on the origin of diamonds are warranted. While many studies on one aspect or another of diamonds and diamond inclusions have

yielded important information, they often leave room for much speculation. For this reason, multi-disciplinary studies on diamonds from single localities and particularly on single diamonds (e.g. Bulanova, 1995) is important.

For this study, kimberlite and mantle samples have been made available from a previously unrepresented part of the Kaapvaal craton east of Potgietersrus in the Northern Province, South Africa. To date, exploration and mining have been concentrated on three kimberlites from which kimberlite, mantle macrocrysts and diamond samples have been recovered. The current study has been focused on the chemical compositions of the diamonds and their syngenetic mineral inclusions in an attempt to elucidate their origin in terms of source material and mechanism of formation.

Compositions of silicate, sulfide and oxide diamond inclusions have been measured by electron microprobe. This allowed for the identification and interpretation of different diamond growth environments. Eclogitic bulk-rock compositions have been estimated from diamond inclusion compositions in an attempt to place constraints on protoliths for the inclusions and diamond formation temperatures have been estimated indirectly from non-touching garnet and clinopyroxene inclusions.

Infrared absorption characteristics of the diamonds were determined primarily to identify different diamond populations and to obtain information on their time-averaged temperatures of mantle residence from nitrogen contents and aggregation state. This study was aided by a time constraint on the mantle residence of the diamonds obtained from Rb-Sr dating of two of the kimberlites. Infra-red absorption analysis was also undertaken in conjunction with cathodoluminescence images of polished diamond plates which allowed for an integrated study of diamond growth zones (with implications for growth mechanisms) and nitrogen and hydrogen contents.

All diamonds studied for mineral inclusions and infra-red absorption characteristics have been described in detail in terms of physical characteristics (i.e. colour, crystal form, deformation structures etc.) and infra-red absorption analysis was performed on most diamonds with mineral inclusions. This has made possible an integrated study of these characteristics, particularly involving mineral inclusions and infrared absorption characteristics.

Re-Os isotope analysis of syngenetic sulfide diamond inclusions has been undertaken to put age constraints on the inclusions and indirectly on the diamond formation event. Re-Os abundance and Os isotope characteristics also allowed for inferences on the origin of the sulfides. Sulfide diamond inclusions were also analysed for sulphur isotope compositions

which have been compared with different possible sulphur reservoirs to further constrain the origin of the sulfides.

The lithospheric lithologies have been characterised through major element analysis of garnet macrocrysts and bimineralic garnet/clinopyroxene nodules. Equilibration temperatures have been estimated for bimineralic nodules and a geothermal gradient for the lithosphere has been proposed.

Implications from the different analyses undertaken are discussed individually at the end of each chapter. In chapter 10, the results are integrated and a proposed age for the diamonds and implications for their origin are discussed on a local scale (the immediate diamond formation environment) and regional scale. The thermal evolution of the lithosphere as deduced from the geothermometry of diamond inclusions and bimineralic nodules, nitrogen aggregation state of the diamonds and some of their physical properties is discussed. Further, some implications for diamond exploration resulting from the current study are presented.

2. GEOLOGICAL SETTING

2.1 Regional framework

The oldest parts of the Kaapvaal craton consist of granite-greenstone terrains which range from 3.1 Ga to 3.7 Ga in age (de Wit et al., 1992). Already around 3.2-3.3 Ga this ancient crust was underlain by a lithospheric keel at least 150 km thick (Richardson et al., 1984). The Kaapvaal craton is unconformably covered by 2.1-2.7 Ga volcanosedimentary sequences indicating that the craton was stable prior to 2.7 Ga (Brandl and de Wit, 1997). The craton has been subdivided into a number of discrete domains which display different types of tectonic contacts (de Wit et al., 1992). In the western parts of the craton, major terrain boundaries strike NNE-SSW while in the eastern parts terrain boundaries trending ENE-WSW predominate. Whether the sub-terrains are allochthonous or represent tectonically disrupted parts of a former coherent geological province is not clear.

The Klipspringer kimberlites are located south of the southern margin of the Limpopo mobile belt in the north-eastern parts of the Kaapvaal craton (Figure 2.1). The kimberlites intrude the Thabazimbi-Murchinson Lineament (TML) which is one of the major ENE-WSW striking terrain boundaries on the craton. The TML forms the northern margin of the basin in which the Archaean-Proterozoic Transvaal sequence was deposited. It is also the northern limit for the extension of the ~ 180 Ma old Karroo volcanics. Further,

the northern lobe of the 2.05 Ga Bushveld complex is significantly offset from the southern lobe across the TML.

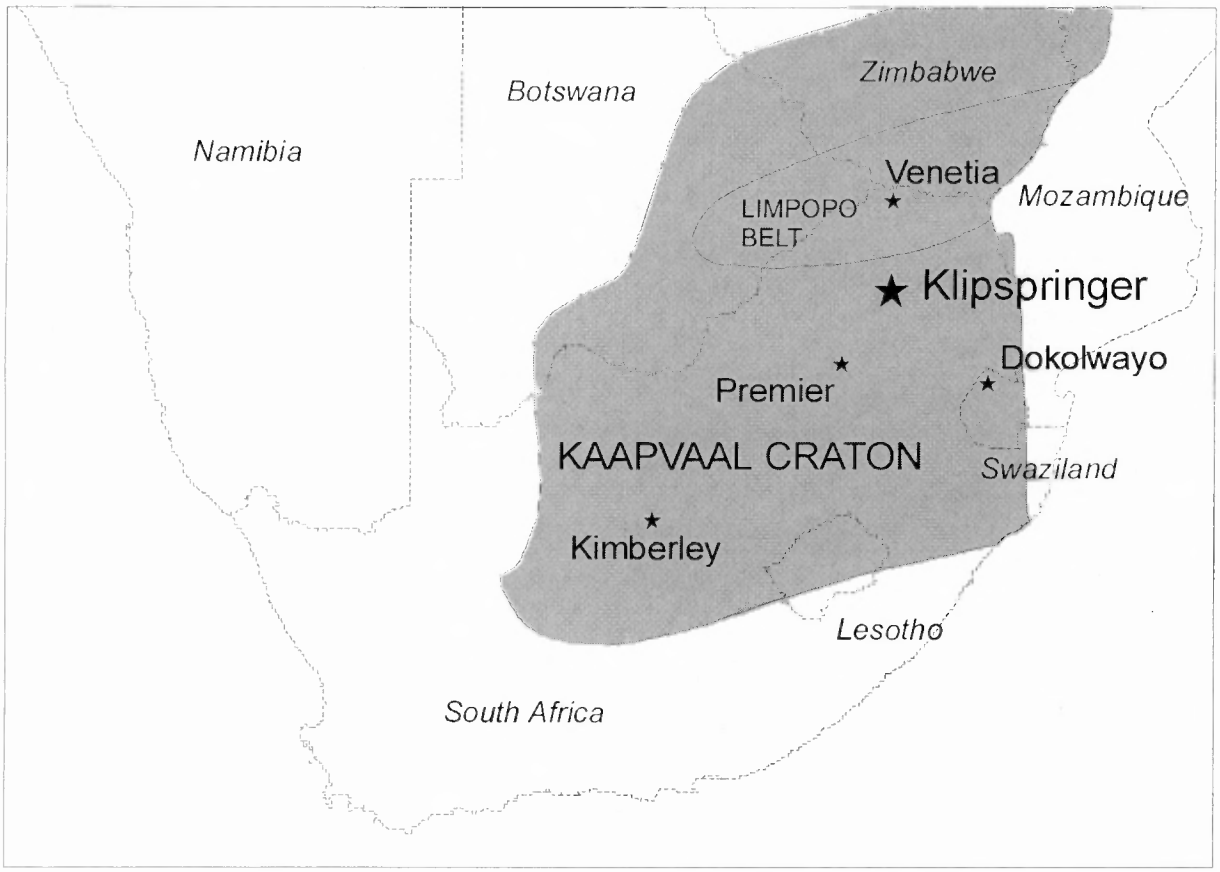

Figure 2.1 The location of the Klipspringer kimberlites in relation to some other kimberlite occurrences and the Limpopo Mobile Belt. The Kaapvaal craton and the Zimbabwe craton merge at the Limpopo Belt.

The history of the TML has been studied in detail by Good (1997) and Good and de Wit (1997). The earliest movements recorded in the TML have been dated at 2.96 Ga and may have originated at the boundary between a Kaapvaal granite-greenstone terrain and the southern margin of the Limpopo mobile belt. A major reactivation of the TML occurred around 2.7 Ga. This age correlates with the formation of the Ventersdorp lavas and associated volcanism in the Witwatersrand basin as well as a major uplift of the Limpopo belt. Nelson et al. (1992) have correlated the ~ 2.7 Ga Ventersdorp lavas with the Fortescue lavas of the Pilbara craton, Western Australia. It has been suggested that a Vaalbara supercontinent (Kaapvaal and Pilbara cratons) possibly existed as far back as ~ 3.6 Ga and that the supercontinent may have fragmented around 2.7 Ga during major intracontinental volcanic and tectonic activities. A second major reactivation of the TML has been recorded

at ~ 2 Ga indicating that the TML probably influenced the emplacement of the Bushveld complex.

Seismic anisotropy data has shown that the lithosphere beneath the TML contains an east-west fast polarisation direction in contrast to the NE-SW direction generally observed for the Kaapvaal craton (Vinnik et al., 1995). This may suggest that formation and/or reactivation of the TML recorded in the crustal rocks can be extrapolated down to lithospheric depths.

2.2 Geological setting and diamond grade of the kimberlites

The studied kimberlites are parts of a kimberlite field consisting of dykes and small pipes. To date, more than ten exploration targets have been identified through drilling and indicator mineral soil anomalies. The kimberlite cluster occurs just north of the northern extent of the Karroo volcanics and the underlying Bushveld complex. Four of the kimberlites, the Main Fissure, the Sugarbird Fissure, Sugarbird Blow and the Marsfontein pipe are included in the present study.

The Main and Sugarbird Fissures intrude the Malmani dolomites of the Transvaal sequence, which was deposited onto the basement in the early Proterozoic. Both kimberlites are en-echelon dykes, which strike parallel to the TML and the Sugarbird Fissure is located about 750 metres north of the Main Fissure. The Main Fissure has been traced through drilling and indicator mineral soil anomalies for more than seven kilometres and the Sugarbird Fissure exceeds four kilometres in length. The Main and Sugarbird fissures have an average width of 1.1 and 1.3 metres respectively. A small pipe, the Sugarbird Blow, is located on the Sugarbird Fissure and it measures about 35m x 40m at surface. The Marsfontein kimberlite is located about 10 kilometres east of the two fissures. It intrudes the Meinhardskraal basement granite and it measures about 40m x 90m at surface.

To date, the Main Fissure, Sugarbird Blow and the Marsfontein kimberlites have been mined to different extents. The Main Fissure has an in situ grade of about 0.7 carats per tonne kimberlite and a 1997 sale realised a diamond price of US$ 126 per carat. The initial diamond grade for the Sugarbird Blow exceeded 1 carats per tonne and the diamonds were valued at US$ 85 per carat. Marsfontein is exceptional on a world-wide scale from its combination of high grade and high quality diamonds. The grade has been estimated to be about 3 carats per tonne and at a 1998 sales the diamonds were valued at about 160 US$ per carat.

3. RB-SR INVESTIGATION OF THE MAIN FISSURE AND SUGARBIRD BLOW KIMBERLITES

3.1 Purposes of the investigation

Rb-Sr isotope analysis of the Main Fissure and Sugarbird Fissure kimberlites has been undertaken while the Marsfontein kimberlite has not been similarly studied due to the lack of suitable samples. Previous Rb-Sr datings with poor precision indicate a Jurassic-Triassic age for the Sugarbird Fissure and in contrast an early Proterozoic age for the Main Fissure (Southernera internal report, 1996). If these indications were correct, an opportunity would exist to study lithospheric mantle brought up by kimberlite at widely different times from two juxtaposed localities. This would allow a study of the evolution of the mantle from early Proterozoic to Cenozoic times at one locality. Rb-Sr analysis was undertaken in an attempt to verify the emplacement ages of the kimberlites.

Knowledge of the age of the kimberlites is also important in the interpretation of the nitrogen aggregation data on the diamonds. The nitrogen aggregation state in a diamond is dependent on the mantle residence time of the diamond and the temperature(s) at which the diamond resided in the mantle (Section 6.1). Time is not as sensitive a parameter as temperature but to be able to better interpret nitrogen aggregation data, it is of importance to know whether the diamonds resided in the mantle for millions or billions of years. For this reason it is necessary to know whether the diamonds (of which some have been dated at ~2.5 Ga, Chapter 9) were brought up by the kimberlites in early Proterozoic or Cenozoic times.

3.2 Principles and problems of the method

The analytical method is described in Appendix 1. The method is based on analysis of kimberlitic phlogopite concentrates and whole-rock samples. Two different types of kimberlite (termed Group I and Group II) have been identified on the basis of Sr and Nd isotope compositions and major and minor element abundance (Smith, 1983; Smith et al., 1985a). Group II kimberlites generally carry abundant phlogopite in contrast to Group I kimberlite, which makes the former group particularly suitable for Rb-Sr dating.

Since the Sr content in mica is more variable than the Rb content, a phlogopite isochron is based on mica concentrates with different intrinsic Sr contents, which translates into different $^{87}Rb/^{86}Sr$ ratios. Thus, preparation of phlogopite concentrates of different grain size, morphology and colour is attempted to strive for a large spread in $^{87}Rb/^{86}Sr$ ratios. Euhedral micas are preferred in the sense that they are cognate with respect to the kimberlite. However, euhedral micas are often very small in size and difficult to clean which makes it difficult to obtain pure mica concentrates. Further, euhedral micas are commonly poikilitic with inclusions of other kimberlite groundmass minerals. This does not give rise to a spurious age if the different minerals were in isotopic equilibrium at the time of crystallisation but introduces a dilution effect since the inclusions are very low in Rb. This would result in model ages that are heavily dependent on a correctly assumed initial $^{87}Sr/^{86}Sr$ ratio. Macrocrystic micas are easier to date since they are larger and clean separates are more easily obtained. Further, they are generally lower in common Sr and consequently have higher Rb/Sr and $^{87}Sr/^{86}Sr$ ratios (Smith et al., 1985b) which yields a better defined isochron or model ages less dependent on the assumed initial $^{87}Sr/^{86}Sr$ ratio. However, the origin of macrocrystic phlogopite is enigmatic and they may not necessarily have been in isotopic equilibrium with the kimberlite at the time of crystallisation.

Allsopp and Barrett (1975) reported isochron ages of 114±8 Ma for large phlogopite nodules, 83±4 Ma for kimberlitic micas and 84±4 Ma for peridotitic nodule micas from the Wesselton kimberlite. The first mentioned age was believed to be anomalously old. This led the authors to suggest that radiogenic Sr might be partially retained in the samples even at mantle temperatures if the phlogopite existed in the form of large masses so that the distance from the interior of the mass to a suitable Sr sink would be too great for equilibrium to be accomplished. The radiogenic Sr is then only partially re-equilibrated in the kimberlite.

The Sanddrift kimberlite was dated at 125 Ma by Smith et al. (1994). Peridotite xenoliths from this locality carry phlogopite, which is similar in appearance to the general mica population and give model ages of about 2250 Ma. When two mica concentrates believed to be contaminated by xenolith mica were incorporated in the regression, an age of 138±8 Ma was obtained. The authors suggested a shallow origin for the xenolith mica with a long residence time below blocking temperature of phlogopite to account for the model age 2250 Ma. As shown by Smith et al. (1985b), this problem is present as well for groundmass mica. These authors dated the New Elands kimberlite at 126 Ma using

groundmass phlogopite concentrates. When two concentrates likely to contain small amounts of unequilibrated crustal mica were incorporated in the regression, an anomalously old age of 140 Ma was obtained. From the examples above it is obvious that introduction of small amounts of foreign, unequilibrated mica can give rise to anomalously old ages even if present only in minor amounts in the mica concentrates.

Smith et al. (1985b) emphasise the importance of homogeneous mica concentrates to avoid combination of micas with different initial $^{87}Sr/^{86}Sr$ ratios and the use of mica chemistry to aid in assessing the results. The authors obtained poorly constrained ages for Roberts Victor and Rietfontein kimberlites, which also showed highly variable phlogopite compositions.

Alteration of kimberlitic micas through deuteric or weathering processes is common. Deuteric alteration does not necessarily result in spurious ages if it occurs in a closed kimberlitic system. On the other hand, weathering induced chloritization and/or serpentinization of the micas typically result in Rb loss (Smith, 1983) and consequently result in spurious old ages. Incipient alteration is not easily recognised but Smith (1983) found a marked colour change in weakly altered mica after leaching in hydrochloric acid (see next section). Despite the possibility of Rb loss during alteration, Brown et al. (1989) presented a high quality isochron age of 121±2 Ma for the Mangawane kimberlite based on a wide range of fresh to altered phlogopites (see further next section).

As pointed out by Allsopp et al. (1989), to avoid problems of isotopically unequilibrated micas and altered micas, sampling of hypabyssal facies kimberlite rather than diatreme facies should be strived for since the latter is more susceptible to weathering and carries more abundant crustal mica.

3.2.1 The leaching technique

The phlogopite grains are commonly "contaminated" by kimberlitic and/or exotic carbonate. Thus, a phlogopite isochron is in part a mixing line between the different phlogopite concentrates and a carbonate end member. Kimberlitic carbonate typically has very high Sr contents (2000-9000 ppm) and low $^{87}Sr/^{86}Sr$ ratios (<0.7050) (Brookins, 1967). If the carbonate contaminant was kimberlitic and thus in equilibrium with the mica it would not give rise to spurious ages. However, the lower measured $^{87}Sr/^{86}Sr$ and $^{87}Rb/^{86}Sr$ yields a model age more dependent on the assumed initial ratio or a less well defined isochron age.

If the carbonate contaminant is of exotic origin it will induce a geological error and give rise to scatter around the regression line.

The leaching method was developed by H.L Allsopp and colleges at the Bernard Price Institute (e.g. Smith, 1983; Allsopp et al., 1989) to get around the problems of carbonate contamination and it involves leaching of the micas in 1-2 M hydrochloric acid for about ten minutes prior to dissolution. Leaching reduces the amount of kimberlitic and exotic carbonate attached to the grains with the effect of increasing $^{87}Rb/^{86}Sr$ ratios and minimising geological error from exotic carbonate. The leaching technique has been shown to drastically decrease the Sr concentration while the intrinsic Rb content and Sr isotope composition of the phlogopite are not affected (Brown et al., 1989).

3.3 Kimberlite petrography and sample description

Main and Sugarbird Fissures have been extensively drilled and core to a depth of 80 metres was available for kimberlite sampling. All samples were collected from hypabyssal facies kimberlite and they were very fresh, free of carbonate veins and xenoliths.

The two dykes are very similar petrographically and they display mostly Group II characteristics. They are macrocrystic kimberlites and subhedral to anhedral macrocrystic olivine often makes up 40-50 modal % of the rock. Phlogopite is very abundant and occurs as anhedral macrocrysts up to a few millimetres in size and as 0.05-1 mm euhedral to subhedral phenocrysts. The dykes are petrographically intermediate between Group I and II kimberlites in that they carry relatively abundant and coarse-grained euhedral perovskite and opaque minerals. The groundmass is dominated by very fine-grained serpentine and calcite while fine-grained apatite and laths of diopside occur subordinately.

Two phlogopite concentrates from the Main Fissure and three from Sugarbird Fissure were prepared for analysis. The micas were very fresh, light brown in colour and no discoloration indicative of alteration was observed either before or after leaching in hydrochloric acid. Crustal micas are generally dark brown in colour due to their relatively high Fe content and such micas were avoided during preparation of the concentrates. Main Fissure concentrates (KJW13/2 and KJW13/3) consist of coarse grained euhedral phenocrysts and subhedral to anhedral macrocrysts respectively. Sugarbird samples (KJW9/2, KJW11/1 and KJW11/2) consist of different size fractions of macrocrysts. Phlogopites in sample KJW11/1 are subhedral while sample KJW9/2 consists of anhedral grains and KJW11/2 consists of very large macrocrysts that broke into smaller pieces during crushing of the sample. Sample

KJW11/1 was split into two samples of which one (KJW11/1-L) was leached in hydrochloric acid while KJW11/1-N was left unleached in an attempt to investigate the Sr isotope composition of the leached Sr. One whole-rock sample from each dyke was analysed in an attempt to better constrain the initial $^{87}Sr/^{86}Sr$ ratio. The whole-rock samples were very "fresh" and showed only very little sign of alteration in the form of incipient serpentinization of olivine.

3.4 Emplacement age and Rb-Sr isotope systematics

Rb and Sr concentrations and isotope ratios are given in Table 3.1. Excluding Sr in sample KJW11/2, Rb and Sr contents of the mica (~ 400-500 ppm and ~ 40-100 ppm respectively) are in the expected range for kimberlitic phlogopite. Leaching of sample KJW11/2 left the Rb concentration virtually unchanged while the Sr content was reduced from 1330 ppm to 428 ppm (compare samples KJW11/2-N and KJW11/2-L). A Sr concentration of 428 ppm in KJW11/2-L is still anomalously high for macrocrystic phlogopite and it is suspected that some carbonate remained attached to the mica after leaching.

Table 3.1 Rb-Sr isotope data for Main Fissure and Sugarbird Fissure whole-rock samples and phlogopite concentrates.

	Rb(ppm)	Sr(ppm)	$^{87}Rb/^{86}Sr$	$^{87}Sr/^{86}Sr \pm 2\sigma_m$
KJW9/WR	94.8	1213	0.226	0.70754±2
KJW13/WR	59.1	1516	0.113	0.70738±2
KJW9/2-L	469	47.54	28.73	0.76690±2
KJW11/1-L	447	97.51	13.31	0.73568±2
KJW11/2-N	462	1330	1.007	0.70936±2
KJW11/2-L	474	428.4	3.206	0.71398±2
KJW13/2-L	414	42.79	28.18	0.76795±2
KJW13/3-L	449	42.86	30.53	0.77030±2

The samples are shown in an isochron diagram in Figure 3.1 together with a regression line which is based on all samples. The samples are strongly correlated in the isochron diagram, which suggests that the phlogopite concentrates are free of unequilibrated old crustal or mantle mica. A phlogopite isochron is in part a mixing line between different phlogopite concentrates and a carbonate end-member and the age obtained is of geological significance only if both end-members were parts of the same isotopic system. Since the unleached sample KJW11/2-N

(which has not been "cleaned" from the carbonate contaminant) plots on the regression line, the carbonate contaminant had an initial Sr isotope composition similar to the phlogopite. This indicates that the leached Sr was in isotopic equilibrium with the Sr of the phlogopites at the time of crystallisation. Further, the whole-rock samples plot on the regression line, indicating that the kimberlite groundmass, in which calcite is the principle host for Sr, had the same initial $^{87}Sr/^{86}Sr$ ratio as the phlogopite. Thus it is believed that an age of geological significance may be obtained from the data.

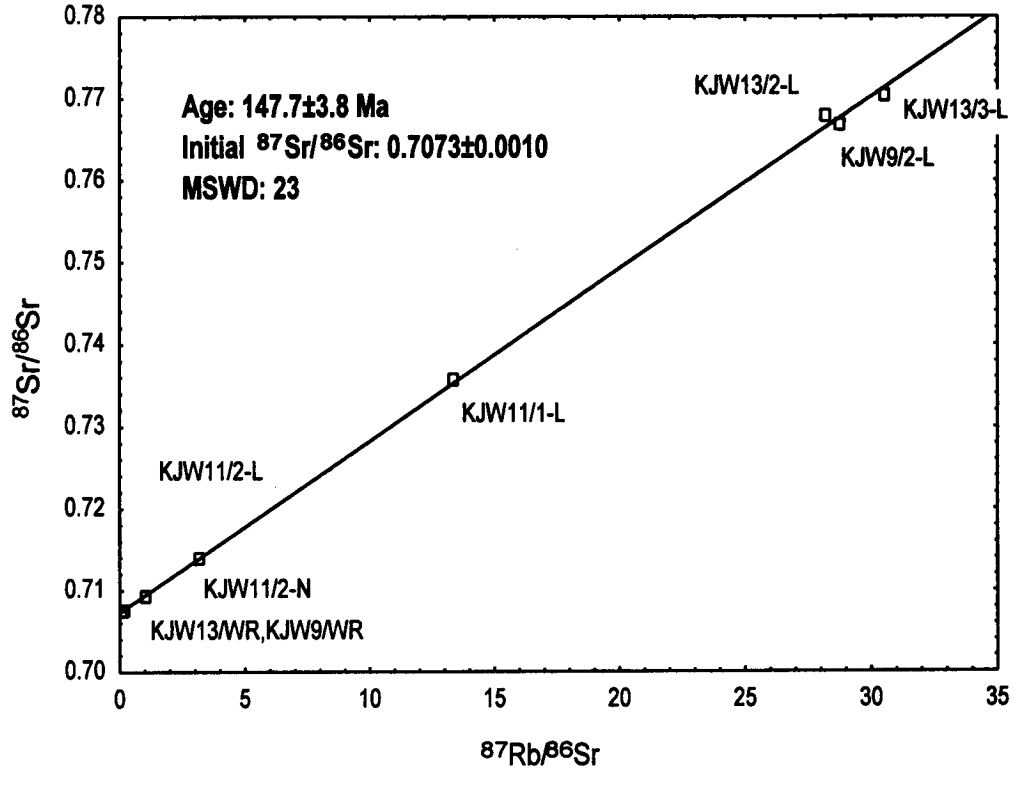

Figure 3.1 Rb-Sr isochron diagram for Main Fissure and Sugarbird Fissure whole-rock samples and phlogopite concentrates. Errors on the age and the initial Sr isotope composition are at the 95 % confidence interval. Analytical errors do not exceed the size of the markers.

The data were regressed according to York (1969) and the scatter around the regression line is assumed to be due to analytical error and a normally distributed error in the initial $^{87}Sr/^{86}Sr$. When all samples are included in the regression, an age of 148±4 Ma and an initial $^{87}Sr/^{86}Sr$ ratio of 0.7073±0.0010 are obtained. This regression yields an errorchron with a MSWD of 23. The fit of the regression line may be drastically improved if samples

KJW11/1, KJW13/2 and the two whole-rock samples are excluded from the regression. This treatment would give a four-point isochron age of 146±1 Ma with an initial $^{87}Sr/^{86}Sr$ of 0.7073±0.000034 and a MSWD of 1.7. However, since the Sr isotope composition of the dolomite country rock is not known, the minor scatter in the isochron diagram cannot be evaluated and there is no obvious reason for any of the samples to be excluded. Further, the age and initial $^{87}Sr/^{86}Sr$ obtained when any samples are excluded are not significantly different from the results when all data are included in the regression.

3.5 Discussion and Conclusions

Since the dating is based on micas from both the Main Fissure and the Sugarbird Fissure, it can be concluded that the two dykes formed contemporaneously around 150 Ma ago. The initial $^{87}Sr/^{86}Sr$ of the phlogopites (and the kimberlites) is similar to the range of 0.7075-0.710 characteristic of Group II kimberlites (Smith, 1983) and confirms the petrographical classification of the dykes as Group II kimberlites. The age is within error of ages obtained for Swartruggens kimberlite dykes (147±4 Ma, Allsopp and Barrett, 1975; 150±3 Ma, Allsopp and Kramers, 1977). The initial $^{87}Sr/^{86}Sr$ ratio of the Swartruggens dykes has not been well constrained but is indicative of Group II kimberlites (Allsopp and Barrett, 1975; Smith et al., 1985b) which is consistent with the petrographical character of the dykes (Klump, 1995). Thus, from the present study, a more-wide spread Group II kimberlite emplacement event may be inferred at around 150 Ma.

The concordant age of the two dykes proves previous age determinations to be wrong and precludes a study of the evolution of the lithospheric mantle over two billion years. Further, the age of the dykes constrains the mantle residence time of dated diamonds (Chapter 9) to about 2.5 Ga.

4. CONCENTRATE GARNETS AND GARNET-CLINOPYROXENE NODULES

4.1 Sampling and nature of the sample

Large, multi-grain mantle xenoliths have not been encountered in the Klipspringer kimberlites. Therefore the underlying mantle has been characterised through concentrate garnet macrocrysts and bimineralic garnet-clinopyroxene nodules.

Garnet macrocrysts were not selected randomly to yield information about the relative abundance of different types of garnet. Instead colour was used as the main selective criteria to make sure that all types of garnets present were covered. However, garnet types occurring more commonly were consciously selected more often. A total of 302 garnet macrocrysts from the Main Fissure, Sugarbird Blow and Marsfontein have been analysed.

Forty-seven lherzolite, eclogite or megacryst garnet-clinopyroxene nodules were found and recovered for mineral analysis. The nodules were all less than 5 millimetre in the longest dimension and all consisted of a bigger garnet with one or two smaller (generally less than one millimetre in size) associated clinopyroxene. Lherzolitic clinopyroxene was generally slightly coarser than eclogitic and megacrystic clinopyroxene. Three of the lherzolitic nodules (BM1, BM2 and BM3) also carried unidentified opaque minerals associated with the clinopyroxene and one lherzolitic nodule (BM4) carried mica believed to be phlogopite from its dark brown colour. The garnets were largely fresh with an alteration (kelyphyte?) rim. Grains with visibly altered clinopyroxene were not analysed and electron microprobe analyses yielding a total of <99 wt.% or >101 wt.% are not included in the results.

4.2 Chemical compositions of garnet macrocrysts

Electron microprobe analysis was performed as described in Appendix 2 with reference to Appendix 5. Chemical compositions of garnet macrocrysts from the Main Fissure, Sugarbird Blow and Marsfontein are given in Appendix 2.1, 2.2 and 2.3 respectively. All mineral compositions are presented as oxides rather than cations to allow for an easy comparison to the data in the literature.

As can be seen in Figure 4.1, low-Cr garnets (<2 wt.% Cr_2O_3) predominate in all three kimberlites. Almost equally common are Ca-rich garnets ranging up to about 7 wt.% Cr_2O_3 which define a trend commonly observed for lherzolitic garnets that have equilibrated at a pressure of about 50 kbars (Gurney and Zweistra, 1995). Low-Ca, high-Cr garnets which are compositionally akin to garnets in harzburgite xenoliths (e.g. from the Premier mine; Danchin and Boyd, 1976) carry up to about 8.5 wt.% Cr_2O_3 and are present at all localities to a subordinate degree. The Marsfontein sample differs from the Main Fissure and Sugarbird Blow samples in that it carries sub-calcic garnets which trend towards a chromium content of about 1.5 wt.% Cr_2O_3 with decreasing calcium reminiscent of a dunitic trend as defined by Grutter (1998).

Garnets carrying more than 2 wt.% Cr_2O_3 are shown in chromium-titanium diagrams in Figure 4.2. High-Cr harzburgitic and lherzolitic garnets generally carry less than about 0.15 wt.% TiO_2 and dunitic garnets from Marsfontein display less than 0.05 wt.% TiO_2. Lherzolitic garnets with about 3-5 wt.% Cr_2O_3 trend towards increasing TiO_2 up to about 0.5 wt.% TiO_2. At all three localities, some garnets occur which carry less than 3 wt.% Cr_2O_3 and between 0.25 and 0.6 wt.% TiO_2. These garnets deviate somewhat from the general lherzolitic trends (clearest displayed in the Main Fissure sample) and may belong to a megacryst suite presented below.

Several studies have shown that megacrysts have crystallised from a differentiating magma and may be petrogenetically related to their host kimberlite (e.g. Gurney et al., 1979a; Moore et al., 1992; Bell et al., 1995; Smith et al., 1995). Megacrysts occur in both Group I and Group II kimberlites but they differ somewhat in composition. Garnet megacrysts from Group II kimberlites generally trend towards higher Cr_2O_3 (up to ~ 5 wt.%), higher Mg-number (up to ~ 91) and lower TiO_2 (down to ~ 0.4 wt.%) (Moore and Gurney, 1991; Bell et al., 1995) compared to those from Group I kimberlites (e.g. Gurney et al., 1979a). From now on in this study, the generally adopted term Cr-poor megacrysts represents garnet megacrysts from Group I kimberlites while "Group II megacrysts" is used for garnet megacrysts from Group II kimberlites.

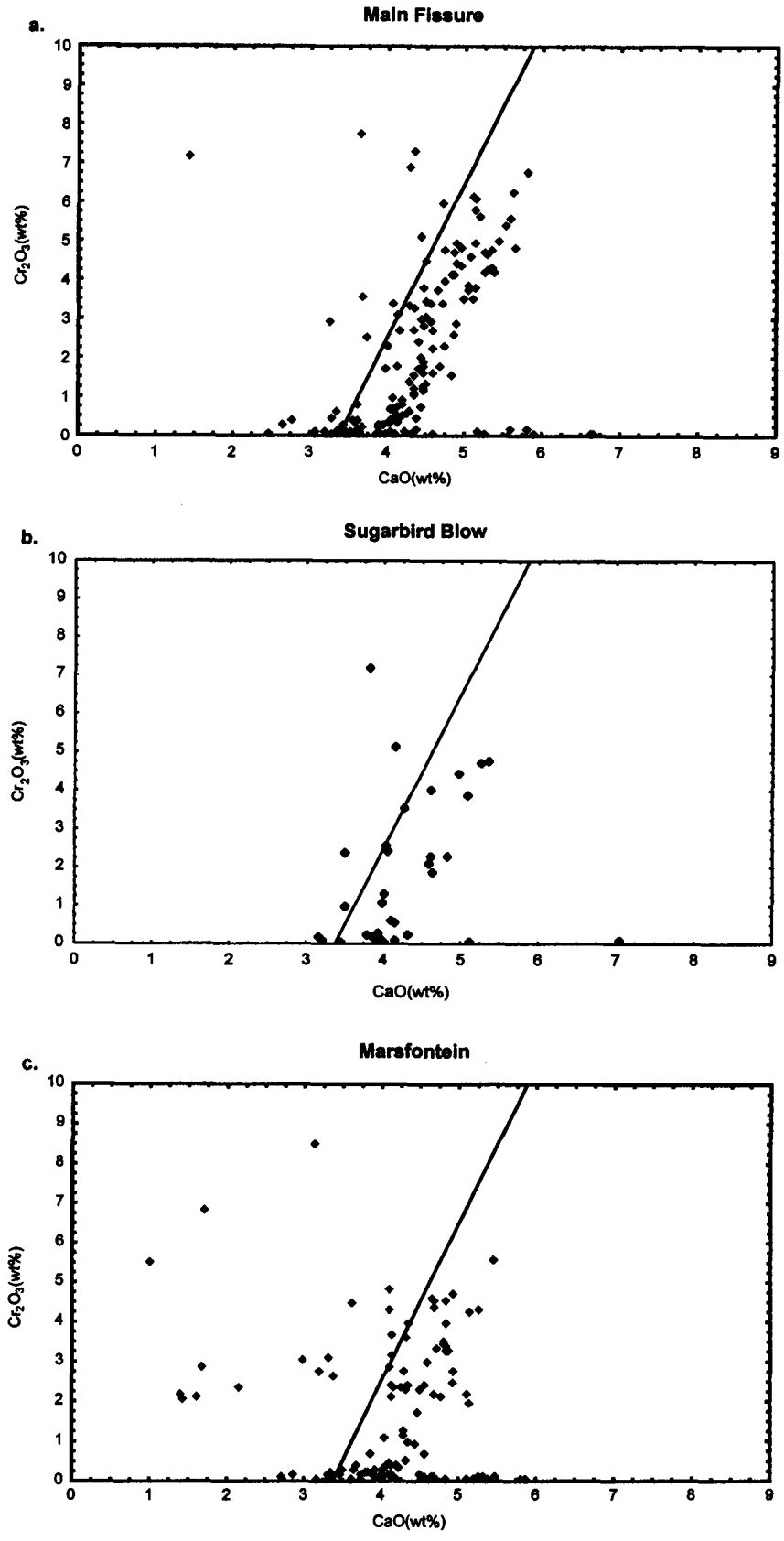

Figure 4.1 Chromium vs. calcium for concentrate garnets shown separately for the three localities. Solid line defines a lherzolitic trend at 50 kbars pressure (Gurney and Zweistra, 1995). Note the trend towards dunitic compositions (low-Ca and low-Cr; Grutter, 1998) displayed by some Marsfontein garnets.

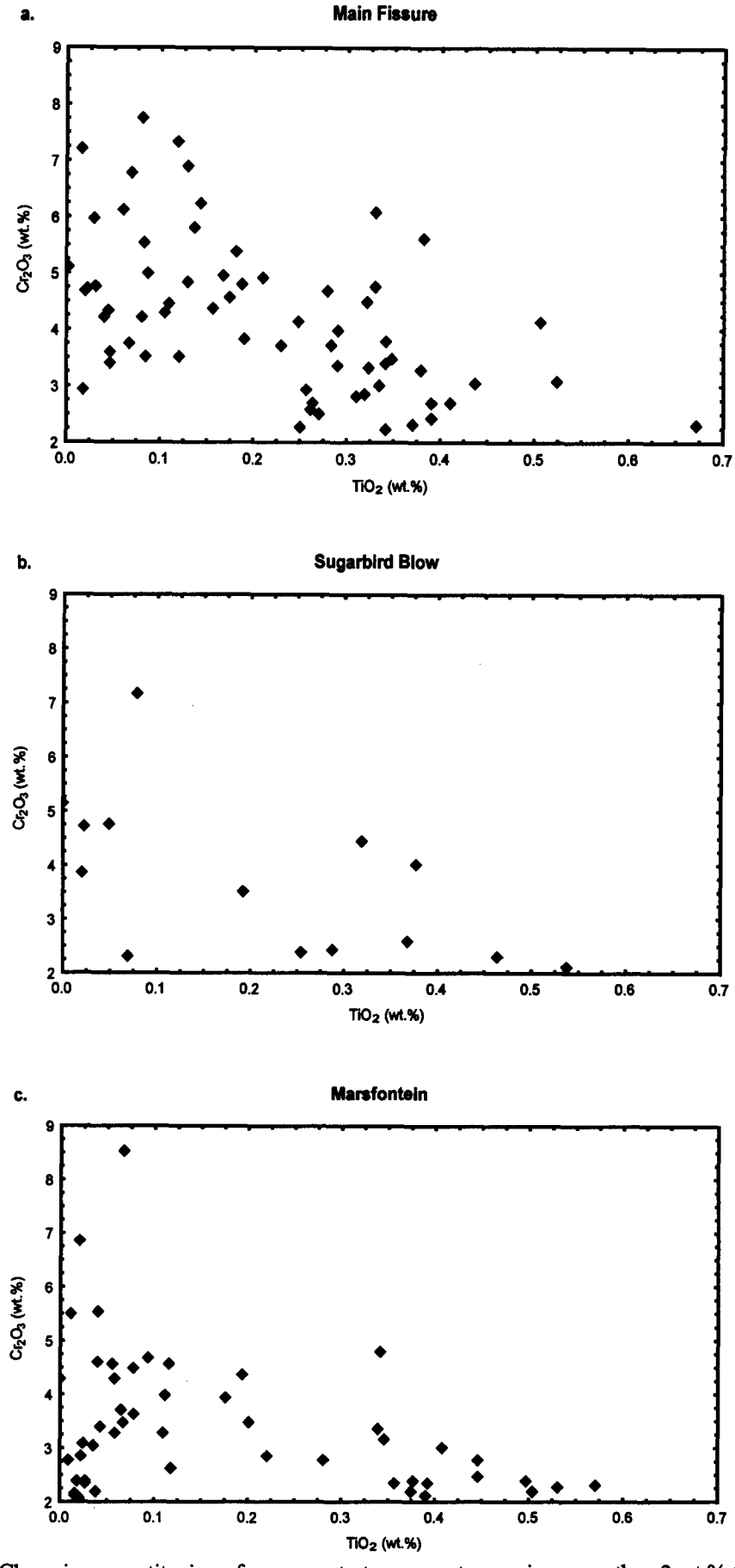

Figure 4.2 Chromium vs. titanium for concentrate garnets carrying more than 2 wt.% Cr_2O_3.

The bulk of the Cr-poor garnets (<2 wt.% Cr_2O_3) range from about 65 to 90 in Mg-number (Figure 4.3). Data from the Kimberlite Research Group data base (University of Cape Town) shows that Cr-poor megacrysts and Group II megacrysts from world-wide localities very seldom display Mg-numbers below 75 while Mg-numbers for eclogitic garnets commonly range down to about 40. This suggests that some of the Klipspringer garnet macrocrysts with Mg-numbers below 75 can be assigned to an eclogitic paragenesis. At higher Mg-numbers it is however difficult to distinguish between eclogitic, megacrystic and even lherzolitic garnets. Most low-Cr garnets range from about 0.2 to 0.5 wt.% TiO_2 (Figure 4.4). In this range of TiO_2, eclogitic garnets from world-wide localities very rarely exceed 0.25 wt.% Cr_2O_3 and megacrystic garnets seldom carry less than 0.25 wt.% Cr_2O_3 (Kimberlite Research Group data base, University of Cape Town). Further, Cr-poor megacrysts generally carry between 0.5 and 1.5 wt.% TiO_2 while most Group II megacrysts display a restricted range of 0.5-0.8 TiO_2 with some compositions extending down to about 0.2 wt.% TiO_2 (Kimberlite Research data base, University of Cape Town). This suggests that many Klipspringer low-Cr garnets with more than 0.25 wt.% Cr_2O_3 and TiO_2=0.2-0.5 wt.% represent Ti-poor varieties of Group II megacrysts that extend up to about 3 wt.% Cr_2O_3 as mentioned in the end of the last paragraph. Considering that Group II megacrysts may carry up to 5 wt.% Cr_2O_3 (see above) it may be that some lherzolite garnets have been wrongly classified and perhaps should be assigned to the megacryst paragenesis.

MacGregor and Carter (1970) first recognised the occurrence of two different types of eclogite (termed Group I and Group II) largely based on textural characteristics. McCandless and Gurney (1989) showed that garnet and clinopyroxene in Group I eclogites are generally enriched in Na_2O and K_2O respectively compared to these minerals in Group II kimberlites. They correlated the mineral composition of Group I eclogites with equilibration pressures similar to what is required for diamond genesis.

Figure 4.5 shows TiO_2-Na_2O relationships for Klipspringer low-Cr garnets. Inserted in the diagrams is a division line at 0.09 wt.% Na_2O separating between Group I and Group II eclogitic garnets (McCandless and Gurney, 1989). Today a value of 0.07 wt.% Na_2O may be more commonly used in diamond exploration to discriminate between "diamond indicator" garnets and garnets which have equilibrated at comparatively lower pressures (Gurney and Zweistra, 1995). A division line between eclogitic and Cr-poor megacrystic garnets and an approximate limit of the extension of Group II megacrysts to lower TiO_2 are also shown in Figure 4.5. The two latter discriminations are based on data from the

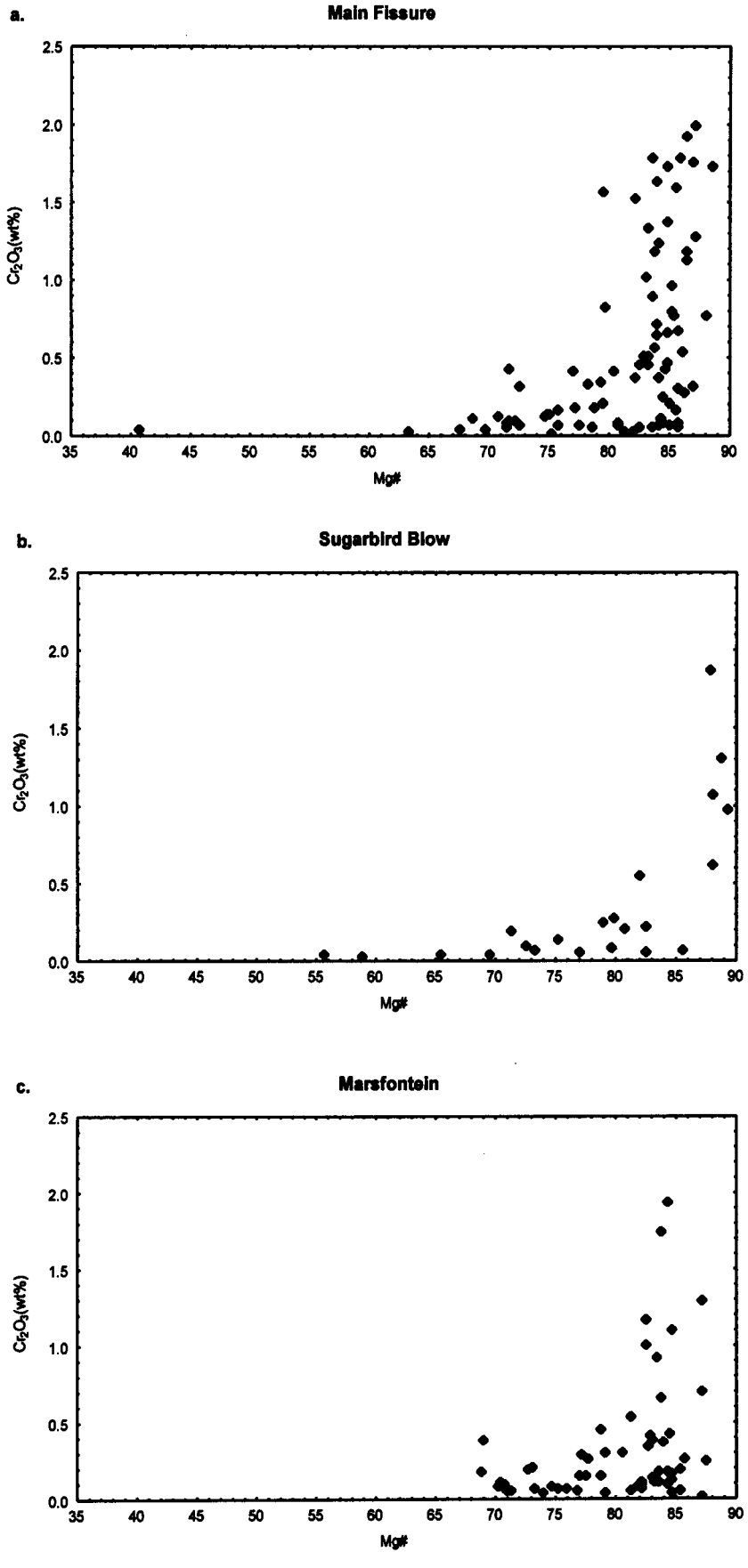

Figure 4.3 Chromium vs. Mg-number for low-Cr (< 2 wt.%. Cr_2O_3) concentrate garnets.

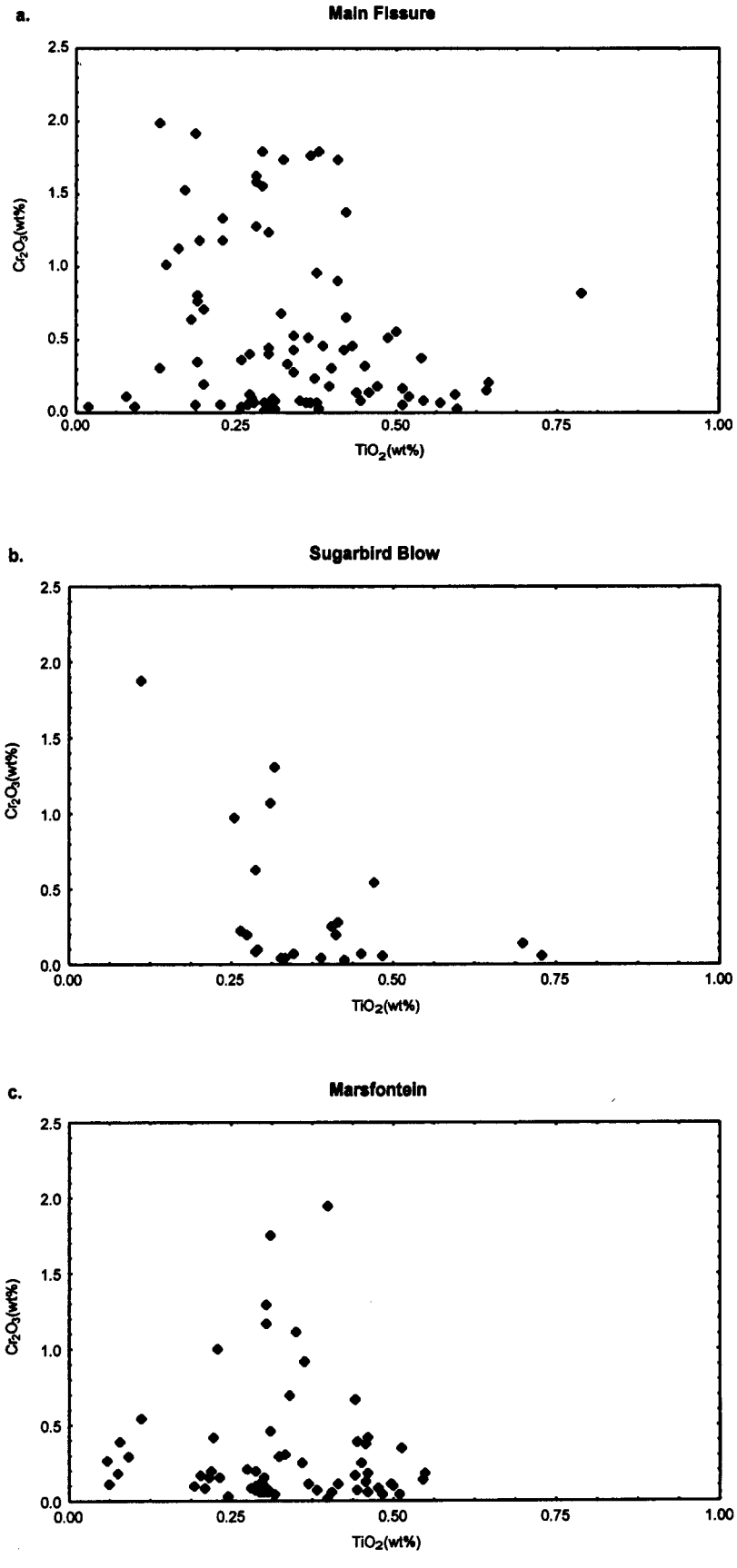

Figure 4.4 Chromium vs. titanium for low-Cr (<2 wt.% Cr_2O_3) concentrate garnets.

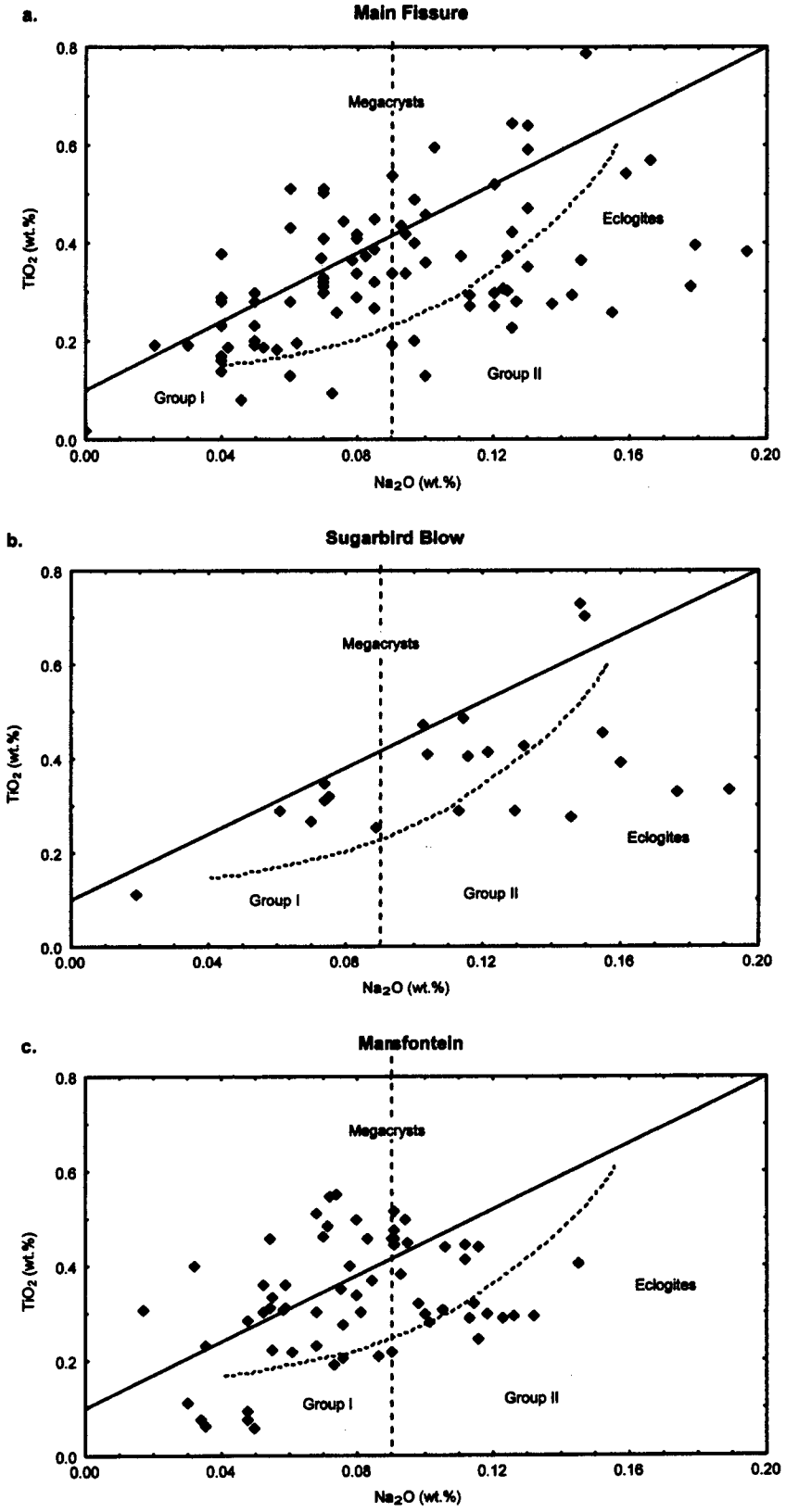

Figure 4.5 Titanium vs. sodium for low-Cr (<2 wt.% Cr_2O_3) concentrate garnets. Dashed line separates Group I and Group II eclogite (McCandless and Gurney, 1989). Solid line separates Cr-poor megacrysts and eclogitic garnets and dotted line shows the extension of Group II megacrysts to lower TiO_2 (Kimberlite Research Group data base, University of Cape Town).

Kimberlite Research Group data base (University of Cape Town). The data suggest that both Group I and Group II eclogitic garnet is present at all three localities and that the former is more common than the latter in the Main Fissure and Sugarbird Blow while they are equally common in the Marsfontein kimberlite. In the compositional area of about 0.05 to 0.12 wt.% Na_2O it is difficult to assign garnets carrying more than 0.2 wt.% TiO_2 to one or other paragenesis. However, most of these garnets are believed to belong to the Ti-poor Group II megacryst paragenesis mentioned above since they display higher Cr_2O_3 than expected for eclogitic garnets at these levels of TiO_2 as mentioned above.

4.3 Chemical compositions of garnet and clinopyroxene from bimineralic nodules

Chemical compositions for garnet and clinopyroxene from bimineralic nodules are found in Appendix 2.4a and 2.4b respectively. Bimineralic nodules have been divided into four groups based on the compositions of the garnets and clinopyroxenes. Two peridotitic varieties are present. Lherzolite I consists of six nodules with garnets which display a lherzolitic trend similar to that displayed by many garnet macrocrysts. A single nodule represents Lherzolite II with a garnet carrying about 9 wt.% Cr_2O_3 which deviates from the Lherzolite I trend with a lower calcium content of about 4.5 wt.% CaO (Figure 4.6a). Mg-numbers for the peridotitic garnets range from 82 to 86 (Figure 4.6b) and they carry about 0.1 wt.% TiO_2 except for one Lherzolite I garnet which deviates from the rest with about 0.35 wt.% TiO_2 (Figure 4.6c).

Nodules with garnets carrying less than 3 wt.% Cr_2O_3 have been divided into an eclogitic and a megacrystic paragenesis similar to the garnet macrocrysts. This grouping may not be completely accurate. However, while eclogitic garnets may occur in the megacryst group, the eclogitic group is not believed to contain any megacrystic garnets. Eclogitic and megacrystic garnets display a similar range of about 3.5-4.5 wt.% CaO while the latter generally is higher in Cr_2O_3 (Figure 4.6a). Most megacrystic garnets have Mg-numbers above 76 and the ones with Mg-number lower than 76 are too high in chromium to be of an eclogitic origin (Figure 4.6b). All garnets displaying Mg-numbers below 74 and Cr_2O_3 below 0.5 wt.% have been assigned to the eclogitic paragenesis since these compositions are extremely unusual for megacrysts.

Two eclogitic garnets (from nodules BM51 and BM59) carry about 2 wt.% Cr_2O_3 and display Mg-numbers of about 84 (Figure 4.6b). These garnets are believed to be Group II eclogitic garnets rather than megacrysts due to their very low TiO_2 contents (Figure 4.6c).

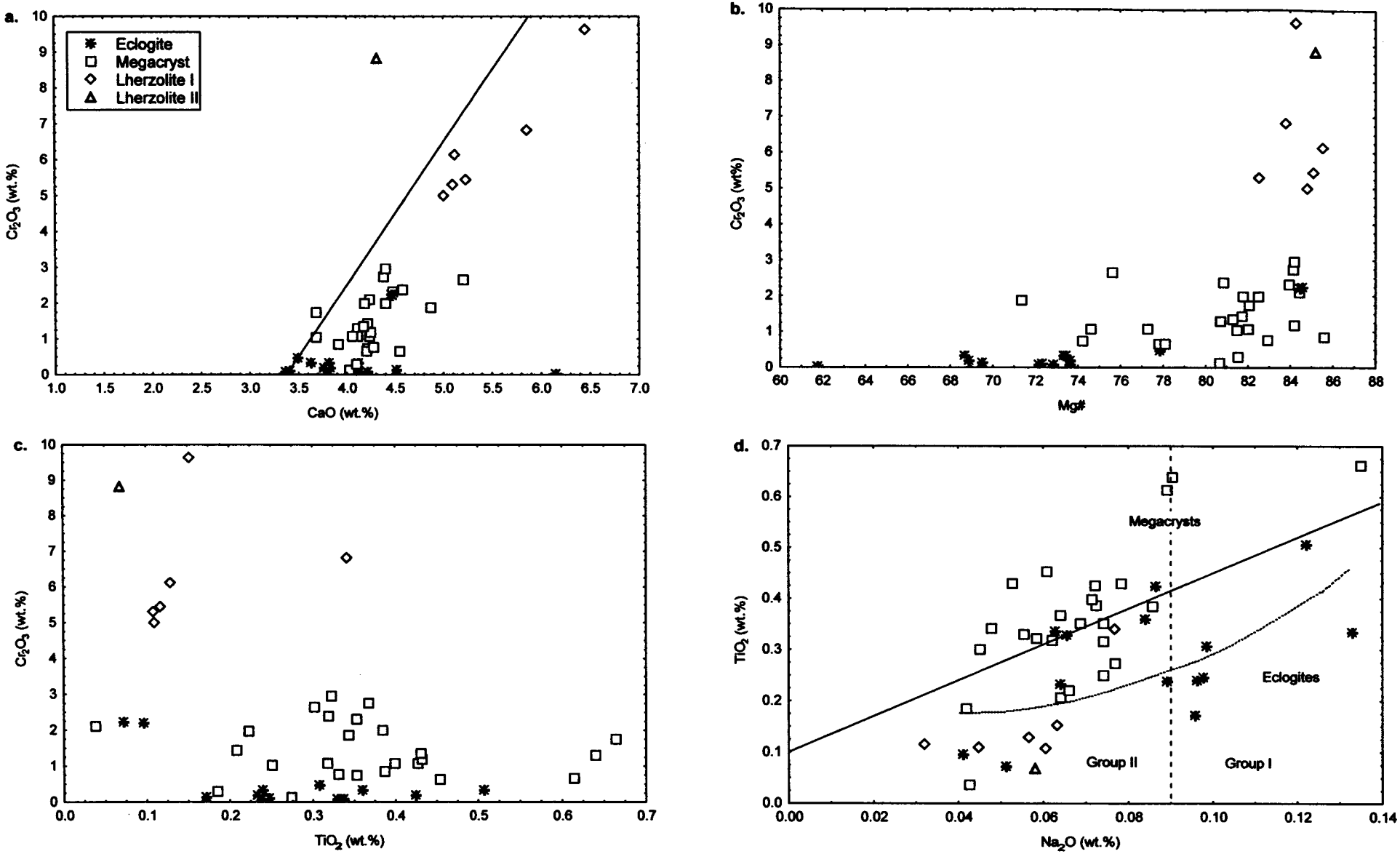

Figure 4.6 Inter-element relationships for garnets from garnet-clinopyroxene nodules. Inserted in Figure 4.6a is a solid line reflecting lherzolitic garnet compositions at 50 kbars pressure (Gurney and Zweistra, 1995). Dashed line in Figure 4.6d discriminates between Group I and Group II eclogites (McCandless and Gurney, 1989) and solid line separates Cr-poor garnet megacrysts from eclogitic garnets with Group II garnet megacrysts ranging down to dotted line in TiO_2 (Kimberlite Research Group data base, University of Cape Town).

The garnet from sample BM11 displays higher CaO, lower Mg#(grt) and lower TiO_2 than all other eclogitic garnets (Figures 4.6a, b and c) and trends towards kyanite eclogite garnets in composition.

TiO_2-Na_2O compositions for garnets with less than 3 wt.% Cr_2O_3 are shown in Figure 4.6d. It can be seen that most garnets assigned to the megacryst paragenesis are similar in composition to Cr-poor megacrysts world-wide while some extend to lower TiO_2 similar to Group II megacrysts from world-wide localities. Further some eclogitic garnets carry more than 0.09 wt.% Na_2O indicative of Group I eclogites while the two Ti-poor eclogitic garnets carry 0.04-0.05 wt.% Na_2O indicative of Group II garnets. The garnet from sample BM11 described above carries more than 0.13 wt.% Na_2O.

The two peridotitic groups are easily recognised in the clinopyroxene compositions. Lherzolite I clinopyroxenes display a Ca-number of about 46 and carry about 3 wt.% Cr_2O_3 while the one Lherzolite II clinopyroxene is distinctively higher in chromium ($Cr_2O_3 \approx 6.5$ wt.%) and displays a lower Ca-number of about 41 (Figure 4.7a). Further, Lherzolite I clinopyroxenes contain about 2.5-3 wt.% Na_2O compared to about 5 wt.% Na_2O for the Lherzolite II clinopyroxene (Figure 4.7b). The peridotitic clinopyroxenes are all low in potassium ($K_2O \approx 0.01$-0.02 wt.%) (Figure 4.7c). FeO contents are similar for all peridotitic clinopyroxene (FeO≈1.5-2 wt.%) while Lherzolite I is slightly lower in magnesium compared to Lherzolite II (Figure 4.7c).

Eclogitic and megacrystic clinopyroxene carry less than 1.5 wt.% Cr_2O_3 and span a range in Ca-number from about 38 to 47 (Figure 4.7a). Similar to the garnets, the megacrystic clinopyroxenes are generally higher in chromium than the eclogitic clinopyroxenes. The eclogitic clinopyroxenes trend towards higher Al and Na contents (Figure 4.7b) indicative of a higher jadeite content. Most low-Cr clinopyroxenes display potassium levels below 0.04 wt.% K_2O while some trend up to above 0.10 wt.% K_2O (Figure 4.7c). McCandless and Gurney (1989) proposed a value of 0.08 wt.% K_2O in omphacite to distinguish between Group I and Group II eclogites, the former being higher in K_2O. While the clinopyroxene from two of the nodules classified as Group I eclogites based on the garnet chemistry carry more than 0.08 wt.% K_2O, the other four display low levels of less than 0.04 wt.% K_2O. Similar to the garnet, the clinopyroxene from nodule BM11 deviates compositionally from the bulk of the eclogitic clinopyroxenes to higher Al_2O_3, Na_2O, K_2O, Ca-number but lower MgO (Figures 4.7a, b, c and d). This supports the idea that nodule BM11 represents a paragenesis akin to kyanite eclogite. The two

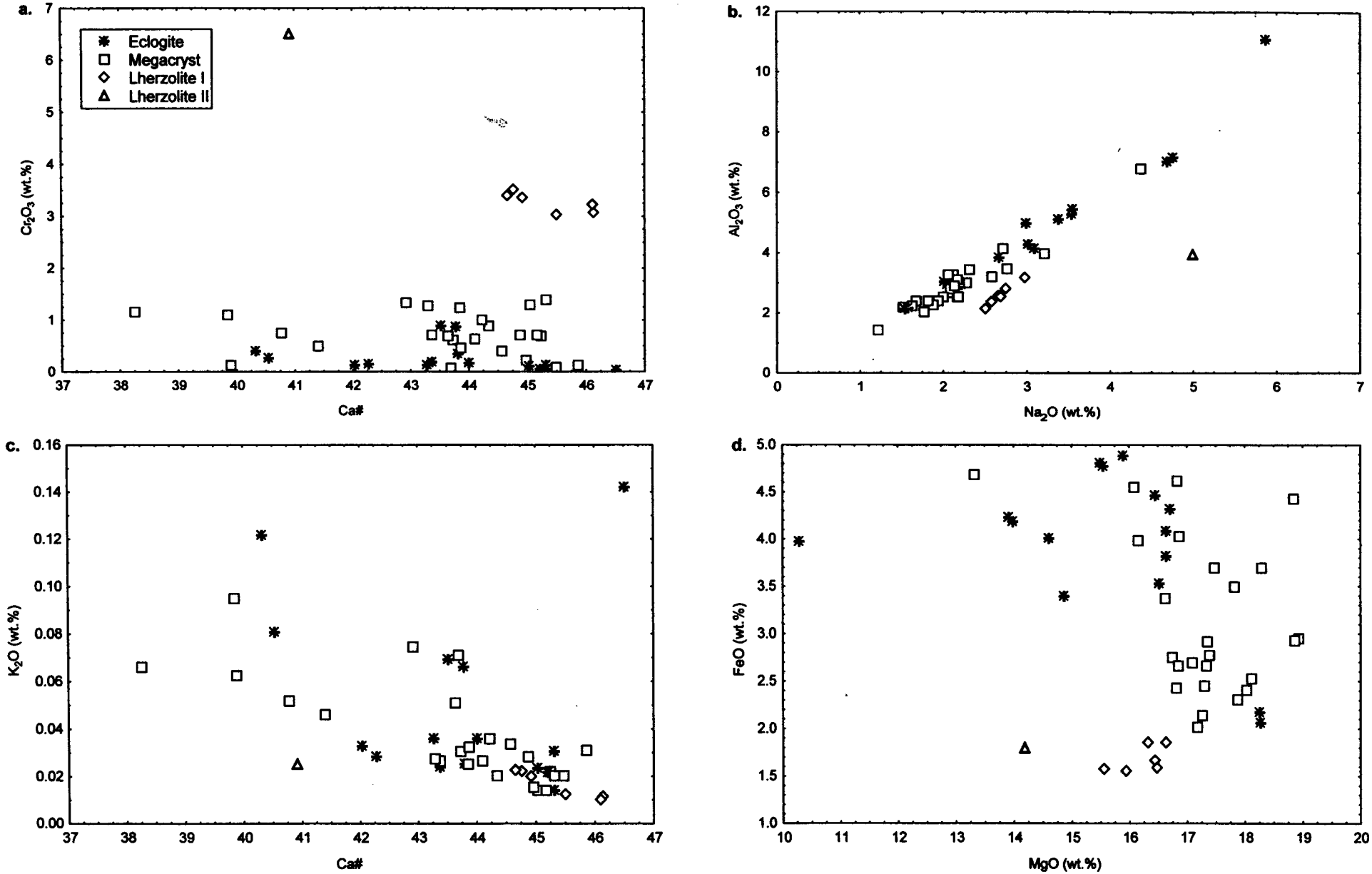

Figure 4.7 Inter-element relationships for clinopyroxenes from garnet-clinopyroxene nodules.

clinopyroxenes from BM51 and BM59 (which were classified as Group II eclogites based on their garnet compositions) are lower in Al_2O_3, Na_2O and FeO but higher in MgO than the rest of the eclogites. Further, they display low levels of about 0.02 wt.% K_2O.

4.4 Geothermometry on bimineralic nodules

While no reactions involving garnet and clinopyroxene result in a sufficient volume change to yield information on pressure of equilibration, several garnet-clinopyroxene geothermometers have been derived experimentally (Raheim and Green, 1974; Mori and Green, 1978; Ellis and Green, 1979; Ganguly, 1979; Saxena, 1979; Krogh, 1988; Pattison and Newton, 1989; Ai, 1994; Berman, 1995). The basis for garnet-clinopyroxene geothermometry is the temperature dependence of the Fe^{2+}-Mg cation exchange between the two minerals. A cation exchange reaction involves little change in volume compared to change in entropy and thus the reaction is more sensitive to temperature than pressure.

Four commonly used geothermometers (Ellis and Green, 1979; Krogh, 1988; Ai, 1994 and Berman, 1995) have been applied to the Klipspringer eclogite and lherzolite nodules. Ganguly (1979) has not been used since it should only be applied when clinopyroxenes display X_{Ca} (molar proportion of Ca present in the octahedrally co-ordinated site in the garnet) between 0.40 and 0.45 and many Klipspringer clinopyroxene display $X_{Ca}<0.40$. The Pattison and Newton (1989) geothermometer has not been used since Berman (1995) is a re-evaluated version of the Pattison and Newton (1989) data. The different calibrations have been investigated and the derived temperatures have been compared in order to assess the results.

4.4.1 Comparison of different geothermometers

The relation between the Fe^{2+} and Mg contents of garnet and clinopyroxene is commonly expressed as K_d, which is the distribution coefficient for Fe^{2+} and Mg partitioning between the two minerals; $K_d=(Fe/Mg)^{grt}/(Fe/Mg)^{cpx}$. Ellis and Green (1979) performed experiments on basaltic compositions and compositions within the system CaO-MgO-FeO-Al_2O_3-SiO_2 in the range 24-30 kbars and 750-1300 °C. They showed that K_d is strongly dependent on the concentration of Ca in both garnet and clinopyroxene due to non-ideal Ca-Mg substitution and they treated the dependence of $\ln K_d$ on X_{Ca} as rectilinear. However, the Ellis and Green (1979) data is indicative of a curvilinear rather than a rectilinear

relationship between $\ln K_d$ and X_{Ca} (Figure 3 in Ellis and Green, 1979). As mentioned by the authors, $\ln K_d$ is not solely dependent on the Ca content of garnet but the X_{Ca} term in their geothermometer represents the net effect of the influence of different solid solutions on $\ln K_d$.

As discussed by Krogh (1988), the substitution of Ca into the octahedrally co-ordinated sites in garnet will lead to an expansion of these sites due to the large size of Ca^{2+} compared to Fe^{2+} and Mg^{2+}. This may possibly distort the structure with the generation of non-equidimensional octahedrally co-ordinated sites as a consequence and the smaller Fe^{2+} and Mg^{2+} ions may begin to occupy sub-sites within the expanded octahedrally co-ordinated sites. Since Mg^{2+} is smaller than Fe^{2+}, it is expected to more readily enter these sub-sites up to an extreme Ca content where Fe and Mg will occupy the sub-sites randomly. This theory would support a curvilinear rather than rectilinear relationship between $\ln K_d$ and X_{Ca}. Krogh (1988) used the experimental data of Raheim and Green (1974), Mori and Green (1978) and Ellis and Green (1979) and derived a geothermometer by treating the relation between $\ln K_d$ and X_{Ca} as such. Applying the derived geothermometer to eclogites from the Tromso nappe complex in the Scandinavian Caledonides, Krogh (1988) concluded that $\ln K_d$ is not dependent on the Mg-number of the garnet [Mg#(grt)] or the Na content of the pyroxene (within the experimental range: Mg#(grt)=0.17-0.55 and Na<0.44 atoms per formula unit).

X_{Ca} ranges from about 0.1 to 0.5 in the data sets used by Ellis and Green (1979) and Krogh (1988). A consequence of treating the relation between $\ln K_d$ and X_{Ca} as curvilinear rather than rectilinear will be slightly lower $\ln K_d$ at the high and low ends of the X_{Ca} range while the reversed is true in the mid-range of X_{Ca}.

Ai (1994) investigated a large set of previously published experimental data (see Ai, 1994 for references) covering a range of 10-60 kbars and 600-1500 °C. Similar to Krogh (1988), Ai (1994) found no relationship between calculated temperatures and Na content of clinopyroxene while contrary to Krogh (1988), Ai (1994) demonstrated a negative relationship between $\ln K_d$ and Mg#(grt). Ai (1994), similar to Krogh (1988), applied a curvilinear relationship between $\ln K_d$ and X_{Ca} and invoked a linear dependence of $\ln K_d$ on Mg#(grt). However, a close investigation of Ai's (1994) presentation of the relationship between $\ln K_d$ and Mg#(grt) (Figure 1 in Ai, 1994) reveals that for Mg#(grt)>75-80, there is a strong negative linear correlation between $\ln K_d$ and Mg#(grt) for experimental data at different temperatures. However, for Mg#(grt)<75-80 the data scatter widely and indicate a less negative (if any) correlation between $\ln K_d$ and Mg#(grt).

The experimentally derived geothermometer of Pattison and Newton (1989) yields distinctly lower temperatures than many other geothermometers (Table 6 in Pattison and Newton, 1989) and the derived thermodynamic data is indicative of strong non-ideality in either or both garnet and clinopyroxene solid solutions. Berman et al. (1995) re-evaluated the data of Pattison and Newton (1989) which was derived at 15 and 29 kbars in a temperature range of 800-1200 °C. X_{Ca} ranged from 0.2 to 0.5 in the garnet product. Berman et al. (1995) evaluated and incorporated new experimental uncertainties in the derivation of thermodynamic parameters and estimated temperatures with the new formulation were 70-200 °C higher than those of Pattison and Newton (1989) and more consistent with other estimations. Similar to Ai (1994), Berman et al. (1995) found that $\ln K_d$ and Mg#(grt) are negatively correlated.

Only very limited experimental data exist for Na-rich compositions to evaluate the effect of the jadeite content of clinopyroxene upon $\ln K_d$. Ellis and Green (1979) found that Na contents up to about 30 mole % jadeite in the clinopyroxene product did not seem to affect the K_d. As mentioned above, Krogh (1988) and Ai (1994) (both of which partly based their geothermometers on the Ellis and Green (1979) data) report that K_d seems not to be influenced by the jadeite content. Koons (1984) suggests that at high jadeite contents (and consequently low Fe^{2+}+Mg contents in the M1 site), Fe^{2+} may show preference for the M2 site in the enstatite-jadeite substitution. However, this effect was not apparent for clinopyroxene with less than 70 mole % jadeite.

4.4.2 Temperature estimations for eclogites and lherzolites

All Klipspringer clinopyroxenes contain less than 70 mole % jadeite and the non-ideality in the Fe^{2+}-Mg substitution in clinopyroxene induced by Na is therefore believed to be negligible in the present study. The possible presence of ferric iron is a source of error since the electron micro-probe cannot distinguish between divalent and trivalent iron. However, the sub-cratonic lithosphere is fairly reduced (Haggerty, 1986) and cationic totals close to four (based on six oxygen per formula unit) rather than higher than four suggest that ferric iron is not present in the clinopyroxene in amounts that would affect the temperature estimations. From now on the terms EG, KR, AI and BER will be used for the Ellis and Green (1979), Krogh (1988), Ai (1994) and Berman (1995) geothermometers.

Temperatures estimated at 40, 50 and 60 kbars are given in Table 4.1 together with K_d, $\ln K_d$, X_{Ca} and Mg#(grt).

Table 4.1 Estimated temperatures (°C) for Klipspringer garnet-clinopyroxene nodules.

					EG			KR			AI			BER		
Eclogites	K_d	$\ln K_d$	X_{Ca}	$Mg\#_{grt}$	*40 kbar*	*50 kbar*	*60 kbar*	*40 kbar*	*50 kbar*	*60 kbar*	*40 kbar*	*50 kbar*	*60 kbar*	*40 kbar*	*50 kbar*	*60 kbar*
BM8	2.51	0.92	0.11	73	1069	1108	1146	986	1030	1073	1017	1105	1194	1057	1069	1077
BM10	2.37	0.86	0.09	78	1079	1118	1157	980	1024	1068	1012	1103	1194	1042	1055	1064
BM11[a]	2.85	1.05	0.16	62	1070	1107	1144	1037	1078	1119	1059	1142	1225	875	895	910
BM14	2.85	1.05	0.12	69	1024	1061	1098	947	988	1029	969	1052	1136	949	966	978
BM15	2.62	0.96	0.09	69	1038	1076	1114	940	982	1025	988	1075	1161	1007	1022	1033
BM16	2.63	0.97	0.10	69	1047	1079	1117	948	990	1033	992	1078	1165	1006	1021	1031
BM17	2.71	1.00	0.11	73	1038	1076	1113	955	997	1038	947	1062	1147	1021	1034	1043
BM20	2.79	1.03	0.11	74	1022	1059	1096	933	975	1016	952	1036	1121	1004	1018	1028
BM31	2.25	0.81	0.08	72	1104	1144	1184	1006	1051	1097	1065	1159	1252	1020	1035	1045
BM32	2.29	0.83	0.09	72	1092	1132	1172	992	1036	1081	1049	1142	1234	1012	1027	1037
BM51[b]	2.90	1.06	0.11	84	1013	1049	1086	932	972	1013	908	991	1073	990	1004	1013
BM59[b]	2.73	1.00	0.11	85	1040	1077	1115	962	1004	1046	943	1028	1113	1022	1035	1043
BM62	2.35	0.85	0.10	74	1091	1130	1170	1002	1046	1091	1044	1135	1227	1073	1084	1091
Lherzolites																
BM1	3.29	1.19	0.13	85	976	1011	1047	904	942	981	864	942	1020	907	924	936
BM2	2.99	1.10	0.17	84	1057	1093	1139	1026	1066	1106	972	1054	1135	973	987	996
BM3	3.71	1.31	0.13	83	931	965	999	856	893	930	816	890	964	851	869	883
BM4	3.03	1.11	0.15	84	1033	1069	1105	987	1026	1066	942	1023	1103	959	974	984
BM60	2.97	1.09	0.13	86	1023	1059	1096	961	1001	1042	921	1003	1084	959	973	984
BM61	3.23	1.17	0.14	85	991	1026	1061	926	965	1004	882	961	1039	921	937	948
BM52[c]	2.44	0.89	0.11	85	1092	1131	1170	1023	1066	1110	1010	1099	1189	997	1011	1021

[a]Nodule akin to kyanite eclogite

[b]Nodules classified as Group II eclogites

[c]Lherzolite II nodule

EG - Ellis and Green (1979)
KR - Krogh (1980)
AI - Ai (1994)
BER - Berman et al. (1995)

A pressure of 50 kbars corresponds to an approximate depth of the entrance into the diamond stability field (Kennedy and Kennedy, 1976) for an assumed geotherm of ~ 40 mW/m^2. In the following sections, temperatures estimated with the different geothermometers at a pressure of 50 kbars are compared in order to assess the different calibrations and thus derive reliable temperatures.

4.4.2.1 Eclogite temperatures

Using EG and KR, the eclogites display temperature ranges of 1049-1144 °C and 972-1078 °C respectively (Table 4.1). In Figure 4.8, temperatures derived for the eclogites using the different geothermometers are compared to each other. Comparing EG and KR, the former yields up to about 100 °C higher temperatures than the latter. The eclogitic garnets range in X_{Ca} from 0.08 to 0.16. As mentioned above, at these low values of X_{Ca} a high discrepancy in temperature between EG and KR is expected due to the first order and quadratic equations respectively describing the relation between $\ln K_d$ and X_{Ca}. The linear decrease in the EG-KR temperature difference with increasing X_{Ca} is an effect of a less rapid increase of $\ln K_d$ with increasing X_{Ca} for EG compared to KR due to the different mathematical treatments of the relationship between $\ln K_d$ and X_{Ca}. Since the relationship between $\ln K_d$ and X_{Ca} is better expressed with a quadratic equation than a first order equation (as discussed above), KR is believed to yield more realistic temperatures than EG for the eclogites especially at lower X_{Ca} where EG distinctly overestimates the true temperature.

The bulk of the eclogitic temperatures estimated using AI range between 1036 °C and 1159 °C. The two nodules that were classified as Group II eclogites based on their major element compositions (BM51 and BM59) deviate from the bulk of the samples towards lower temperatures (991 °C and 1028 °C respectively), approaching KR temperatures (Figure 4.8). BM51 and BM 59 display Mg#(grt) of 84 and 85 respectively which are distinctly higher than the range displayed by the rest of the garnets (Mg#(grt)=62-78). As mentioned in the previous section, a correlation between $\ln K_d$ and Mg-number based on the experimental data used by Ai (1994) seems spurious for samples with garnet Mg#(grt)<75-80 while for Mg#(grt)>75-80, a correlation between $\ln K_d$ and Mg-number is apparent. Thus, the AI temperature range displayed by the bulk of the eclogites is believed to be artificial while the estimations for BM51 and BM52 may approach a true temperature.

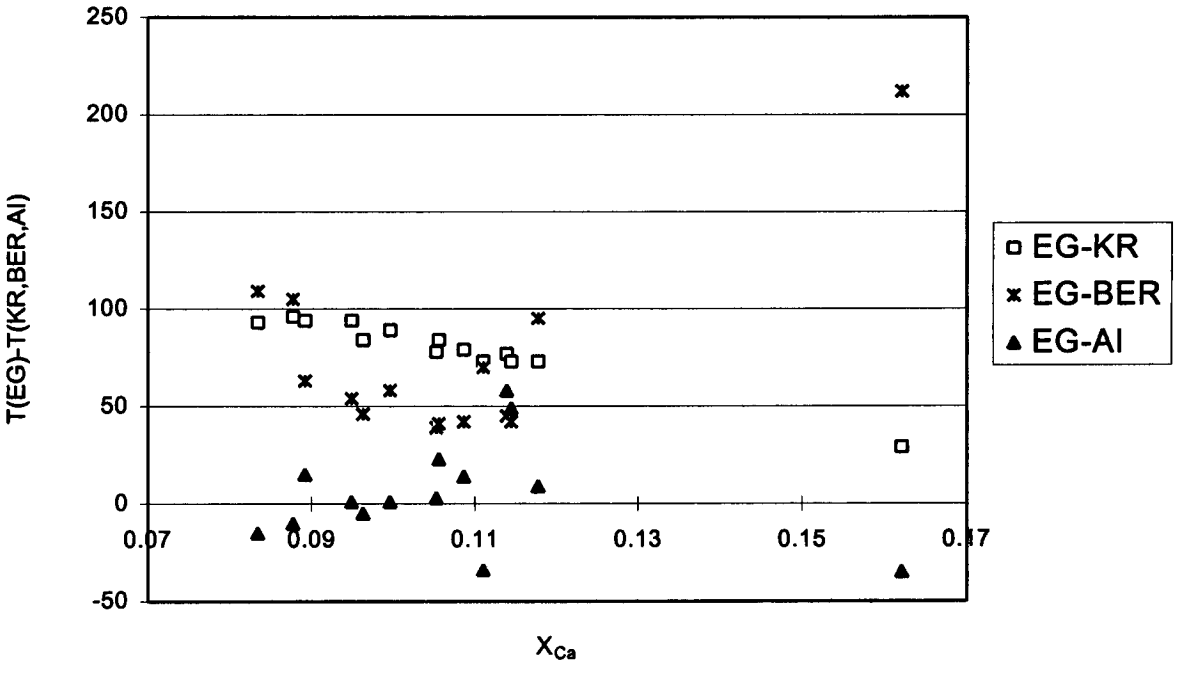

Figure 4.8 Comparison of eclogite temperatures estimated with different geothermometers at an assumed pressure of 50 kbars. See text for references corresponding to the used short forms for the geothermometers.

Eclogite temperatures estimated with BER range from 966 °C to 1084 °C if BM11 (which is compositionally similar to kyanite eclogite) is excluded. These temperatures are some 50 °C higher than those of EG and approach (and in some cases coincide with) those of KR. BM11 yields a temperature of 895 °C using BER. This sample was classified as a Group I eclogite and thus it is believed to originate from depths within the diamond stability field. and the estimated temperature seems anomalously low. BM11 has a distinctly higher X_{Ca} than the other eclogites and it may be that the Berman et al. (1995) calibration does not account properly for the non-ideal substitution of Ca in garnet (and clinopyroxene) at higher X_{Ca}.

From the analysis of the different calibrations and the data, it is believed that KR and BER yield most realistic temperatures for the eclogites (except for sample BM11), which then display a range of ~ 960-1090 °C at 50 kbars. In the literature, KR and BER are not commonly used in estimating equilibration temperatures for eclogite. A compilation of temperatures for Kaapvaal eclogites estimated using EG at an assumed pressure of 50 kbars (Gurney and Harte, 1980) displays a range of ~ 950-1450 °C. Even though EG is believed not to be as adequate as KR and BER, the range in EG temperatures displayed by the Klipspringer eclogites (1049-1144 °C) is indicative of fairly low equilibration temperatures compared to many other Kaapvaal eclogites.

Temperatures estimated with KR at assumed pressures of 40, 50 and 60 kbars are displayed in Figure 4.9 together with lithospheric model geotherms of 35, 37 and 40 mW/m^2 and the graphite/diamond phase transition (Kennedy and Kennedy, 1976). At 40 kbars, the temperatures range across the 40 mW/m^2 geotherm outside the diamond stability field. At 50 kbars, the temperatures range across the 37 mW/m^2 geotherm and at 60 kbars they correspond to model geotherms of about 35-37 mW/m^2. Further, at any assumed pressure sample BM11, which is akin to kyanite eclogite, yields the highest temperature while the Type II eclogites (BM51 and BM52) plot at the lower end of the temperature array. The significance of this and the observed temperature ranges is discussed in Section 4.5.

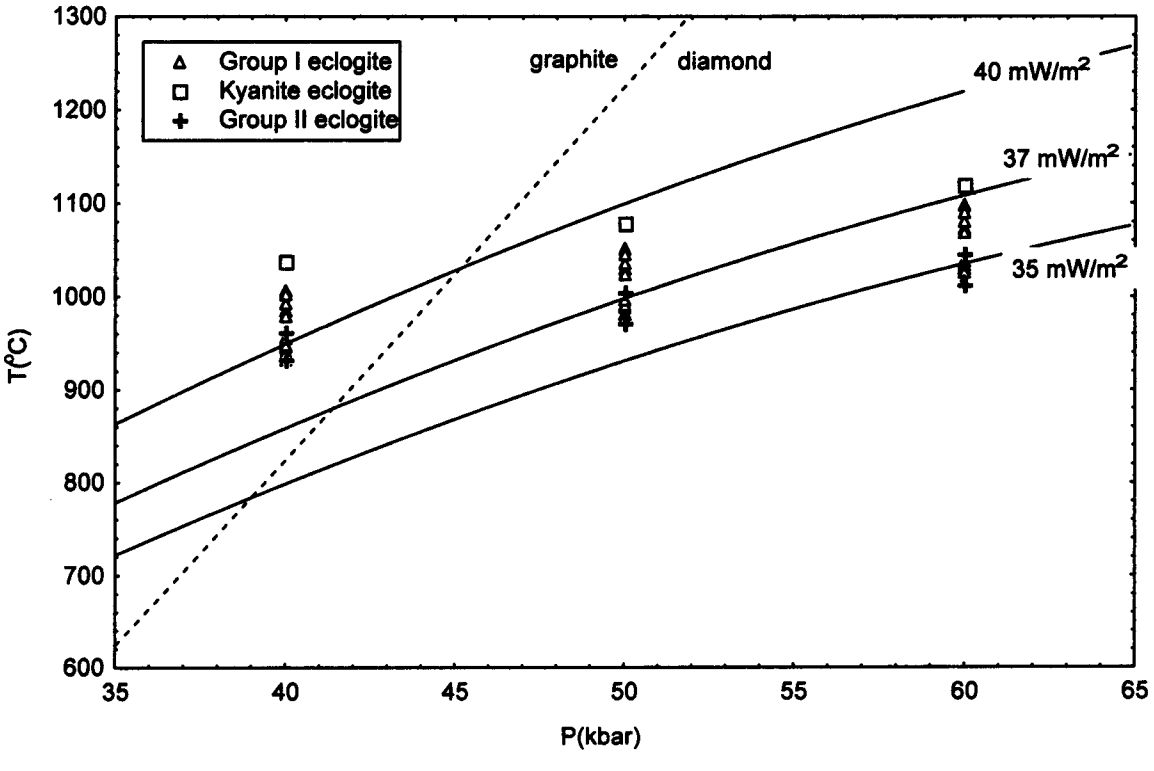

Figure 4.9 Eclogite temperatures estimated at pressures 40, 50 and 60 kbars using the Krogh (1988) geothermometer. Conductive model geotherms are from Pollack and Chapman (1977) and the diamond/graphite boundary is from Kennedy and Kennedy (1976).

4.4.2.2 Lherzolite temperatures

Temperatures estimated for the lherzolites using EG range from 965 °C to 1093 °C compared to a range of 893-1066 °C for KR temperatures. Lherzolite I garnets generally display slightly higher X_{Ca} (0.13-0.17) than the eclogitic garnets. Consequently temperatures estimated using EG and KR for the lherzolites are fairly similar to each other but the former are still some 20-70 °C higher than the latter. This is displayed in Figure 4.10 where KR, BER and AI temperatures are compared to EG temperatures.

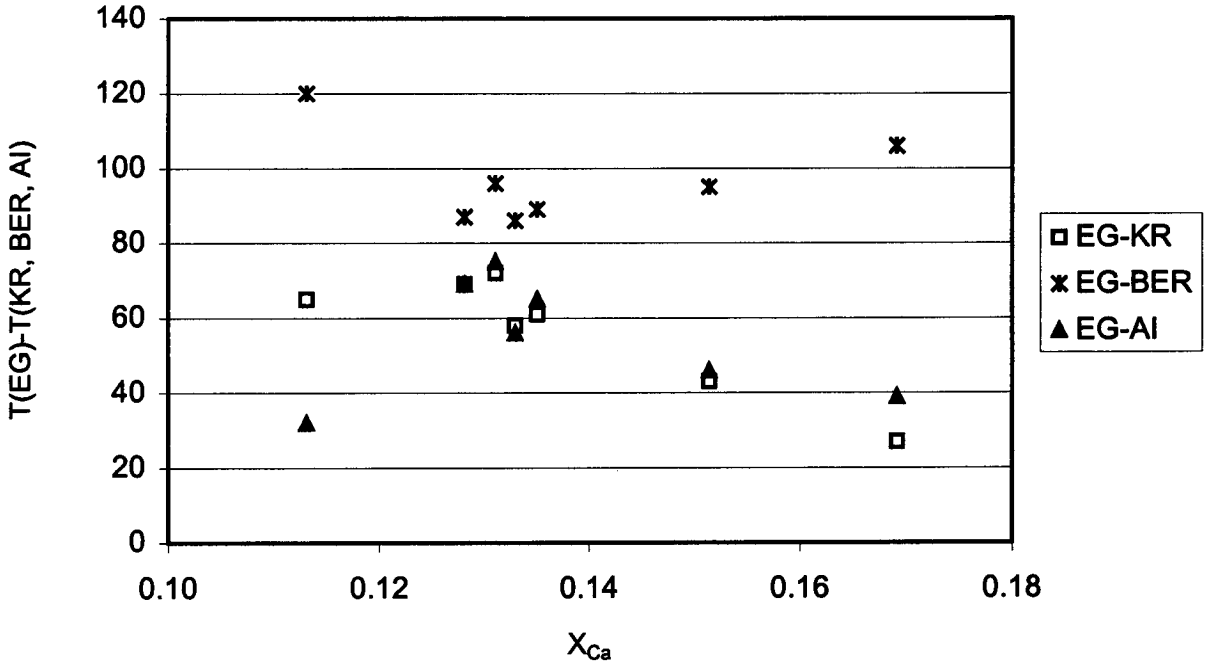

Figure 4.10 Comparison of lherzolite temperatures estimated with different geothermometers at an assumed pressure of 50 kbars. The lherzolite II nodule displays the lowest X_{Ca}. See text for references corresponding to the used short forms for the geothermometers.

Contrary to the case of the eclogites, lherzolite I temperatures using AI (890-1054 °C) are very similar to those using KR and the derived temperatures do not differ by more than 12 °C for any individual sample (Table 4.1). This is due to the higher Mg#(grt) of the lherzolites (Mg#(grt)=83-86) in which range $\ln K_d$ in the experimental data used by Ai (1994) is well correlated with the Mg-number of the garnets.

Lherzolite I temperatures estimated with BER display a range of 924-987 °C and are slightly lower compared to estimations with KR and AI. The temperature difference

increases with increasing X_{Ca}. The reason for this is not understood but as mentioned above, the Berman et al. (1995) geothermometer may be inaccurate at higher X_{Ca} because the calibration is not accounting properly for the non-ideal substitution of Ca.

The lherzolite II sample (BM52) displays a wider range in calculated temperatures than individual lherzolite I samples (Figure 4.10) which is due to the comparatively elevated EG temperature for BM52. X_{Ca} for BM52 is 0.11 and for reasons mentioned above, the EG temperatures are spurious at this low X_{Ca}. The range of temperatures from 1011 °C to 1099 °C for BM52 obtained using the other thermometers is difficult to assess but may be indicative of a slightly higher temperature of equilibration for BM52 compared to lherzolite I nodules.

From the analysis of the different calibrations and the data, it is believed that KR and AI yield most realistic temperatures for lherzolite I nodules which then display a range of ~ 890-1070 °C at 50 kbars with the lherzolite II nodule yielding a temperature at the higher end of this range.

Temperatures estimated for the lherzolites at 40, 50 and 60 kbars using KR are displayed in Figure 4.11 together with model geotherms of 35, 37 and 40 mW/m^2 and the diamond/graphite phase boundary (Kennedy and Kennedy, 1976). The lherzolites span a wider range in temperature at any assumed pressure compared to the eclogites (Figure 4.10).

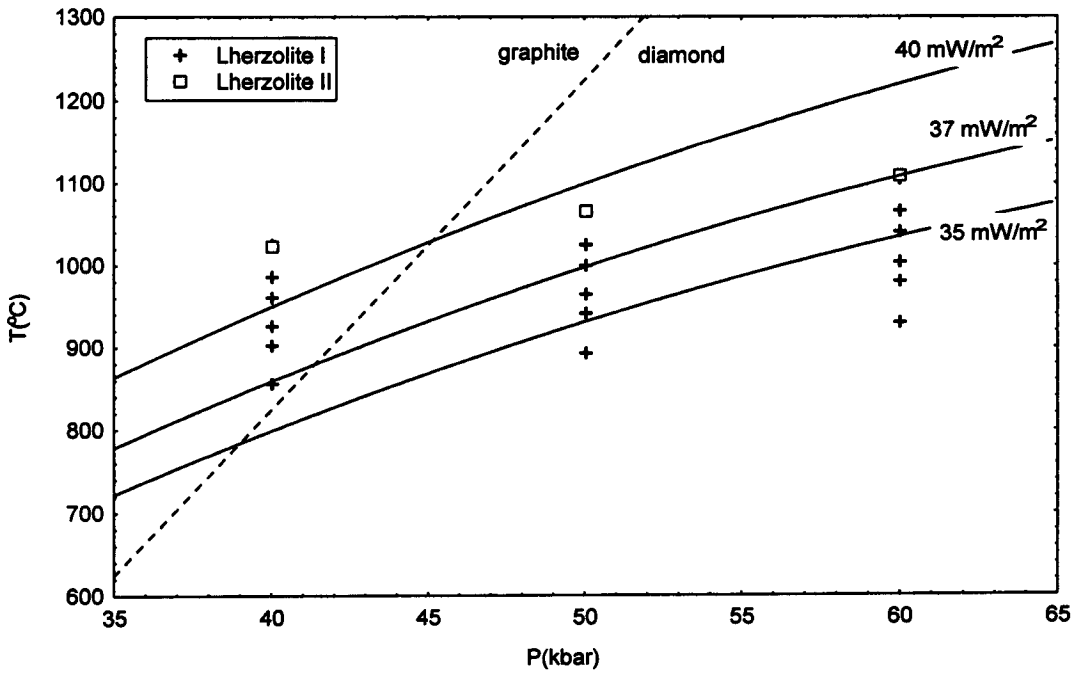

Figure 4.11 Lherzolite temperatures estimated at pressures 40, 50 and 60 kbars using the Krogh (1988) geothermometer. Conductive model geotherms are from Pollack and Chapman (1977) and the diamond/graphite boundary is from Kennedy and Kennedy (1976).

4.5 Discussion and Conclusions

The major element chemistry of garnet macrocrysts shows that the Klipspringer lithosphere consists predominantly of lherzolite and eclogite. Magmaphile element depleted harzburgite is present to a lesser extent. The mantle sampled by the Marsfontein intrusion is different to the mantle sampled by the Main and Sugarbird Fissures in that highly refractory dunite is represented to a limited extent.

The chemical compositions of eclogitic garnet macrocrysts and bimineralic nodule garnets indicate the presence of both Group I and Group II eclogite of which the former is more common as indicated by the commonly elevated Na contents of the garnets. Elevated Na contents of garnet are not always matched by elevated K contents of clinopyroxene as often is the case for eclogite xenoliths (McCandless and Gurney, 1989). However, McCandless and Gurney (1989) found that only 65 % of analysed diamondiferous eclogite could be correctly classified as Group I eclogites based on the K_2O content of clinopyroxene. Removal of K from clinopyroxene through metasomatism or decompression melting has been noted (Switzer and Melson, 1969; Mysen and Griffin, 1973; Reid et al., 1976).

Garnet megacrysts are common and are compositionally akin to megacrysts from Group II kimberlites which is consistent with the classification of the Main and Sugarbird Fissures as Group II kimberlites (Chapter 3). However, the megacrysts trend towards unusually low Ti contents similar to those reported by Daniels and Gurney (1989) for megacrysts from the Group II Dokolwayo kimberlite. Daniels and Gurney (1989) inferred that the garnet megacrysts were derived from a garnet-ilmenite megacryst suite to explain their low levels of TiO_2 compared to garnets from a second ilmenite-free megacryst suite from Dokolwayo. In the Cr-poor megacryst suite (from Group I kimberlites), the on-set of ilmenite crystallisation has been shown to occur at a garnet Mg-number of about 75 and continued fractionation results in depletion in Ti and Cr as well as a decreasing Mg-number of the garnets (e.g. Gurney et al., 1979a). This suggests that Dokolwayo Ti-poor megacrysts crystallised at a late stage of magmatic fractionation. In contrast to Dokolwayo megacrysts, Klipspringer low-Ti garnet megacrysts are characterised by high Mg-numbers (up to 90 compared to 66-73 for Dokolwayo garnet megacrysts) and high levels of Cr_2O_3 (perhaps above 2 wt.% compared to <0.3 wt.% for Dokolwayo garnet megacrysts). The Cr_2O_3 contents of garnets even from deformed or sheared lherzolites which generally extend to lower values than those of coarse lherzolites are seldom below 2 wt.% (e.g. Boyd and

Nixon, 1975; Danchin, 1979). Therefore, the bulk of the garnets with Cr_2O_3=0.25-2 wt.% and TiO_2=0.2-0.5 wt.% are believed to be megacrysts. The high Cr_2O_3, high Mg-numbers and low TiO_2 of Klipspringer garnet megacrysts may indicate that they did not co-crystallise with ilmenite but formed at an early stage before any substantial enrichment of Ti occurred in the megacryst parental magma.

While equilibration pressures for the nodules are not known, the compositions of the eclogites carry some information on this. As mentioned above, Group I eclogites are believed to be akin to diamondiferous eclogite and have been proposed to originate from depths corresponding to pressures where diamond is stable (McCandless and Gurney, 1989) i.e. from pressures in excess of ~ 40-50 kbars depending on the local geotherm. A first indication on the thermal state of the lithosphere in the study area is given by the temperatures estimated for the Group I eclogites. These temperatures correspond to a geotherm of ~ 35-38 mW/m^2 at assumed of 50 and 60 kbars and the data plot within the diamond stability field. For an assumed pressure of 40 kbars, the temperatures coincide with a ~ 40 mW/m^2 geotherm and the data plot outside the diamond stability field. This suggests that the local geotherm is lower than ~ 40 mW/m^2.

It has been shown that the incorporation of K into clinopyroxene is pressure dependent and requires a minimum pressure of 32 kbars (Erlank and Kushiro, 1970). While the K content of clinopyroxene is dependent on the K content of the environment of formation (Harlow, 1999), the elevated and lower K_2O contents of the kyanite eclogite (BM11) and the Group II eclogites (BM51 and BM59) respectively compared to the Group I eclogites may indicate comparatively higher and lower pressures of equilibration. This would be consistent with the kyanite eclogite yielding the highest temperatures and the Group II eclogites plotting at the lower end of the temperature range at any assumed pressure. Some information on the local geotherm may be derived from the inference that the kyanite eclogite and the Group II eclogites define high and low extremes of pressures of equilibration respectively. Assuming a geotherm of ~ 39-40 mW/m^2, the kyanite eclogite would have equilibrated at ~ 50 kbars and the Group II eclogites yield pressures of ~ 40 kbars. The Group I eclogites would have equilibrated at intermediate pressures and they plot either close to or below the limit of the diamond stability field. This contradicts a proposed origin of Group I eclogites from within the diamond stability field and may suggest a highest probable geotherm of ~ 39 mW/m^2. At an assumed geotherm of ~ 37 mW/m^2, the Group I eclogites plot well within the diamond stability field as do the Group II eclogites.

This contradicts a proposed origin for Group II eclogites from outside the diamond stability field. Thus, the current data is suggestive of geotherm of about ~ 37-39 mW/m^2 for the study area.

The depth of origin for the lherzolites cannot be constrained. However, assuming that all lherzolites equilibrated along a steady-state geotherm, the comparatively wide range in temperature displayed by the lherzolites is suggestive of a substantial difference in equilibration pressure between the individual lherzolite nodules (Figure 4.11). With a lithosphere geotherm of 37-39 mW/m^2, as inferred from the eclogites, the lherzolites may span equilibration pressures of ~35-60 kbars. They are certainly derived from both within the diamond and the graphite stability fields. The comparatively high temperature displayed by the lherzolite II nodule and its comparatively lower Ca content indicate that it was derived from a deeper environment more depleted in magmaphile elements, within the diamond stability field.

5. PHYSICAL CHARACTERISTICS OF THE DIAMONDS

5.1 Introduction

Diamonds exhibit several physical characteristics, which can be attributed to different processes occurring, and conditions prevailing at diamond crystallisation, subsequently during residence in the mantle and during transport of the diamond in the kimberlite (Robinson et al., 1989). Studies of these characteristics have revealed broad inter-cratonic differences such as the high abundance of colourless octahedra amongst Russian diamonds and the comparatively common occurrence of large diamonds in Southern Africa (Gurney, 1989). On an intra-cratonic scale, sub-populations have been recognised on a regional scale as well as in adjacent kimberlites (Robinson et al., 1989).

Robinson et al. (1989) proposed a sequence of events which affect diamonds. This includes crystallisation, residence in the upper mantle, plastic deformation, resorption and etching, crystal breakage and further etching. While the primary crystal form and to some extent colour are dependent on the nature of the crystallisation environment, the authors suggest that the latter four processes take place during transport of the diamond in the kimberlite. Thus, studies of "primary" and "secondary" physical characteristics may give information on the mantle environment in which the diamonds were formed and their subsequent history in the kimberlite respectively.

5.2 The nature of the sample

Physical properties of the Klipspringer diamonds have not been studied in an attempt to characterise the diamond population(s) at a statistically significant level. Instead, physical properties have been described for all diamonds on which mineral inclusion and/or FTIR studies were performed with the aim of discovering possible correlations between different characteristics. However, even though the samples are not sufficiently large for satisfying statistical analysis of the physical properties, some distinctive features may be recognized.

The cut-off size in the diamond recovery at the Klipspringer mine is 1.7 mm. Main Fissure diamonds labelled "1700-" were recovered from the tailings and thus are less than 1.7 mm in size while the rest of the diamonds range between 1.7 and ~3 mm in size. Main Fissure and Sugarbird Blow diamonds were collected primarily for mineral inclusion

studies and thus they were selected randomly in respect of physical characteristics. If the presence of certain inclusions is correlated with any physical characteristic, then the sample selected for the study can have a bias. Most Marsfontein diamonds were collected primarily for FTIR studies and flat or fractured stones suitable for the technique were primarily selected. Further, diamonds of different colours were consciously selected. Thus, the Marsfontein sample is certainly not quantitatively representative of Marsfontein sub-populations.

5.3 Physical characteristics

Physical characteristics of the diamonds are presented in Appendix 3.1. The terminology used in describing the diamonds and abbreviations used in Appendix 3.1 are presented in Appendix 3. During selection of diamonds for this study, thousands of Klipspringer diamonds have been briefly observed. In the results below, some general observations made during the sample collection are included although these observations are not included in Appendix 3.1.

5.3.1 Colour

Colourless diamonds constitute 77 % of the diamonds in the Sugarbird Blow sample while brown-pink diamonds constitute 5 % of the diamonds. Data for the Main Fissure sample excluding the <1.7 mm fraction is similar to that of the Sugarbird Blow sample with 73 % colourless stones and 10 % brown-pink stones. This indicates that in the size range 1.7-3 mm colourless diamonds predominate and are equally common in the Main Fissure and Sugarbird Blow samples while brown-pink diamonds are much less common. The <1.7 mm fraction of the Main Fissure diamonds (diamonds labelled 1700-) contained 38 % colourless stones and 29 % brown-pink stones. This indicates that in the case of the Main Fissure diamonds, the number of brown-pink stones increase partly at the expense of colourless stones with decreasing diamond size.

As mentioned above, the data for Marsfontein diamonds are biased due to selective sampling. However, from observations of Marsfontein diamonds during collection of the sample, it can be concluded that colourless stones predominate similar to the case of the Main Fissure and Sugarbird Blow. These results correlate well with the over-all impression from observations made during sample collection.

Homogeneous light green diamonds and diamonds with discrete distinctive green haloes on the surface (observed during sample collection) occur subordinately. Green discolouration is caused by α-particle damage of the diamond lattice and at temperatures above 600 °C, the colour caused by radiation changes from green to brown (Vance et al., 1973). This suggests that green colouration post-dates kimberlite eruption and the homogeneous light-green colour observed is most likely to have been caused by U-bearing ground water. Perovskite, which often carries substantial U, is common in the kimberlites and is likely responsible for the discrete green haloes observed on some diamonds.

Other colours that have been observed include light-yellow, brown-yellow and off-white. Loubser and Wright (1973) ascribed yellow colour of diamonds to N3 defects (see Section 6.1). The three brown-yellow stones all display lamination lines and their colour may be a result of deformation of yellow diamonds.

5.3.2 Crystal form

The octahedron and the cube are the two primary crystal forms of diamond. The former is far more common than the latter at most localities world-wide. Resorption of octahedra and cubes by oxidising agents at elevated temperatures commences at the 4-fold axes of octahedra and at the corners of cubes and finally results in a tetrahexahedroidal (TTH) crystal form (Robinson, 1979). The progressive conversion of an octahedron to a THH is shown in Figure 5.1 and the complete conversion to THH removes a minimum of 45 % of the original octahedron.

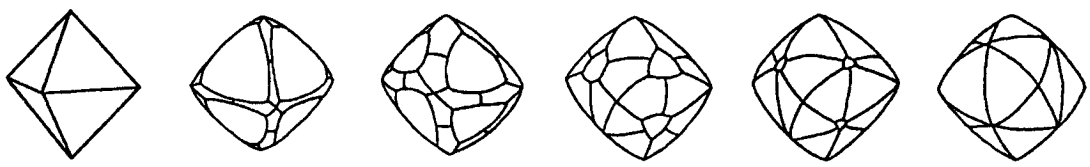

Figure 5.1 Different stages of resorption of a sharp-edged octahedron to the complete conversion into a tetrahexahedroid (from Robinson, 1979). Percent notations indicate the part of the original volume of the octahedron that is still preserved.

Almost all Main Fissure and Sugarbird Blow diamonds display THH morphology. Thus, they have been heavily resorbed and their primary crystal form cannot be directly recognised. Subordinately primary crystal faces are preserved and they are all indicative of octahedral growth. During sample collection it was observed that Marsfontein diamonds are distinctly less resorbed than Main Fissure and Sugarbird Blow diamonds and they often display remnants of octahedral crystal faces. Macles occur only to a very limited degree in all kimberlites. One diamond (SB-6) displayed pseudohemimorphism (half octahedron-half THH), which may indicate that the diamond was partially protected from resorption perhaps whilst protruding from the surface of a host xenolith.

Crystal regularity indicates if the form of a diamond is regular (equidimensional), elongated and/or flattened or irregularly distorted. Main Fissure and Sugarbird Blow diamonds are regular only to a minor extent while most diamonds are distorted in some way. This may either be due to a distorted primary crystal form or perhaps due to preferential resorption in certain directions. This feature cannot be correlated with any other physical characteristics.

5.3.3 Crystal state and fracture surfaces

Following Chinn (1995), crystal state has been divided into four categories namely whole (no volume loss), chipped (<10 % volume loss), broken (10-50 % volume loss) and fragment (>50 % volume loss).

The bulk of Klipspringer diamonds are whole while many stones (almost 50 % in the case of Main Fissure diamonds) are chipped, broken or fragments. The sample probably over-estimates rather than under-estimates the amount of whole stones since inclusion-bearing diamonds are prone to break across the site of an inclusion during decompression (see below) and diamonds with mineral inclusions (consequently not broken) were preferentially selected.

Some fracture surfaces are associated with cubo-octahedral pits believed to have hosted mineral inclusions. This suggests that some fracturing of the diamonds occurred as a result of differential expansion between the diamond and the inclusion from decompression during the ascent of the diamond to surface as first suggested by Sutton (1928). Fracture surfaces are also associated with ruts, which in some cases follow the fracture surfaces.

Many fractured diamonds display "fresh" stepped octahedral or subchoncoidal breakage surfaces. Equally common to "fresh" fracture surfaces are resorbed or lightly

etched fracture planes. The latter show up in the form of traces of the inner structure of the diamond.

5.3.4 Surface features

The dominant surface features developed on resorbed THH surfaces of Main Fissure diamonds include elongate hillocks, microhillocks and terraces. Elongate hillocks are developed across THH surfaces and the elongation is parallel to the strike of octahedral growth layers. Consequently, the form of the hillocks must be partly determined by the different resistance to resorption of individual octahedral growth layers (Robinson, 1979). Robinson (1979) observed that elongate hillocks are generally least prominent on the most heavily resorbed surfaces. Elongate hillocks on Main Fissure diamonds are generally subdued which may be indicative of substantial resorption. In the case of Sugarbird Blow, elongated hillocks may be obscured by extensive corrosion sculpture (see below).

Concentric terraces are developed around 6-fold THH axes. Terraces probably develop where octahedral layers occur which are more resistant to resorption. They are never associated with the cubic growth form (Robinson, 1979). Terraces are common on Main Fissure and Sugarbird Blow diamonds larger than 1.7 mm in size. Amongst Main Fissure diamonds smaller than 1.7 mm in size, terraces are rarely present. This does not necessarily indicate a cubic primary morphology. It may reflect an unstratified octahedral morphology. The latter explanation is preferred since many of these diamonds exhibit other octahedral features such as negative trigons on fracture surfaces.

Similar to terraces, zig-zag patterns, which develop around 4-fold THH axes possibly due to truncated, "complex rectilinear" (Seal, 1963) octahedral growth layers (Robinson, 1979), are very common amongst Sugarbird Blow and Main Fissure diamonds except for the <1.7 mm fraction. This supports the indication from the presence of terraces that many Klipspringer diamonds at least partly have a primary octahedral structure.

The term corrosion sculpture was first used by Gorina (1971) and corresponds to "pock marks" (Wagner, 1914; Williams, 1932) and "etch pits" (Orlov, 1977). Robinson (1979) describes corrosion sculpture as fairly deep, elliptical to irregular depressions with a curved out-line which are 50 μm to 0.3 mm wide and occur on THH surfaces. Corrosion sculpture is very common on Sugarbird Blow diamonds while it is almost absent amongst Main Fissure and Marsfontein diamonds. In most cases, the corrosion sculpture is very extensive and has eradicated any previous "smooth" resorption surface.

Lamination lines are closely spaced lines, which run parallel to cleavage planes of the diamond and result from plastic slip (Harris, 1992). Plastic deformation requires temperatures in excess of 1000 °C at 30 kbar while at higher pressures, plastic deformation can occur at lower temperatures (De Vries, 1975). After diamond crystallisation, plastic deformation is the first physical process to affect the diamond and it may be related to the development of the kimberlite conduit (Harris et al., 1984; Robinson et al., 1989). Lamination lines are reported in Appendix 5 as wide (>100 μm spacing) or fine. The occasional presence of scotch-plaid texture (two sets of lamination lines crossing) is also indicated. Sugarbird Blow diamonds display lamination lines to a very minor extent. However, lamination lines are prominent only on resorbed surfaces and the bulk of the Sugarbird Blow diamonds are covered with corrosion sculpture, which may obscure possible lamination lines. Thus, the lack of lamination lines does not necessarily indicate that these diamonds have not undergone plastic deformation. When Main Fissure diamonds are considered, about 70 % of the diamonds <1.7 mm in size display lamination lines compared to about 38 % of diamonds in the 1.7-3 mm size range.

Ruts are narrow, elongated depressions on the diamond surface. They are referred to by Orlov (1977) as etch channels. Robinson (1979) report that most ruts trace octahedral or subchoncoidal planes on THH surfaces while others are associated with inclusion cavities, developed at the contact of interpenetrating twin crystals or display a sinuous form. Ruts are common amongst Klipspringer diamonds from all three localities. Some follow octahedral and subchoncoidal planes as can be seen in fractured diamonds. In other cases they are irregular or sinuous and sometimes it appears as if they have developed in cracks leading into mineral inclusions. Orlov (1977) suggests that sinuous ruts develop from etchants that penetrate along cracks in the host xenolith. In some stones, the ruts seem to have been the point of incipient etching which has continued across a broader area of the THH surface.

5.4 Discussion and Conclusions

A comparison of the diamond population(s) sampled by the Main Fissure and the Sugarbird Blow is difficult since primary growth features generally are obscured due to resorption. However, the similar abundance of different coloured diamonds in the size range 1.7-3 millimetres and the common occurrence of elongated and/or flattened THH (which reflects distorted primary octahedra) at both localities suggest that the kimberlites have sampled

diamonds from the same population(s). This is supported by the common presence of terraces and zig-zag patterns both on Main Fissure and Sugarbird Blow diamonds.

Previous studies have shown that deformation laminae are common on pink and brown diamonds (Harris, 1992). These colours have been attributed to graphitisation along deformation glide planes (Urusovskaya and Orlov, 1964). Plastic deformation of the diamonds is likely the cause of the colour of the pink-brown (and subordinately occurring light pink) diamonds since deformation laminae have been observed on all except one of the pink-brown diamonds from the Main Fissure and Sugarbird Blow. The common occurrence of deformation laminae on diamonds less than 1.7 mm in size compared to larger diamonds is consistent with the higher number of pink-brown diamonds amongst the smaller diamonds. While all pink-brown diamonds (except one) display lamination lines, this feature is not exclusive to pink-brown diamonds but occur as well on colourless stones. This may suggest that some diamonds were plastically deformed at pressures outside the stability field of graphite.

Haggerty (1986) suggests that resorption occurs in the mantle and pre-dates the entrainment of the diamond into the kimberlite. In contrast, Robinson et al. (1989) propose that resorption occurs in the kimberlite and the liberation of diamonds from their host xenolith at different depths accounts for different degrees of resorption. This may suggest that Main Fissure and Sugarbird Blow diamonds were released from their host xenoliths at an early stage in the kimberlite compared to Marsfontein diamonds. Alternatively the oxygen activity was comparatively higher in the Main Fissure and Sugarbird Blow magmas. Plastic deformation pre-dates resorption and has been proposed to occur during development of the kimberlite conduit (Harris et al., 1984; Robinson et al., 1989). This may suggest that <1.7 mm sized, deformed diamonds were released at an early stage in the kimberlite and attained the smaller size through extensive resorption.

Trigons post-dating corrosion sculpture has previously been observed and they require a temperature of at least 950 °C to form (eg. Phaal, 1965), which consequently is a lower temperature limit for the formation of corrosion sculpture. In the Kimberley mines, diamonds from deeper levels commonly display corrosion sculpture while this feature is absent amongst shallow level diamonds (Wagner, 1914). Thus, corrosion sculpture seems to develop after the emplacement of the kimberlite magma into the diatreme. Robinson (1979) also recognizes corrosion sculpture as a late stage feature based on textural relationships. The common occurrence of corrosion sculpture amongst Sugarbird Blow diamonds in contrast to Main Fissure diamonds may be a result of different chemical features of the

kimberlite magmas. Alternatively, the Sugarbird Blow magma may have been emplaced into a lower confining pressure if it only slightly post-dates the Sugarbird dyke. Gorina (1971) and Robinson (1979) suggest a gaseous agent to produce corrosion sculpture. The different intrusion styles may have facilitated gas development in the case of Sugarbird Blow while the confining pressure was too high for a transition from fluid to gas in the Main Fissure magma.

Etching of diamonds requires a temperature of at least 450 °C (Robinson, 1979). Thus, the observed stepped octahedral or subchoncoidal "fresh" fracture planes are most likely caused during mining and/or recovery of the diamonds. While fractures displaying resorption may pre-date or develop during the major resorption event responsible for the THH form, fractures displaying light etching probably formed at a relatively late stage, subsequent to the major resorption event.

Some Klipspringer diamonds display complex octahedral growth as evident from cathodoluminescence images (Chapter 6). This type of growth may be reflected on the resorbed surfaces as zig-zag patterns. If so, the common occurrence of zig-zag patterns indicates that this type of unusual complex growth is common amongst Main Fissure and Sugarbird Blow diamonds.

6. FOURIER TRANSFORM INFRARED SPECTROSCOPY ON THE DIAMONDS

6.1 Introduction

Due to substitutional impurities, most diamonds display absorption in the mid-infrared (IR) range. Robertson et al. (1934) first grouped diamonds into Type I and Type II based on the fact that the former group displayed IR and ultraviolet (UV) absorption in contrast the latter group. Today, diamonds have been further subdivided into Types IaA, IaB, Ib, IIa and IIb (see Clark et al., 1992; Evans, 1992 for detailed reviews).

Diamonds display intrinsic lattice absorption in the region 4000-1500 cm^{-1} due to two- and three phonon transitions. Type IIa diamond, which is virtually free of substitutional impurities and very rare, displays only this type of IR absorption. Type IIb diamond is extremely rare and contains trace amounts of boron, which causes absorption in the 2-phonon region at 2460 cm^{-1}. Nitrogen is thought to be incorporated at diamond growth as single atoms substituting for carbon atoms in the diamond lattice. Type Ib, IaA and IaB diamond contain nitrogen in different lattice arrangements. Type Ib diamond carries dispersed nitrogen atoms at concentrations of about 50 to 300 atomic ppm (Evans, 1992). It is comparatively rare in nature but constitutes most synthetic diamonds. It displays absorption at 1130 cm^{-1}. During residence at mantle pressures and temperatures, dispersed nitrogen aggregates to form A aggregates characteristic of IaA diamond. From uniaxial stress measurements, Davies (1976) concluded that A aggregates consist of two adjacent nitrogen atoms. This was confirmed by Jones et al. (1992) through local-density-functional theory. Further aggregation results in B aggregates characteristic of IaB diamond (Evans and Qi, 1982). Loubser and Van Wyk (1981) suggested from electron paramagnetic resonance properties that B aggregates are four nitrogen atoms arranged tetrahedrally about a vacancy in the diamond structure, again confirmed by Jones et al. (1992). The characteristic absorption peak of Type IaA diamond is at 1282 cm^{-1} with a subsidiary peak at 1215 cm^{-1} while Type IaB diamond displays absorption at 1174 cm^{-1} and, to a lesser extent, at 1282 cm^{-1}. A third contribution to the absorption peak at 1282 cm^{-1} is the D component (Clark and Davey, 1984), which has been ascribed to platelets (Woods, 1986; Evans et al., 1995) (see further below). Type IaAB diamond contains A and B aggregates in different proportions and the nitrogen concentration ranges from a few hundred to several thousand ppm. A aggregates are believed to migrate in pairs to form B aggregates with

subordinate pairing of A aggregates and dispersed nitrogen to form N3 centres, which do not display any absorption in the IR range of electromagnetic radiation (Evans and Qi, 1982; Woods, 1986).

The amount of aggregation that occurs in a diamond is dependent on the amount of N present and on mantle residence time and temperature. Estimation of the amount of aggregation can be used together with experimentally derived absorption coefficients to estimate the amount of nitrogen. If the correct activation energy for the aggregation reaction is known, the interdependent parameters of time and temperature of mantle residence for the diamond can be calculated from the nitrogen content and aggregation state. Temperature is the more sensitive parameter and if the mantle residence time is known only at the scale of hundreds of millions to billions of years, the temperature at which the diamonds were stored can be fairly well constrained. Conversely, storage temperature must be precisely defined for the nitrogen aggregation state to be useful as an age indicator. If none of the parameters is known, information on nitrogen aggregation state may still be useful in recognising different diamond populations.

Irradiation of diamonds has been shown to enhance the nitrogen aggregation through the introduction of vacancies and interstitial atoms (Collins, 1980; Allen and Evans, 1981). These types of point defects can also be produced by plastic deformation of diamonds (Evans, 1992). The relationship between plastic deformation and enhancement of nitrogen aggregation is not well understood but must be considered when evaluating IR data.

Platelets are planar features occurring in the cubic planes of the diamond, which can be observed by electron microscope (Evans and Phaal, 1962). They range in size from 8 nm up to a few μm (Evans and Qi, 1982) and they cause a local-mode absorption peak around 1359-1374 cm^{-1} termed B'. The position of the platelet peak varies with the size of the platelets (Sobolev et al., 1968; Hanley et al., 1977; Clackson et al., 1990): the larger the platelet, the lower the wave number. There is a direct correlation between the intensity of the B' peak (I[B']) and X-ray spike intensity (Sobolev et al., 1968) and thus, the platelet peak intensity, or more correctly the integrated platelet area (Woods, 1986) is an indication of the platelet concentration. "Regular" IaAB diamonds show a strict positive proportionality between I[B'] and the absorption coefficient for B aggregates at 1282 cm^{-1} (μ^B[1282]) which is not the case for "Irregular" IaA/B diamonds (Woods, 1986). Irregular diamonds are highly aggregated (close to pure IaB) with a smaller or deficient platelet peak, a feature ascribed to catastrophic degradation of the platelets (Woods, 1986). This theory has been confirmed through high-P/T experiments (Evans et al., 1995) in which a

concurrent disappearance of the B' and D peaks in highly aggregated diamonds was observed at high temperatures. This further confirms that the D peak contribution at 1282 cm^{-1} is related to platelets as mentioned above. Evans et al. (1995) further observed that the disappearance of platelets was correlated with the appearance of dislocation loops with voidites which are octahedra 1-10 nm in size (Barry, 1986), probably consisting of solid nitrogen (Bruley and Brown, 1989).

Debate exists concerning the composition of the platelets with nitrogen (Lang, 1964; Lang, 1974; Barry et al., 1985; Bursill and Glaisher, 1985) and carbon (Woods, 1976 and Woods, 1986) as preferred major constituents. Nitrogen concentrations in platelets are lower than required by the Lang (1964) and Berger and Pennycock (1982) models and conductivity studies indicate that only 3 % of the nitrogen in diamonds occurs as planar features (Berman et al., 1975). Based on an excellent agreement between I[B'] and μ^{B}[1282] in many IaAB diamonds and on the Loubser and Van Wyks (1981) model for the formation of B aggregates (see above), Woods (1986) suggested that platelets are formed from expelled carbon atoms during the formation of B aggregates with nitrogen as a minor impurity. Carbon as a major constituent of platelets has been confirmed by electron energy-loss spectroscopy (Bruley, 1992; Fallon et al., 1995). As mentioned by Mendelssohn and Milledge (1995) this provides an explanation for the degradation of platelets since a carbon atom would easily relax back into the diamond lattice at higher temperatures. Mendelssohn and Milledge (1995) suggest that the state of the platelet peak may alone provide information on the temperature at which aggregation occurred without any constraint on the mantle residence time for the diamond. Based on the examination of many thousands of IR spectra for diamonds, they have observed that platelet peak development occurs at different rates relative to the amount of B aggregates. A simulated series of spectra with different rates of platelet peak development (i.e. platelet peak strength compared to total intensity at 1282 cm^{-1}) are shown in Appendix 6.1. While platelet degradation may be explained by catastrophic heating events as mentioned above, the series in Appendix 6.1 from Type N to Type K diamonds may simply reflect aggregation in increasingly warmer thermal regimes. The decrease in platelet peak height would then be ascribed to a higher reluctance for platelet carbon atoms to relax back into the diamond lattice at higher temperatures (Woods et al., 1990).

Two correlated peaks at 3107 cm^{-1} and 1405 cm^{-1} have been attributed to H (Chrenko et al., 1967). Vibrations of sp^2 bonds in the vinylidene group (>C=CH_2) most likely situated at internal surfaces such as inclusion-matrix interfaces have been suggested

to cause the observed peaks (Woods and Collins, 1983). While no experimental data on correlating H peak intensities to H concentrations have been undertaken to date, H peak intensities can be used to in a semi-quantitative way to investigate and compare diamonds and different areas within individual diamonds.

Carbon dioxide has been seen to cause IR absorption at 650 cm^{-1} and 2376 cm^{-1} (Schrauder and Navon, 1993). However, CO_2 has not been detected in any Klipspringer diamonds wherefore it will not further be considered. Some diamonds from the Slave Province, Canada display absorption at 1430 cm^{-1}, which has been ascribed to the presence of the carbonate ion (CO_3^{2-}) (Mendelssohn and Milledge, 1995).

6.1.1 Qualitative cathodoluminescence of diamonds

When bombarded by electrons, diamonds emit electromagnetic waves from excitation and subsequent relaxation of electrons, a phenomenon referred to as cathodoluminescence (CL). Point defects such as substitutional impurities (N, H, B, Al), intrinsic defects (vacancies and interstitials) and their various combinations can be quantitatively investigated in CL spectra (e.g. Hanley et al., 1977; Zezin, 1990). Many peaks in the CL spectra remain unidentified and luminescence intensity is not directly related to the concentration of optical centres (Davies, 1979) wherefore CL as a quantitative method is not yet well developed.

A detailed presentation of the origin of CL is beyond the scope of this thesis and the reader is referred to Davies (1979) or Clark et al. (1992). Different types of point defects yield different types of colour luminescence which provides a way to study compositional heterogeneities and the internal structure of diamonds (e.g. Clark et al., 1992). This has proved useful in evaluating the nature of diamond growth through studies of CL images of polished diamond plates (e.g. Zezin, 1990; Bulanova, 1995).

Nitrogen is the major impurity in natural diamond. Semi-conductive properties of diamonds is a result of that electron acceptor centres in the diamond are compensated by donor centres (Collins and Lightowlers, 1979). Blue Band A emission has been suggested to originate from donor-acceptor pair recombination with close pairs predominating to give blue radiation, and paired nitrogen aggregates (A aggregates) in Type Ia diamonds may be the donor responsible for the blue Band A emission (Davies, 1979 and references therein). This is in agreement with that most natural diamonds display blue CL colours while synthetic diamonds often display green CL colour from their rapid growth and more dispersed acceptors and donors. Aluminium has been suggested as an acceptor in diamond

to explain the semi-conductive properties (Dean, 1965) but is more likely to have a major role in gettering nitrogen (Collins and Lightowlers, 1979). This is supported by the observation of dark, non-luminescent, nitrogen deficient, Type II areas surrounding garnet diamond inclusions which may be due to gettering of nitrogen by aluminium associated with the inclusion (Milledge et al., 1989). Non-luminescent areas of diamonds have been shown to correlate with deficiency in nitrogen as seen from FTIR data (e.g. Taylor et al., 1995).

6.2 Principles and problems of the method

Practical procedures, instrumental settings and principles for evaluation of the quality of absorption spectra are described in Appendix 4. Here, some main concerns about how the IR absorption data are used will be presented. All investigated Klipspringer diamonds are of Type IaAB with or without significant H contents. Thus, the following presentation will concentrate on principles for using IaAB absorption characteristics in time-temperature determinations.

The absorption peak at 1282 cm^{-1} has frequently been used together with absorption coefficients for A and B aggregates to estimate the amount of aggregation. As pointed out by Jones et al. (1992) and Mendelssohn and Milledge (1995), this peak is frequently off-scale but other data in the one-phonon region can be successfully used. Here a spread sheet developed by Mendelssohn and Milledge (1995) has been used which investigates the Platelet peak ~ 1365 cm^{-1} (T), Raman edge ~ 1328 cm^{-1} (E), IaA_{max} ~ 1282 cm^{-1} (P), Dip ~ 1242 cm^{-1} (D), IaB_{max} ~ 1174 cm^{-1} (Q) and the subsidiary peaks at 1174 cm^{-1} (R) and 1010 cm^{-1} (S). Assuming that any IaAB spectrum is a linear combination of two pure end-members (IaA and IaB), simulated intermediate envelopes can be used to estimate the amount of aggregation. A set of simulated envelopes with positions of the mentioned items used for the aggregation estimation is shown in Figure 6.1. For highly aggregated samples, Q varies considerably while if less than 10 % B aggregates contribute to the peak at 1282 cm^{-1}, E is unreliable and R and S are small compared to P. Further, for high nitrogen contents P, D and Q may be off-scale. For this reason each spectrum must be assessed and treated individually as described in Appendix 4. The position of Q also varies with the amount of aggregation (e.g. Davies, 1981) and the IaA absorption at ~ 1215 cm^{-1} gets swamped by the IaB (~ 1174 cm^{-1}) absorption at about IaB=7 % (Mendelssohn and

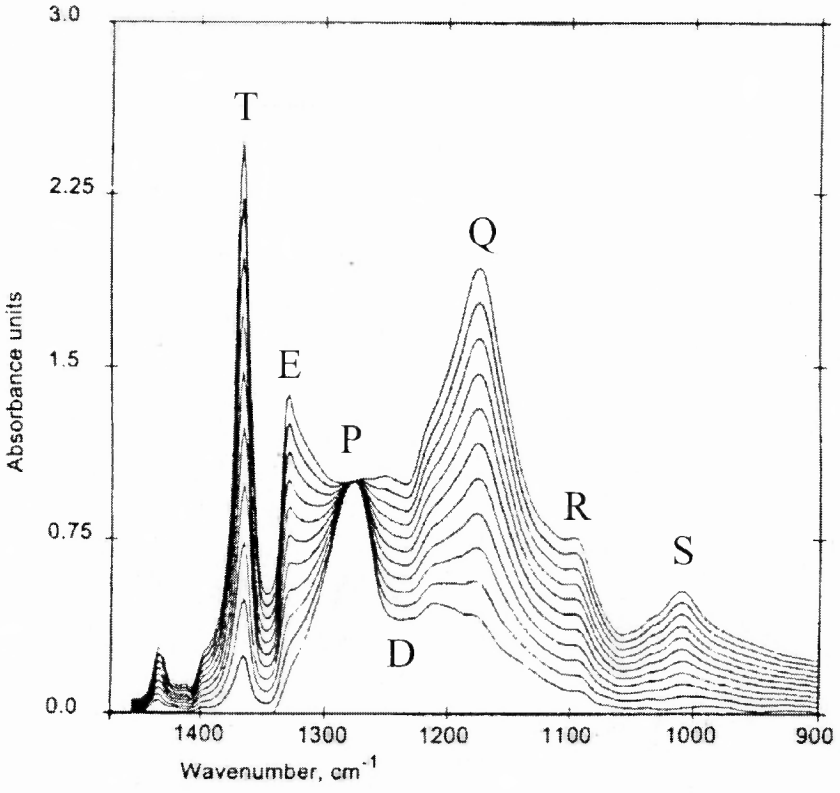

Figure 6.1 Simulated envelopes for the IaA-IaB aggregation sequence with locations for peaks used in the estimation of the amount of nitrogen aggregation (after Mendelssohn and Milledge, 1995).

Milledge (1995). Thus, at low aggregation (%B≤10) the position of Q may be used to estimate the amount of aggregation.

Since the thickness of the specimen is not known, the measured absorption was normalised to the intrinsic absorption of the diamond in the three-phonon region at 1992 cm^{-1}, which is 1.23/mm. The incident intensity corresponds to an absorbance A=3.0. Thus, diamonds thicker than ~2.5 mm would give unreliable data. In practice, even thinner specimens can give unreliable data since the baseline is seldom at zero. Further, as mentioned above, the P peak is frequently off-set even for fairly thin samples since $\mu^{A}[1282]$=1/mm diamond for 160 ppm of A aggregates (see below) which gives an absorbance A=3 at a nitrogen concentration of 480 ppm for a one millimetre thick diamond. However, most frequently this arises for little aggregated stones (i.e. with a strong IaA peak) in which the position of Q might successfully be used instead.

Nitrogen concentration is derived from:

$N(ppm) = \mu(1282\ cm^{-1}) \times [N/mm(IaA) + N/\%B \times (\%B\ used)]$ (Mendelssohn and Milledge, 1995),

where $N/\%B = [N(B)-N(A)]/100]$ and N(A) and N(B) are experimentally derived nitrogen concentrations corresponding to absorption coefficients per millimetre diamond at 1282 cm^{-1} for A and B aggregates respectively. Much effort has been put into relating nitrogen concentrations and the absorption coefficients for A and B aggregates at 1282 cm^{-1} (e.g. Kaiser and Bond, 1959; Evans and Qi, 1982 Woods et al., 1990) and some disagreement exists. However, calculated temperatures do not vary more than a few degrees when different derived absorption coefficients are applied. Here, following Mendelssohn and Milledge (1995), absorption coefficients $\mu^{A}[1282]=1/mm$ for 150 ppm and $\mu^{B}[1282]=1/mm$ for 650 ppm have been used.

Assuming that the formation of B aggregates from A aggregates obeys second order kinetics, time-averaged mantle residence temperatures can be estimated as follows:

T_{NA} (° C) = $-E_A/R \times \{\ln(([N_{tot}/N_{(A)}]-1)/[t_{MR} \times N_{tot} \times A])\}^{-1}-273.15$

where:

N_{tot} = total amount of N (atomic ppm)

E_A/R (activation energy for A to B aggregation/the gas constant)= 81160 K

E_A = 7.03 eV (Taylor et al., 1990)

$N_{(A)}$ = N present as A aggregates (atomic ppm)

A (Arrhenius constant) = $2.94181 \times 10^5\ s^{-1}ppm^{-1}$

T_{MR} = assumed mantle residence time (years)

6.5 IR absorption characteristics of Klipspringer diamonds

6.5.1 Diamond plates

Five diamond plates have been analysed in traverses for IR absorption characteristics. The IR characteristics have been interpreted in conjunction with cathodoluminescence (CL) images of the plates. The diamonds were cut on two parallel sides and CL images were

recorded on both sides in an attempt to correlate different growth zones, which would aid in the interpretation of FTIR data. However, due to technical problems during cutting, the plates could not be cut in specifically desired directions. The analytical procedure for CL is described in Appendix 6. On the CL images, approximate locations for analysed spots are indicated. Exact locations could not be determined since the IR microscopes used were not equipped with a sensitive position control. Spectral information for the analysed plates is given in Appendix 4.2.

Some Klipspringer diamonds have been dated at 2.5±0.3 Ga (Chapter 9) and it is proposed in Chapter 10 that diamond formation may have been associated with the formation of the ~ 2.7 Ga Ventersdorp lavas. The Main Fissure and Sugarbird Fissure kimberlites have been dated at ~ 150 Ma (Chapter 3). Thus, some of the diamonds resided at mantle temperatures for about 2.5 Ga. An assumed mantle residence time of 2.5 Ga was used in the derivation of all temperatures discussed below.

The CL images presented were obtained with an electron microscope (front sides) and through an optical microscope with a photographic attachment (rear sides). This is the reason why some of the rear side images below show inclusions within the diamond while the front side images solely reflect the surface compositions of the plates. Bright luminescence in the CL images presented correspond to light blue luminescence while grey to dark grey luminescence correspond to darker blue tinges. No other CL colours have been observed. From now on, the terms Type I and Type II diamond are used in the meaning of nitrogen carrying and nitrogen deficient diamond respectively.

PLATE P6-9

In the centre of diamond P6-9 is a rounded seed (only vaguely discernible), which has been resorbed prior to later growth (Figure 6.2). Surrounding the seed are several thin layers of varying luminescence colours arranged in a semi-circular pattern reminiscent of "agate texture" only rarely observed previously (Seal, 1965; Bulanova et al., 1995; Zezin et al., 1992). The seed and "agate texture" zone are cut by irregular octahedral growth of Type I diamond. The planar interfaces between the central zone and the octahedral growth suggest that the innermost octahedral zone co-crystallised with the different agate-textured zones diamond rather than that resorption of the central part was followed by octahedral growth. Alternatively the octahedral layers originate from recrystallisation of a pre-existing agate-textured diamond. The local disruption of the octahedral growth is suggestive of either

FRONT SIDE

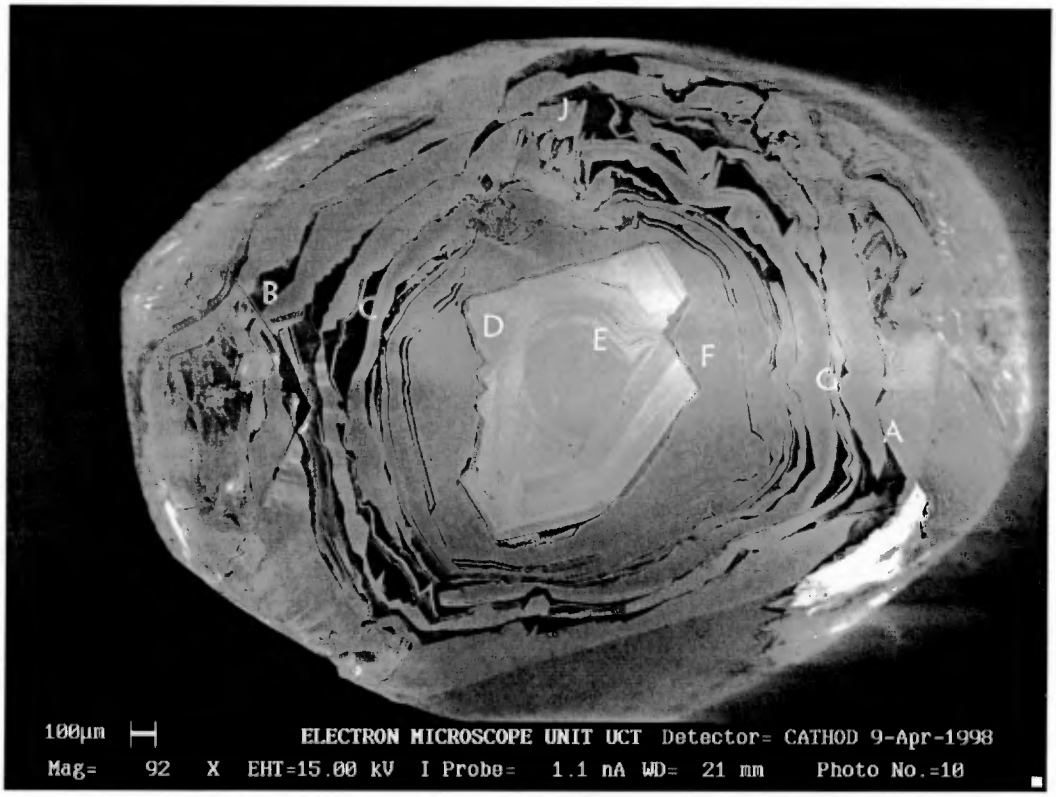

REAR SIDE

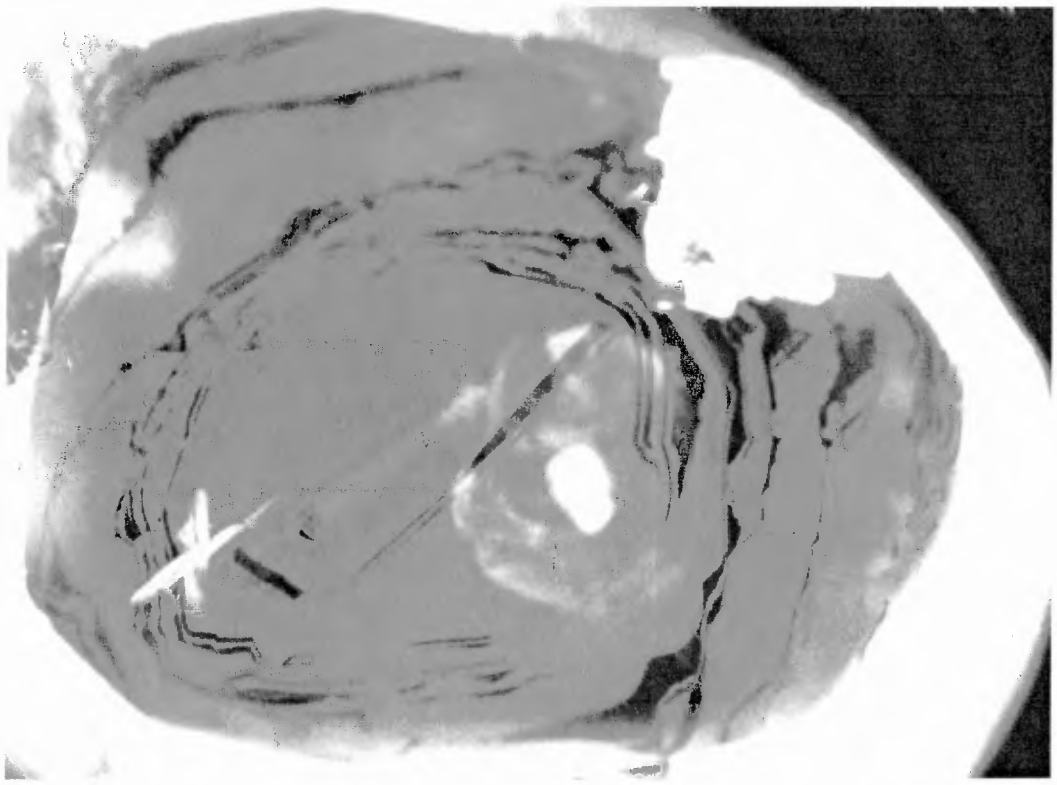

Figure 6.2 Cathodoluminescence images of diamond plate P6-9. The rear side is rotated slightly in the clockwise direction in relation to the front side. The front side to rear side scale relation is about 1:1.5.

brittle fracturing or that the diamond has been partly etched or resorbed while the remainder of the diamond was protected by its host rock. The rest of the plate displays alternating zones of luminescent Type I diamond and non-luminescent Type II diamond. The growth zones are in places complex but generally the Type I diamond displays a rounded outline while the Type II diamond often trends towards octahedral growth best displayed in the upper left parts of front side of the plate. Most growth zones on the front side and the rear side of the plate can be broadly correlated except that the central agate texture does not penetrate to the rear side of the plate.

Plate P6-9 displays a wide range in N concentration (373 to 900 ppm) while the amount of N present as B aggregates is fairly similar for all analyses (14.3 to 23.6 %). Small platelet peaks (μ[1365]=0.2-0.7) are consistent with low but significant levels of B aggregates as expected for regular diamonds. In a diagram of the amount of N present as B aggregates versus N concentration (Figure 6.3), Plate P6-9 displays a horizontal array of data yielding temperatures of 1088 °C to 1107 °C.

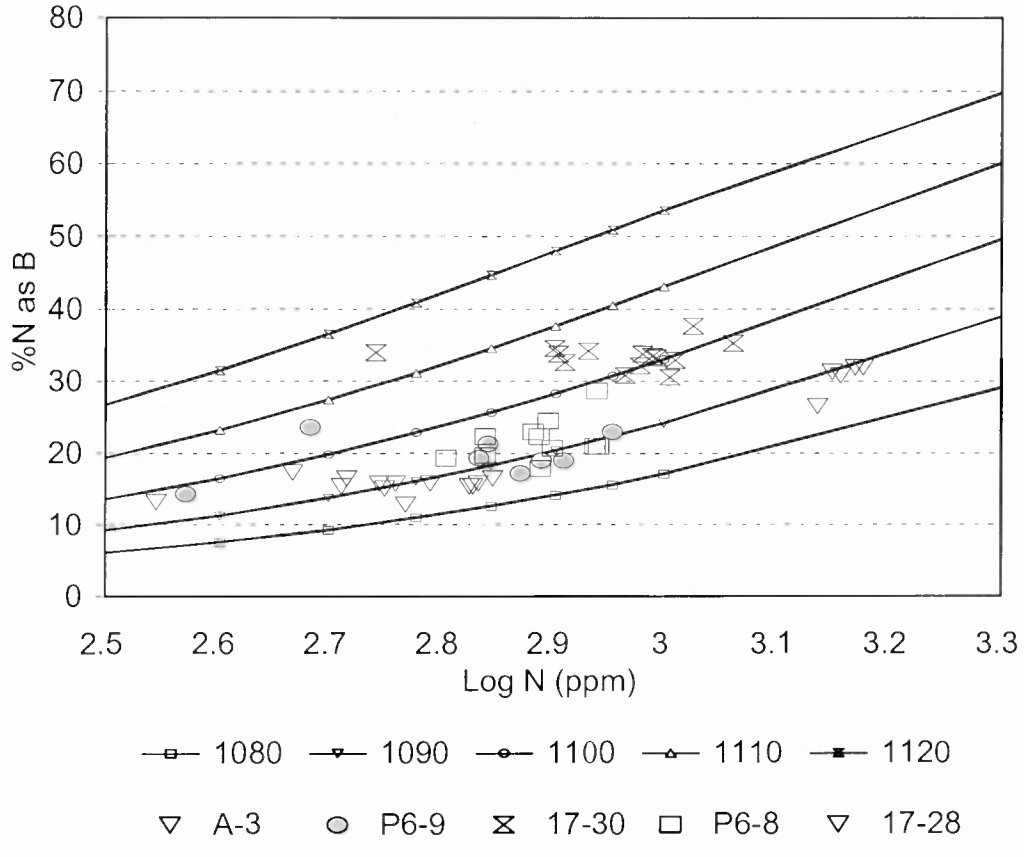

Figure 6.3 The amount of nitrogen present as B aggregates versus the nitrogen content for Klipspringer diamond plates. The inserted isotherms were calculated for a mantle residence time of 2.5 Ga.

As will be shown below, many of the analyses of this plate, other plates and many rough diamonds are considered to give spurious results due to sampling of more than one growth zone. A hypothetical case of analysis of a diamond plate consisting of both Type I and Type II diamond is shown in Figure 6.4. Here a core of Type I diamond with 1000 ppm N of which 50 % is present in B aggregates and a platelet concentration corresponding to μ[1365]=1 is surrounded by N deficient Type II diamond. Analysis x samples only Type I diamond which gives a N concentration of 1000 ppm, N present as B aggregates of 50 % and a platelet peak intensity of 1. Analyses y samples 50 % Type I and 50 % Type II diamond which results in a N concentration of 500 ppm and a platelet peak intensity of 0.5 while per cent N present as B aggregates remains at 50 %. Analysis z would of course not detect any N or platelets. Further, analysis y would display a H peak intensity, which is intermediate between analyses x and z. A concentration of 500 ppm N with 50 % of the N present in B aggregates for analysis y is spurious with an overestimation of the mantle residence temperature for an assumed mantle residence time as a result.

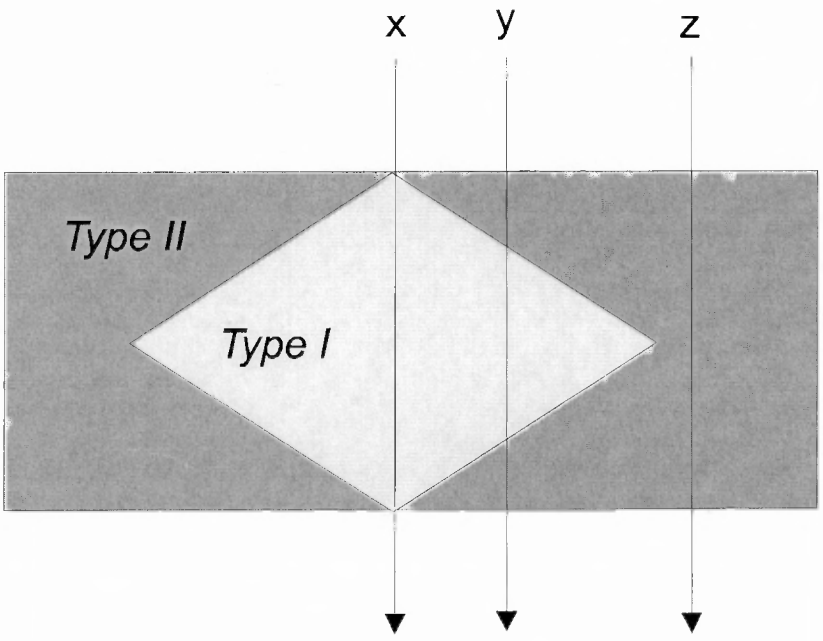

Figure 6.4 Cross section of a hypothetical mixed Type I/Type II diamond with locations for hypothetical IR analyses x, y and z discussed in the text.

Analyses B and C of plate P6-9 partially sample Type II diamond to judge from the location of the analysed spots on the front side of the plate. Accordingly they display low N concentrations of 373 and 482 ppm respectively (Figure 6.5a). Further, these analyses

exhibit depletion in H compared to the rest of the samples (Figure 6.5b) which suggests that the Type II diamond is depleted in H as well as N compared to the Type I parts of the diamond. Analyses A, F, G and J (the central group of data in Figure 6.5b) are from different parts of the plate outside the octahedral zone and yield enriched levels of both N and H compared to analyses B and C. According to the CL images these analyses sample predominantly Type I diamond which explains their higher N concentration and again indicates that the Type I diamond is enriched in H compared to the Type II diamond. Analyses D and E sample the central octahedral and octahedral/agate texture parts on the front side of the plate respectively. Only little Type II diamond can be observed in these central areas of the plate and these analyses give the highest N concentrations. As mentioned above, the bulk of the analyses likely have sampled some Type II diamond. Thus, the slightly higher N concentrations of analyses D and E is suggestive of sampling of pure Type I diamond rather than that the octahedral part of the diamond should be enriched in N compared to more peripheral Type I diamond. The high and low H peak intensities displayed by analyses D and E respectively indicate a heterogeneity that may be related to different growth conditions for the "agate-texture" and octahedral zones. Note also the concurrent high platelet peak intensity (~0.7) and low H peak intensity for analysis E.

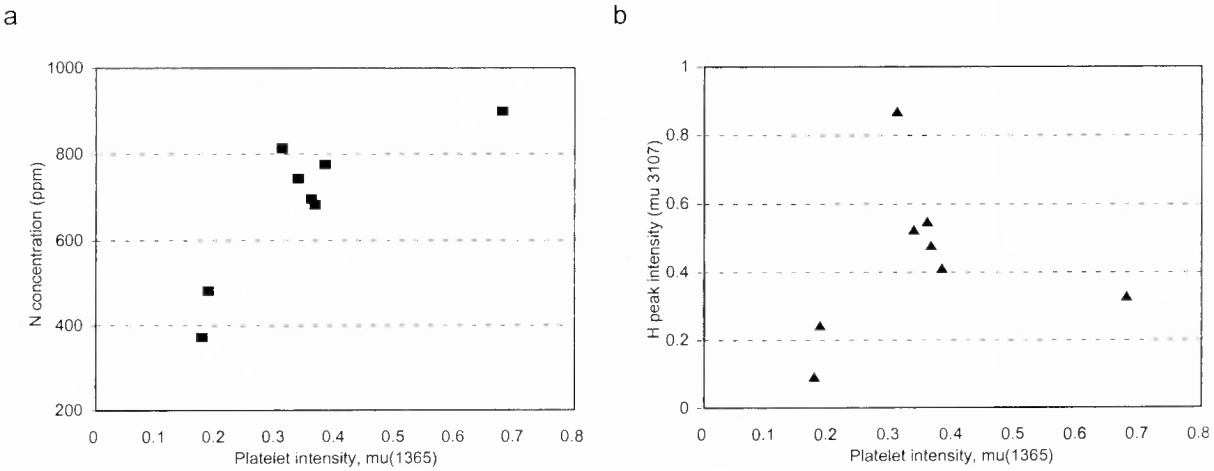

Figure 6.5 Variations in nitrogen concentration and hydrogen peak intensity with platelet peak intensity for diamond plate P6-9.

Although some differences are apparent, the core of Plate P6-9, as represented by analyses D and E, displays very similar IR absorption characteristics to the rest of the plate. Analyses D and E from the central parts of the diamond together with analyses F and J which have the highest N concentrations of the more peripheral analyses are likely to have sampled only little or no Type II diamond and are best suitable for temperature estimations. Thus, the

time averaged estimated temperature of mantle residence for Plate P6-9 is closer to 1085-1090 °C than 1100-1110 °C as suggested by analyses B and C.

PLATE A-3

CL images of Plate A-3 are shown in Figure 6.6. The front side reveals that the inner parts of Plate A-3 consist of a core displaying "agate texture" which is disrupted in a similar way to the core of Plate P6-9. The "agate texture" is surrounded by locally resorbed Type I diamond. Outwards follow irregular octahedral zones of Type I and Type II diamond, which as well are locally resorbed. The intermediate parts of the plate display alternating zones of Type I and Type II diamonds similar those of Plate P6-9. Again, the Type I zones display a rounded outline while the Type II zones trend towards octahedral growth locally. The peripheral part of the plate consists of a broad rim of Type I diamond.

The nitrogen (N) content of plate A-3 ranges from 351 to 703 ppm while the amount of N present as B aggregates displays a very restricted range of 12.8 % to 17.3 %. These characteristics are visualised in Figure 6.3 where calculated temperatures for Plate A-3 stretch horizontally across the 1090 °C isotherm from ~ 1085 °C to ~ 1100 °C. Small normalised platelet peaks are present in all spectra (μ[1365]=0.2 to 0.5) in accordance with the small but significant presence of B aggregates.

The complex structure of Plate A-3 is reflected in the variations in H and N concentrations. Most analysed spots exhibit small amounts of H with normalised peak intensities at 3107 cm^{-1} (μ[3107]) ranging up to ~ 0.4. The variations in H peak intensity and N concentration with the intensity of the platelet peak indicate the presence of two groups of data. Group I displays H peak intensities between 0.3 and 0.4 while H peak intensities are below 0.2 for Group II (Figure 6.7b). N concentrations are above and below about 580 ppm for Group I and Group II respectively (Figure 6.7a). Group I consists of six analyses which are all from within the octahedral parts of the plate (analyses J to O) and calculated temperatures for Group I range from 1085 °C to 1090 °C. Group II represents analyses from outside the octahedral zones across the alternating Type I and Type II diamond zones and into the Type I rim of the plate. Calculated temperatures for Group II analyses range from 1091 °C to 1098 °C and the estimated temperature increases with decreasing N concentration. Group II temperatures are believed to be artificial over-estimations at the assumed residence time for several reasons. Since the core of the diamond for obvious reasons is older than the more peripheral parts of the diamond, the

FRONT SIDE

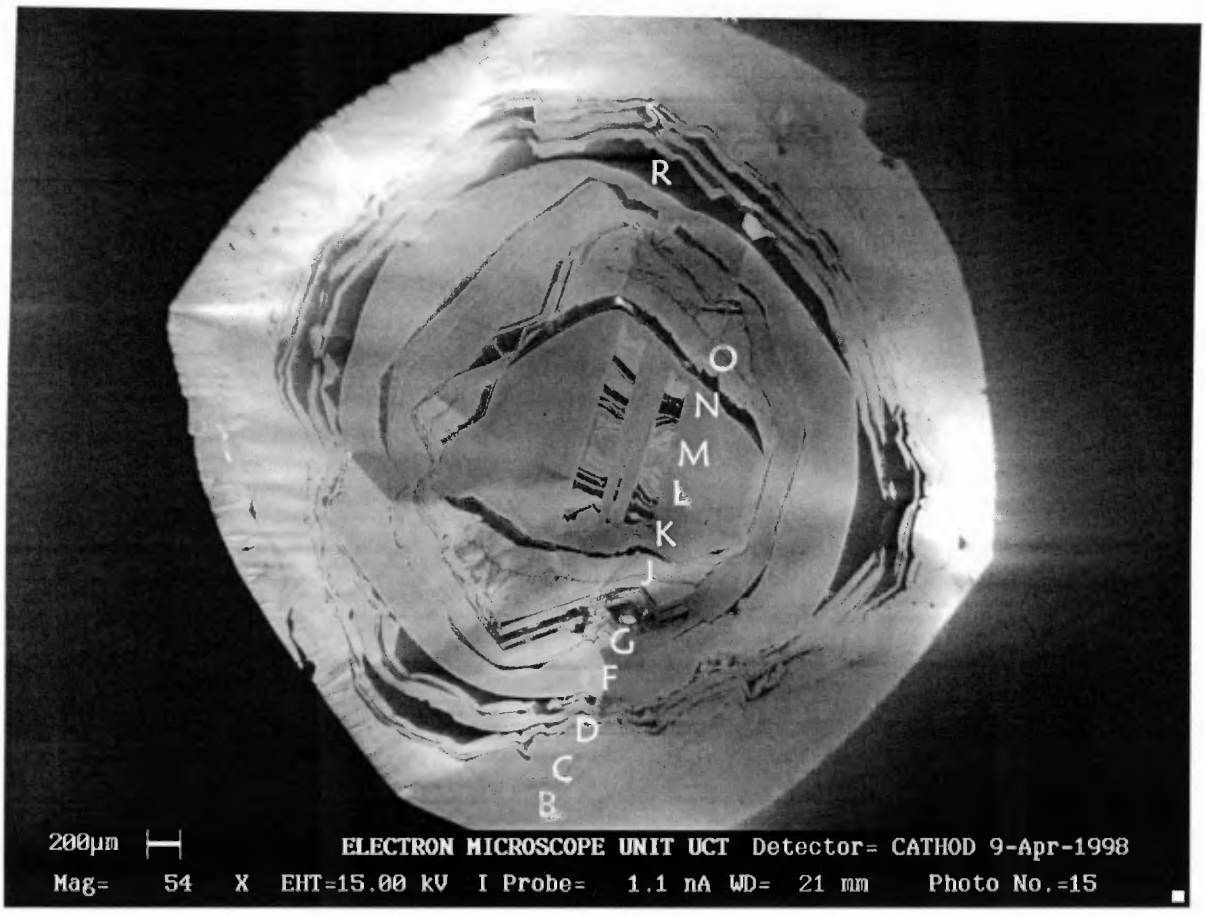

REAR SIDE

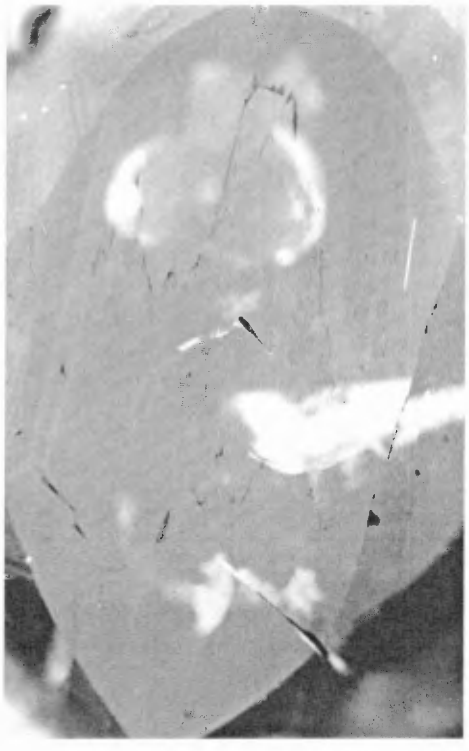

Figure 6.6 Cathodoluminescence images of diamond plate A-3. The scales and orientation of the plate in the two images are similar.

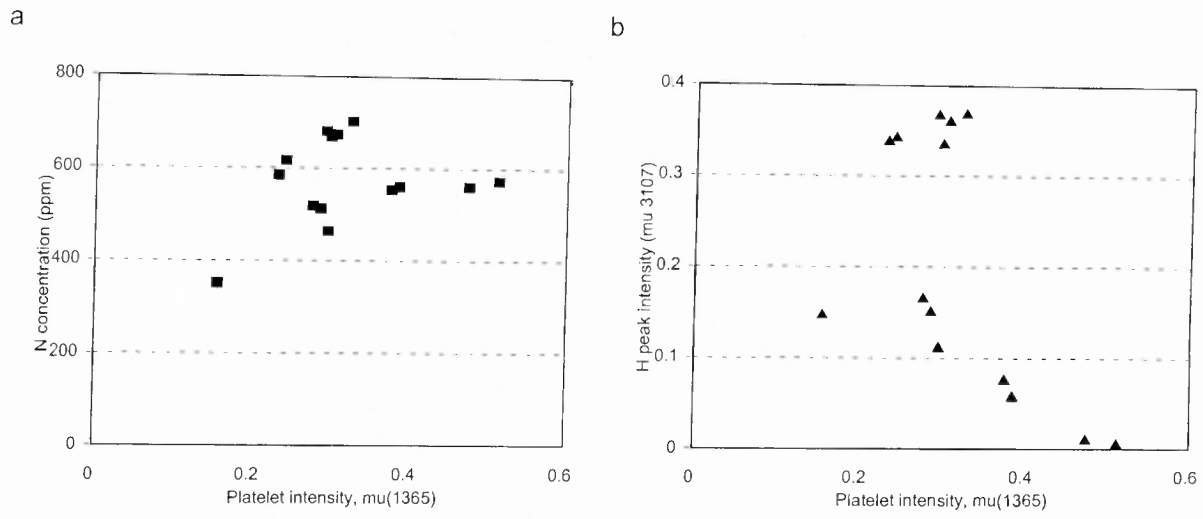

Figure 6.7 Variations in nitrogen concentration and hydrogen peak intensity with platelet peak intensity for diamond plate A-3.

estimated temperatures indicate that the rim for some time resided in a hotter environment than the core (unless other parameters than time and temperature have affected the aggregation of nitrogen), which is not possible. Further, within Group II there is no systematic temperature variation with distance from the rim. This suggests that the observed inter-parameter variations and the estimated temperatures for Group II result at least partly from mixed sampling of different types of diamond.

Since growth zones on the front side of the plate are not present on the rear side (Figure 6.6), the nature of the extension of the zones observed on the front side into the diamond is not known. Due to the complex growth patterns displayed by this diamond and due to the thickness of the plate (~ 2 mm), individual analyses are likely to have sampled more than one type of diamond. Analysis R on Plate A-3 displays the lowest N concentration of all analyses, which probably is due to sampling of Type II diamond to a large extent (Figure 6.6). Together with analysis S, analysis R yields the highest estimated temperature. Contrary to analysis R, analyses B and C sample mainly Type I diamond of the rim zone. These analyses display the highest N concentrations of the Group II analyses and result in the lowest temperature estimations. This suggests that the horizontal array in Figure 6.3 is likely to be explained at least partly by different amount of sampling of Type I and Type II diamond.

The concurrent decrease in H with increasing N for Group II analyses (cp. Figures 6.7a and 6.7b) may suggest that the Type I diamond may be depleted in H compared to the Type II diamond. However, Group II display very low levels of H (μ[3107]=0-0.17) and at

these low levels the estimated peak intensity is very sensitive to fringing and correct base-line correction. Although the low concentrations of platelets recorded (μ[1365]=0.17-0.5) are also sensitive to the base-line correction procedure, the correlation between N concentration and platelet peak intensity for Group II analyses which trend towards 300 ppm N instead of towards the apex in Figure 6.7a argues against mixed sampling of two pure end-members of Type I and Type II diamond. Since no Type II diamond is present on the rear side of Plate A-3, Type II diamond zones observed on the front side are likely to extend inwards under the core zone. Thus, the slight scatter of Group I data towards lower N concentration could be due to mixed sampling of Type I and Type II diamond. In this case however, a lower H content for the Type II diamond than for pure Type I diamond is suggested since H peak intensity decreases with decreasing N concentration (cp. Figures 6.7a and 6.7b). If the Type II diamond is deficient in H, Group II analyses may simply represent mixtures of different zones of Type I diamond and Type II diamond. The Type I rim of the plate represented by analyses B and C would consequently be H deficient in contrast to the Type I diamond of the interior of the diamond. Hydrogen deficient Type II diamond seems plausible in the light of results from Plates P6-9 and 17-30 (see below).

Put in a bigger perspective, the variation in estimated temperatures for Plate A-3 is limited. However, Group I samples are believed to have seen little sampling of Type II diamond and analyses B and C have likely sampled pure Type I diamond for which reasons a time-averaged temperature for a mantle residence time of 2.5 Ga for diamond A-3 is likely to be closer to 1085-1090 °C than 1100 °C.

PLATE 17-30

Plate 17-30 consists of a complex Type I diamond core partly displaying cubo-octahedral growth and which is partly resorbed (Figure 6.8). The core is surrounded by a thin zone of Type II diamond. The intermediate parts of the plate display homogeneous octahedral Type I diamond, which is truncated by the outermost alternating Type I and Type II zones reminiscent of Plates A-3 and P6-9. Similar to the previous plates, in the peripheral parts, the Type I diamond displays a rounded outline while the Type II diamond trends towards regular octahedral growth.

Plate 17-30 is similar to the previously described plates in that it displays a wide range in N concentration (552 to 1154 ppm) for a restricted range of N present as B aggregates (Figure 6.3). However, there are some distinctive differences in IR absorption

FRONT SIDE

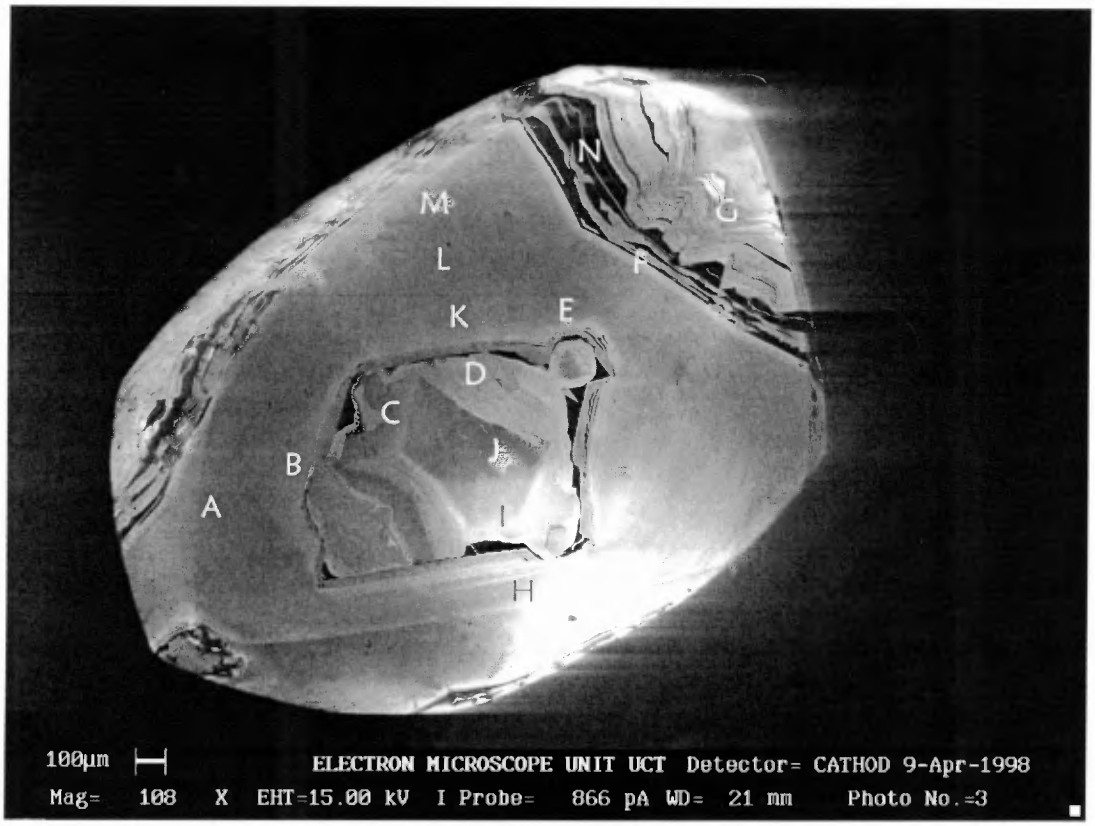

REAR SIDE

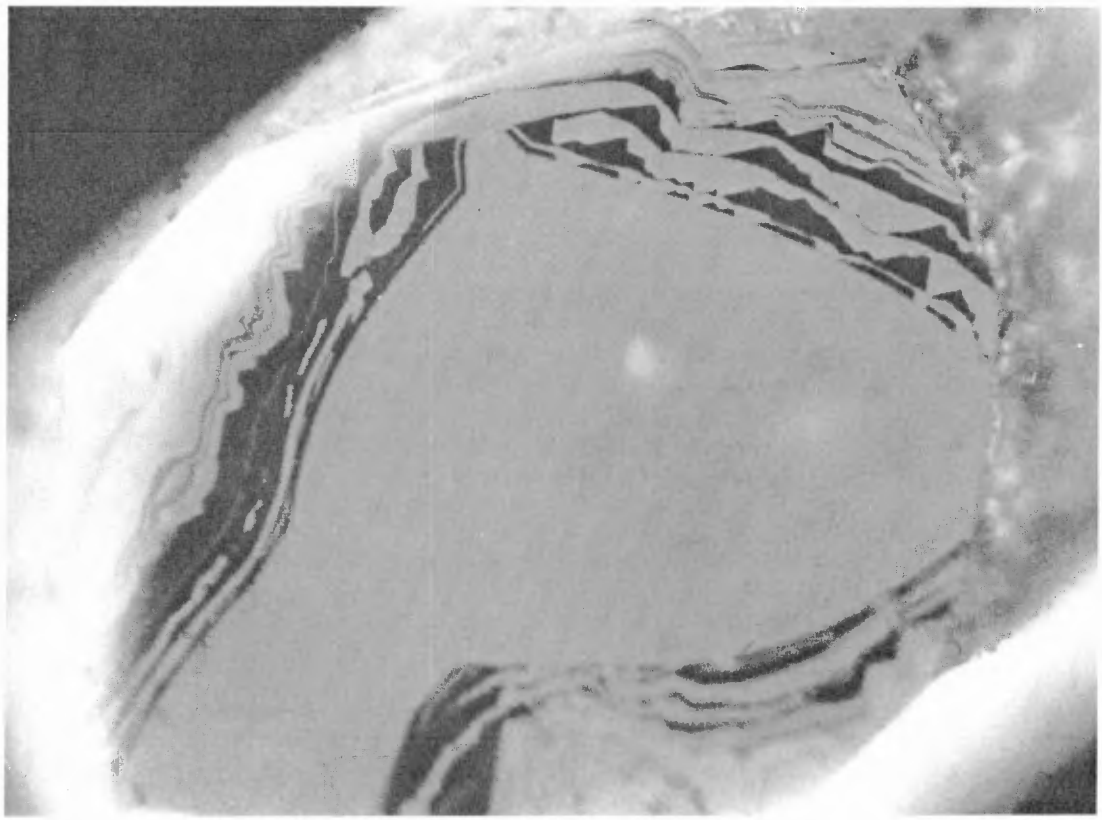

Figure 6.8 Cathodoluminescence images of diamond plate 17-30. The scale proportions between the front side and rear side is about 1:1.5. The orientation of the diamond in the two pictures is close to coincidental.

characteristics between this plate and the ones previously described. The N concentration of Plate 17-30 ranges up to ~ 1200 ppm (Figure 6.9a) and is some 300-400 ppm higher than that of Plates A-3 and P6-9. At the same time the amount of N present as B aggregates is some 10-20 % higher so that the calculated temperature for Plate 17-30 (1098 °C to 1116 °C) are only slightly higher than what was recorded for Plates A-3 and P6-9. Further, Plate 17-30 is very rich in H with μ[3107] ranging from ~ 0.5 to ~2.2 (Figure 6.9b). The five analyses that give the highest H absorption display an unusual range in platelet peak position (T[cm^{-1}]=1376-1382) (Figure 6.9c), the reason for which is not understood. These five analyses are from now on referred to as the "High-T" group. As mentioned in Section 6.1, platelets generally cause absorption between 1359 cm^{-1} and 1374 cm^{-1} and the wave number is normally correlated with the size of the platelets so that bigger platelets cause absorption at lower wave numbers. Rarely very weak peaks have been observed at 1384 cm^{-1}, which may possibly be due to trace amounts of boron (Mendelssohn and Milledge, 1995).

The CL images (comparing front and rear sides) show that the alternating Type I/Type II zones dip gently inwards (from front to rear side) along the sides of the diamond while the zones sampled by analysis N appear to dip vertically. Thus, analysis N has likely sampled substantial amounts of Type II diamond. This is reflected in its comparatively low N concentration (552 ppm). Similar to Plate P6-9, a low H concentration for the Type II diamond is suggested from the comparatively low H concentration of analysis N (Figure 6.9b). Analyses A, F, G, L and M which constitute the High-T group have sampled the outermost parts of the octahedral zone and the peripheral alternating Type I and Type II zones. Analysis N together with the High-T group display a broad positive correlation between H peak intensity and N concentration (cp. Figures 6.9a and 6.9b) which likely is due to sampling of different amounts of Type I and Type II diamond.

The central parts of the diamond (represented by analyses B, C, D, E, H, I, J and K) display lower H contents (μ[3107]=1-1.5) than the more peripheral parts and H for all analyses (except analysis N), and particularly for the central analyses, are negatively correlated with platelet peak intensity (Figure 6.9b). This correlation is not obviously mirrored by a correlation between the N concentration and platelet peak intensity. Thus, while H and N variations for the peripheral group above was ascribed to partial sampling of Type II diamond, the over-all picture and especially the centrally located analyses indicate a

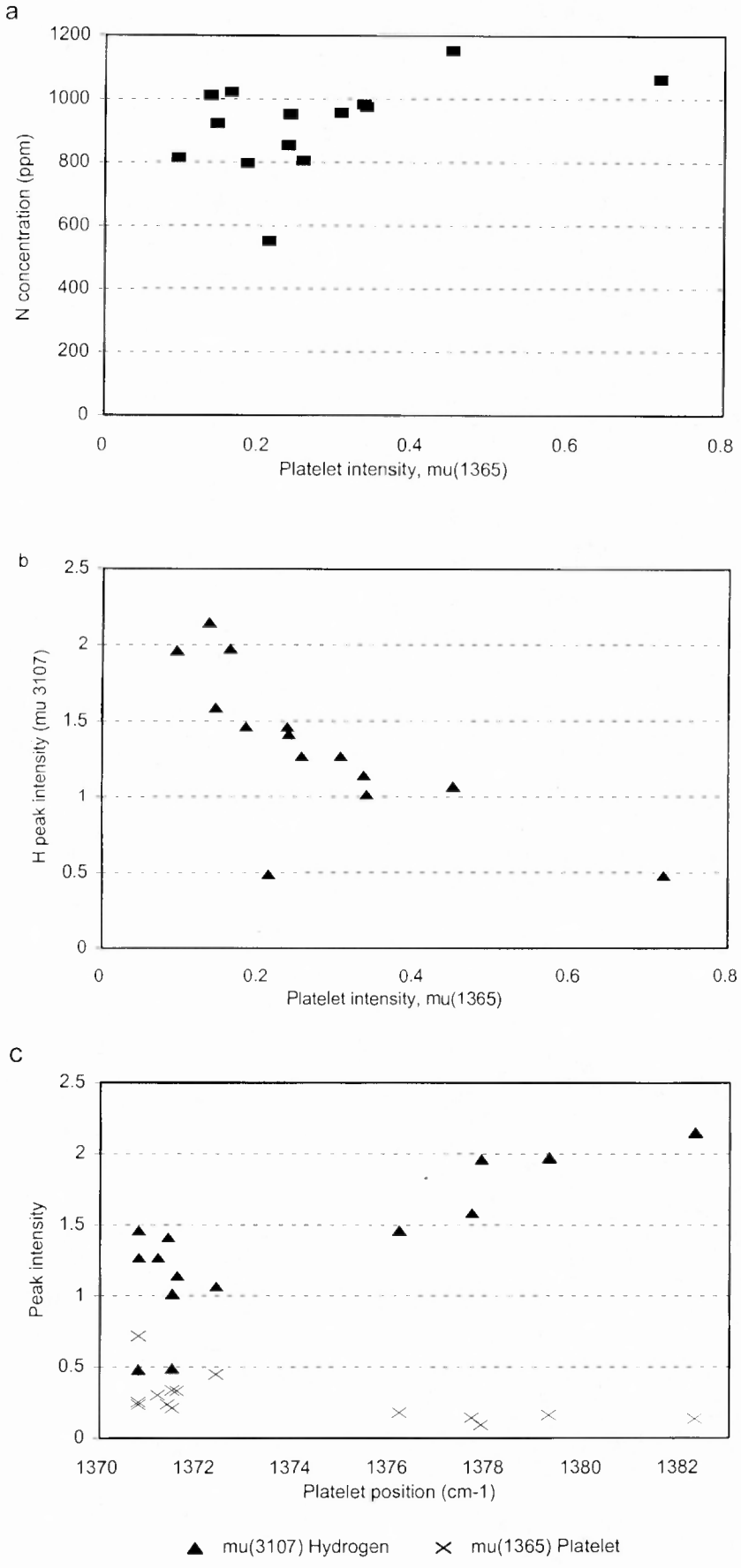

Figure 6.9 Relations between nitrogen concentration, hydrogen peak intensity and platelet peak intensity and position for diamond plate 17-30.

correlation between H content and platelet peak intensity that is not related to partial sampling of Type II diamond.

The continuation of the core and the surrounding Type II zone into the diamond is unknown, so IR absorption characteristics of the central parts of the plate are difficult to assess since individual analyses may represent a mixture of different types of diamond. The most reliable estimations of mantle residence temperatures for the peripheral analysis are based on analyses G and L (1098 °C and 1100 °C respectively) which are highest in N and H and thus probably sampled the least Type II diamond. Although it cannot without reservation be assumed that the peripheral parts of the diamond are not billions of years younger than the central parts, analysis B which has the highest N concentration and probably has sampled the least Type II diamond of the analyses from the central parts as well gives a temperature of 1100 °C. While the difference is not prominent, these temperatures are slightly higher than those of the other investigated plates. Further, Plate 17-30 displays a lower platelet peak evolution relative to the amount of B aggregation compared to the other plates which is further discussed in Section 6.6.

PLATE P6-8

The CL image of Plate P6-8 (Figure 6.10) displays a growth history that is different to the previously presented plates. The central part of the front side displays "rounded", hummocky growth zones with slightly variable luminescent Type I diamond. The intermediate parts of the plate display uninterrupted octahedral growth of variable luminescent Type I diamond. The octahedral layers may have been resorbed (upper part of the front side) and they are followed by a darker luminescent layer which displays a rounded outline (perhaps due to resorption). In the peripheral parts, the regular octahedral Type I growth zones continue.

Nitrogen concentrations for Plate P6-8 are at the same level as for the previously presented plates but they define a more narrow range of 638 to 875 ppm (Figure 6.11a). The different analysed spots of Plate P6-8 display very similar IR absorption characteristics. The three outermost analyses (A, B and O) are lowest in nitrogen (N<700 ppm) and they all, at least partly, sample the dark-blue luminescent resorbed zone. Otherwise there are no systematic variations in IR characteristics with distance from the rim.

FRONT SIDE

REAR SIDE

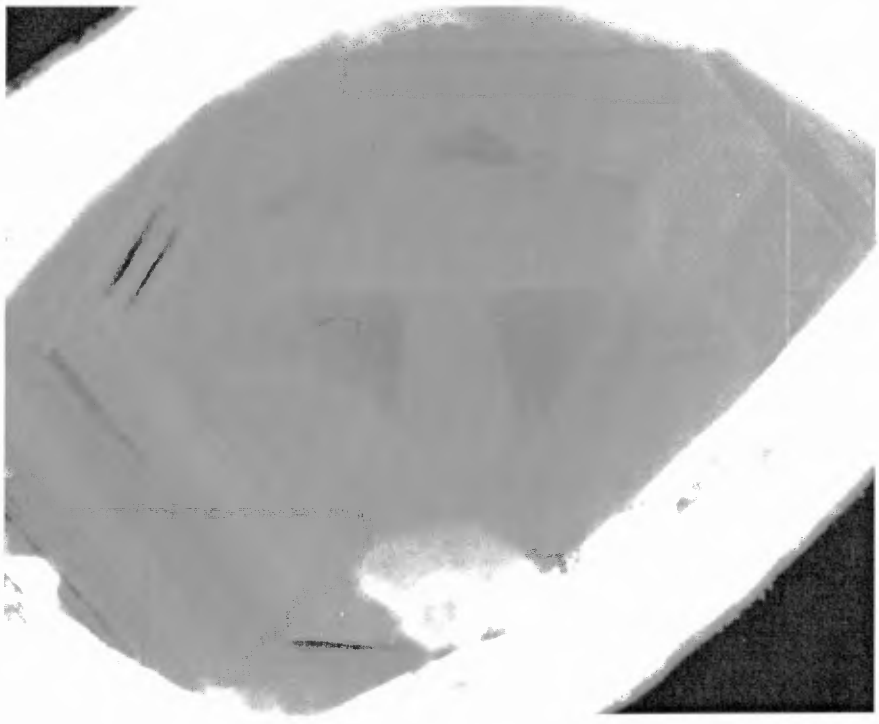

Figure 6.10 Cathodoluminescence images of diamond plate P6-8. The scale in the rear side image is similar to that in the front side image as is the orientation of the plate in the two images.

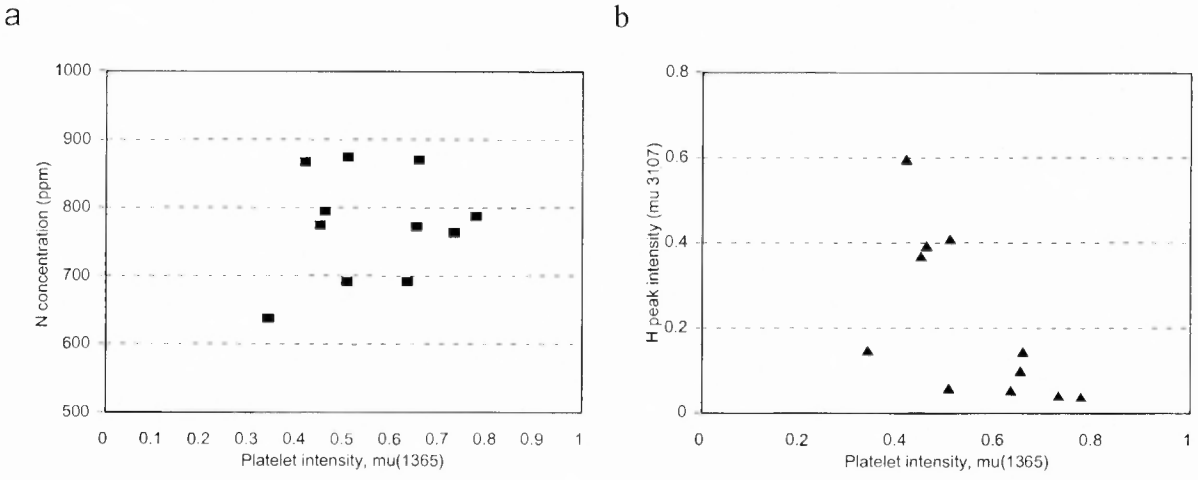

Figure 6.11 Variations in nitrogen concentration and hydrogen peak intensity with platelet peak intensity for diamond plate P6-8.

H peak intensities for most samples are significant but low (μ[3107]<0.2) while analyses F, L, M and N (all from the intermediate octahedral zones) are slightly enriched in H (μ[3107]=0.35-0.6) (Figure 6.11b). This may reflect that some octahedral zones enriched in H have been partially sampled. Alternatively, localised areas rich in sub-microscopic inclusions with diamond/inclusion interfaces suitable to host the vinylidene group have been sampled. It is interesting to note that similar to Plate 17-30, Plate P6-8 displays a broad negative correlation between H peak intensity and platelet peak intensity while there is no systematic variation between N concentration and platelet peak intensity. While the latter is not expected from mixed sampling of Type I and Type II diamond since Plate P6-8 does not contain any Type II diamond, the correlation between H and platelet peak intensities again (see Plate 17-30) suggests that the concentration of platelets may be related to the H content.

Calculated temperatures range from 1088 °C to 1099 °C and they follow a broad isothermal envelope in Figure 6.3. The four samples enriched in H give slightly lower temperatures, which is discussed further in Section 6.6.

PLATE 17-28

This diamond displays continuous octahedral growth from core to rim (Figure 6.12). Different octahedral zones can be distinguished from their slightly different intensity in luminescence.

FRONT SIDE

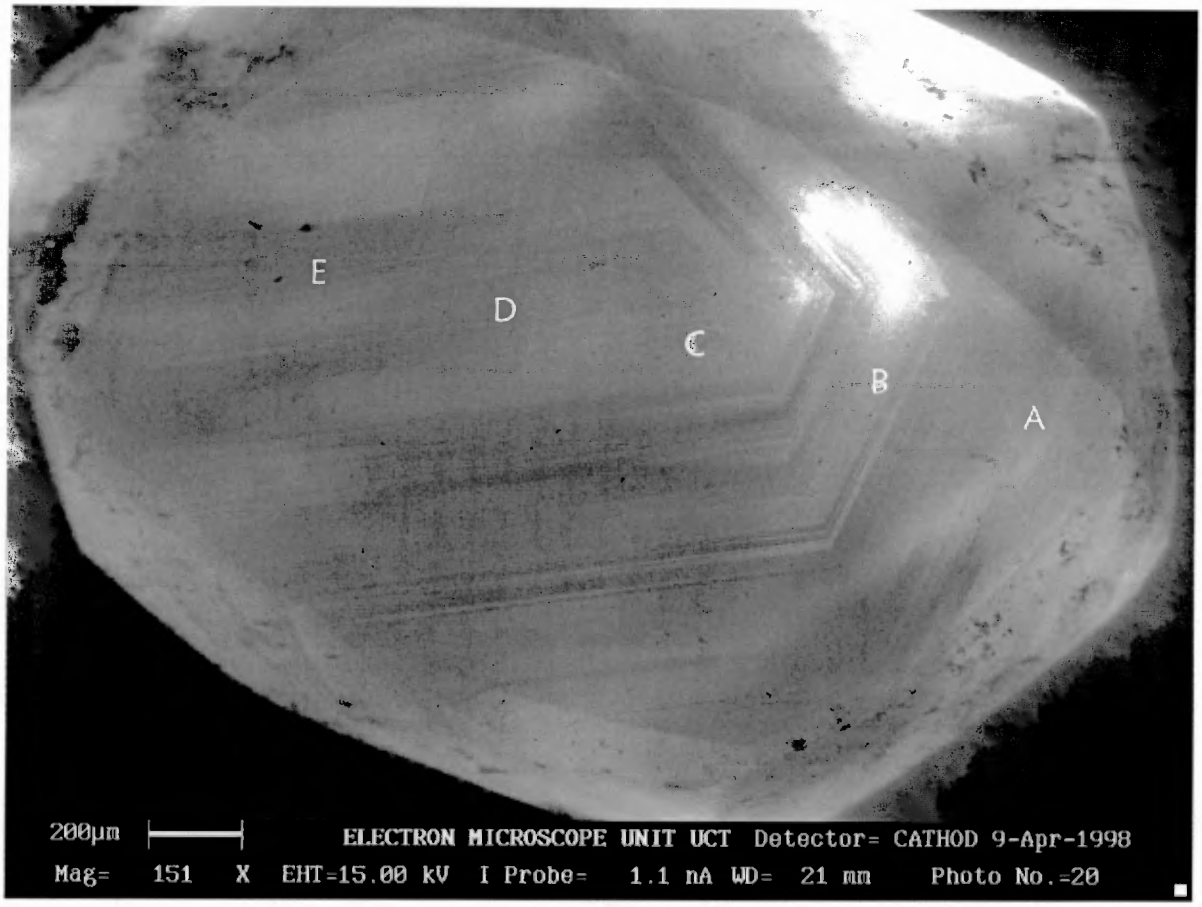

REAR SIDE

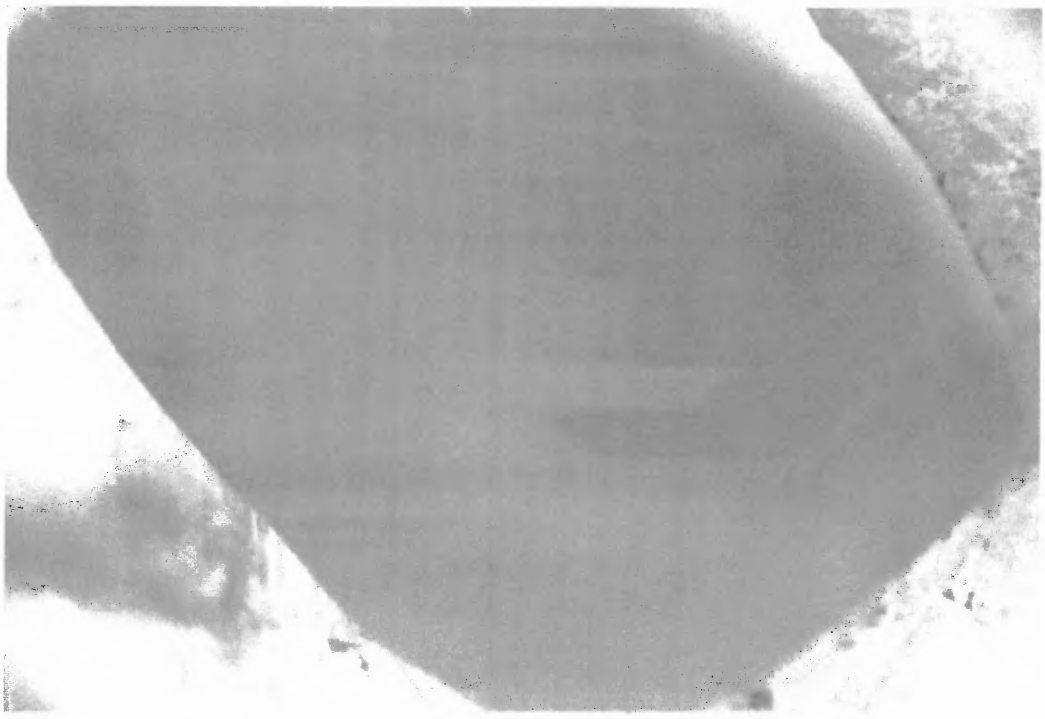

Figure 6.12 Cathodoluminescence images of diamond plate 17-28. The rear side image is rotated slightly in the clockwise direction compared to the front side image. The scale is similar in the two images.

Compared to the previously presented plates, Plate 17-28 displays distinctly higher N concentrations ranging from 1370 to 1505 ppm (Figure 6.13a). Nitrogen concentrations decrease from core to rim, which may reflect a continuous depletion in N of the medium the diamond grew from. Alternatively, the diamond grew in a fluid under an increase or decrease in temperature with a decreasing K_d(diamond/fluid) for nitrogen with the change in temperature. However, as yet no experiments have been undertaken in support or against this theory.

The amount of N present as B aggregates ranges from 26.6 to 32 % and the data form a tightly coherent group in a %NasB versus N concentration diagram (Figure 6.3). Calculated temperatures range from 1087 °C to 1091 °C which is similar to the most reliable estimations for Plates A-3, P6-9 and P6-8.

Plate 17-28 is virtually deficient in H while it displays substantial platelet peak intensities (Figure 6.13b). The higher platelet peak intensities compared to previous plates at approximately the same amount of aggregation is a result of the higher N concentration of Plate 17-28 and consequently a higher concentration of B aggregates and expelled C atoms available for platelet formation.

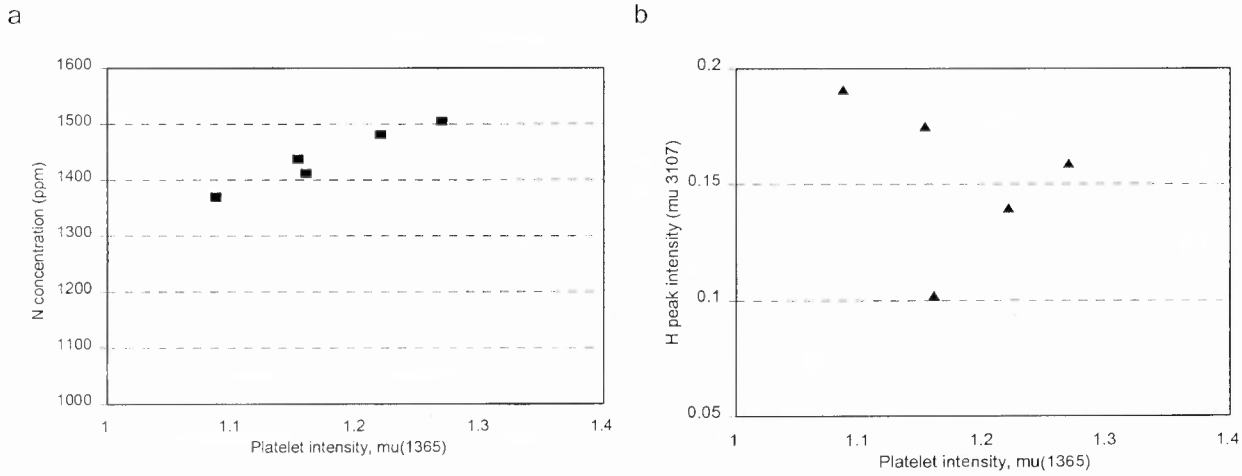

Figure 6.13 Variations in nitrogen concentration and hydrogen peak intensity with platelet peak intensity for diamond plate 17-28.

6.5.2 Rough diamonds

A total of 137 rough diamonds have been investigated for IR absorption characteristics: 72 from the Main Fissure, 41 from Sugarbird Blow and 23 from Marsfontein. Analyses were performed mainly on pieces from diamonds cracked for mineral inclusion studies while

diamonds labelled 1700- (from the Main Fissure) and Mars- (from Marsfontein) were analysed as whole stones. Pieces from cracked diamonds were selected carefully in an attempt to sample both the interior and the rim of the diamond. Spectral information from the IR analyses is given in Appendix 6.3. Multiple analyses from individual stones that showed significant variation in IR absorption properties are included in all the following figures and within-stone variations are presented separately below.

The amount of nitrogen present as B aggregates is plotted versus the nitrogen concentration separately for the three localities in Figure 6.14. In comparing the three localities, the immediate observation is that the Main Fissure and Sugarbird Blow display a similar picture. The bulk of the diamonds from these kimberlites (~ 60 % and ~ 80 % for the Main Fissure and Sugarbird Blow respectively) form a well constrained group (from now on termed the Low-T group) that range from about 500 to 1300 ppm in nitrogen and plot around the 1090 °C isotherm. At face value, estimated time-averaged temperatures range from about 1075 to 1115 °C. However, much of the scatter amongst the Low-T diamonds is believed to be due to sampling of different growth zones within the diamonds to varying extent. Comparing Figures 6.3 and 6.14, it is evident that the data from diamond plates believed to reflect mixed sampling of Type I and Type II diamond cover most of the range in N concentration and aggregation state displayed by the Low-T, rough diamonds. This suggests that the analyses of the Low-T rough diamonds also have partially sampled Type II diamond with slight over estimations in mantle residence temperature for the bulk of the diamonds as a consequence.

About 25 % and 17 % of the diamonds from the Main Fissure and Sugarbird Blow respectively cover a range in nitrogen concentration similar to that of the Low-T group but are far more aggregated and yield temperatures of about 1150 °C to 1180 °C for an assumed mantle residence time of 2.5 Ga (Figure 6.14).

While the two temperature groups together comprise almost all diamonds from Sugarbird Blow, some Main Fissure diamonds straddle along the 1180 °C isotherm down to about 30 ppm nitrogen while others deviate from the Low-T group towards higher nitrogen contents up to about 2500 ppm. The latter are from now on termed the High-N group. Further, a few diamonds straddle between the two temperature groups, which may be explained by sampling of multiple growth zones of mixed High-T and Low-T diamonds (see below). Three Main Fissure diamonds (P3-2, 950W-3 and 17-7) are deficient in N and thus fall into the category of Type II diamonds. It is interesting to note that these diamonds

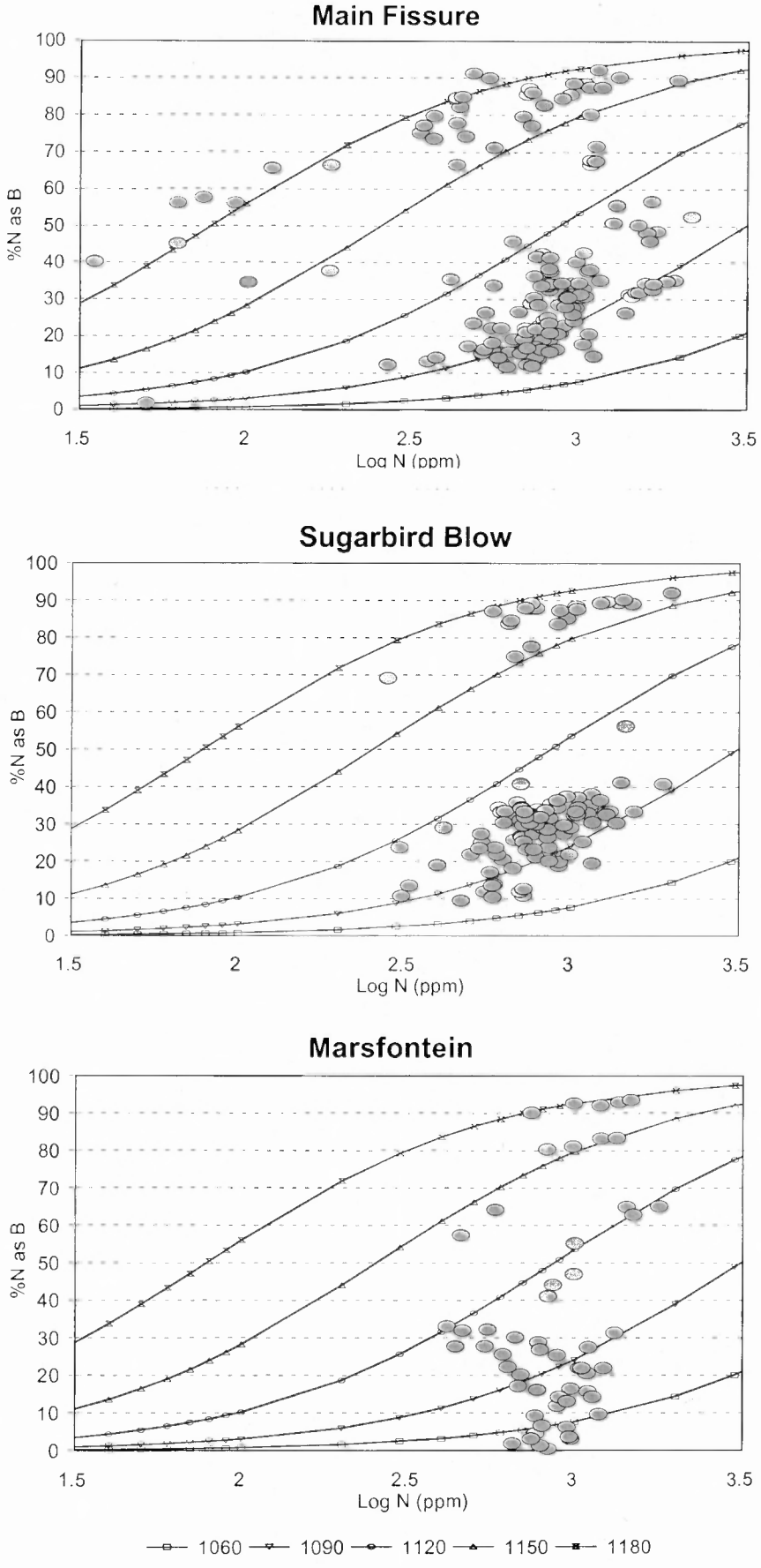

Figure 6.14 Amount of nitrogen aggregation versus nitrogen concentration for Klipspringer rough diamonds. Inserted curves are isotherms ranging from 1060°C to 1180°C calculated for a time of 2.5 Ga.

carry peridotitic or websteritic mineral inclusions. All other diamonds investigated for IR characteristics carried mineral inclusions which have been assigned to an eclogitic paragenesis.

Many Marsfontein diamonds are similar in nitrogen concentration and aggregation state to either the Low-T or the High-T groups discussed. However, some Marsfontein diamonds straddle in between the two groups similar to some Main Fissure diamonds while many Marsfontein stones yield temperatures below 1070 °C (Figure 6.14). This suggests that the Marsfontein kimberlite has sampled a little aggregated diamond population that is not present in the Main Fissure and Sugarbird Blow kimberlites.

The different diamond populations present are effectively discriminated on the basis of estimated time-averaged mantle residence temperature and platelet peak position (Figure 6.15). The High-T and Low-T groups are well defined for the Main Fissure and Sugarbird Blow and many Marsfontein diamonds can be assigned to either of these groups while others have calculated temperatures below 1080 °C as mentioned above. It can be seen in Figure 6.15 that the High-T group displays lower platelet peak positions than the Low-T group. As mentioned in the introduction, platelet size and platelet peak position are generally negatively correlated. Thus, the picture given by Figure 6.15 indicates a bigger platelet size for the High-T group compared to the Low-T group, which suggests that the platelets present in the High-T diamonds have not been substantially degraded.

This is supported by the platelet evolution as indicated by the relation between platelet peak intensity and the concentration of B aggregates (Figure 6.16). In Figure 6.16, the High-T and Low-T groups occur above and below a platelet peak intensity of approximately 1.5. Further, the High-N group mentioned above that is present in the Main Fissure is clearly distinguished as are the little aggregated Marsfontein diamonds which plot on or close to zero platelet peak intensity. The Low-T and the High-N groups display a coincidental platelet evolution as indicated by the constant increase in platelet peak intensity with increased amount of B aggregates. It is interesting to note that the platelet evolution rate for the High-T group is slightly higher (lower slope) than that for the Low-T group. This is the opposite to the common observation that nitrogen aggregation at higher temperature coincides with a relatively lower platelet peak intensity (see Section 6.1). Since the incident IR intensity corresponds to an absorption A=3, platelet peak intensities above A=3 may not be accurate. However, if platelet peak intensities up to 3 are considered, the High-T group still displays slightly higher platelet peak intensities for a set B aggregate nitrogen content compared to the Low-T group.

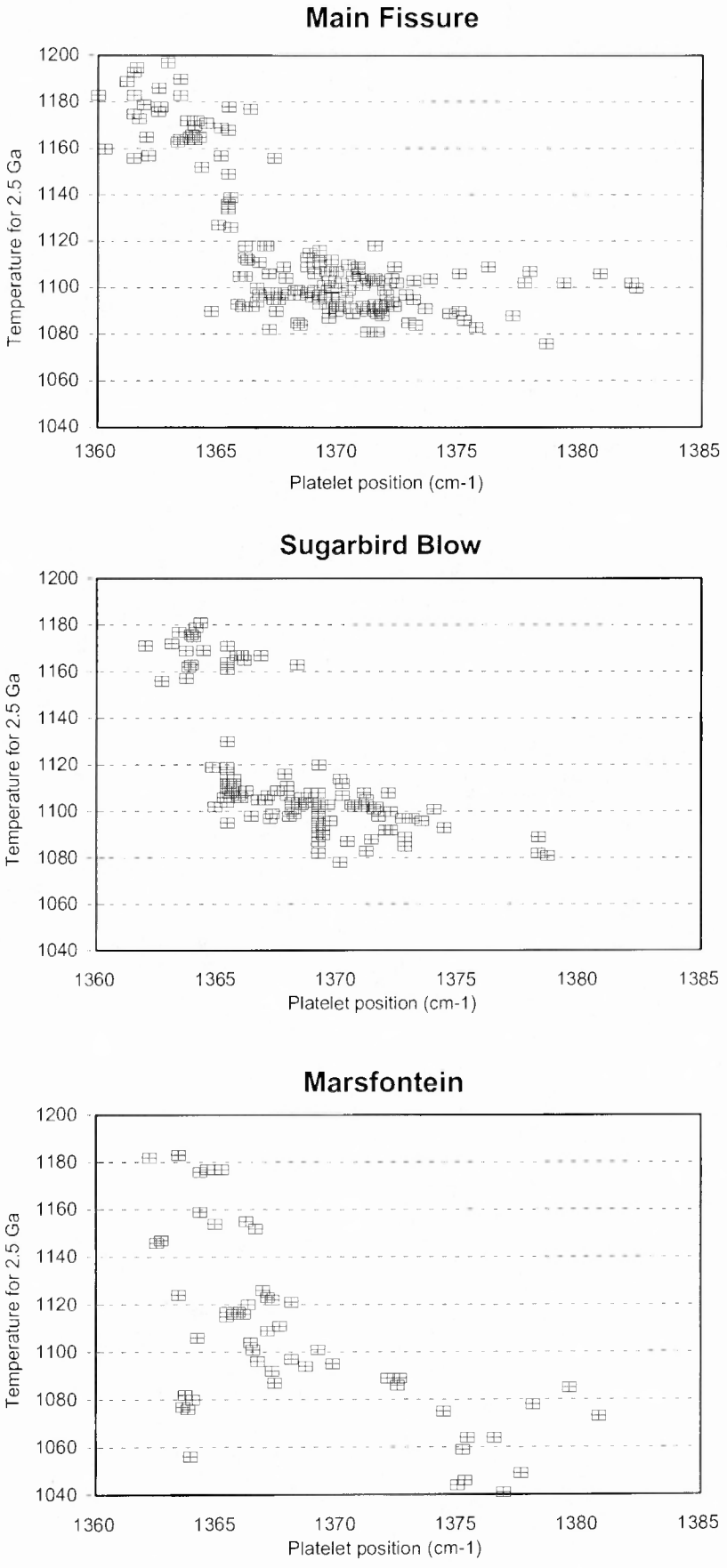

Figure 6.15 Estimated mantle residence temperature versus platelet peak position for Klipspringer diamonds. Temperatures were estimated for an assumed time of 2.5 Ga.

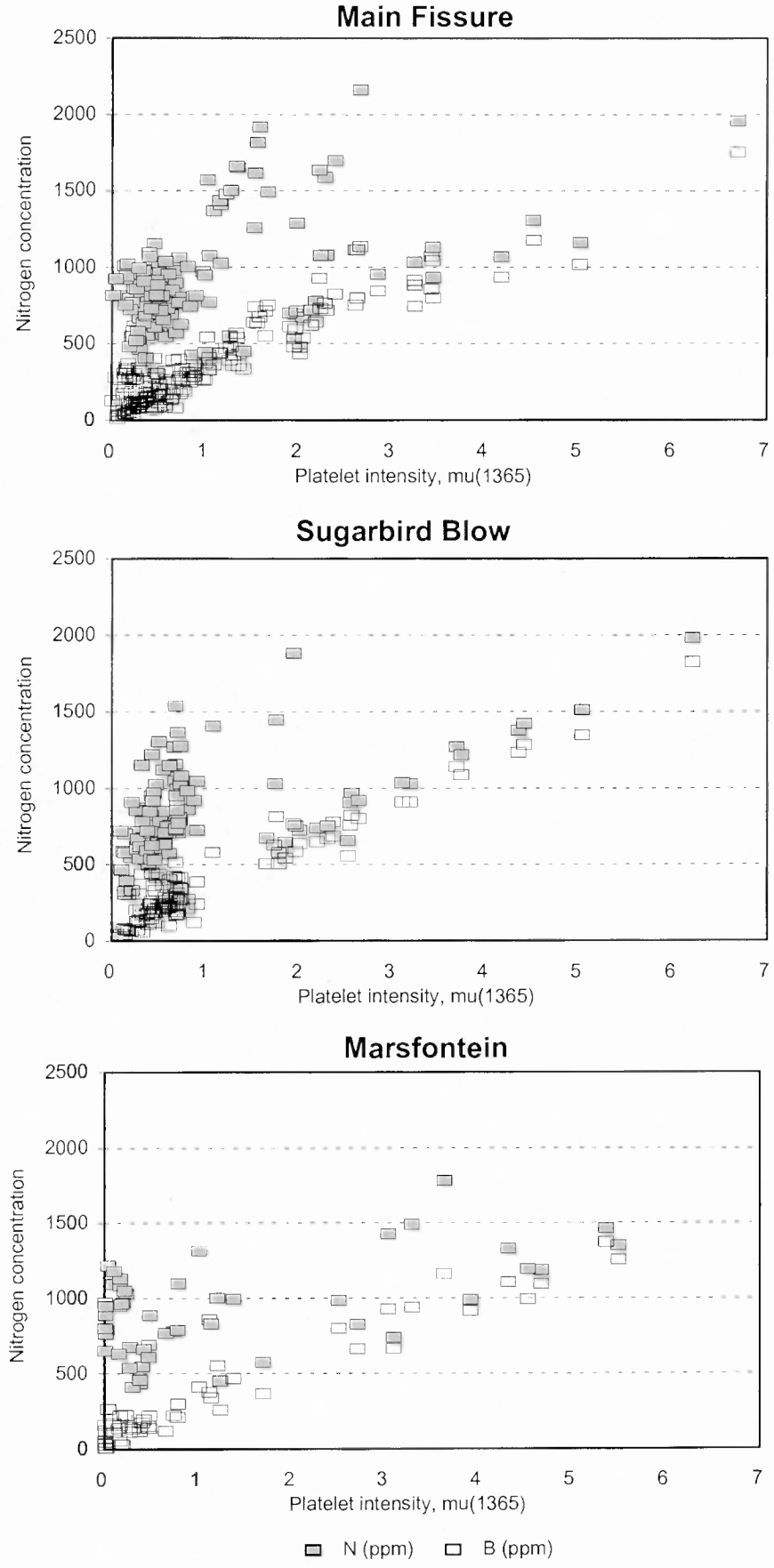

Figure 6.16 Total amount of nitrogen and nitrogen present as B aggregates versus platelet peak intensity for Klipspringer diamonds.

A detailed investigation of the platelet evolution for the Low-T group (Figure 6.17) reveals that some data from all localities deviate from the main trend towards lower platelet peak intensities for constant nitrogen concentration in B aggregates.

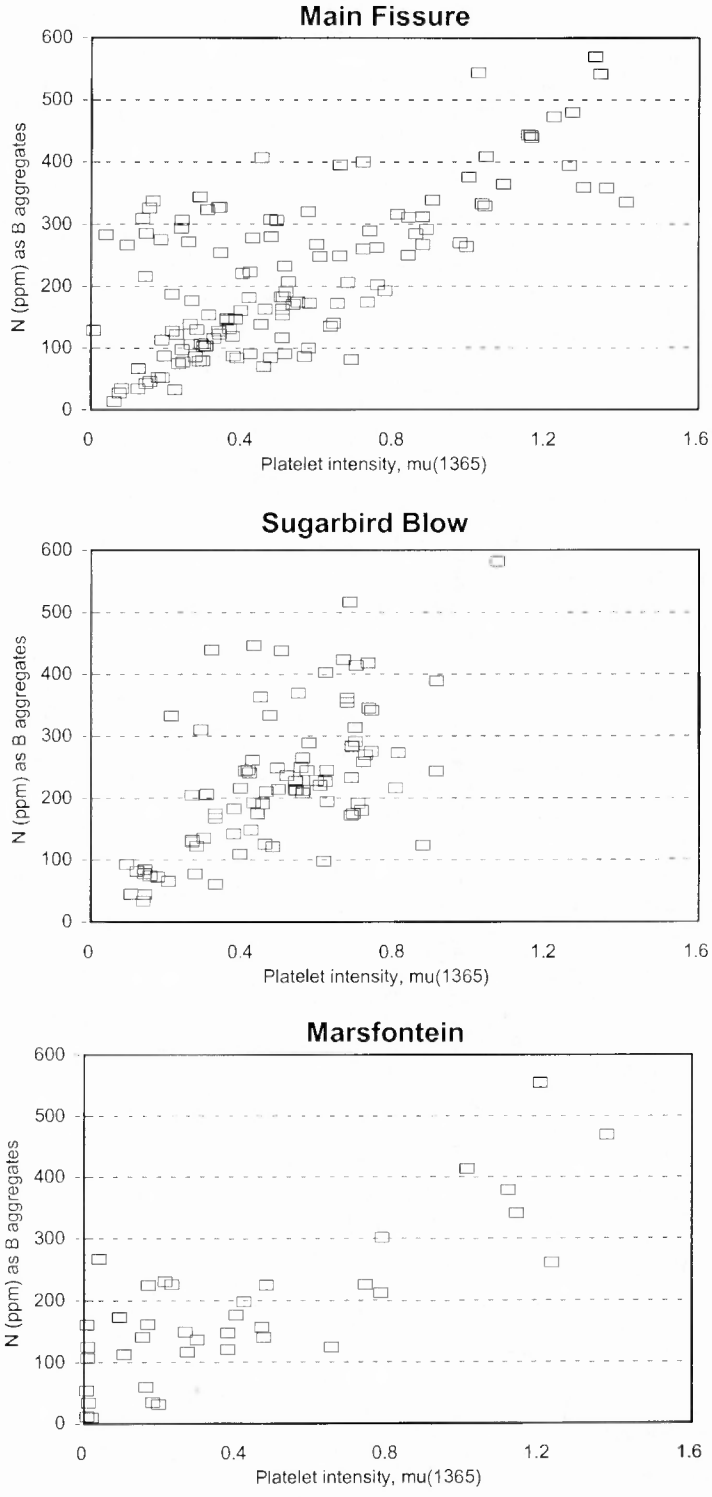

Figure 6.17 Amount of nitrogen present as B aggregates versus platelet peak intensity for Klipspringer diamonds (enlargement of the low B (ppm)/low mu (1365) region of Figure 6.16).

As mentioned in the previous section, data for three of the diamond plates (17-30, A-3 and P6-9) indicates that the platelet peak intensity is related to the H content. This relation is clearly displayed in Figure 6.18 where the relationship between the H peak intensity and platelet evolution rate expressed as the ratio between the amount of nitrogen as B aggregates and the platelet peak intensity is investigated. The broad positive trend in Figure 6.18 supports the thesis that the platelet peak intensity is related to the H content. The H intensities for the High-T group are generally below 0.1 while a high proportion of the Low-T diamonds display H intensities above 0.1.

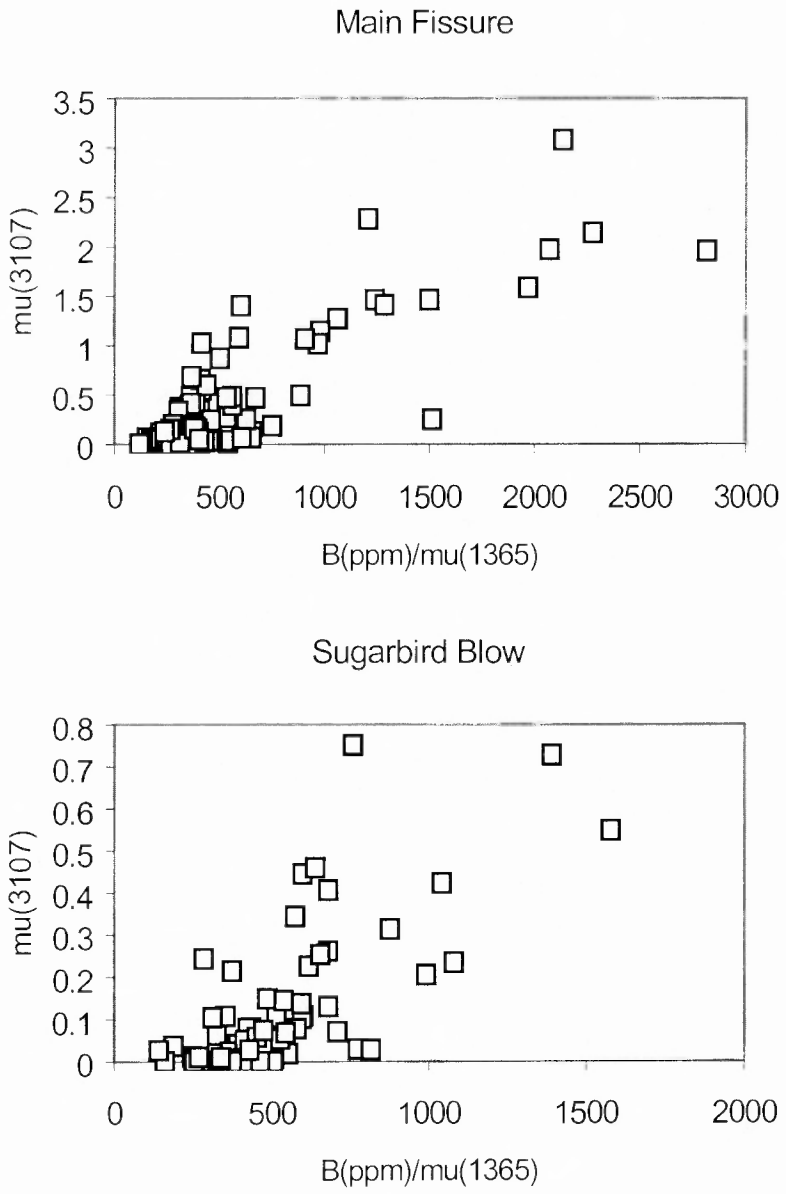

Figure 6.18 Relationship between hydrogen content and platelet evolution as indicated by the ratio of nitrogen content in B aggregates over platelet peak intensity. Note the different scales on both axes.

Variations in IR absorption characteristics within individual diamonds are shown in Figure 6.19. As mentioned above, some zones of some diamonds display High-T type N aggregation while other zones plot in the Low-T group. The different zones within these diamonds are connected with tie-lines in Figure 6.19. In these cases the analyses yielding highly aggregated nitrogen are from pieces of cracked diamonds without any observed THH surface and thus probably from areas closer to the core of the diamond. On the contrary, samples displaying Low-T characteristics are all from more peripheral fragments of a cracked diamond. In Figure 6.19 it can further be seen that some diamonds display approximately constant aggregation for a range in nitrogen content similar to some of the diamond plates investigated. Again, this may be ascribed to partial sampling of Type II diamond. Finally, some diamonds plot along the isotherms as expected for diamonds with different growth zones that are all of the same age and have resided under similar temperature conditions but carry different amounts of nitrogen.

6.6 Discussion and Conclusions

As shown above, three of the diamond plates are dominated by an unusual growth pattern of alternating Type I and Type II diamond. The repetitive growth pattern and the continuous symmetry of the different zones suggest that the outline of the rounded Type I diamond zones reflect rounded growth rather than resorbed regular octahedral growth. The tendency of Type II zones towards octahedral growth suggests a slower rate of growth under less C supersaturated conditions (Sunagawa, 1984a,b) compared to the Type I zones. However, the absence of pronounced regular octahedral growth is suggestive of an over-all high rate of diamond growth. IR analysis has shown that the Type II diamond is depleted in N as well as H compared to the Type I diamond. Thus, the three diamonds in question are believed to have grown from alternating fluids (or magmas) comparatively enriched and depleted respectively in C, N and H.

The presence of other diamond populations is evident from the two diamond plates, which display continuous, uninterrupted octahedral growth. These two diamonds must represent two different octahedral populations since one is distinctly enriched in N compared to the other.

Although variations in IR absorption characteristics within and between the five diamond plates have been evaluated in detail, put in a bigger perspective most variations displayed by the plates are fairly restricted. The total range in calculated time-averaged

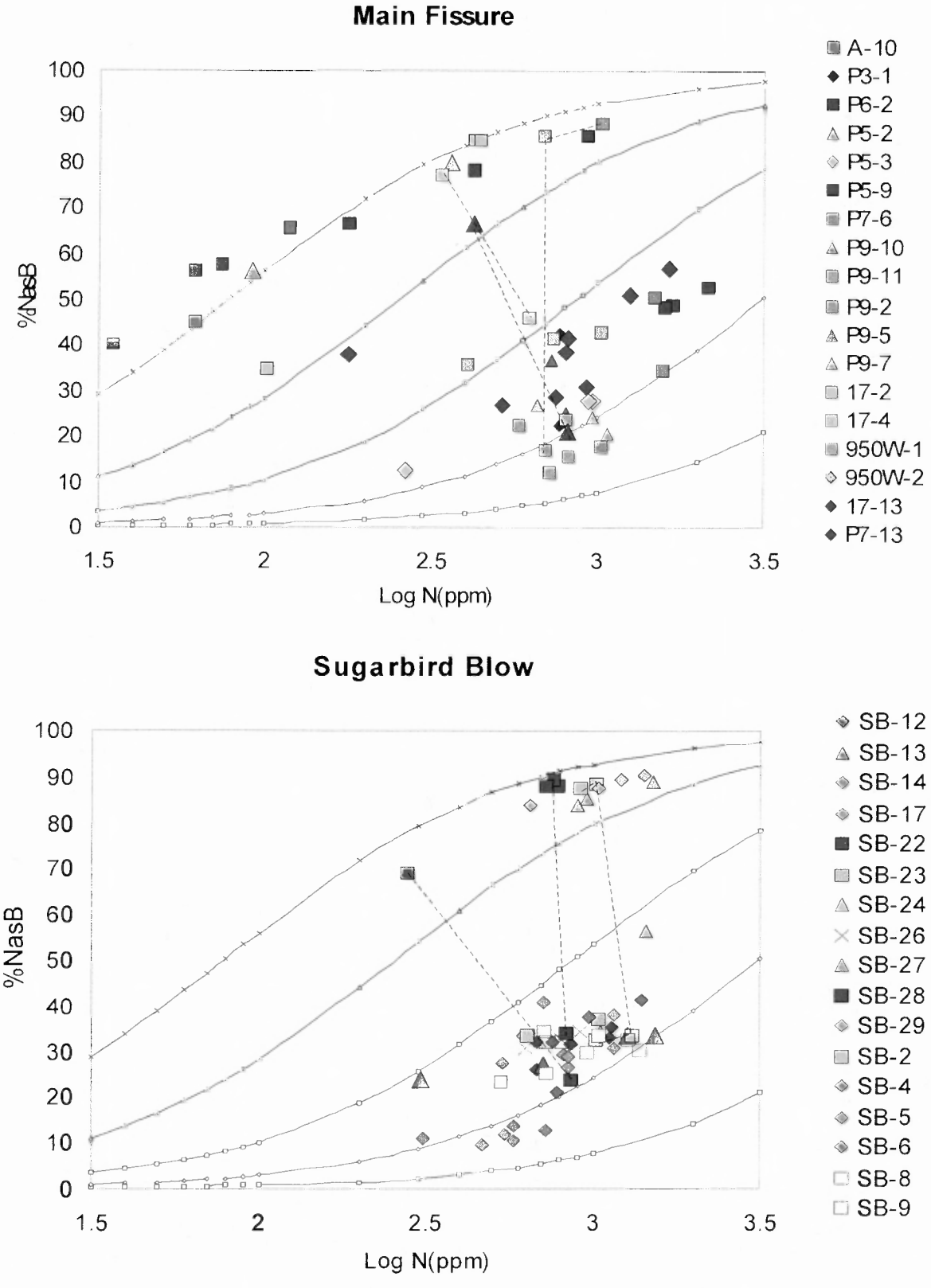

Figure 6.19 Variations in nitrogen content and aggregation state for individual diamonds from the Main Fissure and Sugarbird Blow. Diamonds occurring in both the High-T group and the Low-T group are highlighted with tie-lines. Isotherms range from 1060 °C to 1180 °C as in Figure 6.14.

temperatures (1085-1116 °C) is relatively narrow. It cannot without reason be assumed that the peripheral parts of the diamonds are as old as the cores. However, the similarities in nitrogen content and aggregation state between central and peripheral parts of the individual diamonds suggests that the peripheral parts are not younger than the cores at a scale of billions of years. Since time is an insensitive parameter affecting nitrogen aggregation it cannot be excluded that the peripheral parts of the diamonds are some million years younger than the cores.

From the above detailed evaluation of the data with rejection of data considered to be artificial from partial sampling of Type II diamond, plates A-3, P6-8, P6-9 and 17-28 define a fairly narrow isothermal envelope (Figure 6.3). This may indicate that these diamonds are of the same age and have experienced the similar time-average mantle residence temperatures of ~1090 °C.

The suggested best estimation of a time-averaged mantle residence temperature for Plate 17-30 (~ 1100 °C) is slightly but significantly higher compared to the other plates (Figure 6.3). As shown above, Plate 17-30 is distinctly enriched in H compared to the other plates and further it displays a lower rate of platelet peak development than the other plates. Assuming that the mantle residence time of all plates is the same, theoretically, this could reflect nitrogen aggregation and platelet peak development at a slightly higher temperature for Plate 17-30. The lower rate of platelet development would then be ascribed to a higher amount of platelet carbon atoms that have relaxed back into the diamond lattice. Alternatively, diamond 17-30 was similar to the other diamonds but has seen a heating event perhaps with associated plastic deformation, which resulted in platelet degradation (Woods, 1986) and enhanced aggregation of nitrogen (Evans, 1992). Since the age of every individual diamond is not known, it cannot be excluded that diamond 17-30 is billions of years younger in age than the other investigated diamonds. It must then have resided in a mantle substantially warmer than an average of 1100 °C for the observed aggregation state to develop. This could perhaps more likely explain the difference in platelet peak development than a time-averaged temperature difference of about 10 °C between the plates. However, the observed diamond growth patterns of alternating Type I and Type II diamond for Plates A-3, P6-9 and 17-30 are very unusual and would argue that these diamonds are cogenetic. A correlation between platelet peak evolution and H content has been recognised for Plate 17-30. A plausible dependence of the platelet peak evolution on H content is further discussed below.

The dominating type of rough diamonds have been assigned to a "Low-T" group. Since the mantle residence time of the Low-T group rough diamonds has been estimated to be ~ 2.5 Ga from the age of these diamonds (Chapter 9) and the age of the kimberlites (Chapter 3), their time-averaged mantle residence temperatures may be constrained. With many of the temperatures derived for the Low-T diamonds being regarded as over-estimations due to partial sampling of Type II diamond, a time-averaged mantle residence temperature of about 1075 to 1090 °C, similar to the diamond plates, is suggested for the Low-T group.

The less common "High-T" group rough diamonds (estimated mantle residence temperatures of 1150-1180 °C for 2.5 Ga) cannot without reservation be assumed to be similar in age to the Low-T group rough diamonds. The absence of data between the two well separated groups in Figure 6.13 indicates that they represent two petrogenetically unrelated populations. This precludes that they formed at the same event during falling or increasing temperature but is rather indicative of two discrete diamond formation events. However, the presence of individual diamonds, which display both Low-T and High-T zones suggests that the two populations are spatially related. If the High-T parts of these diamonds are younger than the Low-T parts, the latter should have seen the nitrogen aggregation enhancing process experienced by the former. This clearly cannot be the case, so the High-T diamonds are believed to be at least as old as the Low-T diamonds. This is supported by the observation that High-T analyses of High-T/Low-T diamonds are from the central parts of the diamonds and suggests that in some cases the High-T diamonds have acted as nucleation sites for the Low-T diamonds.

As mentioned in the introduction of the chapter, it has been shown that plastic deformation may enhance nitrogen aggregation. In the case of the Main Fissure, 89 % of the diamonds of the High-T group show evidence of plastic deformation mainly in the form of deformation laminae while this is the case for only 26 % of the Low-T diamonds (Chapter 4). Sugarbird Blow diamonds generally have a very corroded surface on which deformation laminae are not prominently exposed so here a visual assessment of the extent of plastic deformation is not useful. The High-T diamonds are not likely to be plastically deformed equivalents of the Low-T diamonds since some diamonds display both High-T and Low-T zones and since very little data scatters in between the two well defined groups. Rather, the difference in the extent of plastic deformation perhaps reflects that the High-T group has experienced comparatively higher temperatures in conjunction with shear-stress prior to the formation of the Low-T diamonds.

Both the Low-T and the High-T diamonds have well developed platelet peaks as expected for regular diamonds that have not experienced substantial platelet degradation. However, the slightly higher rate of platelet peak evolution for the High-T group compared to the Low-T group (Figure 6.15) contradicts the idea that aggregation at higher temperatures yields a slower platelet formation rate (Mendelssohn and Milledge, 1995). It has been shown that the Low-T group generally is higher in H compared to the High-T group and that the H content is broadly positively correlated with the rate of platelet formation (Figure 6.17). This firstly indicates that the Low-T diamonds formed in an environment comparatively enriched in H supporting the suggestion above that the two groups represent two different diamond formation events. Further, it may suggest that the presence of H prohibits platelet formation which would provide an explanation for the slightly lower platelet evolution rate of the Low-T group.

The paragenetic associations for the High-N group diamonds (range up to 2500 ppm N) and the group of Marsfontein diamonds which yield estimated temperatures down to 1050 °C for 2.5 Ga are not known. The former may represent a population of regular octahedral diamonds as indicated by diamond plate 17-28. The presence of the poorly aggregated Marsfontein diamonds may partly explain the substantially higher diamond grade of the Marsfontein kimberlite compared to the Main Fissure and the Sugarbird Blow.

7. DIAMOND MINERAL INCLUSIONS

7.1 Introduction

Since diamonds are chemically inert and have high physical strength, mineral inclusions trapped within them do not re-equilibrate with the environment surrounding the diamond. Thus, mineral inclusions in diamonds provide a way to study the environment when the diamonds were formed. For brevity, from now on the word 'inclusion' will be used for 'mineral inclusion in diamond'.

7.1.1 Genetic relations between inclusion and host diamond

In the study of inclusions it is important to establish whether an inclusion is proto-, syn- or epigenetic with respect to the diamond. Inclusions that display irregular morphology, or their own morphology, probably grew independently of the diamond into which they were later incorporated (Meyer, 1987). They are referred to as protogenetic and may be unrelated to the diamond formation event. Epigenetic inclusions postdate diamond formation and are mostly alteration products of proto- and syngenetic inclusions (Meyer, 1987). Syngenetic inclusions are by far the most important group in that they are co-genetic with the diamond and may provide information on the mineralogy and chemistry of the diamond growth environment. Some studies have shown that inclusions may be crystallographically oriented with the host diamond (Harris and Gurney, 1979 and references therein). As pointed out by Pearson and Shirey (1999), crystallographic orientation of an inclusion with respect to the diamond is not unequivocally indicative of a syngenetic relationship between the two since it cannot be excluded that the inclusion predates the diamond. Harris and Gurney (1979) suggested that observed octahedral and cubo-octahedral inclusion morphologies, which are not consistent with the crystal structure of the inclusion mineral, result from the greater form energy of diamond imposing its morphology on the inclusion. Cubo-octahedral morphology has been widely used as a criterion for the identification of syngenetic inclusions. Most inclusions do not display the above mentioned morphologies characteristic of proto- and syngenetic inclusions but are partly rounded or irregular with rounded and stepped faces (Harris and Gurney, 1979). These morphologies may also be indicative of syngenetic growth (Harris and Gurney, 1979) and it is striking that they are not reported in

the literature whilst they are comparatively common in nature. Basic criteria in distinguishing between protogenetic and syngenetic inclusions put forward by Pearson and Shirey (1999) includes size and shape of the inclusions. It seems reasonable to assume that silicate inclusions that are much smaller than their xenolithic counterparts, if they have any developed crystal faces, cannot be protogenetic with respect to the diamond. Mendelssohn (1971) suggested that imposed diamond morphologies could be a result of etch pits in diamond acting as nucleation sites for inclusions with later diamond growth capturing the inclusion. Healing of cracks in diamond has been observed in cathodoluminescence studies (Taylor et al., 1995) but epigenetic inclusions with octahedral or cubo-octahedral forms is questioned by Harris and Gurney (1979) partly since the theory is not consistent with inclusions having an imposed morphology in all directions. However, octahedral or cubo-octahedral epigenetic inclusions may occur as replacement minerals of syngenetic inclusions.

Sulfide is the most commonly occurring inclusion in diamonds worldwide (Gurney, 1989) while it is a minor constituent of mantle xenoliths. Sulfides frequently are located close to the centre of the diamond and are commonly found as multiple inclusions in one diamond (Bulanova, 1995; Bulanova et al., 1996; the present study; Westerlund unpublished data). These features taken together leave little doubt that sulfide inclusions are intimately associated with diamond growth and thus, in most cases, are syngenetic. Further, sulfide inclusions also often display octahedral or cubo-octahedral morphology.

7.1.2 Mineral inclusion parageneses

Identification of more than 20 syngenetic inclusion minerals to date shows that most of them can be assigned to either the peridotitic or the eclogitic paragenesis (Table 7.1). Studies of diamond inclusions from worldwide localities show that olivine, enstatite, chrome-pyrope, chrome-spinel and sulfides are the most common inclusions in peridotitic diamonds while eclogitic diamonds most frequently carry omphacite, pyrope-almandine and sulfides (e.g. Gurney et al., 1979b; Gurney et al., 1984a; Gurney et al., 1984b; Gurney et al., 1985; Sobolev, 1983; Harris and Collins, 1985; Jaques et al., 1989). Peridotitic inclusions predominate worldwide as well as in South Africa where a compilation of inclusion data from 21 kimberlites shows that peridotitic inclusions are about three times more abundant than eclogitic inclusions (Gurney, 1989). However, for South Africa, the data may be biased

Table 7.1 Mineral inclusions recovered from diamonds worldwide (modified from Meyer, 1987; Harris, 1992 and Chinn, 1995 with additions from Harte and Harris, 1994).

Syngenetic inclusions			Lower mantle origin	Epigenetic inclusions	Uncertain origin
Peridotitic	*Eclogitic*	*Websteritic*			
Olivine	Omphacitic cpx	Cpx	Mg-wustite	Serpentine	Phlogopite
Enstatite	Pyrope-Almandine	Opx	(ferropericlase)	Calcite	Muscovite
Cr-pyrope	Sulfides	Garnet	Majoritic garnet	Graphite	Amphibole
Cr-spinel	Kyanite	Phlogopite	Mg-Si-perovskite	Haematite	Wollastonite
Sulfides	Sanidine		Ca-Si-perovskite	Kaolinite	Magnetite
Cr-diopside	Coesite			Acmite	Titanomagnetite
Mg-ilmenite	Corundum			Richterite	Sphene
Zircon	Ruby			Perovskite	Moissanite*
Cohenite	Ilmenite			Mn-ilmenite	Apatite
Native iron	Rutile			Spinel	Si-Ti-K phase
Diamond	Chromite			Xenotime	Ti-K-Al silicate
Clouds	Diamond			Sellaite	Staurolite
	Clouds			Goethite	Plagioclase
				Cr-Sr-loparite	Albite
				Cr-chevkinite	

*has been found to co-exist in individual diamonds both with majoritic garnet and peridotitic diopside (Moore et al., 1986)

since eclogitic inclusions are more common in bigger diamonds (>2 mm) (as indicated from Finsch and Premier diamonds) and stones studied for inclusions generally are below this size. Locally (e.g. Orapa Mine, Botswana) eclogitic inclusions predominate (Gurney et al., 1984a) corresponding well to the higher relative abundance of diamondiferous eclogitic xenoliths (Shee, 1978). In contrast, diamondiferous eclogitic xenoliths are well known from the Roberts Victor mine (Hatton, 1978) while about 80 % of the inclusions are peridotitic (Gurney et al., 1984b). An over-view over South African localities shows that there is generally no correlation between inclusion abundance and diamondiferous xenolith abundance (Harris and Gurney, unpublished data).

The depletion in magmaphile elements characteristic of peridotitic xenoliths is even more pronounced in peridotitic inclusions which have been protected from re-equilibrating with the surrounding mantle. Olivine and orthopyroxene display high and restricted magnesium contents with Mg-numbers between 91 and 95 (Meyer, 1987). Garnet and clinopyroxene of the peridotitic paragenesis display restricted ranges in composition compared to those of the eclogitic paragenesis (Figures 7.1a and 7.1b). Pyrope carries up to about 25 wt.% MgO but rarely more than 5 wt.% CaO and depletion in aluminium with chromium contents up to about 18 wt.% Cr_2O_3 brings about the introduction of the knorringite end-member ($Mg_3Cr_2Si_3O_{12}$) to balance the magnesium. Eclogitic garnet inclusions and omphacite are very similar chemically to their xenolithic counterparts and display wide ranges in calcium and Mg number (Figures 7.1a and 7.1b). High sodium contents of pyrope-almandine and potassium contents of omphacite (both up to and sometimes above 0.5 wt.%) mirror the abundance of these elements in diamondiferous eclogite xenoliths and extend to higher levels. Sobolev et al. (1984) report on garnet and omphacite inclusions from south-eastern Australia with up to 32 wt.% and 23 wt.% calcium respectively and they suggest the presence of a separate calc-silicate paragenesis. The low aluminium content of the omphacite is not consistent with the presence of kyanite and the term grospyte was introduced to distinguish the group from kyanite-bearing grospydite. In Figure 7.1b, clinopyroxene from the calc-silicate suite plot around the diopside-hedenbergite join.

Sulfide occurs in both the peridotitic and eclogitic parageneses but is not always easily assigned to one or the other. Subdivision of sulfides from Siberian diamonds into peridotitic and eclogitic based on the nickel content has been suggested with values of 8 wt.% nickel (Yefimova et al., 1983) and 12 wt.% nickel (Bulanova et al., 1996) proposed to

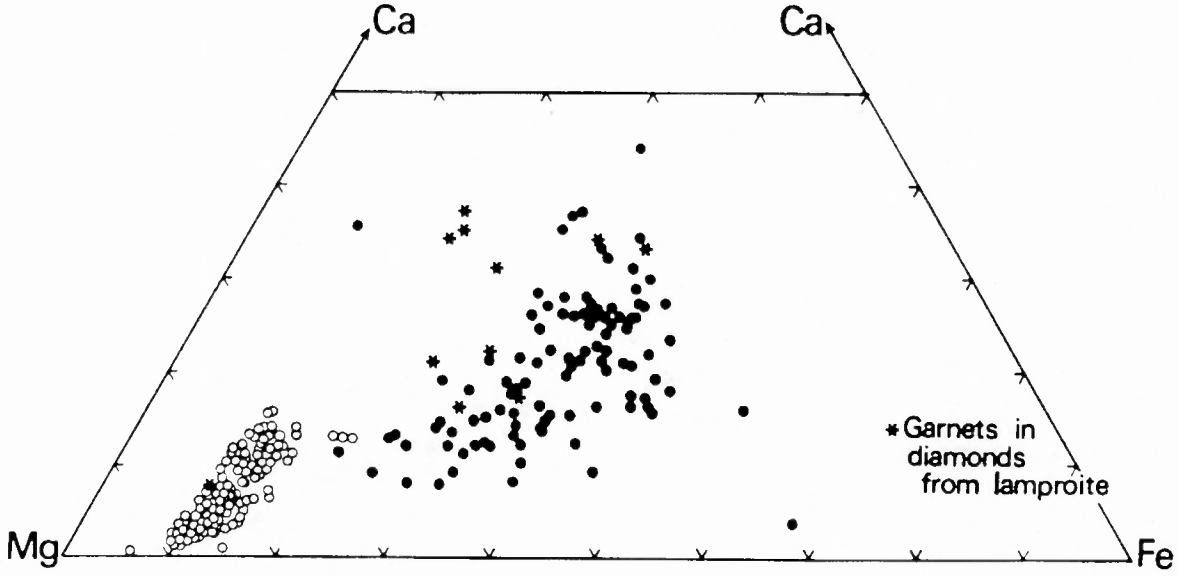

Figure 7.1a Ca-Mg-Fe plot of peridotitic (open circles) and eclogitic (filled circles) diamond inclusion garnets from worldwide localities. Also shown are garnet inclusions from diamonds hosted by lamproite (from Meyer, 1987).

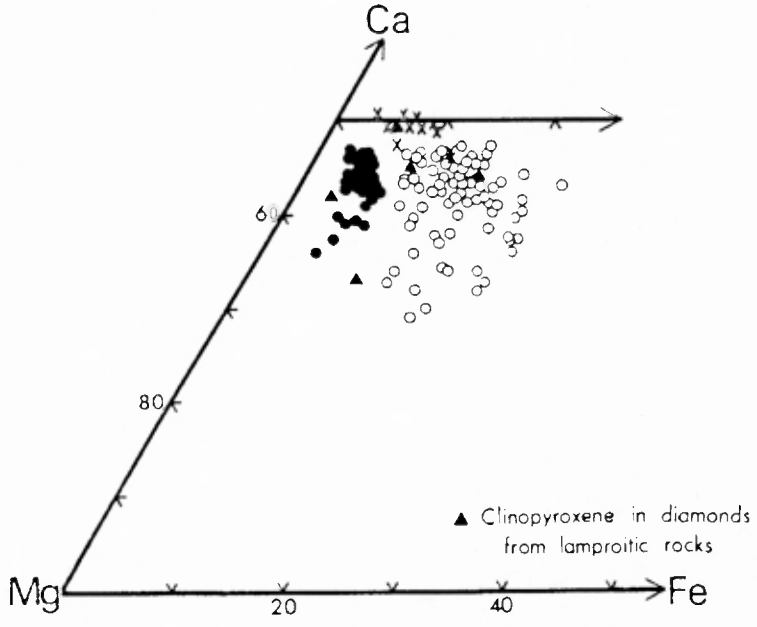

Figure 7.1b Ca-Mg-Fe plot of peridotitic (filled circles), eclogitic (open circles) and calc-silicate suite (crosses) diamond inclusion clinopyroxenes from worldwide localities. Also shown are clinopyroxene inclusions from diamonds hosted by lamproite (from Meyer, 1987).

separate between the two parageneses. These "cut-off" values are based on the Ni contents of sulfides coexisting with peridotitic or eclogitic silicate minerals in individual diamonds. In the latter study, sulfides carrying more than 20 wt.% nickel were assigned to a peridotitic paragenesis whilst some transitional sulfides carrying between 12 wt.% and 20 wt.% nickel were proposed to perhaps be of a pyroxenitic paragenesis. Data for African sulfide inclusions (Deines and Harris, 1995) are indicative of slightly higher "cut-off" values with some sulfides displaying transitional values. Low-nickel sulfides predominate at the Koffiefontein mine whilst peridotitic inclusions predominate amongst silicate inclusions. Further, less than 20 % of the sulfides have nickel contents compatible with being in equilibration with mantle olivine, which led Deines and Harris (1995) to suggest the presence of a separate sulfide paragenesis. However, rhenium-osmium characteristics of low- and high nickel sulfide inclusions show great similarity with eclogitic and peridotitic xenoliths respectively which argues against the need to invoke a separate sulfide paragenesis (Pearson et al., 1998a). The "transitional" sulfides from Deines and Harris (1995) may belong to a pyroxenite paragenesis similar to the transitional Siberian sulfides (Bulanova et al., 1996)

The discovery of inclusions such as Mg-wustite (ferropericlase) (e.g. Scott-Smith et al., 1984; Moore et al., 1986; Wilding 1990; Davies et al., 1999; Harte et al., 1998), majoritic garnets (e.g. Moore and Gurney, 1985; Wilding, 1990) and Mg-Si-perovskite and Ca-Si-perovskite (e.g. Harte and Harris, 1994; Harris et al., 1997; Hutchinson, 1997; Davies et al., 1999) implies that some diamonds originate from greater depths than previously believed. Mg-wustite and Mg-Si-perovskite are stable only below 650 km (Ringwood, 1982; Irifune and Ringwood, 1993) and pyroxene in solid solution with garnet is related to very high pressures corresponding to depths as large as 450 km (Irifune et al., 1989). This suggests that some diamonds have their origin in the transition zone and lower mantle.

7.2 Mineralogy and chemistry of diamond inclusions

101 silicate/oxide inclusions and 56 sulfide inclusions have been recovered from a total of 81 diamonds from Main Fissure, Sugarbird Blow and Marsfontein. 76 of the diamonds have been assigned to the eclogitic paragenesis while 3 diamonds are peridotitic and another 2 are believed to be of a websteritic paragenesis. All recovered sulfide inclusions were assigned to the eclogitic paragenesis based on their low Ni contents. Detailed statistical information on the relative abundance of sulfide and silicate/oxide inclusions is obscured by

biased sampling but sulfide is by far the most common inclusion in Main Fissure and Sugarbird Blow diamonds. The number of Marsfontein diamonds studied is not large enough for a substantive comment on the relative proportions of silicate/oxide and sulfide inclusions. Major element compositions were determined as described in Appendix 5.

7.2.1 Silicate and oxide inclusions

No strictly octahedral or cubo-octahedral morphologies have been observed amongst the silicate and oxide inclusions. However, all inclusions except for clinopyroxene are close to equidimensional and they often have a cubo-octahedral outline with some curved surfaces. Clinopyroxene often fits in to the above description but in some cases exhibits an elongated form. All inclusions are considered to be syngenetic based on the criteria discussed in Section 7.1.1. Recovered inclusions are presented in Table 7.2. It can be seen that the Main Fissure has a strong component of eclogitic diamonds as indicated from silicate and oxide inclusions. For Sugarbird Blow there is an inferred strong eclogitic component but the number of stones is too small to give a statistically significant result. In the case of Marsfontein, the only conclusion that can be drawn is that eclogitic diamonds are present and almost certainly common. Pyrope-almandine and omphacite are equally abundant and dominate the silicate/oxide population with kyanite, coesite, rutile, chrome-pyrope, olivine, orthopyroxene and diopside present only to a minor extent. Multiple inclusions from individual stones are fairly common with up to ten garnets recovered from one diamond (P5-2). However, only seven diamonds carry two or more mineral species and no touching mineral pairs have been found which prevents any thermobarometric investigations of the equilibration conditions immediately before the diamonds were brought up to from the lithosphere. Three diamonds carry non-touching garnet and omphacite which may give information on the temperature of formation of the inclusions and indirectly the diamonds (see Section 7.4).

7.2.1.1 Eclogitic garnet inclusions

Chemical compositions for eclogitic garnet inclusions are found in Appendix 5.1. Throughout this chapter, mineral inclusion compositions are plotted as cations rather than oxides to facilitate an evaluation of cation substitutions and thus the petrogenetic processes responsible for the compositional differences between different inclusions.

Table 7.2 Silicate and oxide inclusions recovered from Main Fissure, Sugarbird Blow and Marsfontein diamonds.

Diamond	Eclogitic inclusions					Peridotitic inclusions		Others
	Pyrope-Almandine	*Omphacite*	*Kyanite*	*Rutile*	*Coesite*	*Pyrope*	*Olivine*	*Orthopyroxene*	
Main Fissure									
P3-1	1								
P3-2						1			
P5-1	1			1					
P5-2	10								
P5-3	4								
P5-9							2		
P6-1	4								
P7-3		1							
P7-4	1								
P7-13	2								
P8-1		1							
P8-2	3	3							
P9-1		1							
P9-2		6							
P9-3					1				
P9-4									1*
P9-6		4							
P9-14		1							
17-2	2								
17-3	1								
17-4		1							
17-7					2				1**
17-13	1								
17-21		3							
A-10	1			3					
MDA-1	3								
950W-1		1							

Table 7.2 continued

Diamond	Eclogitic inclusions					Peridotitic inclusions			Other
	Pyrope-Almandine	*Omphacite*	*Kyanite*	*Rutile*	*Coesite*	*Pyrope*	*Olivine*	*Orthopyroxene*	
Main Fissure									
950W-2	2	1							
950W-3							5	1	
Sugarbird Blow									
SB-1			2						
SB-2	2	6							
Blow-3	1								
Blow-6	1								
TB-5	1								
TB-10		2							
TB-14	2								
NFB		1							
Marsfontein									
M1-1	1								
M1-2	5								
Total:	**49**	**32**	**2**	**4**	**3**	**1**	**7**	**1**	**2**

*Orthopyroxene probably belonging to a websteritic paragenesis
**Clinopyroxene probably belonging to a websteritic paragenesis

Since Ca, Fe and Mg are the only abundant elements that display a substantial variation in eclogitic garnets, their composition can be adequately displayed in a Ca-Fe-Mg plot. In Figure 7.2, garnet inclusion compositions are plotted together with clinopyroxene inclusion compositions which will be presented in the next section. Klipspringer low-Cr garnet inclusions span a very wide compositional range (CaO=3.2-22.5 wt.%, FeO=8.7-21.2 wt.%, MgO=5.5-19.1 wt.%) which covers most compositions displayed by eclogitic garnet inclusions worldwide and extends beyond to compositions highly enriched in the grossular component (Figure 7.2).

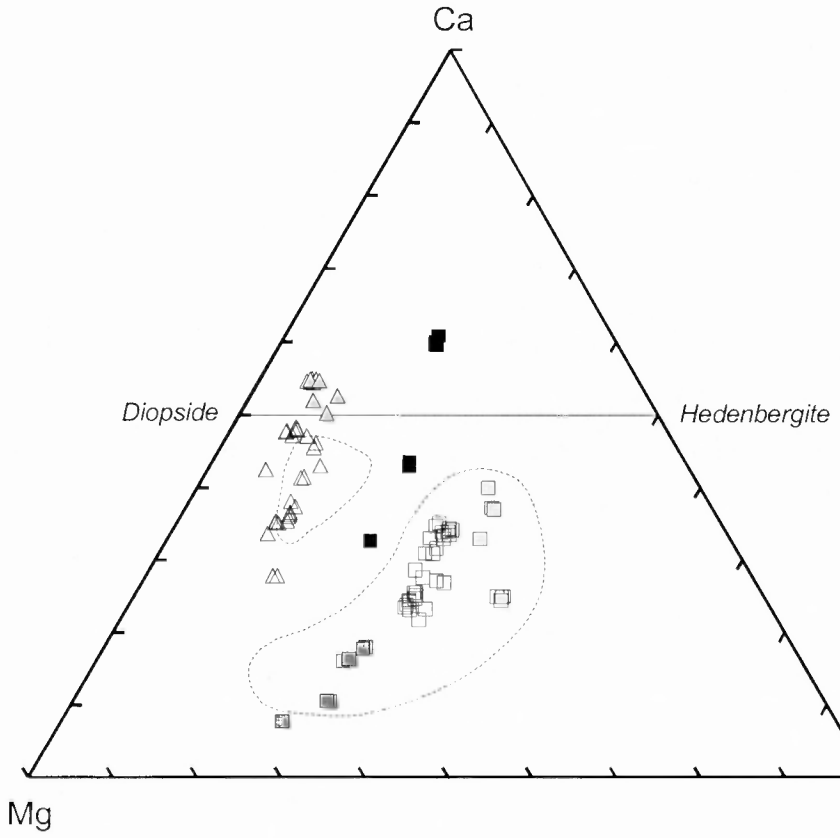

Figure 7.2 Ca-Mg-Fe diagram for Klipspringer eclogitic garnet diamond inclusions (squares: KG-I=white, KG-II=dark grey, KG-III=black, KG-IV=light grey) and clinopyroxene diamond inclusions (triangles: High-Al group=grey). Inserted fields reflect worldwide compositions of eclogitic garnet and clinopyroxene inclusions (from Meyer, 1987). Horizontal line joins the diopside and hedenbergite pyroxene end-members.

Within the wide compositional range, four different groups with restricted compositions and well defined compositional trends can be distinguished. The majority of the garnets form a tightly coherent group (referred to as KG-I, "Klipspringer Garnet inclusions-I") that plot to the Fe-poor, Ca-rich and Mg-rich side of the field for worldwide garnets (Figure 7.2). The most Ca rich garnets in this group are compositionally similar to garnets in diamond bearing

kyanite eclogite xenoliths (Hatton, 1978; Shee, 1978) while the bulk of the garnets trend towards lower Ca. KG-I garnets display a narrow range in Fe for a range in Mg-numbers of 48-57 (Figure 7.3a) and Ca is negatively correlated with Mg-number (Figure 7.3b). The range in Mg-number is a consequence of a concurrent slight decrease in Fe and a pronounced decrease in Mg with the compositional evolution (cp. Figures 7.3c and 7.3d, note the different scales on the y-axes).

KG-II garnets trend away from KG-I garnets towards more refractory compositions (Figure 7.2) with Mg-numbers of 62-72 and they are compositionally similar to garnets from bimineralic eclogite xenoliths (Hatton, 1978; Shee, 1978). Figure 7.3a and 7.3b display continuous trends of increasing Fe and Ca with decreasing Mg-number from KG-II garnets to KG-I garnets. However, Fe increases slightly with decreasing Mg-number for KG-II contrary to KG-I and Ca increases at a slower rate with decreasing Mg-number for KG-II compared to KG-I. Figure 7.3c shows that Fe and Ca are positively correlated for KG-II garnets contrary to KG-I garnets and in Figure 7.3d it can be seen that Mg decreases with Ca at a higher rate for KG-II than for KG-I garnets. The simultaneous increase in Fe and decrease in Mg with increasing Ca (Figures 7.3c and 7.3d) explains the observed range in Mg-number. Large-scale chemical disequilibrium is displayed by multiple inclusions from two diamonds (P5-2 and P8-2) which are represented by their inclusions both in group KG-I and KG-II.

Four inclusions from two diamonds contain very high levels of about 22 wt.% CaO which translates into a grossular component of more than 60 % (Figure 7.2). This level of CaO is distinctly lower than the CaO content of ~ 32 wt.% observed in garnets of the calc-silicate suite from south-eastern Australia (Sobolev et al., 1984) but distinctly higher than garnets from diamond bearing kyanite eclogite xenoliths (Hatton, 1978; Shee, 1978). The composition is similar to what has been observed for garnets in grospydite xenoliths (Lappin, 1978; Smyth and Hatton, 1977). From major element variations it may be inferred that these high-Ca inclusions constitute an end-member of KG-III (Figure 7.2). KG-III displays a range in Mg-number of 53-64 and is distinctly depleted in Fe and enriched in Ca at any Mg-number compared to the other groups (Figures 7.3a and 7.3b). Similar to the other groups, KG-III garnets display well defined trends of decreasing Fe and Mg with increasing Ca (Figures 7.3c and 7.3d). However, contrary to other groups, Fe is positively correlated with Mg# (Figure 7.3a).

KG-IV garnets plot to the Mg-poor, Fe-rich and Ca-rich side of the field for eclogitic garnet inclusions from world-wide localities (Figure 7.2). It can be seen in

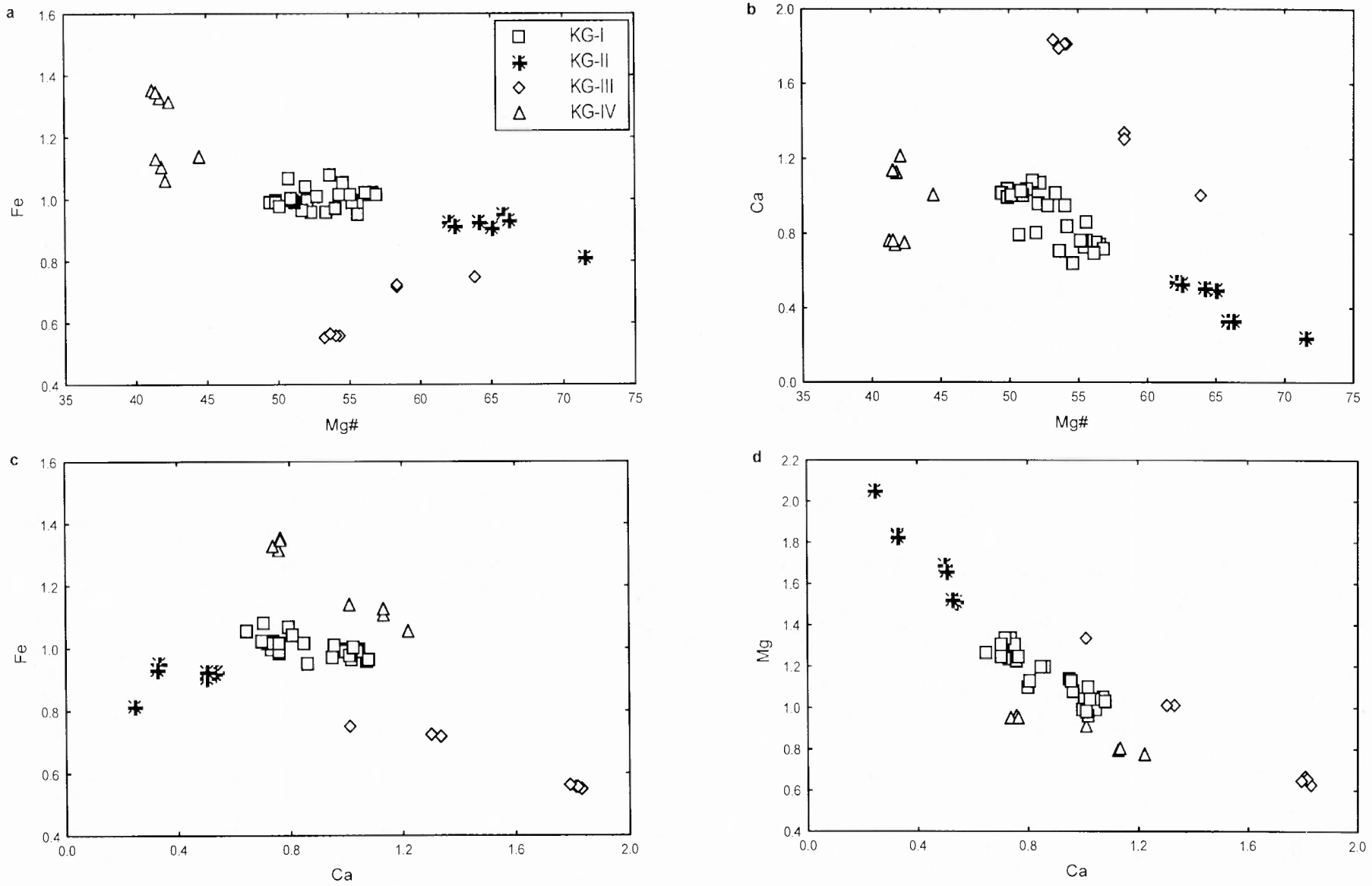

Figure 7.3 Inter-element relationships for diamond inclusion garnets. Units on element axes are in cations per garnet formula unit.

Figure 7.2 that they form a trend of increasing Ca with fairly low and constant Mg-numbers of 41-44. The restricted range in Mg-number is clearly displayed in Figures 7.3a and 7.3b. A comparison of Figures 7.3c and 7.3d reveals that the low Mg-numbers are a consequence of distinctly elevated Fe and lower Mg for KG-IV garnets compared to the other groups. Further the restricted range in Mg-numbers is due to the same rate of decrease in Fe and Mg for the KG-IV garnets (cp. Figures 7.3c and 7.3d, again note the different y-axis scales). Further variation diagrams for the garnet inclusions are shown below in Figure 7.4.

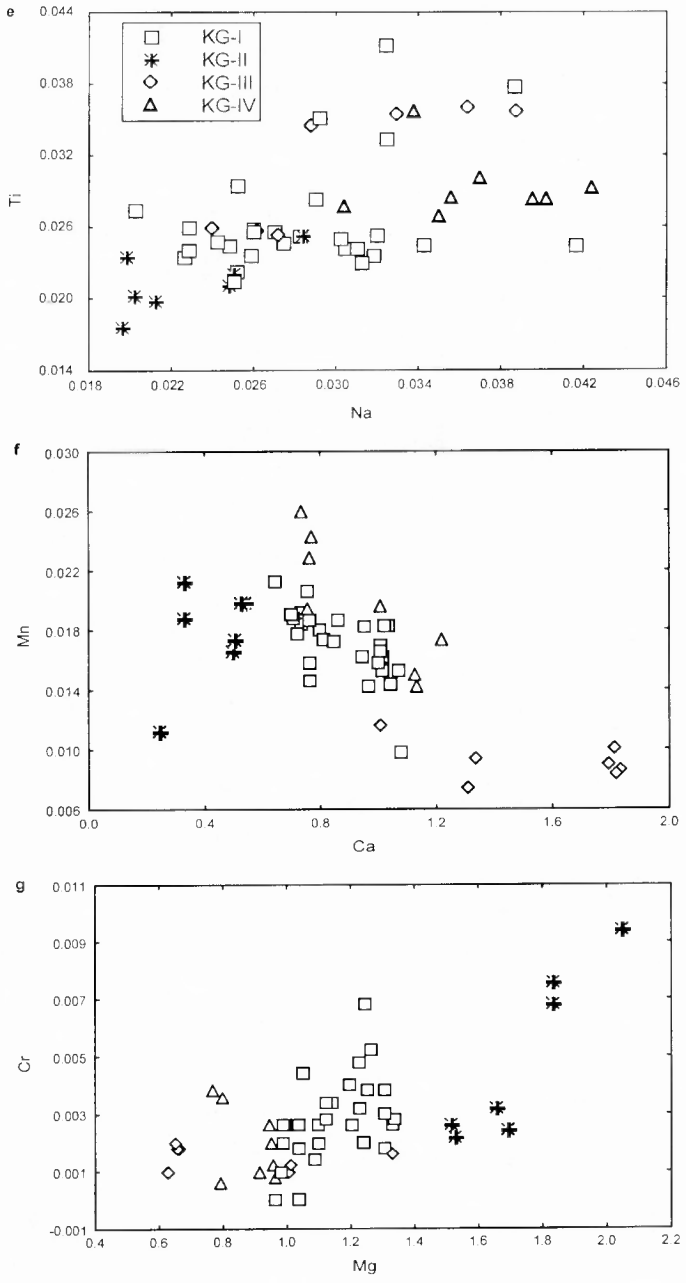

Figure 7.4 Inter-element relationships for the garnet inclusions showing their Ti, Na, Mn and Cr characteristics.

Garnets from all groups contain trace levels of Na (Na_2O=0.14-0.29 wt.%) which is broadly correlated with Ti (Figure 7.4a). KG-II garnets plot to the lower end of the array consistent with their relatively refractory major element character described above and KG-IV trend towards the upper part of the array consistent with their more evolved nature as indicated by their low Mg numbers. Variations in Mn contents mirror that of Fe in accordance with the similar geochemical behaviour of these elements (cp. Figures 7.3c and 7.4b). Cr is broadly correlated with Mg (Figure 7.4c). Again the comparatively depleted and evolved characters of Group II and Group IV respectively are apparent from their high Cr/high Mg and low Cr/low Mg contents. KG-III garnets are very poor in Cr even for increasing Mg and may have formed in an environment almost entirely depleted in Cr.

Multiple inclusions from several KG-I, KG-II and KG-IV diamonds display small but distinctive differences in composition (Figure 7.5). Variations are in most cases outside analytical error and the within diamond variation is often highly systematic as seen when more than two inclusions from one diamond are present. Further, the variations are not concordant with the main geochemical trends displayed by the different KG-groups. The observed small-scale chemical disequilibrium could have several sources of explanation and is discussed further in Section 7.5.

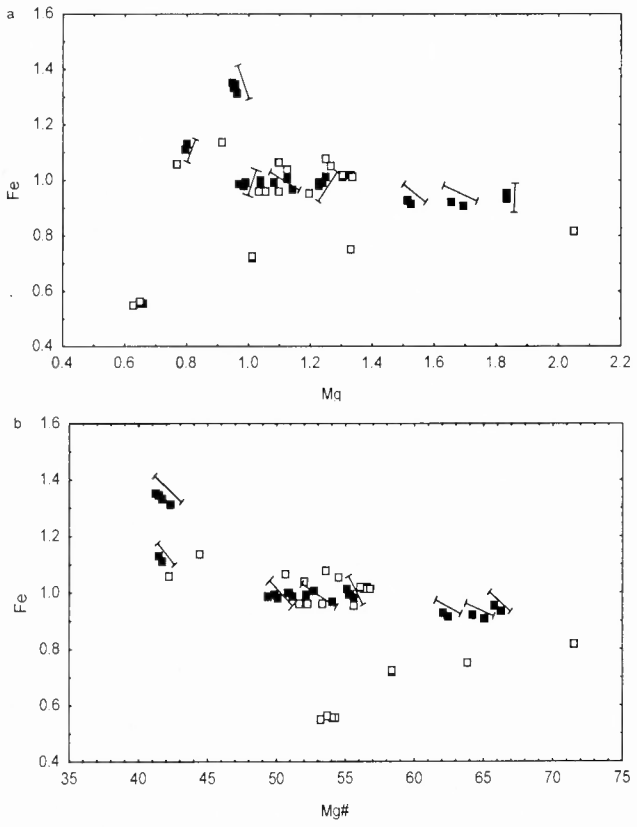

Figure 7.5 Fe-Mg characteristics showing 'small-scale' disequilibrium between multiple inclusions from individual stones (filled squares). 'Small-scale' chemical disequilibrium is high-lighted with arrows.

7.2.1.2 Eclogitic clinopyroxene inclusions

Chemical compositions for eclogitic clinopyroxene inclusions are found in Appendix 5.2. Similar to the garnets, Klipspringer omphacite inclusions display a wide and somewhat unusual range in composition. In a Ca-Mg-Fe diagram (Figure 7.2) they plot partly within and partly outside the Fe-poor side of the field for eclogitic clinopyroxene worldwide (Meyer, 1987) and accordingly have fairly high Mg-numbers of 77-88. This is mainly due to their low FeO contents which range from about 1.5 to 6 wt.% with half of the omphacites having <3 wt.% FeO. Further, the Klipspringer clinopyroxene compositions extend beyond both the most Mg-rich and Ca-rich compositions for clinopyroxene from worldwide locations (Figure 7.2).

Different populations are not as easily recognised for the omphacite inclusions as for the garnet inclusions. The bulk of the omphacites (from now on referred to as the Omphacite Main group "OM") plot below the diopside-hedenbergite join in Figure 7.2 and display a strong positive ~1:1 correlation between Al and Na (Figure 7.6a) indicative of a substantial jadeite component. OM range from low-Al/high-Fe/high-Mg to high-Al/low-Fe/low-Mg (Figure 7.6a-c). In Figures 7.6a and 7.6b three different sub-groups within OM (not the ones indicated in the legend) may be recognised from their different levels of Al, Fe and Na. However, these sub-groups almost certainly have no petrogenetic connotations but are artificial due to lack of data.

Three diamonds (950W-2, P8-2 and SB-2) contain both garnet and omphacite inclusions and the garnets from these diamonds were assigned to KGI-I and KGI-II (see previous section). In Figure 7.6, omphacites from these diamonds have been grouped together with an omphacite from diamond NFB as OM-I. Two other sub-groups within OM (OM-II and OM-III) may be distinguished and the three sub-groups may be discriminated from their Ca and Mg contents (Figure 7.6d). OM-II displays higher Ca than OM-I (Figure 7.6e) while OM-III displays lower Ca and slightly higher Mg (Figure 7.6c) than OM-I. Further, Ca is positively correlated with Na for OM-III contrary to the other groups. OM-III, which displays lowest Ca and highest Mg, may be petrogenetically connected to the most refractory garnets of KGI-II.

Nine omphacites which plot on or above the diopside-hedenbergite join in a Ca-Mg-Fe diagram (Figure 7.2) form a distinct group which is referred to as the High-Al group. These omphacites carry up to 16.3 wt.% CaO and plot distinctly above clinopyroxene from the calc-silicate suite (Sobolev et al., 1984) due to their comparatively lower Mg contents

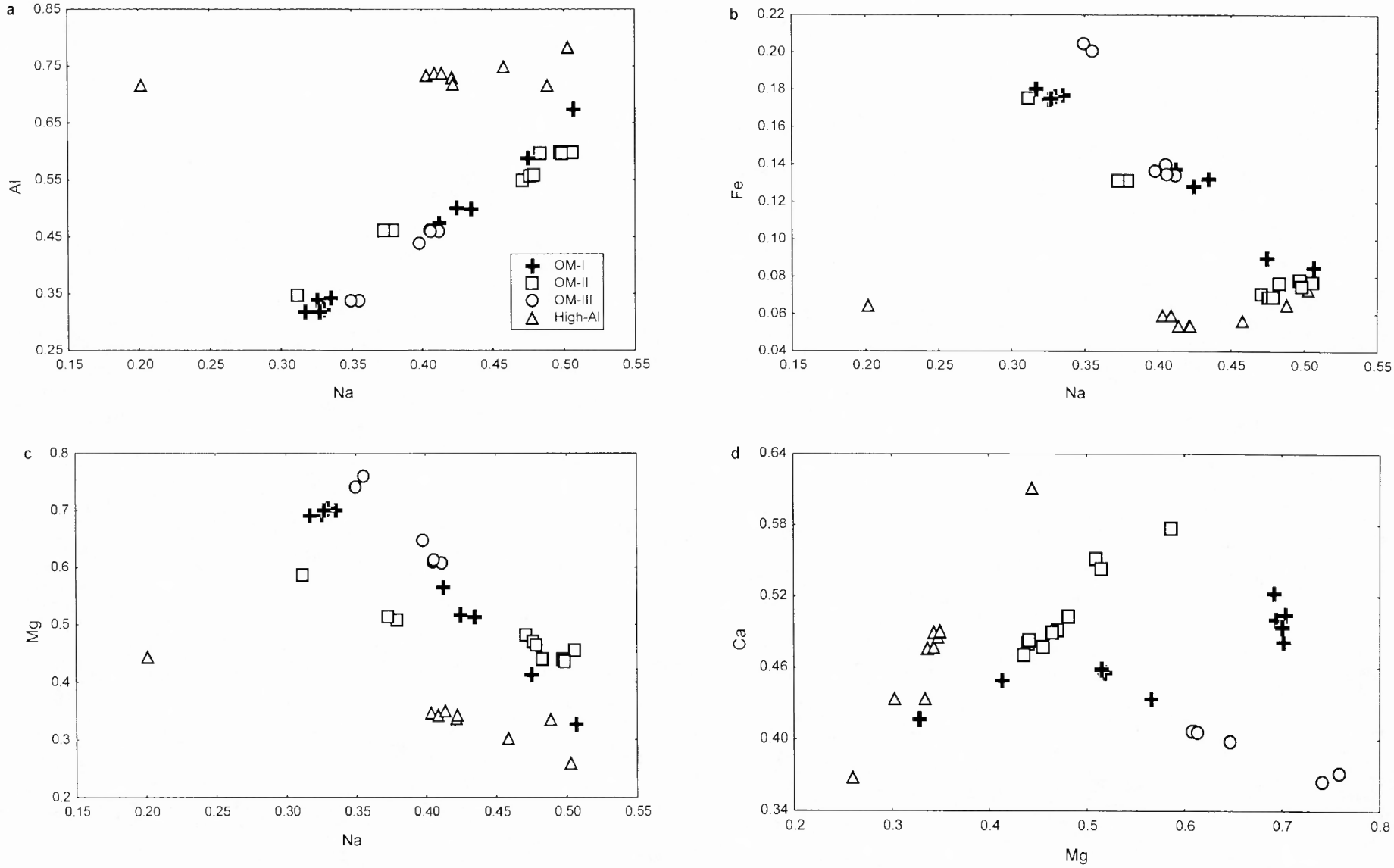

Figure 7.6 Inter-element relationships for diamond inclusion omphacites. Units on element axes are in cations per clinopyroxene formula unit.

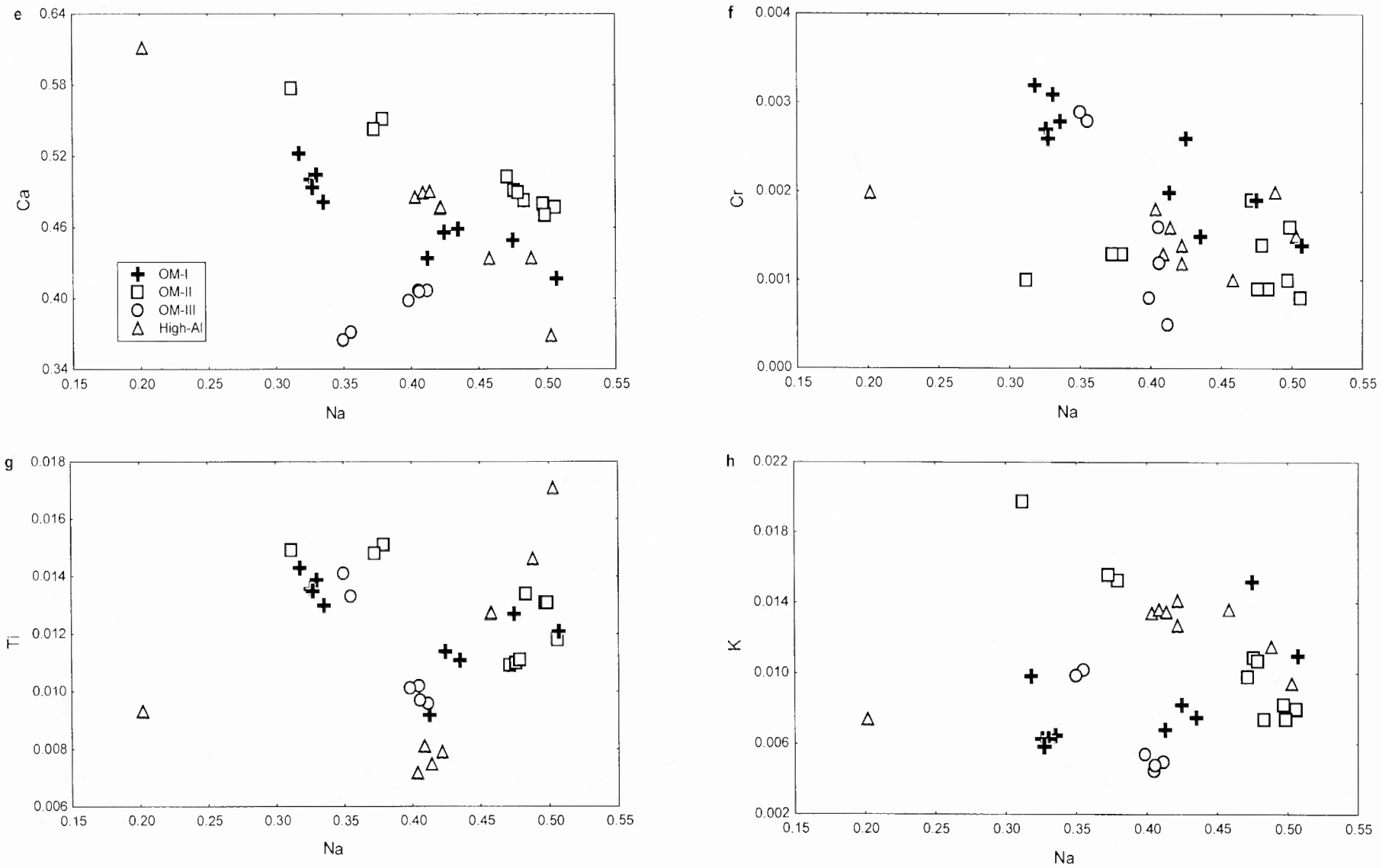

Figure 7.6 continued

and further, they display extremely high Al contents (Al_2O_3 ~17-19 wt.%). The High-Al group is fairly constant in Fe while Ca and Mg decrease with increasing Na (Figures 7.6b, c and e). As in the case of omphacite inclusions worldwide, most Klipspringer omphacites are compositional mixtures of the jadeite ($NaAlSi_2O_6$) and diopside-hedenbergite $Ca(Fe,Mg)Si_2O_6$ end-members (Meyer, 1987) with enrichment in the jadeite component as indicated from a strong positive correlation between Na and Al. Jaques et al. (1989) report on omphacites with Al_2O_3 up to 20 wt.% accommodated almost entirely as jadeite. Klipspringer High-Al omphacites deviate from a correlation between Na and Al to lower Na (Figure 7.6a) which cannot support the accommodation of Al entirely as jadeite. Clinopyroxene end-members have been calculated according to Hatton (1978) and are shown in Appendix 5.5. Most omphacites range between Jd21-Jd52 and Di23-Di56 with up to 27 % enstatite in P9-1 and up to about 12 % Ca-tschermakite that accommodates some Al. The High-Al clinopyroxenes show various amounts of site deficiency as evident from cation totals lower than four. Cawthorn and Collerson (1974) and Wood (1976) report on site deficiency in aluminous pyroxene, which has been ascribed to vacancies in the M2 site, and the pseudojadeite component ($Ca_{0.5}AlSi_2O_6$) has been invoked as an explanation for the site deficiency (Cawthorn and Collerson, 1974; Smyth 1977; Smyth, 1980). The High-Al group omphacites have calculated pseudojadeite between 7 and 18 % with sample P9-2e showing an extremely high pseudojadeite content of 28 %. Six of the High-Al omphacites are from diamond P9-2 and they display "large-scale" major element disequilibrium similar to some KG-I/KG-II garnets.

Klipspringer omphacites display ranges of 0.03-0.12 wt.% Cr_2O_3, 0.27-0.67 wt.% TiO_2, and 0.10-0.42 wt. % K_2O which are similar to what is normally observed for omphacite diamond inclusions (e.g. Gurney et al., 1979a,b; Gurney et al., 1985). None of the designated groups displays systematically higher or lower levels of either Cr, Ti or K compared to the other groups (Figure 7.6f, 7.6g and 7.6h). However, it is interesting to note that the most Na-poor clinopyroxene in the High-Al group also is slightly depleted in K.

7.2.1.3 Other eclogitic inclusions

As can be seen in Table 7.2, besides pyrope-almandine and omphacite, kyanite, coesite and rutile have been identified as eclogitic inclusions. Chemical compositions for these inclusions are given in Appendix 5.3. Two kyanites with distinctively light blue colour were the only inclusions present in diamond SB-1 and thus cannot be directly associated with any

pyrope-almandine or omphacite compositions. The compositions of the kyanites are close to stoichiometric kyanite with some Fe present (FeO=0.23 wt.% and 0.27 wt.%). As mentioned in section 7.2.1.1, some garnet inclusions of group KG-I mirror the compositions of kyanite bearing eclogites and the most Ca rich garnets of group KG-III were classified as grospydite garnets. Thus the kyanites may be related to either of these parageneses.

Coesite has been found as single inclusions in diamonds (e.g. Gurney et al., 1984a; Hall and Smith, 1984; Moore and Gurney, 1989; Daniels and Gurney, 1989) and Otter and Gurney (1989) reported on a coesite inclusion coexisting with a pyrope-almandine with a grossular component of 35 %. Sobolev (1983) defined a coesite eclogite diamond inclusion paragenesis devoid of kyanite and different to a kyanite eclogite diamond inclusion paragenesis devoid of coesite. Coesite in eclogite xenoliths is rare but has been reported from a grospydite carrying garnet with about 19 wt.% CaO (Smyth and Hatton, 1977). One inclusion with a composition close to pure SiO_2 from diamond P9-3 and two from diamond 17-7 have been recovered. Although the minerals have not been identified with X-ray diffractometry, they are believed to be coesite rather than quartz from their primary setting within the diamonds similar to other inclusions. While in diamond P9-3, the coesite occurred as a single inclusion, diamond 17-7 also carried a clinopyroxene believed to belong to a websteritic paragenesis (see section 7.2.1.5).

Rutile has quite commonly been observed as a diamond inclusion (e.g. Otter and Gurney, 1989; Daniels and Gurney, 1989) and in diamonds from Western Australia rutile coexists with omphacite, pyrope-almandine and coesite inclusions (Hall and Smith, 1984). Sobolev (1983) reported on rutile present in a wide variety of Siberian eclogitic diamond inclusion parageneses from bimineralic (pyrope-almandine/omphacite) to grospydites. One rutile from diamond P5-1 and three from diamond A-10 have been recovered. The rutiles carry minor quantities of Fe and Al similar to other diamond inclusion rutiles while their low Cr contents are different from rutile in metasomatised peridotites (Haggerty, 1989). Both diamonds also carried garnets that are amongst the lesser evolved group KG-I garnets (low Ca, high Fe, high Mg) which suggests that Klipspringer rutile inclusions are related to a paragenesis with a composition similar to bimineralic eclogites.

7.2.1.4 Peridotitic inclusions

Chemical compositions for recovered peridotitic inclusions are given in Appendix 5.4. A pyrope with a composition of 24.6 wt.% MgO, 1.72 wt.% CaO and 12.5 wt.% Cr_2O_3

occurred as a single inclusion in diamond P3-2. The sub-calcic nature of the pyrope precludes that it crystallised in equilibrium with clinopyroxene but is indicative of a harzburgitic or dunitic paragenesis. Grutter (1998) showed that sub-calcic garnet xenocrysts of the dunitic paragenesis generally have less than about 10 wt.% Cr_2O_3 for CaO<1.8 wt.% while those of the harzburgitic paragenesis can have 6-16 wt.% Cr_2O_3 at these low levels of CaO. This suggests that the recovered pyrope should be assigned to a harzburgitic rather than a dunitic paragenesis.

Two and five olivines were recovered from diamonds P5-9 and 950W-3 respectively. Fe and Mg contents for all olivines yield Mg-numbers of 93, which is in the middle of the range displayed by peridotitic olivine inclusions worldwide (Meyer, 1987). Chromium ranges up to fairly high levels of 0.11 wt.% Cr_2O_3 while Ni contents (0.23-0.30 wt.%) are slightly lower than commonly observed (e.g. Daniels and Gurney, 1989; Moore and Gurney, 1989) At some localities bimodal distributions of Mg-number for olivine inclusions have been observed. Daniels and Gurney (1989) reported that less refractory olivines (Mg#=92) did not co-exist with sub-calcic garnet inclusions. Moore and Gurney (1989) assigned a less refractory group of olivine inclusions (Mg#=90-92) to a lherzolitic paragenesis and Gurney et al. (1985) assigned less refractory olivine inclusions (Mg#=91-93) to a harzburgitic paragenesis different from a harzburgitic paragenesis to which a more refractory population (Mg#=94.5-95) was assigned. The fairly high Mg-number and Cr contents of Klipspringer olivine inclusions suggests that they are related to the sub-calcic pyrope of a harzburgitic paragenesis described above while it cannot be ruled out that the olivines belong to a dunitic paragenesis.

An orthopyroxene was recovered from the same diamond (950W-3) as five of the olivines presented above. The orthopyroxene has a Mg-number of 94 which is in the middle of the range displayed by orthopyroxene inclusions from worldwide localities (Meyer, 1987). In this respect it is similar to the olivines recovered from the same diamond. Its composition (Mg#=94, CaO=0.47 wt.% and Cr_2O_3=0.45 wt.%) precludes equilibration with clinopyroxene which, together with its co-occurrence with the olivines described above, suggests that it formed in equilibrium with the olivines and should be assigned to a harzburgitic paragenesis or perhaps a dunitic paragenesis.

7.2.1.5 Websteritic inclusions

One clinopyroxene from diamond 17-7 differs from the omphacite inclusions described above with distinctly lower K, Na, Ti, and Al and higher Mg and Ca (Appendix 5.2). Its low Cr_2O_3 (0.17 wt.%) is not consistent with a peridotitic origin while Cr_2O_3 and MgO (18 wt.%) is higher than expected for calc-silicate suite clinopyroxenes (Meyer, 1987). It is suggested that this clinopyroxene is a fairly refractory representative of a websteritic paragenesis. As mentioned above, diamond 17-7 as well carries coesite inclusions. Coesite has never before been found as an inclusion coexisting with websteritic minerals or in websteritic xenoliths. It may be that diamond 17-7 has grown in two separate environments at different stages of the diamond growth.

A single orthopyroxene recovered from diamond P9-4 displays a distinctly lower Mg- number (Mg#=90) than the orthopyroxene of a harzburgitic paragenesis described above (Appendix 7.4). Further, it is virtually deficient in Cr and carries about 0.8 wt.% and 0.3 wt.% CaO and Na_2O respectively. Since the Mg-number of mafic mineral inclusions commonly is higher than their xenolith counterparts, this orthopyroxene is not likely to belong to a dunitic, harzburgitic or lherzolitic paragenesis. Rather, it should be ascribed to a websteritic paragenesis.

It must here be noted that a garnet from diamond Blow-6 which was assigned to group KG-II garnets above has a composition which is indistinguishable from many websterite xenolith garnets (e.g. from Orapa; Shee, 1978 or Roberts Victor; Hatton, 1978). However, while it is impossible to assign this garnet to one or the other paragenesis it will remain classified as an eclogitic KG-II garnet.

7.2.2 Sulfide inclusions

Klipspringer sulfide inclusions often occur as multiple inclusions that are located close to the centre of the diamond which is suggestive of a syngenetic relationship between the sulfide and the host diamond. The size of the recovered inclusions range from about 60 to 300 μm. Main Fissure and Sugarbird Blow sulfides differ somewhat from Marsfontein sulfides regarding morphology. The former are bulky, most often with fairly well developed crystal faces that are slightly rounded but define a cubo-octahedral outline. Occasionally one or more crystal faces are completely planar. Further, the sulfides display an irregular surface structure with pits up to 20 μm in size showing a rectangular or hexagonal outline.

These pits have been observed only in pyrrhotite and have not been observed in chalcopyrite. Corresponding topographically elevated features have not been observed in inclusion pits in cracked diamonds, which excludes the structures being imposed by diamond. The pits may represent sites of entrapment of fluids, which in such a case could provide a new way to study the composition of fluids associated with diamond growth in a sulphur-rich environment. Marsfontein sulfides do not display this pitted surface texture but are bulky with well developed planar crystal surfaces and exhibit cubo-octahedral or more irregular forms. All sulfides studied are surrounded by black rosettes in contrast to silicate inclusions. None of the rosettes have been analysed for chemistry but display colours reminiscent of chalcopyrite and bornite.

In the interpretation of the mineralogy it is important to note that the sulfides were polished down to a minimum surface area needed for accurate ion-probe analyses in order to save the bulk of the sulfides for Re-Os analyses. Thus, the exposed mineralogy may not be representative of the whole grain. However, all sulfides were polished in random crystallographic directions and yet they display great similarities mineralogically, which suggests that the mineralogy observed for an individual grain is broadly representative of the whole grain. Sulfides from the Main Fissure and Sugarbird Blow exhibit similar mineral chemistry and are described as one population below. Chemical compositions of the sulfides are given in Appendix 5.5.

Individual inclusions from the Main Fissure and Sugarbird Blow are dominated by pyrrhotite, which always constitutes more than 90 % of a grain. Pyrrhotite is close to Fe_7S_8 in composition but contains up to 2.4 wt.% nickel which either substitutes for Fe in the pyrrhotite structure or occurs in sub-microscopic pentlandite exsolution. Copper and cobalt concentrations in pyrrhotite reach a maximum of 0.4 and 0.2 wt.% respectively. Pentlandite occurs as flame-like exsolution (maximum 5 μm wide and 40 μm long) and reaches up to about 10 % in modal abundance. Variations in nickel and cobalt concentrations in pentlandite are artefacts due to difficulties in analysing the fine scale exsolution. Total nickel content of the Main Fissure and Sugarbird Blow sulfide inclusions, as estimated from the nickel contents of pyrrhotite and pentlandite, range between 1-5 wt.% which is indicative of eclogitic sulfides (Bulanova et al., 1996) as discussed in Section 7.1.2. Chalcopyrite always occurs at the rim of the crystals and is close to stoichiometric chalcopyrite in composition. When pentlandite is in contact with chalcopyrite the former always occurs around the rim of the latter indicating descending crystallization order from chalcopyrite to pentlandite. Marsfontein sulfides fit into the mineralogical description above

but the sample cannot be taken as fully representative of Marsfontein sulfides since inclusions from only three diamonds have been studied. Pyrrhotite in the Marsfontein sulfides appears to be slightly higher in nickel (1.8-4.8 wt.%) than pyrrhotite in the Main Fissure and Sugarbird Blow sulfides. However, this might be due to sub-microscopic pentlandite exsolution.

Experiments on phase relations in the Cu-Fe-Ni-S system (Craig and Kullerud, 1969) show that above 1000 °C a pyrrhotite-rich Fe-Ni monosulfide solution coexists with sulfide melts. With decreasing temperatures from 1000 °C pyrrhotite becomes enriched in nickel relative to the sulfide fluid and at 850 °C chalcopyrite crystallises and coexists with a monosulfide solution carrying a maximum of 30 % nickel. At 610 °C pentlandite appears through exsolution from the monosulfide solution. This suggests that the observed mineral relations are consistent with incorporation of a monosulfide solution and a co-existing sulfide fluid at the time of diamond formation. It is believed that rapid decompression during transport of the diamonds to surface has generated cracks around the inclusions and subsequently chalcopyrite nucleated and grew at the monosulfide solution/diamond interface as well as in decompression cracks surrounding the inclusion creating the black rosettes described above. With decreasing temperature pentlandite exsolved from the monosulfide solution and left pure pyrrhotite behind.

7.3 Estimation of eclogite compositions from mineral inclusion chemistry

7.3.1 Samples and background for the estimations

As mentioned in section 7.2.1, three diamonds (950W-2, P8-2 and SB-2) carry both pyrope-almandine and omphacite as non-touching inclusions. Further, in diamond P8-2, two distinctive compositions of both pyrope-almandine and omphacite were observed. In a Ca-Mg-Fe plot (Figure 7.7), tie-lines connecting the different pairs do not cross which indicates that the minerals in the individual pairs may have been in chemical equilibrium at crystallisation. Bulk rock eclogite compositions have been estimated from these pairs in order to compare the compositions with possible protoliths. Bulk rock chemistry was also estimated from KG-III garnets and High-Al omphacites since they may be petrogenetically related as proposed in Section 7.5. In this case estimations were made for the most evolved minerals from each group, as indicated by major element variations.

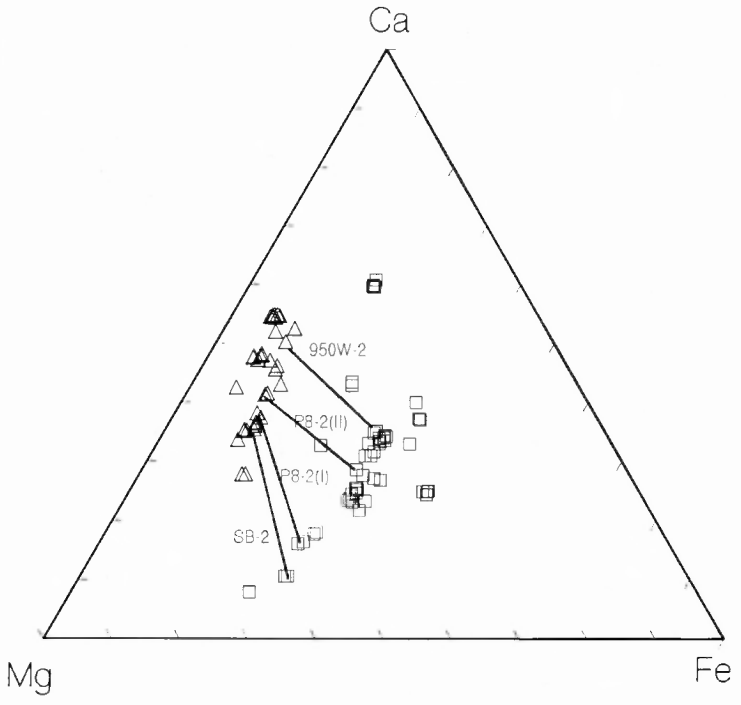

Figure 7.7 Ca-Mg-Fe diagram for eclogitic garnet (squares) and omphacite (triangles) inclusions. Non-touching garnet and omphacite inclusion pairs from individual diamonds are connected with tie-lines.

Bulk rock compositions have been estimated assuming equal modal amounts of garnet and clinopyroxene. The minerals from diamond 950W-2 are similar in composition to their counterparts in kyanite eclogites and the most evolved KG-III garnet (P3-1) and High-Al omphacite (P7-3) are similar in composition to these minerals in grospydites (Section 7.2.1). Kyanite eclogites and grospydites commonly carry between 5 and 20 modal per cent kyanite (e.g. Ater et al., 1979; Shee, 1978; Smyth and Hatton, 1977; Lappin, 1978). Therefore, bulk rock estimations based on inclusions from 950W-2 and P3-1/P7-3 were also performed assuming 10 and 20 modal % kyanite. The estimations took into consideration the specific weight of each mineral.

7.3.2 Estimated bulk rock compositions

The results are presented in Table 7.3. Selected compositions for mid-ocean ridge basalts (MORB), mid-ocean ridge (MOR) cumulates and Archaean komatiites which have been suggested as protoliths for mantle eclogites (see Chapter 1) are given in Table 7.4. All estimated compositions display low levels of SiO_2 which range from 44.2 wt.% to 46.5 wt.%. This level of SiO_2 is below that generally displayed by MORB and MOR cumulate

Table 7.3 Bulk rock compositions estimated from garnet and omphacite inclusion. Equal modal proportions of garnet and omphacite were assumed and specific gravities of the minerals were used to estimate weight proportions. Indices (0,) (10) and (20) indicates the modal% of kyanite assumed.

	SB-2	P8-2(I)	P8-2(II)	950W-2(0)	950W-2(10)	950W-2(20)	P3-1/P7-3(0)	P3-1/P7-3(10)	P3-1/P7-3(20)
SiO_2	46.8	46.9	46.7	46.1	45.2	44.2	46.7	45.7	44.6
TiO_2	0.48	0.38	0.55	0.44	0.41	0.38	0.63	0.58	0.53
Al_2O_3	15.4	17.5	17.5	19.2	23.7	28.1	20.6	25.0	29.3
Cr_2O_3	0.12	0.06	0.06	0.06	0.06	0.05	0.04	0.04	0.03
FeO	10.9	10.2	10.2	9.46	8.53	7.60	5.90	5.34	4.77
MnO	0.21	0.18	0.18	0.14	0.12	0.11	0.09	0.08	0.07
MgO	15.0	13.1	10.3	7.86	7.08	6.29	5.38	4.84	4.31
CaO	8.28	8.69	11.3	12.2	11.0	9.71	16.6	14.9	13.2
Na_2O	2.30	2.89	3.04	3.52	3.17	2.81	3.59	3.23	2.87
K_2O	0.08	0.07	0.08	0.11	0.10	0.09	0.10	0.09	0.08
Total	99.6	99.9	99.9	99.1	99.3	99.4	99.6	99.8	99.8

Table 7.4 Selected compositions of MORB, MOR cumulates and komatiites from the literature. Total Fe is given as either FeO or Fe_2O_3.

	MORB (1)	MORB (2)	Cumulate (3)	Cumulate (3)	Cumulate (3)	Cumulate (3)	Cumulate (3)	Cumulate (3)	Cumulate (3)
SiO_2	49.7	49.4	48.9	50.5	48.1	47.2	45.3	50.0	50.0
TiO_2	1.55	1.37	0.34	0.31	0.17	0.12	0.10	0.34	0.06
Al_2O_3	15.2	15.9	15.6	20.5	25.0	19.7	22.0	17.5	29.1
Cr_2O_3									
FeO	10.3	9.54							
Fe_2O_3			8.17	4.65	3.29	4.59	5.09	3.87	1.44
MnO	0.18	0.17	0.13	0.08	0.05	0.08	0.07	0.08	0.02
MgO	8.01	7.14	14.8	8.34	7.02	14.0	14.3	9.45	3.00
CaO	11.2	11.1	11.4	13.0	14.2	12.8	11.3	16.0	13.1
Na_2O	2.59	2.74	1.78	2.67	2.07	1.21	1.02	1.86	3.21
K_2O	0.30	0.33	0.02	0.02	0.01	0.04	0.28	0.01	0.02
Total	100.28	100.25	101.17	100.02	99.95	99.67	99.38	99.11	99.93

	Komatiite (4)	Komatiite (5)	Komatiite (5)	Komatiite (6)	Komatiite (6)	Komatiite (6)
SiO_2	49.1	47.3	41.5	50.1	48.5	52.6
TiO_2	0.41	0.35	0.48	1.21	1.30	0.65
Al_2O_3	4.65	7.95	9.60	9.91	10.0	6.96
Cr_2O_3	0.37					
FeO	11.4	11.9	13.5	13.5	14.5	11.1
Fe_2O_3						
MnO	0.20	0.20	0.25	0.18	0.23	0.17
MgO	23.2	24.9	21.9	11.0	10.8	13.1
CaO	10.2	7.18	6.30	11.8	12.1	10.8
Na_2O	0.03	0.01	0.04	0.26	0.22	0.11
K_2O	0.28	0.22	0.32	1.24	1.54	1.61
Total	99.84	99.98	93.89	99.13	99.19	97.14

1. le Roex et al. (1987), MORB from the Mid-Atlantic ridge
2. le Roex et al. (1989), MORB from the Southwest Indian ridge
3. Meyer et al. (1989), MOR cumulates from the Southwest Indian ridge
4. Parman et al. (1997), Komatiite from the Barberton greenstone belt, South Africa
5. Polat et al. (1999), Komatiites from the late Archaean Wava greenstone belts, Superior Province, Canada
6. Jahn et al. (1982), Basaltic komatiites of the Onverwacht Group, South Africa

while the latter may display this level of SiO_2 and komatiites may range down to ~ 40 wt.% SiO_2.

The reconstructed bulk rocks span a wide range in composition. SB-2 displays the most refractory composition with 46.8 wt.% SiO_2, 10.9 wt.% FeO, 15.4 wt.% Al_2O_3 and 8.28 wt.% CaO. SB-2 is compositionally similar to the most refractory MOR cumulates (Table 7.3) while its MgO content is higher than what is commonly observed for MORB. Komatiites may range down to ~ 15 wt.% MgO (and down to ~ 10 wt.% MgO for basaltic komatiites) while the Al_2O_3 content of SB-2 is distinctly higher compared to that generally displayed by komatiites.

The bulk rock composition for 950W-2 is sensitive to the modal abundance of kyanite assumed (cp. 950W-2(0), 950W-2(10) and 950W-2(20)). Estimated compositions display ranges of 6.29-7.86 wt.% MgO, 7.60-9.46 wt.% FeO, 19.2-28.1 wt.% Al_2O_3 and 9.71-12.2 wt.% CaO. All compositions are too fertile to be akin to komatiite. Further, even the most refractory composition (950W-2(0); kyanite-free estimation) display distinctly higher Al_2O_3 (19.2 wt.%) than commonly displayed by MORB. All estimated compositions are however covered by the compositional range displayed by the MOR cumulates. 950W-2(0) (kyanite-free estimation) is similar in composition to kyanite bearing eclogite (Hatton, 1978; Shee, 1978) while if 10 modal % and 20 modal % kyanite is added to the mineralogy (950W-2(10) and 950W-2(20)) respectively Al_2O_3 distinctively exceeds the range observed for kyanite eclogite and enters that of grospydite (Smyth and Hatton, 1977; Lappin, 1978). Since garnet from 950W-2 is akin to kyanite bearing eclogite garnet rather than grospydite garnet, this suggests that only minor kyanite was associated with the 950W-2 paragenesis. Thus, the composition of a hypothetical protolith for this paragenesis is probably closer to that of 950W-2(0) than those of 950W-2(10) and 950W-2(20).

Chemical compositions for P8-2(I) and P8-2(II) are similar to each other and intermediate between those of SB-2 and 950W-2(0). They display compositions of 13.1 wt.% and 10.3 wt.% MgO respectively, 10.2 wt.% FeO, 17.5 wt.% Al_2O_3 and 8.69 wt.% and 11.3 wt.% CaO respectively. P8-2(I) and P8-2(II) are much too elevated in Al_2O_3 to resemble even basaltic komatiites while they are fairly similar to MORB in composition. However, their MgO and Al_2O_3 contents are slightly higher than what is commonly observed for MORB while they are compositionally akin to some MOR cumulates.

As for 950W-2, the estimated bulk rock chemistry based on P3-1 (garnet) and P7-3 (omphacite) is dependent on the assumed modal content of kyanite. The estimated compositions display ranges of 4.31-5.38 wt.% MgO, 4.77-5.34 wt.% FeO, 20.6-29.3 wt.%

Al_2O_3 and 13.2-16.6 wt.% CaO. These compositions are all distinctly higher in CaO and Al_2O_3 and lower in FeO and MgO compared to MORB and komatiite. The whole estimated compositional range however falls within that of MOR cumulates. P3-1/P7-1(20) with 20 modal % kyanite is very similar in composition to a grospydite from Roberts Victor, which contains 20 modal % kyanite (Lappin, 1978).

Estimated contents of K_2O (0.07-0.011 wt.%) are similar to those of komatiites and MOR cumulates while they are three to four times lower than those of MORB. Similar to K_2O, estimated Na_2O contents (2.60-3.60 wt.%) are similar to those of MOR cumulates. Further, bulk rock levels of Na_2O are similar to those of MORB while they are distinctly higher than Na_2O of komatiites and about two times higher than Na_2O of basaltic komatiites. Estimated TiO_2 contents display a range of 0.40-0.60 wt.%. which is similar only to komatiites. Bulk rock estimations of TiO_2 are lower than basaltic komatiites and distinctly lower than MORB while they are similar to the TiO_2 content of komatiites.

The Al, Ti and Si contents of the reconstructed bulk rocks are heavily dependent on the assumed amount of kyanite, rutile and coesite respectively. Thus, they will be spurious if the assumed modal amount of these minerals is different from the true modal amount in an eclogitic precursor rock. Estimated contents of K and Na, which exclusively occur in garnet and clinopyroxene respectively, are sensitive to the assumed modal abundance of these minerals. Further, large-ion lithophile elements like K and high field strength elements like Ti are very sensitive to partial melting and/or metasomatism of the protolith. Fe, Ca and Mg are the elements which best can reflect the compositions of hypothetical protoliths. In Figure 7.8, FeO and CaO are plotted versus MgO for all estimated bulk-rock compositions. A "dilution" effect from the presence of kyanite is clearly displayed by samples P3-1/P7-3 and 950W-2 for which FeO, CaO and MgO increase with decreasing amount of kyanite. It must be noted that similar "dilution" effects would be caused by the presence of coesite and rutile. The latter has been recovered from diamonds which also carried garnet with a composition similar to the garnets from diamond P8-2 (Section 7.2.1.3). In Figure 7.8, a broad negative correlation between CaO and MgO is apparent. This correlation is very well constrained if sample P-1/P7-3 carries 10 or 20 modal% kyanite and sample 950W-2 is deficient in kyanite as suggested above. Further, it can be seen that FeO and MgO are broadly correlated and FeO increases with increasing MgO.

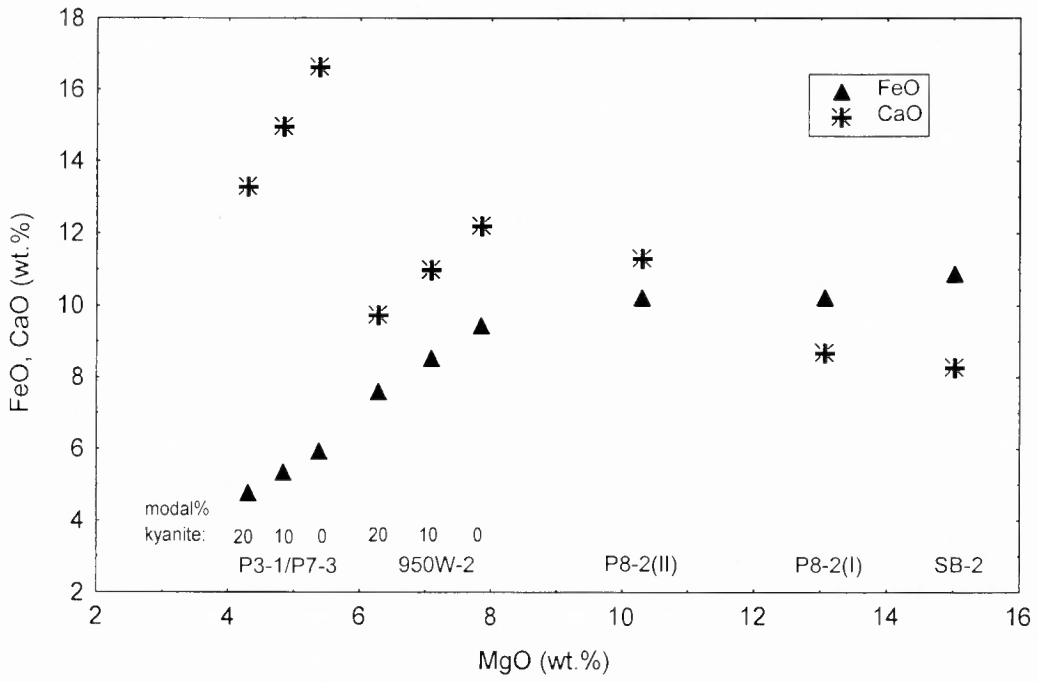

Figure 7.8 Inter-element relationships for bulk compositions estimated from garnet and omphacite inclusion pairs discussed in the text.

7.4 Diamond inclusion geothermometry

As mentioned in Section 7.3.1, touching minerals suitable for pressure or temperature estimations are absent while non-touching garnet/clinopyroxene pairs were recovered from three diamonds. This may allow for estimations of formation temperatures for these minerals and indirectly the diamond host. Temperatures have been estimated using the experimentally calibrated geothermometers of Ellis and Green (1979), Krogh (1988), Ai (1994) and Berman et al. (1995). For a background to Fe^{2+}-Mg cation exchange geothermometry as well as a comparison and evaluation of the different geothermometers, see Chapter 4.

Temperature estimations are subject to some assumptions. A true temperature will only be obtained if the minerals were in chemical equilibrium at the time of formation. This cannot simply be assumed since the inclusions may have been incorporated into the diamond at different times, in different chemical environments and/or under different temperature conditions. This may be the case for some inclusions as evident from the 'large-scale' disequilibrium observed for multiple garnet inclusions from two diamonds (see above). Another source of error is that the amount of Fe^{3+} in the minerals is not known since

electron microprobe analysis cannot discriminate between Fe^{2+} and Fe^{3+}. However, diamonds are believed to originate from a comparatively reduced lithosphere (Haggerty, 1986) and it is assumed that all iron is present as Fe^{2+}.

7.4.1 Samples for geothermometry

Klipspringer garnet and clinopyroxene diamond inclusions were shown above in a Ca-Mg-Fe diagram (Figure 7.7) with tie-lines connecting non-touching garnet and omphacite from diamonds 950W-2, P8-2 and SB-2. In the case of diamonds P8-2, both garnets and omphacites display different chemical compositions. These compositions were combined so that tie-lines are not crossing (P8-2(I) and P8-2(II)) since this more likely connects co-genetic inclusions that were in chemical equilibrium with each other at the time of formation. No tie-lines are crossing which suggests, or at least does not preclude, that the different mineral pairs crystallised under equilibrium conditions. In some cases, multiple inclusions of both garnet and omphacite from individual diamonds display very similar compositions (Appendix 5.1 and 5.2). In these cases, electron microprobe analyses that yielded analytical totals less than 99 wt.% or above 101 wt.% were excluded and an average chemical composition was calculated from the rest of the minerals. None of the clinopyroxenes contain more than 70 mole % jadeite and non-ideal mixing of Na in clinopyroxene is therefore believed to be unimportant (see end of Section 4.4.1)

7.4.2 Formation temperatures of diamond inclusions

Calculated temperatures for assumed pressures of 50 and 60 kbars are given in Table 7.5. Temperatures estimated using the Berman et al. (1995) geothermometer (from now on referred to as BER) at 50 kbars range from 892 °C (950W-2) to 1138 °C (SB-2) and they are conspicuously low. BER temperatures display a negative correlation with the molar abundance of Ca occupying the M1 site of garnet (X_{Ca}). It was suggested in Chapter 4 that BER may not account properly for the non-ideal substitution of Ca in garnet (and omphacite) which is further indicated here and BER temperatures are believed to underestimate the true temperature.

The Ai (1994) geothermometer (from now on referred to as AI) yield the highest temperatures which range from 1223 °C (P8-2(I)) to 1320 °C (P8-2(II)) at 50 kbars and

Table 7.5 Temperatures estimated from garnet-clinopyroxene diamond inclusions from individual diamonds. Temperatures were estimated at assumed pressures (P) of 50 and 60 kbars using the Ellis and Green (1979) (EG), Krogh (1988) (KR), Ai (1994) (AI) and Berman et al. (1995) (BER) geothermometers.

Sample	lnK_d	X_{Ca}	$Mg\#_{grt}$	T(EG)		T(KR)		T(AI)		T(BER)	
				P=50	P=60	P=50	P=60	P=50	P=60	P=50	P=60
SB-2	0.71	0.11	66	1213	1254	1152	1200	1285	1383	1138	1143
P8-2(I)	1.15	0.28	56	1163	1197	1188	1226	1223	1301	941	953
P8-2(II)	0.81	0.16	65	1233	1273	1233	1278	1320	1414	1055	1063
950W-2	1.27	0.35	52	1181	1215	1203	1241	1244	1318	892	907

1301 °C and 1414 °C respectively at 60 kbars. As discussed in Chapter 4, AI temperatures for samples with Mg#(grt)<75-80 are spurious due to uncertainty in the dependence of lnK_d on Mg#(grt). It was further shown in Chapter 4 that for eclogites with Mg#(grt)>75-80 AI temperatures approach those of other geothermometers while at lower Mg#(grt) AI likely overestimates the true temperature. Mg#(grt) for the current samples are 52, 55, 64 and 66 and they are positively correlated with estimated temperatures. For these reasons, AI temperatures are believed to be spuriously high.

Ellis and Green (1979) and Krogh (1988) (from now on referred to as EG and KR) give very similar temperature ranges of 1163-1233 °C and 1152-1233 °C respectively at 50 kbars. However, the two geothermometers do not display a co-variation in temperatures with the different samples. They yield identical temperatures (1233 °C) at 50 kbars for sample P8-2(II) which displays a X_{Ca} of 0.16. For samples with higher X_{Ca} (P8-2(I) and 950W-2) KR gives slightly higher temperatures than EG while the reverse is true for sample SB-2 with X_{Ca}=0.11. KR and EG temperatures vary less than 25 °C for samples with X_{Ca} between 0.16 and 0.35 while for sample SB-2 (X_{Ca}=0.11) the temperatures differ by 61 °C. This is consistent with the treatment of the dependence of lnK_d on X_{Ca} as curvilinear and rectilinear by KR and EG respectively and as discussed in Chapter 4 and the former treatment is believed to be more accurate.

Based on the current results and the discussion on geothermometers and results from geothermometry on eclogite nodules in Chapter 4, KR is believed to yield the most realistic temperatures for eclogitic samples. KR temperatures also vary independently of both X_{Ca} and Mg#(grt). Temperatures using KR display ranges of 1152-1233 °C and 1200-1278 °C at 50 and 60 kbars respectively and as mentioned above they are very similar to EG temperatures at X_{Ca} above 0.11. In Figure 7.9, estimated temperatures at 50 kbars using EG

are compared to EG temperatures for eclogitic diamond inclusions at 50 kbars from other southern African localities. It can be seen that Klipspringer temperatures (1163-1233 °C) are fairly similar to those displayed by samples from Orapa (1135-1212 °C). Some Premier temperatures (1159-1363 °C) are similar to Klipspringer temperatures while most of the Premier samples yield higher temperatures as evident from the average temperature of 1285 °C. The temperature ranges displayed by Jwaneng (1110-1131 °C) and RoVic (1250-1275 °C) inclusions are distinctly lower and higher respectively compared to Klipspringer temperatures.

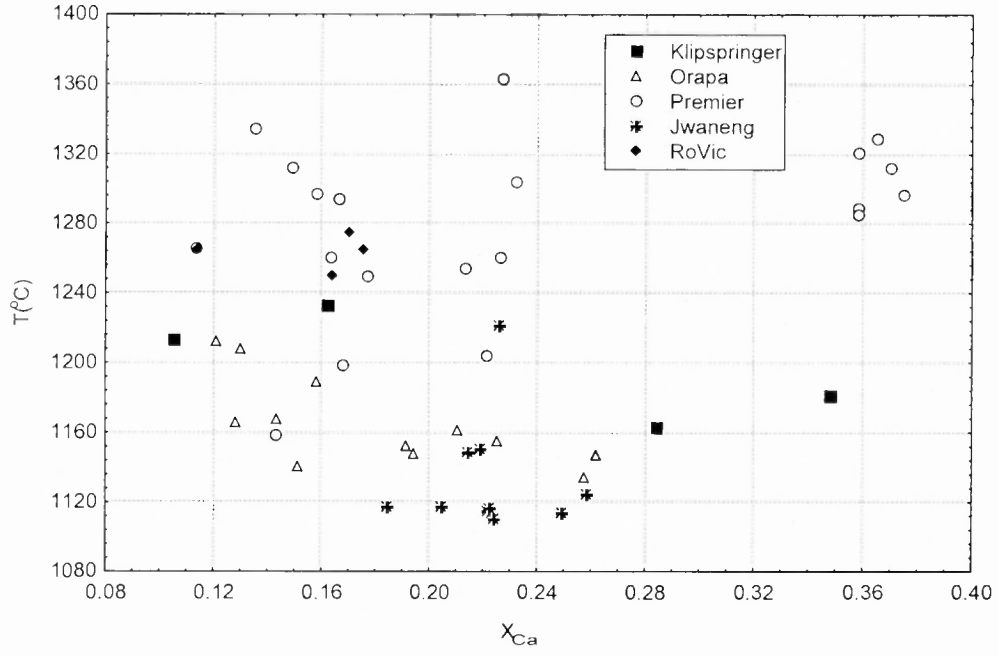

Figure 7.9 Comparison of estimated equilibration temperatures for Klipspringer eclogitic diamond inclusion and those of eclogitic diamond inclusions from other southern African localities (Orapa: Gurney et al., 1979a; "RoVic"=Roberts Victor: Gurney et al., 1979b; Premier: Gurney et al., 1985; Jwaneng: Gurney et al., 1995). Temperatures estimated at 50 kbars using the Ellis and Green (1979) geothermometer.

7.5 Discussion and Conclusions

Silicate and sulfide inclusion compositions indicate that eclogitic parageneses strongly dominate amongst Klipspringer diamonds. Based on garnet and clinopyroxene inclusion compositions, the presence of both rutile and garnet in two individual diamonds, and the occurrence of kyanite inclusions, four eclogitic parageneses have been recognised: A bimineralic±kyanite, a bimineralic±rutile, a grospydite and an "Fe-rich" paragenesis.

Whether the diamond inclusion garnets are products of high-pressure igneous fractionation in the mantle (e.g. MacGregor and Carter, 1970; Hatton and Gurney, 1977) or have inherited their chemistry from subducted oceanic crust (Jagoutz et al., 1984; Sautter and Harte, 1986; Ater et al., 1984) the geochemical trends observed suggest that garnets within each individual group (KG-I to KG-IV) may be linked by magmatic fractionation. The continuous elemental trends from KG-II (bimineralic±kyanite) to KG-I (bimineralic±rutile) indicate that these groups may be petrogenetically linked through fractionation. The "large-scale" chemical disequilibrium displayed by garnets from two individual diamonds which occur both in KG-I and KG-II supports that these two parageneses are petrogenetically linked. However, the change in elemental trends from a positive (KG-II) to a negative (KG-I) correlation between Fe and Ca and the higher Mg content of KG-II suggest that the onset of crystallisation of KG-I garnets was marked by the disappearance of a Mg-rich phase such as orthopyroxene. The higher Ca levels of KG-III (grospydite paragenesis) and the higher Fe levels of KG-IV (Fe-rich paragenesis) for a constant Mg-number compared to KG-I and KG-II indicate that neither KG-III nor KG-IV is related to KG-I and KG-II through a simple petrogenetic process. Thus, at least three petrogenetically unrelated eclogitic parageneses are believed to be present amongst Klipspringer diamonds.

Most Klipspringer omphacites are fairly similar chemically and cannot easily be assigned to any specific garnet inclusion groups. However, the High-Al group is distinctly different from the other omphacites. To the authors knowledge, omphacite carrying up to 28 mole % pseudojadeite has not been reported for either clinopyroxene inclusions or xenolithic clinopyroxene before. Smyth et al. (1989) report on a substantial pseudojadeite component in omphacites from grospydites and kyanite eclogites which show extensive exsolution of garnet and kyanite from the clinopyroxene. Further, the authors emphasize that cation/oxygen ratios of 0.6 and 0.67 for kyanite and pyroxene respectively imply that kyanite exsolution demands a pyroxene precursor with substantial pseudojadeite. The degree of alteration of clinopyroxene in eclogite xenoliths has been observed to correlate well with the deviation from stoichiometric clinopyroxene of unaltered pyroxene remnants (Smyth, 1980). Pseudojadeite may be present in the clinopyroxene structure in substantial amounts only at pressures in excess of ~20-25 kbars (Gasparik, 1985), and Smyth (1980) invokes the reaction $2Ca_{0.5}AlSi_2O_6 \rightarrow CaAl_2Si_2O_6 + 2SiO_2$ to explain the breakdown of pyroxene observed. This implies that the original pyroxene composition with elevated pseudojadeite is not preserved due to breakdown during and/or after kimberlite

emplacement. Since inclusions are protected by the diamond host from re-equilibration with the surrounding environment, the observed pseudojadeite contents of the High-Al omphacites may be indicative of intrinsic compositions of omphacite that cannot be observed in xenolithic omphacite.

Experiments in the system Na_2O-CaO-Al_2O_3-SiO_2 show that the pseudojadeite content of clinopyroxene is strongly pressure dependent and increases with increasing pressure up to ~35 kbars (Gasparik, 1985). The comparatively small cell volume of non-stoichiometric clinopyroxene would also favour increased stability at higher pressures (Wood and Henderson, 1978). The solubility of K in clinopyroxene increases with increasing pressure under upper mantle conditions (Harlow, 1992). Thus, assuming that K is buffered, the low level of K in P9-2e (which displays the highest pseudojadeite content) compared to the rest of High-Al omphacites (Figure 7.5h) suggests that the increased pseudojadeite is not due to a higher pressure of formation. Rather the amount of pseudojadeite is determined by the bulk composition of the environment of formation.

The geochemical characteristics of the High-Al group omphacites prevent a simple petrogenetic relationship between the High-Al group and any of the Main group omphacites. The extremely high Ca and Al contents together with very low Fe and Mg contents of the High-Al group omphacites suggest that they are genetically linked to KG-III garnets which were proposed to belong to a grospydite paragenesis. Grospydites are enriched in Ca and Al compared to bimineralic and kyanite eclogites and all grospydites reported in literature carry clinopyroxene that displays substantial total cation deficiency (reported by Smyth, 1980). Unless grospydites are specifically located at deeper levels in the lithosphere compared to eclogites, this further indicates that the presence of pseudojadeite is mainly dictated by the bulk composition of the environment.

Since the Al_2O_3 content of garnet is fairly constant at eclogitic rock compositions, the variations in total Al_2O_3 of the environment is reflected in the Al_2O_3 content of clinopyroxene and the possible presence of kyanite and/or corundum. However, high pressure experiments have shown that corundum does not coexist with high pseudojadeite clinopyroxenes but rather with high Ca-Tschermakite clinopyroxenes (Harlow, 1999). The very high Al_2O_3-levels of the reconstructed grospydite bulk composition and particularly the constant level of Al_2O_3 in the High-Al omphacites with increasing and decreasing contents of other oxides indicates that the environment was buffered with respect to Al_2O_3. This suggests that kyanite was present in this grospydite paragenesis. Wood and Henderson (1978) showed that non-stoichiometric clinopyroxene with M2 vacancies is stabilised if

SiO_2 is present in excess of that required for stoichiometric clinopyroxene. This may suggest that coesite was also present in the grospydite paragenesis.

Both the KG-III garnets and the High-Al omphacites display distinctive inter-element variations that can be reconciled with magmatic fractionation. Although kyanite probably was present in the grospydite paragenesis, it is suggested that excessive amounts of Al in the formation environment were initially accommodated partly in pseudojadeite. While Ca increases with decreasing Mg for the KG-III garnets, Ca (and the pseudojadeite content) decreases and Na increases with decreasing Mg for the High-Al omphacites. Since clinopyroxene is the only phase in a deep lithospheric environment that can host Na to an important extent, as Na gets concentrated in the magma due to fractionation of garnet and Na-deficient clinopyroxene, at some point it starts to enter the clinopyroxene. Garnet and clinopyroxene are the only phases to accommodate Ca. Therefore Ca will increase in the garnet as Na enters the clinopyroxene. Bulanova et al. (1988) (in Russian, cited by Bulanova, 1995) interpreted a decrease in the pseudojadeite content of clinopyroxene diamond inclusions as a decrease in pressure of formation based on a qualitative estimation of the pressure sensitivity of pseudojadeite (Jarikov et al., 1984, in Russian, cited by Bulanova, 1995). However, from the discussion above, it is suggested that any information on the pressure of equilibration based on the level of pseudojadeite in clinopyroxene at high pressures and with the bulk composition of the environment unknown may be spurious.

Bulk rock compositions estimated from mineral inclusion chemistry are dependent on the assumed modal abundance of garnet and omphacite. However, because of the comparatively similar major element compositions of these minerals, a modal garnet/omphacite ratio of 60/40 or 40/60 instead of the assumed 50/50 would not substantially affect the estimated bulk rock compositions. Although MOR cumulates and komatiites span wide compositional ranges, some constraints on possible protoliths may be inferred from the data. While the low levels of K_2O mirror those of MOR cumulates and komatiites, they do not alone exclude a MORB protolith since potassium is very mobile and incompatible and thus may have been lost during partial melting or dehydration of a subducting MORB. However, it was shown above that none of the estimated bulk rock compositions based on mineral inclusions is akin to those of MORB or komatiite while all estimated compositions are covered by the range displayed by MOR cumulates from the Southwest Indian Ridge. Assuming an origin for the diamond inclusions from subducted MOR cumulates, the reason for the comparatively lower estimated SiO_2 is not clear. It may be that coesite was present in the different parageneses (as proposed above for the KG-

III/High-Al paragenesis) which has not been accounted for in the bulk rock chemistry estimations. Alternatively, any silica present as an SiO_2 phase may have been lost during subduction and partial melting of the oceanic crust as suggested by Rudnick (1995).

The bulk rock contents of TiO_2 may have been underestimated since rutile (which has been observed as a diamond inclusion) has not been accounted for in the estimations. However, the discrepancy between estimated levels of TiO_2 and those of MOR cumulates is difficult to assess. Data for MOR cumulates has been acquired from only one locality and it may be that TiO_2 contents for MOR cumulates vary more than shown in Table 7.3. Further, a high field strength element like titanium is highly sensitive to the physical conditions prevalent at mantle melting compared to most other major elements. Thus, since an assumed protolith to the mineral inclusions likely is Archaean in age, a slightly different type of mantle melting and MOR cumulate/MORB fractionation during the Archaean due to a higher heat flow and faster MOR spreading rates (Taylor and McLennan, 1995) may have yielded slightly lower levels of TiO_2 for MOR cumulates compared to present day levels.

Garnet inclusion groups KG-I/KG-II and KG-III were shown not to be petrogenetically related to each other in a simple way and the High-Al omphacite inclusion compositions are not compatible with a direct petrogenetic relationship to other omphacite inclusions. However, taking into account the uncertainties introduced by assumptions on modal mineralogies to reconstruct hypothetical protoliths (see Section 7.3.2), these protoliths may have been directly petrogenetically related through magmatic fractionation as shown in Figure 7.7. Since all estimated bulk rock compositions fall within the range displayed by MOR cumulates, it may be that spatially associated MOR cumulates related by magmatic fractionation, which gave rise to the wide compositional range observed, were the precursors to the kyanite and rutile eclogite and grospydite diamond inclusions. The composition of the most Al-rich hypothetical bulk rock resembles that of a feldspar-rich cumulate or anorthosite, which has previously been suggested as a precursor to Al-rich eclogites by Jagoutz et al. (1984).

It is not clear whether differences between estimated temperatures for Klipspringer eclogitic garnet/omphacite inclusions and those from other Southern African localities reflect different temperature states of the lithosphere, formation at different levels in the lithosphere or differences in the petrogenetic processes. Implications from the estimated temperatures are further discussed in Chapter 10 as well as implications from the observed "small-scale" equilibrium between multiple garnets from individual diamonds.

8. SULFUR ISOTOPE ANALYSIS ON DIAMOND INCLUSION SULFIDES

8.1 Introduction

Sulfur has four stable isotopes of which ^{34}S and ^{32}S are used in investigations of the isotopic composition of sulfur. Fractionation of sulfur isotopes is caused by two processes. (I) Conversion of sulfate to sulfide by anaerobic bacteria with enrichment in ^{32}S in the sulfide (Harrison and Thode, 1958). (II) Isotopic exchange reactions between ions, molecules and solid media where compounds with the greatest bond strength generally become enriched in ^{34}S (Bachinski, 1969). Depending on the nature of petrogenetic processes, different minerals and rocks will display different $^{34}S/^{32}S$ ratios. This is the basis for the use of sulfur isotopes as a petrogenetic tracer. Sulfur isotope characteristics are reported as $\delta^{34}S$, which is the relative difference in per mil between $^{34}S/^{32}S$ in the sample and in troilite from the Canyon Diablo Meteorite (CDT).

8.2 Sulfur isotope characteristics of the mantle

The average $\delta^{34}S$ for the bulk earth is assumed to be similar to the $\delta^{34}S$ of meteorites which is 0±2 ‰ (Thode et al., 1961; Nielsen, 1978). The $\delta^{34}S$ for crustal rocks deviate from CDT by as much as 70 ‰ (Ohmoto and Rye, 1979) while many mantle samples display a small but significant difference from CDT.

Whole-rock Mid-Ocean Ridge Basalts (MORB) from world-wide localities have an average $\delta^{34}S$ of +0.1±0.5 ‰ (Sakai et al., 1984) which is similar to that of meteorites and suggests that the asthenosphere has not undergone any significant sulfur isotope fractionation. Undegassed Ocean Island Basalts (OIB) are slightly higher in $\delta^{34}S$ than MORB (Sakai et al. (1984), which is probably explained by in-put from a source enriched in ^{34}S since fractionation of sulfur isotopes is not likely to occur at mantle melting temperatures. In contrast to this, Sakai et al. (1984) found that degassed basalts from Hawaii displayed $\delta^{34}S$ values as low as -5 ‰. However, this was thought not to reflect the sulfur isotope composition of the source but was ascribed to degassing of SO_2 enriched in ^{34}S. Calc-alkaline basalts from the Japanese Arc (Ueda and Sakai, 1984) and the Mariana Arc (Woodhead et al. 1978) display somewhat heavy sulfur isotope compositions with $\delta^{34}S$

ranging up to +5 ‰. The authors preclude high temperature fractionation as an explanation for the enrichment in ^{34}S and suggest a partial in-put from subducted crustal components enriched in ^{34}S.

While MORB and OIB are similar to CDT in sulfur isotopic composition, the sub-continental lithospheric mantle shows distinct deviations from CDT. Chaussidon et al. (1989) report on spinel and plagioclase lherzolite from Lherz (southern France), Ronda (southern Spain) and Beni Boussera (northern Marocco), which display rare earth element characteristics indicative of residual mantle remaining after partial melting. $\delta^{34}S$ values for primary sulfides in these rocks range from -3.2 to +3.6 ‰, however with a mode of +3 ‰. The authors suggest that this positive deviation from CDT is caused by high temperature fractionation during 10-20 % melting of primitive mantle with a $\delta^{34}S$ of +0.5±0.5 ‰ and hence suggest that primitive mantle is slightly enriched in ^{34}S compared to meteorites. Ionov et al. (1992) also invoke high temperature fractionation during partial melting to explain $\delta^{34}S$ of +3 to +5 ‰ for whole-rock spinel harzburgites from southern Siberia and Mongolia. In the latter case, this theory is mainly based on a broad positive correlation between $\delta^{34}S$ and MgO and a broad negative correlation between $\delta^{34}S$ and CaO.

Sulfur isotope data on sub-cratonic mantle rocks or minerals are scarce. Chaussidon et al. (1989) report on a hexagonal sulfide from a garnet harzburgite with $\delta^{34}S$=-0.1‰. This may indicate that residual peridotite in the sub-cratonic lithosphere is similar to meteorites in sulfur isotope composition in contrast to younger sub-continental residual peridotite. Two sulfide separates from eclogite xenoliths from the Premier and Roberts Victor kimberlites, South Africa have $\delta^{34}S$ values of 0.2 and 2.1 ‰ respectively (Tsai et al., 1979). A pyrrhotite (with minor pentlandite and chalcopyrite) regarded as primary from its pyrite-free mineralogy and its primary setting as a globule in an eclogite xenolith from Koidu (West Africa) displays $\delta^{34}S$ of 1.6 and 1.9 ‰ for two replicate analyses (Chaussidon et al., 1989). This restricted data set indicates a slight positive deviation from CDT for sub-cratonic eclogites.

While the sub-cratonic eclogite sulfides analysed to date display a restricted range in $\delta^{34}S$, eclogitic sulfide diamond inclusions display an exceptionally wide range in $\delta^{34}S$. Chaussidon et al. (1987) report on pyrrhotite diamond inclusions from the Orapa kimberlite, South Africa that range from +2.1 to +9.5 ‰ in $\delta^{34}S$. In a more extensive study on sulfide diamond inclusions, Eldridge et al. (1991) recorded a range in $\delta^{34}S$ from -11 to +14 ‰ for eclogitic sulfides with Ni contents lower than 13 wt.%. Further, low-Ni sulfides from

individual localities displayed a wide range in $\delta^{34}S$: Sierra Leone (+8 to +14 ‰), Orapa (-11 to -2 ‰) and Jagersfontein (-10 to -7 ‰). The observed range in $\delta^{34}S$ cannot be explained by high temperature fractionation and Eldridge et al. (1991) suggested a crustal input with biogenic sulfate reduction or low temperature inorganic hydrothermal precipitation in an oxidising environment to explain large negative values. The authors further speculated on biogenic effects or hydrothermally altered oceanic sea-floor as possible sources for large positive values.

In contrast to eclogitic sulfide inclusions, Eldridge et al. (1991) reported on $\delta^{34}S$ ranging from -4 ‰ to +3 ‰ for peridotitic sulfides and proposed a sub-lithospheric primitive mantle origin for the sulfur to explain the comparatively narrow range in $\delta^{34}S$.

8.3 Particulars about the analytical technique

Sample preparation and the ion-probe analytical procedure are described in detail in Appendix 6. Contrary to previous ion-microprobe studies of sulfur isotopes in mantle sulfides in which duoplasmatron sources have been used, secondary ions were generated with a primary beam of Cs^+ ions in the current study. Cs^+ is more effective than duoplasmatron in producing secondary sulfur ions which allows for extreme energy filtering (set at 250±50 eV) while in previous studies no energy filtering has been used. At low energies, the fractionation factor for $^{34}S/^{32}S$ varies substantially with the energy of the secondary ions which is very sensitive to possible charging of the sample (pers. comm. Erik Hauri, 1998). Thus, by using a primary source of Cs^+ the instrumental fractionation is better controlled. With energy filtering set at 250±50 eV the interference of $^{16}O^{2-}$ is negligible which allows for a low mass resolution to compensate for a lower ion yield due to the extreme energy filtering.

8.4 Sulfur isotope analysis of Klipspringer sulfide diamond inclusions

Sulfur isotope analysis was performed on sulfides from 13, 18 and 2 diamonds from the Main Fissure, Sugarbird Blow and Marsfontein respectively. Multiple inclusions from some individual Main Fissure and Sugarbird Blow diamonds were recovered and a total of 15 and 28 sulfides were analysed from these localities respectively.

Measured $^{34}S/^{32}S$ are presented as $\delta^{34}S$ in Table 8.1. The sulfides display very similar sulfur isotope compositions to each other with a total range in $\delta^{34}S$ of –1.8 to +2.4 ‰. With the estimated total error of ±1 ‰ (see Appendix 8), $\delta^{34}S$ for multiple sulfides from individual diamonds are well within error of each other. Two sulfides (P7-6b and Mars-3) are distinctly different from the rest with $\delta^{34}S$ values of –1.8 and –1.1 ‰ respectively. If these samples are excluded the total range narrows to –0.2 to +2.4 ‰.

Table 8.1 Sulfur isotope analyses on sulfide diamond inclusions. 2σ standard errors on $\delta^{34}S$ are 1 ‰ as estimated in Appendix 8. All analyses are from discrete sulfides while in some cases multiple sulfides from individual diamonds have been analysed indicated by the last letter or number in the sample name.

Main Fissure	$\delta^{34}S$	Sugarbird Blow	$\delta^{34}S$	Marsfontein	$\delta^{34}S$
P5-7	1.0	SB-3.1	0.5	M1/A-1	-0.2
P5-8f	0.7	SB-3.2	2.1	MARS-3	-1.1
P7-5a	1.4	SB-4	1.0		
P7-6b	-1.8	SB-6a	1.7		
P7-9	1.2	SB-6b	0.5		
P8-4	0.3	SB-7	1.9		
P9-6	2.4	SB-8a	2.1		
P9-7a	2.1	SB-8b	0.5		
P9-8b	2.4	SB-9a	2.1		
P9-8c	1.9	SB-9b	0.7		
P9-8e	2.1	SB-10a	0.3		
P9-10	0.7	SB-10b	1.2		
P9-11a	-0.2	SB-10c	0.0		
A-8a	1.9	SB-11a	1.0		
RUS-1	0.0	SB-11b	1.4		
		SB-12.1	1.7		
		SB-12.2	1.7		
		SB-12.3	2.4		
		SB-12.5	1.7		
		SB-13	1.9		
		SB-15	2.1		
		SB-19	0.0		
		SB-21	0.3		
		SB-24	0.7		
		SB-25	-0.2		
		SB-26	1.2		
		SB-28	0.7		
		SB-30	1.7		

While the limited sample from Marsfontein may not be representative of Marsfontein sulfides, Main Fissure and Sugarbird Blow sulfides display very similar sulfur isotope characteristics. Mean values and 2σ error around mean for Main Fissure and Sugarbird

Blow samples are 1.27±0.23 ‰ and 1.16±0.14 ‰ respectively which suggests that these sulfides are part of the same population. If the analytical errors are somewhat worse than estimated (1.3 ‰ instead of 1 ‰) due to underestimation of the precision of the standard, all data except for samples P7-6b and Mars-3 would be within error of each other. This would allow a treatment of all data (except P7-6b and Mars-3) as identical which would justify a calculation of one average value. However, the data does not display a normal distribution (Figure 8.1) which would be expected if the variation in $\delta^{34}S$ was exclusively due to analytical uncertainties. Instead the number of observations are evenly distributed across the range of $\delta^{34}S$ which implies that the observed range is true and has geological significance. Nevertheless, the data define a narrow range in $\delta^{34}S$ with 90 % of the samples being between 0 and +2.4 ‰. Although there is a statistically significant difference between high and low $\delta^{34}S$ samples, no discrete subgroups can be identified.

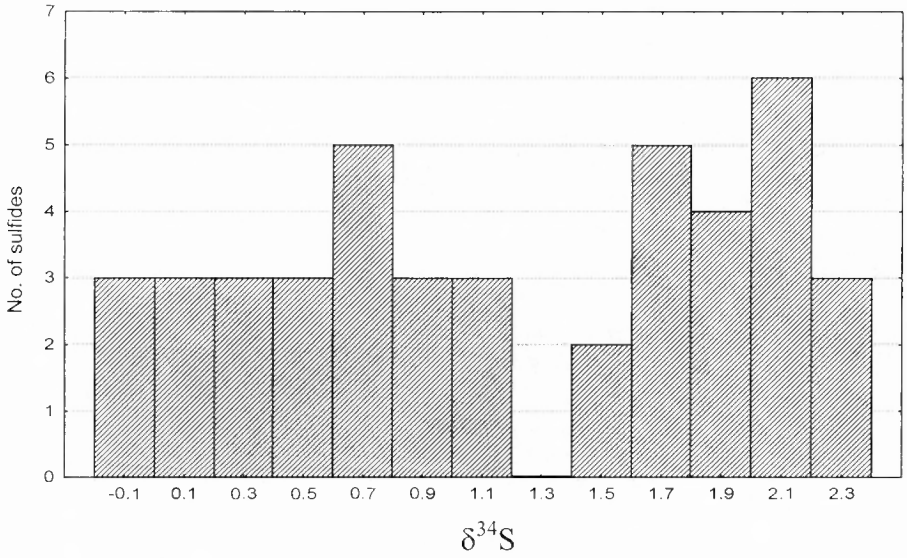

Figure 8.1 Sulfur isotope data for Klipspringer sulfide diamond inclusions displaying the even distribution of samples over the limited range in $\delta^{34}S$.

In Figure 8.2, Klipspringer data is shown together with $\delta^{34}S$ for eclogitic sulfide diamond inclusions from other localities. It is clear that the range in $\delta^{34}S$ previously observed for eclogitic sulfide inclusions is not present in the Klipspringer data. Instead Klipspringer $\delta^{34}S$ values are similar to CDT with the bulk of the sulfides ranging to slightly higher values. It is interesting to note that the range observed for the Klipspringer sulfides mirrors the range recorded for sulfides from eclogite xenoliths (see Section 8.1).

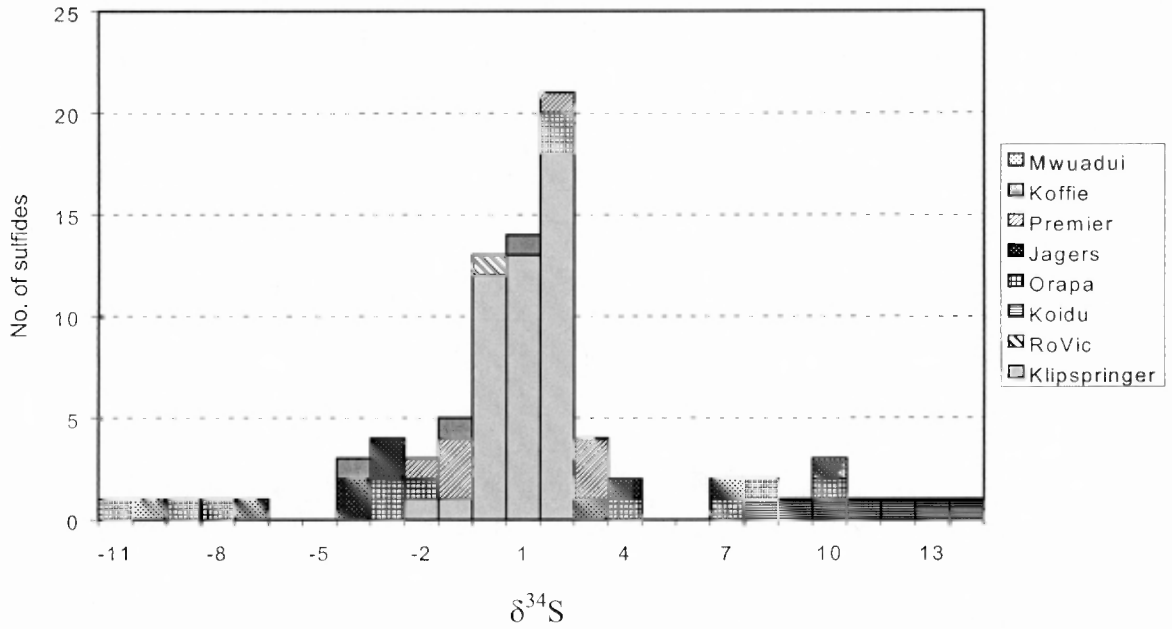

Figure 8.2 Comparison of $\delta^{34}S$ for Klipspringer sulfide diamond inclusions to those of sulfide diamond inclusions from other localities (Chaussidon et al., 1987; Eldridge et al., 1989). 'Koffie'=Koffiefontein, 'Jagers'=Jagersfontein and 'RoVic'=Roberts Victor.

8.5 Discussion and Conclusions

The narrow and continuous range in $\delta^{34}S$ (P7-6b and Mars-3 excluded) suggests that the sulfides acquired their sulfur isotopic compositions from a common source, which had a slightly heterogeneous sulfur isotope composition. Alternatively, the sulfur originates from an isotopically homogeneous source and minor sulfur isotope fractionation has occurred either prior to or during diamond formation.

The very restricted range in $\delta^{34}S$ for the Klipspringer sulfide inclusions and the sulfur composition close to CDT (Figure 8.1) argues against an origin for the sulfur from subducted sediments and/or hydrothermally altered oceanic crust. Although clear signs of subducted oceanic crust are absent in the sulfur isotopes, an origin from mid-ocean ridge cumulates unaffected by biogenic fractionation and hydrothermal alteration may be speculatively proposed. Since no $\delta^{34}S$ data exists for cumulates, this requires assumptions on possible fractionation of sulfur isotopes during the formation of cumulates from a partial mantle melt parental to MORB. Sakai et al. (1984) showed that SO_4^{2-}/S^{2-} ratios for MORB are between 0.15 ‰ and 0.56 ‰. They further reported on SO_4^{2-} enriched in ^{34}S compared to S^{2-} with a maximum difference in $\delta^{34}S$ of about 10 ‰. Even at high temperatures a

fractionation factor of about 2 ‰ is expected between SO_4^{2-} and S^{2-} with SO_4^{2-} being enriched in ^{34}S. While sulfur is partially hosted in the MORB by SO_4^{2-}, the sulfide in the cumulate is most likely present as reduced sulfur in sulfides. Thus, assuming equilibrium crystallisation, the MORB magma would be enriched in ^{34}S compared to the cumulate. Since MORB displays $\delta^{34}S$ of 0.1±0.5 ‰, a MOR cumulate would extend to lower rather than higher $\delta^{34}S$ compared to MORB. This is contrary to the data for Klipspringer sulfides wherefore a cumulate source for the sulfur seems unlikely. However, Fletcher et al. (1989) reported on layered Caledonian gabbro cumulates displaying $\delta^{34}S$ values from –1.2 ‰ to +2.4 ‰ which was ascribed to magmatic isotope fractionation. In the absence of sulfur isotope data for MOR cumulates and taking into consideration that bulk rock compositions based on Klipspringer silicate eclogitic inclusions mirror a wide range of MOR cumulate compositions (Chapter 7), a cumulate source for the sulfur cannot be rejected.

The $\delta^{34}S$ close to CDT for the Klipspringer sulfides may be suggestive of a primitive sub-lithospheric source but the reason for the slight positive deviation of the Klipspringer data compared to CDT is difficult to assess. The eclogitic nature of the sulfides demonstrated by their Ni and Os contents (Chapters 7 and 9) may indicate that they originate from a basaltic melt extracted from the asthenosphere. However, fractionation during melting of a primitive mantle seems unlikely as an explanation for the positive $\delta^{34}S$ values in the light of the enriched rather than depleted ^{34}S previously recorded for residual peridotitic mantle remaining after melt extraction (Chaussidon et al., 1989; Ionov et al., 1992). The occurrence of regions in the asthenosphere enriched in ^{34}S cannot be excluded. Radiogenic isotope characteristics of some Ocean Island Basalts are indicative of the presence of a component of recycled oceanic crust in mantle plumes (e.g. Hauri et al., 1996). Thus, if either the formation of a protolith to the sulfide inclusions or the diamond formation event itself was petrogenetically associated with a mantle plume, $\delta^{34}S$ values deviating from CDT may be expected.

The mechanism for formation of eclogitic diamonds remains enigmatic and it has not yet been well constrained whether eclogitic diamonds are magmatic, metamorphic or metasomatic in origin (Chapter 1). With phase relations unknown at diamond formation, it is difficult to speculate on possible sulfur isotope fractionation at the time of diamond formation. Further, isotope fractionation at diamond formation is difficult to predict due to the lack of experimental data on sulfur isotope fractionation between a sulfide fluid and dissolved sulfur in a silicate fluid.

9. RE-OS ISOTOPE ANALYSIS OF SULFIDE DIAMOND INCLUSIONS

9.1 Introduction

During the last 20 years, several studies on radiogenic isotopes of syngenetic mineral inclusions from diamonds have been undertaken which have greatly improved our knowledge on the timing of diamond formation. Information on the age of diamonds and on trace element abundance in their syngenetic inclusions is of basic importance in understanding the processes that are involved in diamond formation.

In a pioneer study on Pb systematics of sulfide inclusions from the Cretaceous Kimberley and Finsch kimberlites, Kramers (1979) presented model ages in excess of 2 Ga and for the first time it was firmly established that many diamonds are xenogenic rather than cognate with respect to the kimberlite. This has subsequently been supported by numerous studies involving different types of isotopic systems.

Richardson et al. (1984) presented mid-Archaean combined Rb-Sr and Sm-Nd model ages for harzburgitic garnet inclusions that had high Mg and Cr contents and a low Ca content indicative of garnets in residual harzburgite from which magmaphile elements have been removed. At the same time, the garnets displayed Sm/Nd ratios distinctly lower than bulk earth indicative of a strong LREE enrichment and Sm, Nd and Sr concentrations distinctly higher than those of peridotite xenolith garnets. This belies formation from a precursor depleted in elements comparatively less compatible during mantle melting. Further, the garnets displayed radiogenic Sr, which was totally unsupported by their low Rb contents. The result was interpreted as diamond formation around 3.2-3.3 Ga in a metasomatically enriched residual mantle with the metasomatic event predating diamond formation by some 200-300 Ma. Richardson et al. (1984) further suggested that the residual mantle remaining after wide-spread komatiite magmatism around 3.5 Ga may have been the host for the diamonds. This interpretation has been the subject of much debate (Pidgeon, 1989; Richardson, 1989; Pearson et al., 1995a; Shimizu and Sobolev, 1995; Navon, 1999) of which a detailed presentation is beyond the scope of this thesis. However, in this authors assessment, the core argument for Richardson's et al. (1984) interpretation has not yet been successfully overturned and it seems viable to accept that major harzburgitic diamond formation occurred in the Kaapvaal lithosphere in the mid-Archaean, albeit as one of

several diamond forming events of different ages. Certainly the opposite has not been proven.

Richardson et al. (1993) presented a Sm-Nd isochron age of 1930±40 Ma based on lherzolitic garnet and clinopyroxene composites from diamonds of the Premier kimberlite, South Africa. Later, Richardson and Harris (1997) obtained a Sm-Nd isochron age of 2010±10 Ma for harzburgitic garnet composites from diamonds of the Udachnaya kimberlite, Russia. This demonstrates the formation of a second generation of peridotitic diamonds around 2 Ga both in the Siberian and the Kaapvaal mantle (see next section for mid-Archaean peridotitic diamond formation in the Siberian mantle). This age corresponds in South Africa to the age of the Bushveld complex (~2050 Ma; Walraven et al., 1989) and a link between an expected depleted residual mantle after Bushveld magmatism and the lherzolitic diamond inclusions has been suggested (Richardson et al., 1993). Interestingly, some peridotite xenoliths from the Premier kimberlite have Re-Os isotope characteristics indicative of ages around 2 Ga which is in contrast to minimum ages of about 2.4-2.9 Ga generally displayed by Kaapvaal peridotites (Carlson et al., 1999). Since the lherzolitic diamonds at Premier may be petrogenetically related to the Bushveld magmatism, their age is not unequivocally indicative of a broader lherzolitic diamond formation event around 2 Ga.

In contrast to ancient peridotitic diamond formation, Sm-Nd isochron ages based on garnet and clinopyroxene composites from eclogitic diamonds seem to reflect relatively younger diamond formation events. Eclogitic diamonds from the Argyle (Australia), Finsch (South Africa) and Jwaneng (Botswana) kimberlites have been dated at 1540 Ma, 1580±50 Ma and 1580±60 Ma respectively (Richardson, 1986; Richardson et al., 1990, 1999). Premier eclogitic diamonds have an age of 1150±60 Ma (Richardson, 1986) similar to the age of the Premier kimberlite. Orapa diamonds have been dated at 990±50 Ma (Richardson et al., 1990). The similar ages of Finsch and Jwaneng eclogitic diamonds led Richardson et al. (1999) to suggest a regional eclogitic diamond formation event along the western side of the Kaapvaal craton around 1580 Ga.

Due to low Sr and Nd concentrations in garnet and clinopyroxene and the small size of the inclusions, the data presented above has been based on composites of tens to hundreds of inclusions from different diamonds. Although such inclusions have been carefully grouped on the basis of major element chemistry and colour, there is room for some concern as to whether all diamonds from which inclusions for a specific composite

has been assembled are genetically related. On the other hand composite samples may "average out" differences within a population and provide more useful results than single inclusion analysis. This seems likely in the light of data obtained for analyses of large single inclusions of the eclogitic paragenesis (Smith et al., 1991), an experiment specifically designed to circumvent the problem of composites.

During the last ten years, some attempts have been made to date individual diamond inclusion minerals through U-Pb analysis of zircon and the Ar-Ar technique on clinopyroxene. U-Pb studies of zircon inclusions have been hampered by the scarcity of this type of inclusion and by the difficulty in assigning zircons to a specific paragenesis. In the only study undertaken so far, Kinny and Meyer (1994) presented a U-Pb age of 628±12 Ma for a zircon diamond inclusion from the late Cretaceous Mbuji Mayi kimberlite, Zaire.

Ar-Ar analysis of clinopyroxene inclusions may yield spurious ages intermediate between the kimberlite eruption ages and inferred diamond ages (Burgess et al., 1992) and must be interpreted with caution. Analytical difficulties arise due to migration and accumulation of Ar at the diamond/inclusion interface at mantle temperatures while post-eruption temperatures are below the closure temperature for Ar diffusion (Burgess et al., 1992). Phillips et al. (1998) further suggest that due to partial retention of the pre-eruption Ar in the clinopyroxene, analysis of the clinopyroxene inclusion can at best yield an upper estimate of the kimberlite eruption age. Although Burgess et al. (1989) and Phillips et al. (1989) present ages for Premier diamonds similar to those obtained by Richardson et al. (1986), none of the Ar-Ar ages obtained so far (Burgess et al., 1989, 1992, 1998; Phillips et al., 1989, 1998) are unequivocally indicative of diamond formation ages and will not be considered further here.

9.1.1 Re-Os isotope analysis of sulfide diamond inclusions: Background, advantages and previous investigations

Any isotope study of diamond inclusion minerals is limited by the occurrence of the mineral needed for analysis. Zircon inclusions suitable for U-Pb analysis are extremely rare and Sm-Nd analysis of garnet and clinopyroxene inclusions requires pooling of a large amount of inclusions. Sulfide is the most abundant inclusion world-wide (Gurney, 1989) and in most cases there is strong evidence for a syngenetic relation between sulfide inclusions and their host diamonds (see Chapter 7). Both Re and Os are strongly siderophile (Allegre and Luck, 1980) and chalcophile (Foster et al., 1996). As a result sulfide is likely the main host for

these elements in the lithosphere. ^{187}Re decays to stable ^{187}Os by emission of a β particle and the decay constant is fairly low ($\lambda[^{187}Re]=1.666x10^{-11}$ y^{-1}). Therefore, if an appropriate method is applied, Re-Os analysis of sulfide inclusions may contribute substantially to the understanding of the timing of diamond formation. Further, a recently developed method (see next section) under favourable circumstances allows for analysis of single sulfides from individual diamonds. This provides a way to eliminate the problem of analysing composites of sulfides from different diamonds, which may not have a common origin.

As mentioned above and as discussed in Section 9.4, the bulk of the Re and Os in the lithosphere is probably hosted by sulfides. Further, Proterozoic ages obtained from Re-Os systematics of sulfide inclusions from diamonds hosted by Mesozoic and younger Paleozoic kimberlites (see below) indicate that the sulfides have been protected by their host diamond from re-equilibration with the surrounding environment and from metasomatism and weathering which commonly have affected xenolithic sulfides (Tsai et al., 1979; Lorand, 1989). Thus, analysis of Re and Os isotopes in sulfide inclusions may provide "primary" sulfide Re-Os compositions which can contribute to the understanding of the Re-Os budget of the mantle.

The use of compositional and isotopic information on sulfide inclusions has been hampered by difficulties in assigning the sulfides to a specific paragenesis. This has been overcome to some extent by the use of Ni content as a discriminating parameter (see Chapter 7). Os contents of the sulfide inclusions have further aided in this discrimination. Recent work shows that eclogitic sulfide inclusions contain <750 ppb Os (Pearson et al., 1998a, 1998b) while peridotitic sulfides carry between 1ppm and >100 ppm Os (Bulanova et al., 1996; Pearson et al., 1998a, 1998b, 1998c, 1999a, 1999b). Thus, on the basis of both Ni and Os, eclogitic and peridotitic sulfides can be effectively discriminated. Os contents of the proposed pyroxenitic sulfide inclusions (Bulanova et al., 1996) are not known. Further investigations must be undertaken to examine if they can be discriminated from eclogitic and peridotitic sulfide inclusions on the basis of Ni and Os.

Pearson et al. (1999a and 1999b) report on model ages of 3.1-3.5±0.3 Ga for three peridotitic sulfides from one diamond and 3.4±0.3 Ga for a sulfide composite of 2 grains from another diamond from the Udachnaya kimberlite, Russia. Kimberlite emplacement has been dated at 360 Ma (Kinny et al., 1995). All ages are within error of each other which strongly indicates mid-Archaean peridotitic diamond formation in the Siberian mantle. The antiquity of these diamonds was supported by the comparatively high aggregation state of

the nitrogen in the diamonds. The ages are similar to the ages of 3.2-3.3 Ga obtained for peridotitic diamonds from the Bultfontein and Finsch kimberlites, South Africa (Richardson et al., 1984) and a world-wide diamond formation event in the mid-Archaean may be inferred.

In contrast to this, Pearson et al. (1998a), presented a two-point Re-Os isochron with an age of 68±30 Ma based on two peridotitic sulfides from one diamond from the Koffiefontein kimberlite, South Africa, a pipe with the preferred emplacement age of ~ 90 Ma (Davies, 1978). Another suggestion for young diamonds comes from a model age of ~200 Ma obtained for an eclogitic sulfide inclusion from the Dokolwayo kimberlite, South Africa (Westerlund, unpublished data) that is concordant with the age of the kimberlite (203±7 Ma; Allsopp and Roddick, 1984). Together with the 1150±60 Ma age of eclogitic diamonds from the Premier kimberlite (Richardson et al., 1993) which is similar to the age of the Premier kimberlite (1179±36 Ma; Smith, 1983), this may suggest that some diamond formation events are linked to the kimberlite formation events. However, as mentioned by Richardson et al. (1993), the aggregation state of the nitrogen in Premier diamonds indicates crystallization at least 1-10 Ma before the emplacement of the kimberlite.

Two peridotitic sulfide inclusions from two individual alluvial diamonds from eastern Australia give Re-Os model ages of 2.1 and 3.4 Ga and have measured $^{187}Os/^{188}Os$ of 0.12 and 0.11 respectively which is lower than present day chondrite (Pearson et al., 1998c). Although these ages may reflect diamond formation in the Proterozoic and Archaean respectively, it cannot be excluded that the sulfides had initial $^{187}Os/^{188}Os$ below chondritic values and thus may have formed more recently than indicated by the model ages.

Eclogitic sulfide inclusions from the Koffiefontein kimberlite, South Africa were investigated by Pearson et al. (1998a). Assuming that the analysed sulfides from five individual diamonds were cogenetic, an isochron age of 1.05±0.12 Ga was obtained. With this interpretation, the sulfides were considered to have formed from a precursor which was enriched in Re over Os compared to chondrite for some time prior to diamond formation as indicated by an initial $^{187}Os/^{188}Os$ of 0.277. However, sulfides from two of the diamonds displayed chondritic model ages of 2.7 and 2.9 Ga respectively in contrast to model ages of 1.1-1.2 Ga displayed by the other samples. Further, the former group displayed Re/Os ratios of ~ 1 compared to Re/Os ratios of 14-18 for the latter samples. Hence, an alternative

interpretation was put forward for two separate diamond formation events at ~ 2.7-2.9 Ga and ~1.1-1.2 Ga respectively, both with a chondritic source for the Re and Os.

9.2 Principles and problems of the analytical technique

Diamonds with sulfide inclusions for Re-Os isotope analyses were acid treated, visually inspected and cracked as described in Appendix 5. The sulfides often broke into two or three pieces when liberated from the diamonds, which allowed mounting of a smaller piece in epoxy for electron and ion microprobe analyses while the bulk of the grain could be kept for Re-Os analysis. When unbroken sulfides were recovered, the whole grain was mounted in epoxy for probe work and later released from the epoxy through ultrasonic agitation in chloroform for about twenty minutes followed by 5 minutes of agitation of the liberated sulfide. Through treatment in chloroform, the epoxy becomes like an elastic gel that does not dissolve but flakes off in coherent pieces, which do not stick to the sulfide to judge from visual inspection by high-powered microscope. Possible sub-microscopic epoxy stuck to the sulfides is believed not to influence the results since both Re and Os are strongly siderophile elements, which should be virtually absent in the epoxy.

The very small size of the sulfides (~ 100-350 μm in the longest dimension) translates into low levels of Re and Os available for analysis which requires a method capable of producing accurate results at analysis of down to ~ 1 pg Os. This may be accomplished through the combination of a highly sensitive analytical method in combination with a chemical procedure with extremely low blanks. The technique used combines the high ionisation efficiency of N-TIMS (Negative Thermal Ionisation Mass Spectrometry) (Creaser et al., 1991) with a sample preparation procedure developed by Graham Pearson and co-workers at the Carnegie Institution of Washington (e.g. Pearson et al., 1998a), which involves the use of a "clean-up" step used to purify the Os fraction during conventional analyses of higher-level Os samples (Roy-Barman and Allegre, 1995).

The procedures for dissolving the sulfides, extracting Re and Os and N-TIMS analysis are described in detail in Appendix 7. Of main importance in the analytical method is that dissolving of the sulfides and separation of Re and Os is accomplished in one step in a 7 ml vial with subsequent extraction of Re using micro-columns (~ 5 ml volume). This allows for use of a minimum of chemicals, which is the key to the low blanks obtained. Os blanks previously reported range between 5 and 45 fg including filament blanks (Pearson et

al., 1998a) and in the present study total Os blanks range from 4 to 35 fg for six measurements. For a sample containing substantially less than 1 pg Os, Os concentration and $^{187}Os/^{188}Os$ will vary considerably when different blanks of the measured range are used to correct the data. To account for the problem of blank correction, the blank was set to an average of all blanks (17.5 pg) with a 100 % uncertainty.

Previously reported Re blanks range from 100 to 310 fg (Pearson et al., 1998a) which is lower than the 300 to 600 fg obtained in this study. The Re blank was set, as the Os blank, to the average of all Re blank measurements with 100 % uncertainty to account for the variation in the blank measurements. A lower and better constrained Re blank would be desirable. However, for three of the five samples (SB-C1, SB-C2 and Main), the error for blank corrected abundance is lower than four percent with slightly worse errors for the two remaining samples (SB-12 and Mars).

Due to the low weight of the samples, weighing must be accurate to ±20 μg. Weighing errors do not directly affect $^{187}Os/^{188}Os$ and $^{187}Re/^{188}Os$ ratios used in the isochron diagram and in model age calculations. However, the separate blank corrections of Re and Os may introduce uncertainties in Re and Os abundance which propagate into errors in isotopic composition and $^{187}Re/^{188}Os$ ratios. The samples were weighed by difference in a small aluminium tray using a Mettler UMT2 microbalance. The sensitivity for this scale is 0.1 μg but due to charging and drift the accuracy is believed to be ~ 0.5 μg to judge from replicate weighings. Errors introduced into isotopic compositions at this level of accuracy are negligible.

Practical problems in the method include static charging during sample handling and during dry down of the spike (see Appendix 7). To reduce the problem of static charging, the vial lid in which the spike is dried down and to which the sample is transferred was covered in aluminium foil. To ensure complete mixing between the spike and the sample it is essential to dry down the spike in the centre of the lid. This is aided by a small indentation in the centre of the lid.

9.3 Re-Os analysis of Klipspringer diamond inclusions sulfides

The morphology of Klipspringer sulfide inclusions has been described Chapter 7. Prior to Re-Os analyses, the sulfides were analysed for major elements and sulfur isotopes. The mineralogy and major element composition of all sulfides analysed for Re and Os is presented in Chapter 7 and sulfur isotope analyses for most of the sulfides are presented in

Chapter 8. In summary, the sulfides analysed for Re-Os exhibit great similarity in mineralogy, major element chemistry and $\delta^{34}S$. All the analysed sulfides are from diamonds of the Low-T nitrogen aggregation group (Chapter 6).

Sample SB-12, which consists of five sulfides from one diamond with a combined weight of about 20 μg was analysed initially. The analysis gave a concentration of 13 ppb Os which translates into an amount of ~ 0.25 pg Os. This low level of Os yields a poor result from the large analytical error and from a substantial blank correction. The initial analysis of sample SB-12 indicated that analysis of composites rather than single grains (or a couple of grains from one diamond) would be necessary due to a low Os content. This approach is not ideal since it might result in combination of sulfides from different populations that may be of different age or may have formed with different initial $^{187}Os/^{188}Os$. However, the approach is partly justified by the similar mineralogy, major element chemistry and $\delta^{34}S$ displayed by the sulfides (Chapters 7 and 8).

Five samples were analysed of which two (SB-12 and Mars) consist of five and two sulfides respectively from two individual diamonds while samples SB-C1, SB-C2 and Main are composites of 33 sulfides from 19 diamonds, seven sulfides from three diamonds and six sulfides from four diamonds respectively. Samples SB-C1, SB-C2 and SB-12 are from the Sugarbird Blow while Main is from the Main Fissure and Mars is from the Marsfontein kimberlite.

9.3.1 Re-Os abundance

Os contents of four of the samples (SB-12, SB-C1, Main and Mars) range between 13 and 38 ppb and are distinctively lower than the 163 ppb recorded for sample SB-C2 (Table 9.1). These levels of Os are within the range observed previously for eclogitic sulfide inclusions and well below Os concentrations of peridotitic sulfide inclusions (see Section 9.1.1). Thus, the classification of the sulfides as eclogitic based on Ni contents (see Chapter 7) is supported.

Re contents range from 199 ppb to 502 ppb, which is predominantly within the range previously observed for eclogitic sulfide inclusions (Pearson et al., 1998a, 1998b) but extend to slightly higher values. In Figure 9.1, Re and Os contents of the Klipspringer sulfide inclusions are shown together with the Re-Os contents of other sulfide inclusions and some selected rock types. As shown by Pearson et al. (1998a), there is a clear

Table 9.1 Re-Os abundances and isotope ratios for sulfide inclusions in diamonds. Model ages are based on an assumed chondritic source.

	Re(ppb)	Os(ppb)	Re/Os	$^{187}Re/^{188}Os$	$^{187}Os/^{188}Os$	Model age (Ga)
SB-12	262	13	20	430	25.6	3.5±1.7
SB-C1	355	38	9	87	7.3	4.8±0.2
SB-C2	502	163	3	16	0.9	2.8±0.1
Main	370	33	11	90	4.1	2.6±0.2
Mars	199	20	10	65	2.8	2.4±0.5

distinction in Re/Os ratios between eclogitic and peridotitic sulfide inclusions which is mainly controlled by their difference in Os contents. This is in accordance with the wide range in Re/Os observed for silicate rocks, which span a much wider range in Os content than Re content (Allegre and Luck, 1980). A positive correlation between Re and Os for the Klipspringer eclogitic sulfides may be inferred from Figure 9.1 with SB-C2 as the high Re/high Os end-member and SB-12 on the low Re/low Os end. At the same time, SB-C2 and SB-12 have the lowest and highest Re/Os respectively which indicates that Os is the controlling parameter for Re/Os ratios even within this sulfide population.

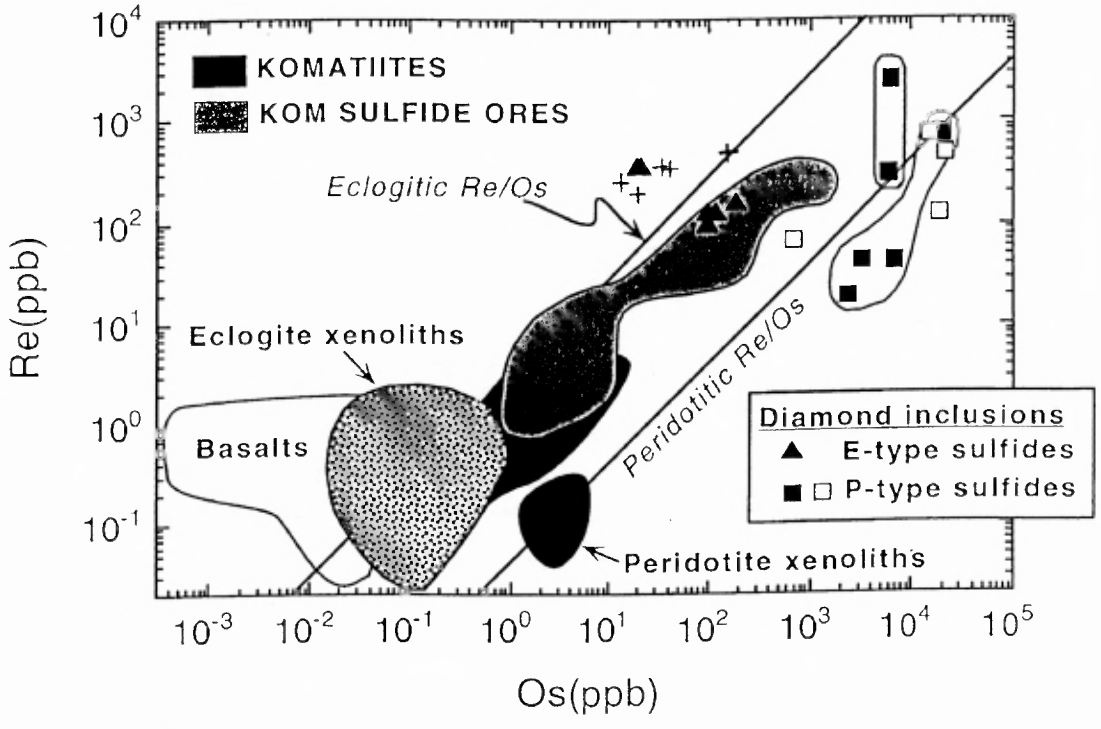

Figure 9.1 Re and Os abundances for sulfide diamond inclusions compared to those of peridotites, eclogites, basalts, komatiites and komatiitic sulfide ores (modified from Pearson et al., 1998a). Squares and triangles are from Pearson et al. (1998a). Klipspringer sulfides are shown as crosses.

The difference in Re/Os between eclogitic and peridotitic sulfide inclusions mirrors the difference in Re/Os between eclogitic and peridotitic xenoliths which suggests that sulfide inclusions of a specific paragenesis and their xenolith counterparts are petrogenetically related. As pointed out by Pearson et al. (1998a), this similarity may suggest that the bulk of the Re and Os in the xenoliths is hosted by unencapsuled sulfides similar to those entrapped by the diamonds. Re/Os ratios for Klipspringer sulfides range from 3 to 20 (Table 9.1, Figure 9.1) which is similar to other eclogitic sulfide inclusions and strengthens the picture of the similarity in Re/Os between eclogitic sulfide inclusions and eclogite xenoliths. The range in Re/Os observed for the Klipspringer sulfide inclusions is similar to that of basalts while it is slightly higher than the Re/Os ratio of komatiites (Figure 9.1).

9.3.2 Re-Os isotope systematics

The analysed samples are presented in an isochron diagram in Figure 9.2, and the immediate observation is that the five data points are broadly correlated and form a trend that is indicative of Archaean ages. However, a regression of all five samples is not meaningful for several reasons. First, most samples would not plot on the regression line within analytical errors and it would be difficult to assess the meaning of the scatter. A true isochron without scatter would be obtained only if the samples are of the same age, were formed from the same source (or different sources with the same $^{187}Os/^{188}Os$ and have behaved as closed systems since the time of formation). The scatter around the regression line could have several explanations. Second, the age obtained (~ 3.7 Ga) would be heavily dependent on sample SB-12, which is very low in Os with low analytical accuracy and substantial blank correction. Finally, the similarity in Re/Os between xenoliths and sulfide inclusions of the eclogitic paragenesis (see previous section) implies that the sulfides are formed from a source that was enriched in Re/Os compared to primitive mantle for some time since this is the case for any possible eclogitic precursor (Pearson et al., 1995; Menzies et al., 1998; Shirey et al., 1998). This would translate into an elevated initial $^{187}Os/^{188}Os$ compared to primitive mantle. The initial $^{187}Os/^{188}Os$ for a regression line through all five samples is about -0.3 which is lower than that for the primitive mantle in the mid-Archaean and clearly contradicts formation from an enriched source.

A regression through Sugarbird samples only (SB-12, SB-C1 and SB-C2) yields a low MSWD of 1.06. However, the regression results in an unfeasible age of 5200±430 Ma which exceeds the age of the earth and a low initial $^{187}Os/^{188}Os$ ratio of –0.6. Bearing in

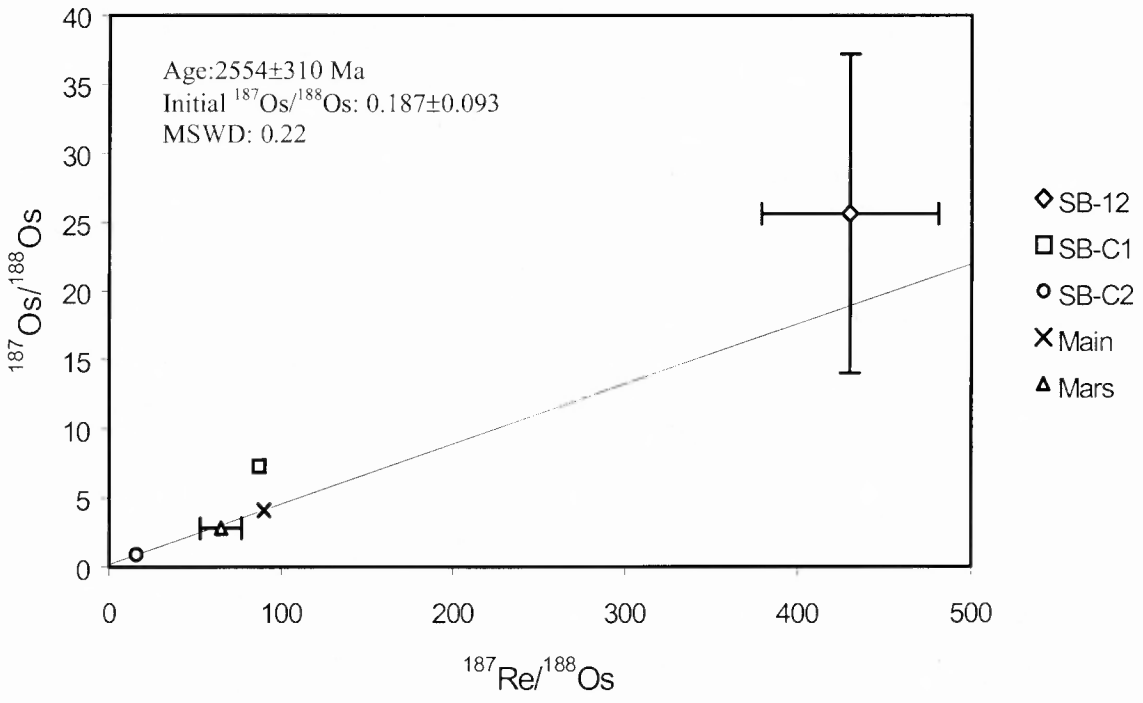

Figure 9.2 Re-Os isochron diagram for sulfide diamond inclusions. The inserted trend-line and the regression data are based on samples SB-C2, Main and Mars. Error bars and uncertainties in the age and initial $^{187}Os/^{188}Os$ are at the 1σ level. Error bars are only shown when extending outside the marker.

mind the proximity of the three sampled kimberlites and the similarities in mineralogy, chemistry and $\delta^{34}S$ displayed by the sulfides, there is no obvious reason as to why Sugarbird samples should be considered as petrogenetically different, and treated separately to the Main Fissure and Marsfontein samples.

Since the accuracy of sample SB-12 is very low, it should not be included in a regression. If the four remaining samples are considered, SB-C1, Main and Mars form a coherent trend in the isochron diagram while SB-C2 plots above this trend. The deviation of sample SB-C2 is further apparent from the difference in model ages (Table 9.1). SB-C2 has a chondritic model age beyond the age of the earth while SB-C1, Main and Mars have chondritic model ages around 2.6 Ga that are all within error of each other. This implies that a significant age may be deduced from regression of the three latter samples. A regression of samples SB-C1, Main and Mars yields an isochron which translates into an age of 2550±310 Ma with an initial $^{187}Os/^{188}Os$ of 0.19±0.09. This regression yields an isochron with a MSWD of 0.22 which passes within error of sample SB-12 and leaves only sample SB-C2 as being significantly different from the other samples.

Several explanations may exist for the deviation of sample SB-C2. This sample consists of seven sulfides from three diamonds and some of the sulfides may simply be different in age compared to the main population. Klipspringer garnet and clinopyroxene inclusions display a wide variation in chemistry with most samples showing similar compositions while some samples are distinctively enriched in magmaphile elements such as Ca and Al. Thus, if some sulfides in sample SB-C2 are petrogenetically connected to silicate "outliers", their source may have been enriched in Re over Os. If all sulfides of sample SB-C2 were formed contemporaneously with the other samples, an elevated initial $^{187}Os/^{188}Os$ for some of the sulfides due to a precursor comparatively enriched in Re over Os may explain its comparatively high model age. However, no variations in major element chemistry or sulfur isotopes have been recorded that would support such a scenario. Alternatively, the Re-Os isotope system of parts of sample SB-C2 may not have been closed since the time of formation. An annealed crack in a diamond can be observed only through cathodoluminescence and has previously been reported to explain disturbance of Re-Os systematics (Pearson et al., 1998a). The highly radiogenic character of sample SB-C2 precludes re-equilibration with a kimberlitic fluid since kimberlites have very low Re/Os ratios (Carlson et al., 1996). Another possibility is that samples SB-C1 and SB-C2 are undisturbed while samples Main and Mars have reequilibrated with an unradiogenic environment. This is considered unlikely since the age obtained from samples SB-C1 and SB-C2 exceeds the age of the earth and yields an unfeasible initial $^{187}Os/^{188}Os$ ratio of -1. From the evaluation of the data, an age of 2550±310 Ma with an initial $^{187}Os/^{188}Os$ of 0.19±0.09 is suggested for at least some of the Klipspringer sulfides (and indirectly the host diamonds), while the reason for the deviation of sample SB-C1 is not clear. The initial $^{187}Os/^{188}Os$ of 0.19±0.09 for the Klipspringer sulfides covers values from that for the primitive mantle at ~2.5 Ga to values significantly higher than the primitive mantle.

Klipspringer sulfides are shown in an isotope evolution diagram in Figure 9.3 together with formation ages of Kaapvaal and Siberian eclogite xenoliths (Pearson et al., 1995b; Menzies et al., 1998) and Os evolution for the eclogites with the highest and lowest Re/Os from each locality. It can be seen that samples Main, Mars and SB-C1 give chondritic model ages ranging from 2.4 Ga to 2.8 Ga while the model age for sample SB-C2 exceeds the age of the earth which would require at least a two-stage process to explain. Useful information from the model age of sample SB-12 is obscured due to the large analytical errors.

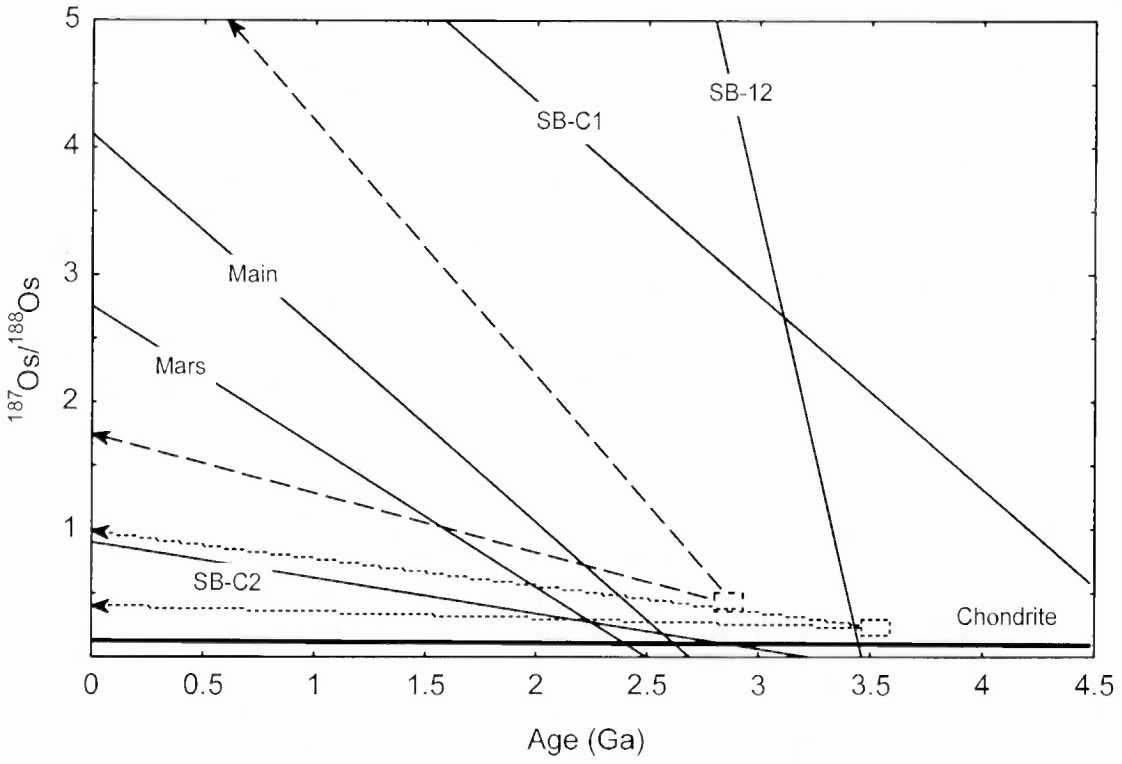

Figure 9.3 Os isotope evolution diagram for sulfide diamond inclusions. Age and Os isotope evolution for high and low extreme Re/Os eclogites from Udachnaya (dashed) (Pearson et al., 1995) and Newlands (dotted) (Menzies et al., 1998) are shown for comparison.

9.4 Discussion and Conclusions

As shown above, Re/Os ratios of Klipspringer sulfide inclusions are similar to those of eclogites and they are suggestive of a basaltic rather than a komatiitic protolith. However, a comparison of Re/Os ratios of the sulfides and plausible sources for the Re and Os requires knowledge of the geochemical behaviour of these elements in the mantle. Experimental data on the partitioning of Re and Os during mantle melting are scarce for Re (Righter et al., 1995; Righter and Hauri, 1997) and absent for Os. Further, experiments with sulfide as a stable phase have not been undertaken. Foster et al., (1996) reported on elevated Re/Os for komatiites compared to associated magmatic sulfide ores which implies that Re is less chalcophile than Os. Based on analysis of minerals separated from single peridotite xenoliths, Hart and Ravizza (1995) suggested that sulfides may be the main host for Os in peridotites. Pearson et al. (1998a) estimate that 0.1 to 0.2 modal % sulfide in peridotite can host all the Re and Os present if Re and Os contents of sulfides in peridotites are similar to those of peridotitic sulfide inclusions. While Os is compatible during mantle melting (Morgan, 1986; Hart and Ravizza, 1995) and is likely to be hosted almost entirely by sulfide in the mantle, the behaviour of Re is less well understood. Based on the coherent variation

of Re and elements such as HREE, Al, Fe, Ca and Y in OIB (Ocean Island Basalts) and MORB (Mid-Ocean Ridge Basalts), Hauri and Hart (1997) concluded that Re is moderately incompatible during mantle melting. The average Re content of MORB is substantially higher than that of OIB similar to the difference in Yb content between MORB and OIB (Hauri and Hart, 1997). For Yb, this difference has been attributed to a relatively higher abundance of residual garnet at formation of OIB (Hoffman et al., 1984; Salters and Hart, 1989). This led Hauri and Hart (1997) to suggest garnet may also be a host for Re in the mantle. However, Hauri and Hart (1997) observed a co-variation between Re and S that was stronger than the co-variation between Re and any other element which suggests that Re is strongly controlled by sulfide. While Re probably is controlled by sulfide to an important extent, some silicate control on Re is required to explain that Re is moderately incompatible during mantle melting while Os is compatible. Thus, if Re and Os contents of sulfide inclusions mirror those of unencapsulated sulfides in the different mantle lithologies (as discussed above) and if the sulfides acquired their Re and Os in the same process as the whole-rock eclogite, one would expect lower Re/Os in sulfide inclusions than in the diamond host rock in which some "additional" Re would be hosted by garnet. Speculating on a precursor to an eclogitic host for Klipspringer diamonds, the affinity to basalts rather than ultramafic rocks would then be even more pronounced since the whole-rock eclogite would have a higher Re/Os than the sulfide inclusions.

Several studies have indicated that eclogite may be the product of subducted oceanic crust (see Chapter 1). As shown above, a hypothetical eclogite petrogenetically associated with the Klipspringer diamonds would show a closer affinity with basalts rather than ultramafic rocks and a speculative origin from subducted oceanic crust for the Re and Os in the sulfide inclusions may be proposed. The initial $^{187}Os/^{188}Os$ of 0.19±0.09 for the Klipspringer sulfides allows for an initial $^{187}Os/^{188}Os$ higher than the primitive mantle which would require a precursor that was enriched in Re over Os compared to primitive mantle for some time prior to diamond formation. However, the comparatively low initial $^{187}Os/^{188}Os$ of the Klipspringer sulfides place constraints on the timing of formation of a hypothetical precursor. A first approximation for this is given by comparison of the Os evolution of the Klipspringer sulfides and Udachnaya and Newlands eclogites. As can be seen in Figure 9.3 Newlands eclogites evolve radiogenic Os fairly slowly due to their low Re/Os akin to komatiites while Udachnaya eclogites display higher present-day $^{187}Os/^{188}Os$ due to their higher Re/Os possibly inherited from subducted oceanic basalts. This indicates that a hypothetical eclogite host of basaltic character for the Klipspringer diamonds must

have formed close in time to diamond formation and must have had a fairly low Re/Os. Even if an eclogite protolith akin to the Udachnaya sample with the lowest Re/Os ratio is assumed, the protolith could not have separated from a primitive mantle more than ~200 Ma prior to diamond formation. Thus, if a subduction scenario is proposed, with the Os in the sulfides originating from a subducted basalt, the diamonds and their eclogite host may well have formed at the same time around 2.5 Ga rather than that the diamonds formed during a tectonothermal event post-dating eclogite formation.

The $^{187}Os/^{188}Os$ of 0.19±0.09 overlaps within uncertainty the $^{187}Os/^{188}Os$ for primitive mantle at 2.5 Ga and a sub-lithospheric origin for the Os of the sulfides cannot be excluded.

10. GENERAL DISCUSSION

10.1 Mechanism of eclogitic diamond formation

It was shown in Chapter 6 that the bulk of the Klipspringer diamonds display low but significant nitrogen aggregation (the Low-T group) while most other diamonds contain highly aggregated nitrogen (the High-T group). Some diamonds from each of the eclogitic/grospyditic garnet inclusion paragenesis (KG-I to KG-IV) occur in the High-T nitrogen aggregation group while other diamonds from each paragenesis occur in the Low-T nitrogen aggregation group. Thus, although the two nitrogen aggregation groups have been suggested to represent different diamond formation events as argued in Chapter 6, their diamond inclusions seem to have acquired their major element compositions from the same source. This supports the conclusion from the FTIR data that the two groups are spatially related and it suggests that the difference in nitrogen aggregation state between the two groups is not a consequence of an origin of the diamonds from different levels and temperature regimes in the mantle. Rather, as suggested in Chapter 6, the High-T diamonds pre-date the Low-T diamonds and the former have seen a heating event (which enhanced the nitrogen aggregation) prior to the formation of the latter.

It cannot be excluded that the High-T group diamonds formed contemporaneously with an eclogitic host and perhaps are of an igneous origin. The two diamonds with multiple garnet inclusions displaying "large-scale" chemical disequilibrium are High-T type diamonds and the one diamond with multiple clinopyroxene inclusions displaying "large-scale" chemical disequilibrium is a High-T/Low-T type diamond. The "large-scale" disequilibrium is difficult to reconcile with a metamorphic origin through solid state diffusion or simple re-crystallisation of pre-existing garnet and clinopyroxene since this would require a substantial chemical disequilibrium on a micrometre scale in the eclogitic host-rock. The observed "large-scale" disequilibrium trends are concordant with the magmatic fractionation trends displayed by the KG-I/KG-II garnets which may imply that the High-T diamonds are of an igneous origin.

From the discussion in the first paragraph it is suggested that the Low-T group diamonds formed in the host-rock for the High-T group diamonds and that their silicate inclusions acquired their compositions from the surrounding host eclogite/grospydite. This could mean that the Low-T group diamonds are metamorphic or metasomatic in origin.

Alternatively, the host eclogite/grospydite was partially re-melted and the Low-T group diamonds precipitated from the melt. As mentioned in Chapter 7, the small size of syngenetic diamond inclusions compared to their xenolith counterparts implies that they co-crystallized with the diamonds. Further, it was argued above that the silicate inclusions acquired their major element compositions from the eclogite host-rock. For these reasons, the diamond inclusions in the Low-T diamonds are believed not to be products of either modal metasomatism or diffusion metasomatism of pre-existing minerals. An igneous origin for eclogitic diamonds has commonly been suggested (see Chapter 1). An igneous origin for the Low-T diamonds may also be suggested from the estimated formation temperatures which are higher than the temperatures recorded for any of the eclogitic nodules and higher than the time-averaged mantle residence temperatures for the diamonds. It was shown in Chapter 7 that different garnet and clinopyroxene mineral inclusion groups display distinctive magmatic fractionation trends which preclude any simple petrogenetic relationship between the different groups. This may imply that the silicate inclusions formed through magmatic fractionation of partial melts from different eclogitic/grospyditic protoliths in the mantle. However, if the Low-T diamonds formed from partial melts of the High-T diamond host-rock, one would expect the silicate inclusions from the Low-T diamonds to display more evolved compositions than the silicate inclusions from the High-T diamonds. Since this is not the case, the Low-T diamonds cannot without reservation be classified as igneous unless the host-rocks were completely re-melted. The alternating zones of Type I and Type II diamond which dominate three of the studied diamond plates (and which were inferred to be common amongst the Low-T group diamonds) with their enrichment and depletion respectively in N and H is not consistent with diamond growth through solid state diffusion in a closed environment as suggested by Haggerty (1986). The Low-T diamonds are therefore not believed to be of metamorphic origin. Neither are these features compatible with precipitation of diamonds from a melt in a closed system. Rather, the Low-T diamond formation was connected to the introduction of a foreign melt or fluid into an eclogite host rock. It may be possible that the diamonds are metasomatic in the sense that they acquired their C, N, H and S from an introduced melt during a heating event while their syngenetic silicate inclusions re-crystallised from pre-existing minerals in the protolith. As indicated by the bulk rock compositions that were reconstructed from mineral inclusion compositions, the eclogitic/grospyditic protoliths for the silicate inclusions mirror mid-ocean ridge cumulates in composition and may themselves have been related through magmatic fractionation (see Chapter 7).

While the bulk of the eclogitic inclusions acquired their compositions from their respective protoliths, an introduced melt/fluid may have been the main source of the C, N, H and S as previously proposed by Deines and Harris (1995). It has been shown that octahedral diamond grows under comparatively low C supersaturation (Sunagawa, 1984a,b). Thus, the presence of alternating fluids enriched and depleted respectively in C, N and H could explain why the Type II diamond zones observed in the polished plates are fairly depleted in N and H and trend towards pronounced octahedral growth contrary to the Type I diamond zones.

The predominance of sulfides amongst Klipspringer diamond inclusions as well as amongst diamonds from world-wide localities suggests that sulfides are intimately associated with diamond formation (e.g. Gurney et al., 1979b; Bulanova et al., 1990). Haggerty (1986) suggested that S (as well as N_2) may act as a catalyst during diamond formation. The solubility of reduced carbon in a sulfide melt is considerably higher than in a silicate melt (Saxena, 1989). The poorly developed octahedral growth zones in the alternating Type I/Type II diamond zones observed in the polished plates (and inferred for the bulk of the Low-T diamonds) may indicate a high growth rate in a sulfide melt (or a sulfur saturated silicate melt) that was highly supersaturated in C as previously suggested (Haggerty, 1986; Bulanova and Spetsius, 1990). The abundance of sulfide was likely the controlling factor for the prevailing redox conditions of the environment. If the introduced melt was the main carrier of C, N, H and S, the higher rate of growth of the Type I diamond may not only have been favoured and characterised by enriched levels of C, N and H but also by a reduced environment suitable for C, N and H to enter the diamond structure and vinylidene groups respectively. An introduced sulfur-rich melt may also have been the main source for the Fe and Ni (both which are strongly chalcophile) of the sulfide inclusions. Unless all the sulfide inclusions are related to only one of the recognised silicate inclusion parageneses, the very similar Fe and Ni compositions as well as S isotope characteristics of the sulfide inclusions is not compatible with the wide compositional range displayed by the silicate inclusions. This supports that the Fe, Ni and S were introduced into the diamond formation environment through a foreign sulfide-rich melt rather than derived from the diamond host-rock.

10.2 Thermal history of the lithosphere

Time-averaged mantle residence temperatures for the Low-T group diamonds are similar to equilibration temperatures for the Group I eclogites and the lherzolite II nodule. These rocks are believed to have recorded the temperatures that prevailed at lithospheric depths corresponding to pressures of 50-60 kbars (i.e. inside the diamond stability field) at the time of kimberlite eruption 150 Ma ago. This suggests that the diamondiferous part of the lithosphere on average cannot have been much hotter at the time of diamond formation (2.5±0.3 Ga) compared to 150 Ma ago and thus implies that a geotherm of 37-39 mW/m^2 was established already around the Proterozoic/Archaean boundary.

The higher temperatures recorded for diamond formation compared to the time averaged mantle residence temperatures for the diamonds and the equilibration temperatures of Group I eclogite nodules may have several explanations (or implications). The small-scale disequilibrium between garnet inclusions from individual Low-T diamonds, which form compositional trends discordant to the fractionation trends, may indicate diamond formation during slightly increasing or decreasing temperatures as mentioned in Chapter 7. Thus, the diamonds may have formed in the lithosphere under thermal perturbation (either during heating or subsequent temperature decrease) with subsequent thermal relaxation back to a steady-state geotherm of ~ 37-39 mW/m^2. This is compatible with a metasomatic origin for the diamonds since such a process probably was associated with a temporarily increased geotherm. A heating event associated with reactivation of the Thabazimbi-Murchinson Lineament (TML) (see further below) just prior to the formation of the Low-T diamonds may provide an explanation for the plastic deformation of the High-T diamonds which are at least as old as the Low-T diamonds (Chapter 6). The smaller size of the High-T diamonds may also suggest that extensive resorption of these diamonds occurred in the mantle at this event prior to the formation of the Low-T diamonds.

Alternatively, the diamonds have formed in or at the base of the lithosphere which was subsequently underplated either by sub-lithospheric material or by subducted oceanic crust. This would decrease the geotherm and consequently lower the temperature of the diamond residence environment. The emplacement of the Bushveld complex may have been associated with major underplating of the lithosphere as indicated by Re-Os data on peridotites from the Premier kimberlite (Carlson et al., 1999).

While it cannot be excluded that the recorded temperatures reflect a mechanical transport of the diamonds to a shallower lithospheric level subsequent to diamond

formation, a metasomatic/igneous process of formation was likely associated with a heating event as mentioned above. Thus, it is believed that the diamonds were formed under thermal perturbance with or without subsequent underplating of the lithosphere whereafter they were stored under thermal conditions similar to those that were prevalent in the mantle 150 Ma ago.

A steady-state geotherm may subsequently have been disturbed by addition of heat to the lithosphere during the Bushveld event. However, for two reasons, the Bushveld event is thought not to have affected the mantle hosting the Klipspringer diamonds to any major extent. First, the high diamond grade of the Klipspringer kimberlites indicates that any major heating event(s) subsequent to diamond formation did not likely obliterate diamonds. Secondly, while the plastic deformation of the High-T diamonds may have been associated with the Bushveld event (and reactivation of the TML) this is contradicted by the lack of plastic deformation amongst the Low-T diamonds since the two diamond populations were spatially related as argued above.

The current geotherm of 37-39 mW/m^2 is similar to xenolith geotherms for the Barkley West-Kimberley area and slightly lower than xenolith geotherms for Finsch and Monastery (Menzies and Baumgartner, 1998). It is indicative of a fairly cool lithosphere which would have been favourable for diamond preservation.

10.3 Geochemical constraints on the source of the diamond inclusions

Plate tectonics operating during the Archaean were probably roughly equivalent to modern-day plate tectonic processes (De Wit et al., 1992). However, a hotter Archaean earth must have been coupled with a higher heat flow which was likely accomplished by faster subduction of younger oceanic plates (Taylor and McLennan, 1995). It was argued in Chapter 9 that a suggested basaltic source for the Os of the sulfide inclusions could have fractionated from the primitive mantle up to ~ 200 Ma prior to sulfide inclusion and diamond formation. Thus, at a faster spreading rate of younger oceanic plates in the Archaean, the Os in the sulfide inclusions may have been derived from a subducted oceanic crust. However, as shown in Chapter 9, the initial Os isotope composition of the sulfides does not exclude the primitive mantle as a source. If it is assumed that the sulfide and silicate inclusions are petrogenetically related, this is somewhat contradictory to the indications from silicate inclusions which may be suggestive of a mid-ocean ridge (MOR) cumulate source for the major elements (Chapter 7). While a hydrothermally altered oceanic

crust with or without accompanying sediments can be excluded as a source for the sulfur of the sulfide inclusions, $\delta^{34}S$ data is compatible with both a MOR cumulate and a sub-lithospheric source.

The data may indicate a decoupling between Os and S of the sulfides and the major elements of the silicates with the former being introduced from the primitive mantle while the latter originate from eclogites derived from subducted oceanic crust. Thus, sub-lithospheric melts which carried the bulk of the Os and S may have been introduced into the lithosphere at 2.5±0.3 Ga while the silicate inclusions acquired their compositions from an older previously subducted protolith as discussed above.

Only five non-eclogitic diamonds have been recovered which precludes a detailed investigation of the origin of these diamonds. Non-eclogitic diamonds are nitrogen deficient, Type II diamonds and have been assigned to a websteritic or a harzburgitic paragenesis based in syngenetic mineral inclusions. Peridotitic Type II diamonds are not common and Taylor (1994) states that Type II diamonds most commonly are eclogitic and reflect an origin from subducted oceanic crust degassed of N_2. Schulze (1986) and Kesson and Ringwood (1989) have proposed a hydrated oceanic lithosphere and melt-depleted island-arc environments respectively as protoliths for harzburgitic diamonds (see Chapter 1). An origin from subducted degassed lithosphere rather than primitive mantle would explain the nitrogen deficiency of Klipspringer harzburgitic (and websteritic) diamonds.

10.4 Significance of the age of the diamonds

The derived age for the Low-T group diamonds carrying sulfide inclusions (2.5±0.3 Ga) has not been recognized for any type of diamonds previously and the Proterozoic/Archaean age is supported (or at least not contradicted) by the fairly aggregated nitrogen of the diamonds.

The lower group of the Ventersdorp lavas occurs in and to the south of the Witwatersrand basin and has been described as a typical continental flood basalt that covers >30000 km^2 and reaches a thickness of up to 2 km (Myers et al., 1990). The lavas have been dated at 2714±8 Ma (Armstrong et al., 1991) which may suggest a genetic link between the Klipspringer diamonds and the Ventersdorp event. Zegers et al. (1998) suggest that the Ventersdorp lavas and their equivalent in Australia, the Mt Roe basalts, may mark the onset of the break-up of the Vaalbara supercontinent. The age of the Ventersdorp lavas and the Klipspringer diamonds further correspond to the age of major reactivation of the

Thabazimbi-Murchinson Lineament (Good and De Wit, 1997) into which the Klipspringer kimberlite later intruded and which has been traced down to mantle depths from seismic anisotropy studies (Vinnik et al., 1995). Based on trace element and Sm-Nd isotope data, Nelson et al. (1992) conclude that partial melting, crystal fractionation and crustal contamination were not significant processes in the formation of the Ventersdorp lavas. Instead the geochemical differences between different magmatic sequences were attributed to formation from a heterogeneous source. The primitive to slightly enriched character of the Ventersdorp lavas is reflected in ε_{Nd}(2.7 Ga) ranging from 0.0 to –3.4 which is believed to reflect the character of the source for the lavas. Chondritic Re-Os model ages of 2.63 Ga and 2.72 Ga obtained for the Ventersdorp lavas (pers. comm. Marian Tredoux) are similar to the established age of 2714±8 Ma (Armstrong et al., 1991) and are indicative of a chondritic source for the lavas. The primitive to slightly fertile character of the Ventersdorp lavas mirrors the chondritic to slightly elevated initial $^{187}Os/^{188}Os$ for the Klipspringer sulfides. This may suggest that melts or fluids related to the Ventersdorp lavas may have been the source of the Os (and the Fe, Ni and S) of the Klipspringer sulfides (and the C, N and H of the diamonds).

10.5 Implications for diamond exploration

Several different diamond populations have been identified from FTIR data and mineral inclusion studies. Sampling of a wide variety of diamondiferous lithosphere may explain the relatively high diamond grade displayed by the Klipspringer kimberlites. The Marsfontein kimberlite carries a low nitrogen aggregation group diamonds for which the mineral inclusion paragenesis has not been identified and which is not present in the other investigated kimberlites. In contrast to the Main Fissure and Sugarbird Blow, the Marsfontein kimberlite also carries abundant dunitic concentrate garnets which may or may not be associated with diamonds. Any or both of these features may explain the exceptionally high diamond grade displayed by the Marsfontein kimberlite.

While peridotitic diamonds predominate world-wide, the present study shows the local importance of eclogitic diamonds. All three kimberlites studied are high-grade diamond deposits where eclogitic diamonds strongly predominate. This is in accordance with the common occurrence of Group I garnet macrocrysts in the kimberlites which shows the importance of eclogitic garnet prospecting in diamond exploration. Further, the high

diamond grade supports that kimberlite dykes may be economically viable (Gurney and Kirkley, 1996).

The emplacement of the dykes into the Thabazimbi-Murchinson Lineament (TML) is of significance for two reasons. First, it indicates that the kimberlite magma is likely emplaced into crustal to deep lithospheric structures. Further, a major lithospheric structure may be favourable for diamond formation since sub-lithospheric magmas or fluids may preferably enter along these structures. Thus, large scale tectonic structures should be primary targets in diamond exploration.

The diamond age derived (2.5±0.3 Ga) and the metamorphic or metasomatic nature of the diamonds have been proposed to perhaps correlate with the break-up of the Vaalbara super continent. The broad scale of this tectono-magmatic event is likely to have been important on a broad scale for diamond formation and thus major lineaments reactivated at this time are interesting diamond exploration targets.

Finally, the age of the Main and Sugarbird Fissures (~ 150 Ma) shows that any petrogenetically related kimberlite magmatism that possibly occurred to the south of the study area may have cross-cut (and thus may not obscured by) the ~ 180 Ma old Karroo volcanics. Thus, kimberlite exploration can perhaps be successfully extended to the south of the study area into the Karroo volcanic rocks.

11. CONCLUSIONS

11.1 Composition and thermal state of the mantle

The lithosphere sampled by the Klipspringer kimberlites is dominated by eclogite and lherzolite, with minor harzburgite and dunite. Group I eclogites (with elevated Na contents in the garnets) believed to originate from within the diamond stability field are more common than Group II eclogites. Garnet megacrysts sampled by the kimberlites are unusually Ti-poor at fairly high Mg-numbers and Cr_2O_3 levels. It is suggested that they represent an early garnet phase which crystallized prior to enrichment of Ti (and crystallization of ilmenite) and depletion of Mg and Cr in a fractionating megacryst parental magma.

A geotherm corresponding to a heat flow of 37-39 mW/m^2 has been inferred from eclogite equilibration temperatures and it is indicative of a fairly cool lithosphere favourable for diamond preservation. Assuming that the lherzolites equilibrated along a 37-39 mW/m^2 steady-state geotherm, estimated equilibration temperatures indicate that they are derived from a wide range of depths corresponding to pressures of ~ 35-60 kbars.

Time-averaged mantle residence temperatures (as deduced from nitrogen aggregation data) for the 2.5±0.3 Ga old diamonds (see 11.4) are similar to the temperatures that prevailed in the diamondiferous part of the lithosphere 150 Ma ago (as indicated by the equilibration temperatures of the mantle nodules). This indicates that a "cool" lithosphere geotherm probably was established already around the Proterozoic/Archaean boundary.

11.2 IR absorption characteristics and internal structure of the diamonds: Implications for multiple diamond formation events and the nature of the formation environment

The bulk of the Klipspringer diamonds are "regular" type I diamonds and most of them carry between 500 and 1300 ppm nitrogen. Two groups which display time-averaged mantle residence temperatures (for 2.5 Ga) of 1075-1090 °C (the Low-T group) and 1150-1180 °C (the High-T group) are present. Some diamonds have High-T type cores and Low-T type rims. This suggests that the diamonds of the two nitrogen aggregation groups were spatially related in the mantle and that the formation of the High-T diamonds predates the formation of the Low-T diamonds.

Poorly developed and complex internal octahedral structures in some of the Low-T diamonds are suggestive of rapid diamond growth under variable C concentrations. Together with variable N and H concentrations of different growth zones this indicates that the diamonds formed in an open environment from a fluid rather than in a closed magmatic environment or through solid state diffusion. The fluid was likely a sulfide fluid or a sulfide saturated fluid (see further 11.4) highly super-saturated in C which would explain the high rate of diamond growth.

A slightly lower rate of platelet peak evolution for the Low-T group diamonds compared to the High-T diamonds is somewhat contradictory to their lower time-averaged mantle residence temperatures. The Low-T diamonds are characterized by elevated H contents compared to the High-T diamonds. It is proposed that the presence of hydrogen may prohibit the formation of platelets or may enhance disaggregation of platelets.

The harzburgitic and websteritic diamonds are nitrogen deficient type II diamonds. This may reflect an origin from degassed oceanic crust/lithosphere which previously has been proposed to explain the nitrogen deficiency of eclogitic diamonds.

11.3 Silicate and oxide diamond inclusions: Implications for the origin of eclogitic/grospyditic inclusions and their host diamonds

In accordance with the high abundance of Group I garnet macrocrysts, eclogitic parageneses strongly dominate amongst diamond mineral inclusions. Out of 39 diamonds investigated for silicate and oxide inclusions, 34 are eclogitic (or grospyditic), 2 are websteritic and 3 are harzburgitic (or perhaps dunitic).

Three eclogitic/grospyditic petrogenetically different silicate/oxide inclusion parageneses are present: A grospydite, a rutile-kyanite eclogite and an "Fe-rich" eclogite paragenesis. Compositional variations within the different groups are compatible with magmatic fractionation. Multiple silicate inclusions from individual High-T group diamonds display "large-scale" chemical disequilibrium and their compositions are concordant with the magmatic fractionation trends displayed by other silicate inclusions. Together with elevated temperatures of formation this may imply an igneous origin for the High-T diamonds.

Some diamonds from each eclogitic/grospyditic inclusion paragenesis occur in the High-T group while other diamonds from each inclusion paragenesis occur in the Low-T group. This supports the implications from the FTIR data alone that the two N aggregation

group diamonds were spatially related in the mantle. Further, this indicates that the silicate inclusions of the Low-T diamonds acquired their compositions from the eclogitic/grospyditic host rocks for the High-T diamonds. Since inclusions from the Low-T diamonds generally do not display more evolved compositions than inclusions from the High-T diamonds, the former are not believed to have crystallised from a partial melt of their eclogitic/grospyditic host-rock. Neither did they form through solid-state diffusion (see 11.2) nor through modal or diffusion metasomatism (see 10.1). Rather, they formed through re-crystallisation of the minerals in the protolith during a thermal event as indicated by their elevated formation temperatures. It is proposed that the Low-T diamond inclusions and their host diamonds formed after thermal perturbation of the lithosphere during heating or subsequent cooling which is consistent with the "small-scale" chemical disequilibrium displayed by multiple inclusions from individual diamonds.

Estimated bulk rock compositions suggest that the eclogitic and grospyditic inclusions acquired their compositions from subducted mid-ocean ridge cumulates. While the compositional trends displayed by the different eclogitic/grospyditic paragenesis precludes any simple petrogenetic relationships between the groups their protoliths may have been related to each other through magmatic fractionation. The grospydite inclusions were derived from a high-Ca, high-Al protolith similar in composition to anorthosite. An extreme range in pseudojadeite (2-28 mole %) content of the grospyditic clinopyroxene inclusions is proposed to be dependent on the composition of the protolith and perhaps magmatic fractionation of a partial melt of the protolith rather than the prevalent pressures of formation of the clinopyroxene.

11.4 Sulfide diamond inclusions and their Re-Os and S isotope characteristics: Implications for the mechanism and regional context of diamond formation

Sulfide inclusions from 42 diamonds are dominated by pyrrhotite and they all belong to a low-Ni eclogitic paragenesis. Sulfide inclusions are by far more common than silicate and oxide inclusions. The very common occurrence of sulfide diamond inclusions supports previous suggestions that sulfides are intimately associated with diamond growth and that sulfur may act as a catalyst during diamond formation. The presence of sulfur would have maintained a reduced environment suitable for reduced carbon, nitrogen and hydrogen to enter the diamond and vinylidene structures.

Contrary to the silicate inclusions, the sulfides probably formed from one common source as indicated by their similar mineralogy and major element compositions and the very restricted range in sulfur isotope ratios. The derived Re-Os age of 2.5±0.3 Ga for some sulfide inclusions of the Low-T diamonds mirrors the age of the Ventersdorp lavas (~ 2.7 Ga). The age also corresponds to the break-up of the Vaalbara supercontinent and an episode of major re-activation of the Thabazimbi-Murchinson Lineament (~ 2.7 Ga) into which the Klipspringer kimberlites later intruded. Further, the primitive to slightly "fertile" Os and S isotope signatures of the sulfides compared to the primitive mantle mirror the primitive to slightly enriched Os and Nd characteristics of the Ventersdorp lavas. It is proposed that the bulk of the Klipspringer diamonds (represented by the Low-T group) were formed contemporary with the Ventersdorp lavas and that sub-lithospheric sulfide saturated melts introduced the C, N, and H of the diamonds and the S, Os, Fe, and Ni of their sulfide inclusions into the eclogitic/grospyditic protoliths. These elements are proposed to be decoupled from the major elements of the silicate inclusions, which, as mentioned, were acquired from the eclogite/grospydite protoliths. The Thabazimbi-Murchinson Lineament would have acted as a path-way for asthenospheric melts to enter the lithosphere.

11.5 The history of the diamonds subsequent to their formation

The frequent brown-pink colouration and the common occurrence of lamination lines amongst the High-T diamonds compared to the Low-T diamonds suggest that the former have experienced a heating event with associated deformation of the diamonds which predates the formation of the latter. This heating event may partly (but not fully) explain the elevated nitrogen aggregation of the High-T diamonds. The event may correspond to the thermal perturbation of the lithosphere associated with the formation of the Low-T diamonds with the shear-stress induced from the re-activation of the Thabazimbi-Murchinson Lineament. The smaller size of the High-T diamonds compared to the Low-T diamonds may suggest that resorption occurred in the mantle during the mentioned thermal event rather than in the kimberlite magma.

Most of the Main Fissure and Sugarbird Blow diamonds are heavily resorbed tetrahexahedra while the Marsfontein diamonds often display partly preserved primary octahedral surfaces. This could reflect different oxidation states of the kimberlite magmas, the release of the diamonds from host xenoliths at different levels in the kimberlite or

perhaps that resorption occurred in the mantle (as already suggested above for the High-T diamonds) under different physical condition at any time between diamond formation and kimberlite eruption.

11.6 The age and isotopic/mineralogic nature of the kimberlites

The Main Fissure and Sugarbird Blow diamonds were transported up from the lithosphere by their host-rocks around 150 Ma ago as shown by Rb-Sr isotope investigations of the kimberlites. Sr isotope characteristics are indicative of Group II kimberlites which is consistent with their Group II-type mineralogy. The age of the kimberlites is similar to that of the Group II Swartruggens kimberlite and a more wide-spread kimberlite emplacement event may be inferred at ~ 150 Ma.

11.7 Implications for diamond exploration from the present study

All three investigated kimberlites have to a large extent sampled the same eclogitic/grospyditic diamond populations to judge from silicate and sulfide inclusions. This is supported by the similar primary growth features (crystal structure and colour) of the diamonds from the different kimberlites as well as their similar secondary morphological features reflecting primary growth characteristics (terraces and zig-zag patterns). The domination of eclogitic diamonds is in accordance with the common occurrence of Group I eclogite garnet macrocrysts and shows the importance of eclogitic garnet prospecting in diamond exploration.

The presence of harzburgitic and websteritic diamonds as well as diamonds with different nitrogen contents and aggregation state compared to the mentioned parageneses partly explains the high diamond grades of the kimberlites. The high diamond grade of the kimberlites shows the importance of kimberlite dykes as exploration targets.

The spatial association between the diamond occurrence and the location of the Thabazimbi-Murchinson Lineament (TML) and the temporal association between diamond formation and a major reactivation of the TML shows the importance of large-scale tectonic structures (which reach down to lithospheric depths) for diamond formation. The break-up of the Vaalbara supercontinent with the re-activation of the TML and the Ventersdorp magmatism was a major tectono-magmatic event which likely was important for diamond formation on a large scale. Thus, large-scale tectonic structures that acted as path-ways for

these lavas and/or were formed or reactivated at the time of the formation of the lavas should be primary targets in diamond exploration.

Kimberlite exploration may be successfully extended southwards into the ~ 180 Ma Karroo volcanics since any kimberlites similar in age to the ones studied would have cross-cut the Karroo volcanics. However, further south and away from the TML it is less likely to find zones of crustal and lithospheric weakness which should be favourable for the intrusion of a kimberlite magma.

REFERENCES

Ai, Y. (1994). A revision of the garnet-clinopyroxene Fe^{2+}-Mg exchange geothermometer. *Contrib.Mineral.Petrol.*, **115**, 467-473.

Allegre, C.J. & Luck, J.-M. (1980). Osmium isotopes as petrogenetic and geological tracers. *Earth Planet.Sci.Lett.*, **48**, 148-154.

Allen, B.P. & Evans, T. (1981). Aggregation of nitrogen in diamond, including platelet formation. *Proc.R.Soc.Lond.*, **A375**, 93-104.

Allsopp, H.L. & Barrett, D.R. (1975). Rb-Sr age determinations on South African kimberlite pipes. *Phys.Chem.Earth*, **9**, 605-617.

Allsopp, H.L. & Kramers, J.D. (1977). Rb-Sr and U-Pb age determinations on southern African kimberlite pipes. *2nd Int.Kimberlite. Conf., Santa Fe, New Mexico, (extended abstracts).*

Allsopp, H.L. & Roddick, J.C. (1984). Rb-Sr and $^{40}Ar/^{39}Ar$ age determinations on phlogopite micas from the pre-Lebombo group Dokolwayo kimberlite pipe. *Geol.Soc.S.Afr., Spec.Publ.No.13*, 267-272.

Allsopp, H.L., Bristow, J.W., Smith, C.B., Brown, R., Gleadow, A.J.W., Kramers, J.D., & Garvie, O.G. (1989). A summary of radiometric dating methods applicable to kimberlites and related rocks. In J. Ross (Ed.), *Kimberlites and Related Rocks, Vol 1. Their Composition, Occurrence, Origin and Emplacement. Geol.Soc.Aus., Spec.Publ. No.14,* (pp. 343-357). Blackwell Scientific.

Armstrong, R.A., Compston, W., Retief, E.A., Williams, I.S., & Welke, H.J. (1991). Zircon ion microprobe studies bearing on the age and evolution of the Witwatersrand triad. *Prec.Res.*, **53**, 243-266.

Ater, P.C., Eggler, D.H., & McCallum, M.E. (1984). Petrology and geochemistry of mantle eclogite xenoliths from Colorado-Wyoming kimberlites: Recycled oceanic crust? In J. Kornprobst (Ed.), *Kimberlites II: The Mantle and Crust-Mantle Relationships,* (pp. 309-318). Elsevier.

Bachinski, D.J. (1969). Bond strength and sulfur isotopic fractionation in coexisting sulfides. *Econ.Geol.*, **64**, 56-65.

Barry, J.C. (1986). Voidites in diamond - do they contain nitrogen? *Ultramicroscopy*, **20**, 169-176.

Barry, J.C., Bursill, L.A., & Hutchinson, J.L. (1985). On the structure of {100} platelet defects in type Ia diamond. *Phil.Mag.*, **A48**, 109-121.

Bell, D.R., Schulze, D.J., Read, G.H., Mattioli, G.S., Shimizu, N., Moore, R.O., & Gurney, J.J. (1995). Geochemistry of Cr-poor megacrysts from the Lace (Group II) kimberlite, South Africa. *6th Int.Kimberlite Conf., Novosibirsk, (extended abstracts),* 52-54.

Berger, S.D. & Pennycock, S.J. (1982). Detection of nitrogen at {100} platelets in diamond. *Nature*, **298**, 635-637.

Berman, R., Hudson, P.R.W., & Martinez, M. (1975). Nitrogen in diamond: Evidence from thermal conductivity. *J.Phys.C: Solid St.Phys.*, **8**, L430-434.

Berman, R.G., Aranovich, L.Ya., & Pattison, D.R.M. (1995). Reassessment of the garnet-clinopyroxene Fe-Mg exchange thermometer: II. Thermodynamic analysis. *Contrib.Mineral.Petrol.*, **119**, 30-42.

Boyd, F.R. & Finnerty, A.A. (1980). Conditions of origin of natural diamonds of peridotite affinity. *J.Geophys.Res.*, **85**, 6911-6918.

Boyd, F.R. & Gurney, J.J. (1982). Low-calcium garnets: Keys to craton structure and diamond crystallization. *Carnegie Institution Wash.YB.*, **81**, 261-267.

Boyd, F.R. & Gurney, J.J. (1986). Diamonds and the African lithosphere. *Science*, **232**, 472-477.

Boyd, F.R. & Nixon, P.H. (1975). Origins of the ultramafic nodules from some kimberlites of northern Lesothoand the Moastery mine, South Africa. *Phys.Chem.Earth*, **9**, 431-454.

Boyd, F.R., Gurney, J.J., & Richardson, S.H. (1985). Evidence for a 150-200-km thick Archaean lithosphere from diamond inclusion thermobarometry. *Nature*, **315**, 387-389.

Boyd, S.R. & Pillinger, C.T. (1994). A preliminary study of $^{15}N/^{14}N$ in octahedral growth form diamonds. *Chem.Geol.*, **116**, 43-59.

Brandl, G. & de Wit, M.J. (1997). The Kaapvaal craton, South Africa. In M.J. de Wit & L.D. Ashwal (Eds.), *Greenstone belts. Oxford Monograph on Geology and Geophysics, 35,* (pp. 581-608). Clarendon Press, Oxford.

Brookins, D.G. (1967). The strontium geochemistry of carbonates in kimberlites and limestones from Riley County, Kansas. *Earth Planet.Sci.Lett.*, **2**, 235-240.

Brown, R., Allsopp, H.L., Bristow, J.W., & Smith, C.B. (1989). Improved precision of Rb-Sr dating of kimberlitic micas: An assessment of a leaching technique. *Chem.Geol.*, **79**, 125-136.

Bruley, J. (1992). Detection of nitrogen at {100} platelets in type IaA/B diamond. *Phil.Mag.*, **66**, 47-56.

Bruley, J. & Brown, L.M. (1989). Quantitative electron energy-loss spectroscopy microanalysis of platelet and voidite defects in natural diamonds. *Phil.Mag.*, **A59**, 247-261.

Bulanova, G.P. (1995). The formation of diamond. *J.Geochem.Exploration*, **53**, 1-23.

Bulanova, G.P. & Griffin, B.J. (1995). The origin of complex "agate" textures in octahedral diamonds from kimberlites. *6th Int.Kimberlite Conf., Novosibirsk, Russia, (extended abstracts),* 74-76.

Bulanova, G.P. & Milledge, H.J. (1995). Origin and history of growth of macrodiamonds from Yakutian kimberlites. *6th Int.Kimberlite Conf., Novosibirsk, Russia (extended abstracts)*, 77-79.

Bulanova, G.P. & Spetsius, Z.V. (1990). Inclusions in diamond and minerals of mantle xenoliths from kimberlites as a source of information on the upper mantle composition. *Int.Mineralogical Ass.Meeting, Beijing, (abstracts),* Vol. 2, 784-785.

Bulanova, G.P., Novgorodov, P.G., & Pavlova, L.A. (1988). A first find of melt inclusion in diamond from Mir pipe. *Geokhimiya*, **5**, 756-765, (in Russian).

Bulanova, G.P., Spetsius, Z., & Leskova, N.V. (1990). Sulfides in diamonds and mantle xenoliths from kimberlite pipes of Yakutiya. *Nauka, Novosibirsk*, (in Russian).

Bulanova, G.P., Griffin, W.L., Ryan, C.G., Shestakova, O.Y., & Barnes, S.-J. (1996). Trace elements in sulfide inclusions from Yakutian diamonds. *Contrib.Mineral.Petrol.*, **124**, 111-125.

Burgess, R., Turner, G., Laurenzi, M., & Harris, J.W. (1989). ^{40}Ar-^{39}Ar laser probe dating of individual clinopyroxene inclusions in Premier eclogitic diamonds. *Earth Planet.Sci.Lett.*, **94**, 22-28.

Burgess, R., Turner, G., & Harris, J.W. (1992). ^{40}Ar-^{39}Ar laser probe studies of clinopyroxene inclusions in eclogitic diamonds. *Geochim.Cosmochim.Acta*, **56**, 389-402.

Burgess, R., Phillips, D., Harris, J.W., & Robinson, D.N. (1998). Antarctic diamonds in south-eastern Australia? Hints from $^{40}Ar/^{39}Ar$ laser probe dating of clinopyroxene inclusions from Copeton diamonds. *7th Int.Kimberlite Conf., Cape Town, (extended abstracts)*, 119-121.

Bursill, L.A. & Glaisher, R.W. (1985). Aggregation and dissolution of small and extended defect structures in type Ia diamond. *Am.Miner.*, **70**, 608

Carlson, R.W., Esperanca, S., & Svisero, D.P. (1996). Chemical and Os isotopic study of Cretaceous potassic rocks from southern Brazil. *Contrib.Mineral.Petrol.*, **125**, 393-405.

Carlson, R.W., Pearson, D.G., Boyd, F.R., Shirey, S.B., Irvine, G., Menzies, A.H., & Gurney, J.J. (1999). Regional age variation of the southern African mantle: Significance for models of lithospheric mantle formation. In J.J. Gurney, J.L. Gurney, Pascoe M.D., & S.H. Richardson (Eds.), *Proc.7th Int.Kimberlite Conf., Vol. 1,* (pp. 99-108). Red Roof Design, Cape Town.

Cartigny, P., Harris, J.W., & Javoy, M. (1998a). Eclogitic diamond formation at Jwaneng: No room for a recycled component. *Science*, **280**, 1421-1424.

Cartigny, P., Harris, J.W., Phillips, D., Boyd, F.R., & Javoy, M. (1998b). Subducted-related diamonds? - The evidence for a mantle derived origin from coupled $\delta^{13}C$-$\delta^{15}N$ determinations. *Chem.Geol.*, **147**, 147-159.

Cawthorne.W.G. & Collerson, K.D. (1974). The recalculation of pyroxene end-member parameters and the estimation of ferrous and ferric iron content from electron microprobe analyses. *Am.Miner.*, **59**, 1203-1208.

Chaussidon, M., Albarede, F., & Sheppard, M.F. (1987). Sulphur isotope heterogeneity in the mantle from ion microprobe measurments of sulphide diamond inclusions. *Nature*, **330**, 242-244.

Chaussidon, M., Albarede, F., & Sheppard, M.F. (1989). Sulphur isotope variations in the mantle from ion microprobe analyses of micro-sulphide inclusions. *Earth Planet.Sci.Lett.*, **92**, 144-156.

Chinn, I. L. (1995). A study of unusual diamonds from the George Creek K1 kimberlite dyke, Colorado. Ph.D. Thesis, University of Cape Town, (unpublished).

Chrenko, R.M., McDonald, R.S., & Darrow, K.A. (1967). Infra-red spectra of diamond coat. *Nature*, **213**, 474-476.

Clackson, S.G., Moore, M., Walmsley, J.C., & Woods, G.S. (1990). The relationship between platelet size and the frequency of the B' infrared absorption peak in type Ia diamond. *Phil.Mag.*, **B62**, 115-128.

Clark, C.D. & Davey, S.T. (1984). One-phonon infrared absorption in diamond. *J.Phys.C: Solid St.Phys.*, **17**, 1127-1140.

Clark, C.D., Collins, A.T., & Woods, G.S. (1992). Absorption and luminescence spectroscopy. In J.E. Field (Ed.), *The properties of natural and synthetic diamond*, (pp. 35-79). Academic Press.

Collins, A.T. (1980). Vacancy enhanced aggregation of nitrogen in diamond. *J.Phys.C: Solid St.Phys.*, **13**, 2641-2650.

Collins, A.T. & Lightowlers, E.C. (1979). Electrical properties. In J.E. Field (Ed.), *The properties of diamond,* (pp. 79-105). Academic Press.

Craeser, R.A., Papanastassiou, D.A., & Wasserburg, G.J. (1991). Negative thermal ion mass spectrometry of osmium, rhenium, and iridium. *Geochim.Cosmochim.Acta*, **55**, 397-401.

Craigh, J.R. & Kullerud, G. (1969). Phase relations in the Cu-Fe-Ni-S system and their application to magmatic ore deposits. *Econ.Geol.Monograph*, **4**, 344-358.

Danchin, R.V. (1979). Mineral and bulk chemistry of garnet lherzolite and garnet harzburgite from the Premier mine, South Africa. In F.R. Boyd & H.O.A. Meyer (Eds.), *The Mantle Sample: Inclusions in Kimberlites and Other Volcanics,* (pp. 104-126), A.G.U.

Danchin, R.V. & Boyd, F.R. (1976). Ultramafic nodules from the Premier kimberlite pipe, South Africa. *Carnegie Institution Wash.YB.*, **75**, 531-538.

Daniels, L.R.M. & Gurney, J.J. (1989). The chemistry of the garnets, chromites and diamond inclusions from the Dokolwayo kimberlite, Kingdom of Swaziland. In J. Ross (Ed.), *Kimberlites and Related Rocks, Vol. 2. Their Mantle/Crust Setting, Diamonds and Diamond Exploration, Geol.Soc.Aus., Spec.Publ.No.14,* (pp. 1013-1021). Blackwell Scientific.

Davies, G. (1976). The A nitrogen aggregate in diamond - its symmetry and possible structure. *J.Phys C:Solid St.Phys*, **9**, L537-L542

Davies, G. (1979). Cathodoluminescence. In J.E. Field (Ed.), *The properties of diamond,* (pp. 165-181). Academic Press.

Davies, G. (1981). Decomposing the IR absorption spectra of diamonds. *Nature*, **290**, 40-41.

Davies, G.L. (1978). Zircons from the mantle. *4th Int.Conf.Geochron.Cosmochron., Isot.Geol., U.S.Geol.Serv.Open File Report*, **78-701**, 86-88.

Davies, R., Griffin, W.L., Pearson, N.J., Andrew, A., Doyle, B.J., & O'Reilly, S.Y. (1999). Diamonds from the deep: Pipe DO-27, Slave craton, Canada. In J.J. Gurney, J.L. Gurney, Pascoe M.D., & S.H. Richardson (Eds.), *Proc.7th Int.Kimberlite Conf., Vol. 1,* (pp. 148-155). Red Roof Design, Cape Town.

de Wit, M.J., Roering, C., Hart, R.J., Armstrong, R.A., de Ronde, C.E.J., Green, R.W.E., Tredoux, M., Peberdy, E., & Hart, R.A. (1992). Formation of an Archaean continent. *Nature*, **357**, 553-562.

Deines, P. & Harris, J.W. (1995). Sulfide inclusions chemistry and carbon isotopes of African diamonds. *Geochim.Cosmochim.Acta* , **59**, 3173-3188.

Droop, G.T.R. (1987). A general equation for estimating Fe3+ concentrations in ferromagnesian silicates and oxides from microprobe analyses, using stoichiometric criteria. *Mineral.Mag.,* **51,** 431-435.

DeVries, R.C. (1975). Plastic deformation and "Work-Hardening" of diamond. *Materials Res.Bull.*, **10**, 1193-1200.

Eldridge, C.S., Compston, W., Williams, I.S., Harris, J.W., & Bristow, J.W. (1991). Isotope evidence for the involvment of recycled oceanic sediments in diamond formation. *Nature*, **353**, 649-653.

Erlank, A.J. & Kushiro, I. (1970). Potassium contents of synthetic pyroxenes at high temperatures and pressures. *Carnegie Institution Wash.YB.*, **68**, 433-439.

Evans, T. (1992). Aggregation of nitrogen in diamond. In J.E. Field (Ed.), *The properties of natural and synthetic diamond,* (pp. 259-290). Academic press.

Evans, T. & Phaal, C. (1962). Imperfections in type I and II diamonds. *Proc.R.Soc.Lond.*, **A270**, 538-551.

Evans, T. & Qi, Z. (1982). The kinetics of the aggregation of nitrogen atoms in diamond. *Proc.R.Soc.Lond.*, **A381**, 159-178.

Evans, T., Kiflaw, I., Luyten, W., van Tendeloo, G., & Woods, G.S. (1995). Conversion of platelets into dislocation loops and voidite formation in type IaB diamonds. *Proc.R.Soc.Lond.*, **A449**, 295-305.

Fallon, P.J., Brown, L.M., Barry, J.C., & Bruley, J. (1995). Nitrogen determination and characterization in natural diamond platelets. *Phil.Mag.A*, **72**, 21-37.

Finnerty, A.A. & Boyd, F.R. (1984). Evaluation of thermobarometers for garnet peridotites. *Geochim.Cosmochim.Acta*, **48**, 15-27.

Fletcher, T.A., Boyce, A.J., & Fallick, A.E. (1989). A sulphur isotope study of Ni-Cu mineralisation in the Huntley-Knock Caledonian mafic and ultramafic intrusions of northeast Scotland. *J.Geol.Soc.London*, **146**, 675-684.

Foster, J.G., Lambert, D.D., Frick, L.R., & Maas, R. (1996). Re-Os isotopic evidence for genesis of Archean nickel ores from uncontaminated komatiites. *Nature*, **382**, 703-706.

Ganguly, J. (1979). Garnet and clinopyroxene solid solutions, and geothermometry based on Fe-Mg distribution coefficient. *Geochim.Cosmochim.Acta*, **43**, 1021-1029.

Gasparik, T. (1985). Experimental study of subsolidus phase relations and mixing properties of pyroxene and plagioclase in the system Na_2O-CaO-Al_2O_3-SiO_2. *Contrib.Mineral.Petrol.*, **89** , 346-357.

Good, N. (1997). Tectonic evolution and structural controls on the fluid flow along the Thabazimbi-Murchinson lineament, northern Transvaal, South Africa. Ph.D Thesis, University of Cape Town, (unpublished).

Good, N. & de Wit, M.J. (1997). The Thabazimbi-Murchinson lineament of the Kaapvaal craton, South Africa: 2700 Ma of episodic deformation. *J.Geol.Soc., London*, **154**, 93-97.

Gorina, I.F. (1971). Crystal morphology of diamonds in Anabaro-Oleneksky Interfluve. In M.I. Rabkin, V.A. Milashev, & L.S. Yegorov (Eds.), *Kimberlite volcanism and prospects for primary diamond content in the north-eastern part of the Siberian platform,* Arctic Geology Research Institute of the USSR Ministry of Geology, Leningrad, (in Russian).

Griffin, W.L., Jaques, A.L., Ryan, C.G., Cousens, D.R., & Suter, G.F. (1988). Conditions of diamond growth: A proton microprobe study of inclusions in West Australian diamonds. *Contrib.Mineral.Petrol.*, **99**, 143-158.

Griffin, W.L., Gurney, J.J., & Ryan, C.G. (1992). Variations in trapping temperatures in peridotite-suite inclusions from South African diamonds: Evidence for two inclusion suites, and implications for lithosphere stratigraphy. *Contrib.Mineral.Petrol.*, **110**, 1-15.

Griffin, W.L., Sobolev, N.V., Ryan, C.G., Pokhilenko, N.P., Win, T.T., & Yefimova, E.S. (1993). Trace elements in garnets and chromites: Diamond formation in the Siberian lithosphere. *Lithos*, **29**, 235-256.

Grutter, H.S. (1998). Chrome-calcium, magnesium number and yttrium characteristics of garnets in depleted lherzolitic, harzburgitic and dunitic mantles. *7th Int.Kimberlite Conf., Cape Town, (extended abstracts)*, 277-279.

Gurney, J. J. (1989). Diamonds. In J. Ross (Ed.), *Kimberlites and Related Rocks, Vol. 2. Their Mantle/Crust Setting, Diamonds and Diamond Exploration, Geol.Soc.Aust., Spec.Publ. No.14,* (pp. 935-965). Blackwell Scientific.

Gurney, J.J. & Harte, B. (1980). Chemical variations in upper mantle nodules from southern African kimberlites. *Phil.Trans.R.Soc.Lond.*, **A297**, 273-293.

Gurney, J.J. & Kirkley, M.B. (1996). Kimberlite dyke mining in South Africa. *Afr.Geoscience Rev.*, **3**, 191-201.

Gurney, J.J. & Zweistra, P. (1995). The interpretation of the major element compositions of mantle minerals in diamond exploration. *J.Geochem.Exploration*, **53**, 293-309.

Gurney, J.J., Jakob, W.R.O., & Dawson, J.B. (1979a). Megacrysts from the Monastery kimberlite pipe, South Africa. In F.R. Boyd & H.O.A. Meyer (Eds.), *The Mantle Sample: Inclusions in Kimberlites and Other Volcanics,* (pp. 227-243). AGU.

Gurney, J.J., Harris, J.W., & Rickard, R.S. (1979b). Silicate and oxide inclusions in diamonds from the Finsch kimberlite pipe. In F.R. Boyd & H.O.A. Meyer (Eds.), *Kimberlites, Diatremes and Diamonds: Their Geology, Petrology and Geochemistry,* (pp. 1-15). A.G.U.

Gurney, J.J., Harris, C., & Rickard, R.S. (1984a). Silicate and oxide inclusions in diamonds from the Orapa Mine, Botswana. In J. Kornprobst (Ed.), *Kimberlites II: The Mantle and Crust-Mantle Relationship*, (pp. 3-9). Elsevier.

Gurney, J.J., Harris, J.W., & Rickard, R.S. (1984b). Minerals associated with diamonds from the Roberts Victor mine. In J. Kornprobst (Ed.), *Kimberlites II: The Mantle and Crust-Mantle Relationship,* (pp. 25-32). Elsevier.

Gurney, J.J., Harris, J.W., Rickard, R.S., & Moore, R.O. (1985). Inclusions in Premier mine diamonds. *Trans.Geol.Soc.S.Afr.*, **88**, 301-310.

Gurney, J.J., Harris, J.W., Otter, M.L. & Rickard, R.S. (1995). Jwaneng diamond inclusions. *6th Int.Kimberlite Conf., Novosibirsk, (extended abstracts),* 208-210.

Haggerty, S.E. (1986). Diamond genesis in a multiply constrained model. *Nature*, **320**, 34-38.

Haggerty, S.E. (1989). Upper mantle opaque mineral stratigraphy and the genesis of metasomites and alkali-rich melts. In J. Ross (Ed.), *Kimberlites and Related Rocks, Vol. 2. Their Mantle/Crust Setting, Diamonds and Diamond Exploration,* (pp. 687-699). Blackwell Scientific.

Hall, A.E. & Smith, C.B. (1984). Lamproite diamonds-are they different? In J.E. Glover & P.G. Harris (Eds.), *Kimberlite Occurence and Origin: A basis for conceptual models in exploration, Geol. Dept. and Univ. Extention, Univ. of Western Australia, Publ. No. 8.,* (pp. 167-212).

Hanley, P.L., Kiflawi, I., & Lang, A.R. (1977). On topographically identifiable sources of cathodoluminescence in natural diamonds. *Phil.Trans.R.Soc.Lond.*, **A284**, 329-368.

Harlow, G.E. (1992). Potassium clinopyroxene at high pressure. *Geol.Soc.Amer., Session 48-A129, (abstract).*

Harlow, G.E. (1999). Interpretation of Kcpx and CaEs components in clinopyroxene from diamond inclusions and mantle samples. In J.J. Gurney, J.L. Gurney, Pascoe M.D., & S.H. Richardson (Eds.), *Proc.7th Int.Kimb.Conf., Vol. 1,* (pp. 321-331). Red Roof Design, Cape Town.

Harris, J.W. (1992). Diamond geology. In J.E. Field (Ed.), *The properties of natural and synthetic diamond,* (pp. 345-393). Academic press, London.

Harris, J.W. & Collins, A.T. (1985). Studies of Argyle diamonds. *Ind.Diamond Rev.*, **3**, 128-130.

Harris, J.W. & Gurney, J.J. (1979). Inclusions in diamond. . In J.E. Field (Ed.), *The properties of diamond,* (pp. 555-591). Academic Press, London.

Harris, J.W., Hawthorne, J.B., & Oosterveld, M.M. (1984). A comparison of diamond characteristics from the De Beers pool mines, Kimberley, South Africa. In J Kornprobst (Ed.), *Ann.Sci.Univer.Clermont Ferrand II, 74,* (pp. 1-13). Elsevier.

Harris, J.W., Hutchinson, M.T., Hursthouse, M., Light, M., & Harte, B. (1997). A new tetragonal silicate mineral occurring as inclusions in lower mantle diamonds. *Nature*, **387**, 486-488.

Harrison, A.G. & Thode, H.G. (1958). Mechanism of the bacterial reduction of sulfate from fractionation studies. *Trans.Faraday Soc.*, **54**, 84-92.

Hart, S.R. & Ravizza, G.E. (1996). Os partitioning between phases in lherzolite and basalt. In H. Basu & S.R. Hart (Eds.), *Earth processes: Reading the isotopic code, Geophys. Monogr. 95,* (pp. 123-134).

Harte, B. & Harris, J.W. (1994). Lower mantle mineral associations preserved in diamonds. *Mineral.Mag.*, **58A**, 384-385.

Harte, B., Hutchinson, M.T., Lee, M., & Harris, J.W. (1998). Inclusions of (Fe,Mg)O in mantle diamonds. *7th Int.Kimberlite Conf., Cape Town, (extended abstracts),* 308-310.

Hatton, C.J. (1978). The geochemistry and origin of xenoliths from the Roberts Victor mine. Ph.D. Thesis, University of Cape Town, (unpublished).

Hatton, C.J. & Gurney, J.J. (1977). Igneous fractionation trends in Roberts Victor eclogites. *2nd Int.Kimberlite Conf., Santa Fe, New Mexico, (extended abstracts).*

Hauri, E.H. & Hart, S.R. (1997). Rhenium abundances and systematics in oceanic basalts. *Chem.Geol.*, **139**, 185-205.

Hauri, E.H., Lassiter, J.C., & DePaolo, D.J. (1996). Osmium isotope systematics of drilled lavas from Mauna Loa, Hawaii. *J.Geophys.Res.*, **101**, 11793-11806.

Helmstaedt, H. & Doig, R. (1975). Eclogite nodules from kimberlite pipes of the Colorado Plateau - samples of Franciscan-type oceanic lithosphere. *Phys.Chem.Earth*, **9**, 95-111.

Hoffmann, A.W. & White, W.M. (1982). Mantle plumes from subducted oceanic crust. *Earth Planet.Sci.Lett.*, **57**, 421-436.

Hoffmann, A.W., Feigenson, M.D., & Raczek, I. (1984). Case studies on the origin of basalts. III. Petrogenesis of the Mauna Ulu eruption, Kilauea, 1969-1971. *Contrib.Mineral.Petrol.*, **88**, 24-35.

Hutchinson, M. T. (1997). Constitution of the sub-lithospheric mantle shown by diamonds and their inclusions. Ph.D Thesis, University of Edinburgh, (unpublished).

Ionov, D.A., Hoefs, J.H., Wedepohl, K.H., & Wiechert, U. (1992). Content and isotopic composition of sulphur in ultramafic xenoliths from central Asia. *Earth Planet.Sci.Lett.*, **111**, 269-286.

Ireland, T.R., Rudnick, R.L., & Spetsius, Z. (1994). Trace elements in diamond inclusions from eclogites reveal link to Archean granites. *Earth Planet.Sci.Lett.*, **128**, 199-213.

Irifune, T. & Ringwood, A.E. (1993). Phase transformations in subducted oceanic crust and buoyancy relationships at depths of 600-800 km in the mantle. *Earth Planet.Sci.Lett.*, **117**, 101-110.

Irifune, T., Hibberson, W. A., and Ringwood, A. E. (1989). Eclogite-garnetite transformation at high pressure and its bearing on the occurrence of garnet inclusions in diamond. In J. Ross (Ed.), *Kimberlites and Related Rocks, Vol. 2. Their Mantle/Crust Setting, Diamonds and Diamond Exploration, Geol.Soc.Aust., Spec.Publ. No.14,* (pp. 877-882). Blackwell Scientific.

Jacob, D.E. & Foley, S.F. (1998). Evidence for Archaean ocean crust with island arc signature from diamondiferous eclogite xenoliths. *7th Int.Kimb.Conf., Cape Town, (extended abstracts)*, 358-360.

Jacob, D.E., Jagoutz, E., Lowry, D., Mattey, D., & Kudrjavtseva, G. (1994). Diamondiferous eclogites from Siberia: Remnants of Archaean oceanic crust. *Geochim.Cosmochim.Acta*, **58**, 5191-5207.

Jagoutz, E., Dawson, J.B., Hoernes, S., Spettel, B., & Wanke, H. (1984). Anorthositic oceanic crust in the Archaean. *15th Lunar and Planetary Science Conference, Houston, (extended abstracts).*

Jahn, B., Grau, G. & Glikson, A.Y. (1982). Komatiites of the Onverwacht group, South Africa: REE geochemistry, Sm/Nd age and mantle evolution. *Contrib.Mineral.Petrol.*, **80**, 25-40.

James, D.E., van der Lee, S., Gao, S., Silver, P., & VanDecar, J. (1997). Kaapvaal project: Preliminary seismic observations and analysis. *Supplement to EOS Trans.Am.Geophys.Union*, 78, No.46, F495.

Jaques, A. L., Hall, A. E., Sheraton, J. W, Smith, C. W., Sun, S-S., Drew, R. M., Foudoulis, C., and Ellingsen, K. (1989). Composition of crystalline inclusions and C isotopic composition of Argyle and Ellendale diamonds. In J. Ross (Ed.), *Kimberlites and Related Rocks, Vol. 2. Their Mantle/Crust Setting, Diamonds and Diamond Exploration, Geol.Soc.Aust., Spec.Publ. No.14,* (pp. 966-989). Blackwell Scientific.

Jarikov, V.A., Ishbulatov, R.A., & Chudinovskih, L.T. (1984). The eclogitic barrier and clinopyroxenes of high pressure, *Geol.Geophys.*, **12**, 54, (in Russian).

Jones, M.Q.W. (1999). A review of heat flow in southern Africa and the thermal structure of the lithosphere. *S.Afr.Geoph.Rev.*, in press.

Jones, R., Briddon, P.R., & Oberg, S. (1992). First-principle theory of nitrogen aggregates in diamond. *Phil.Mag.Lett.*, **66**, 67-74.

Jordan, T.H. (1978). Composition and development of the continental tectosphere. *Nature*, **274**, 544-548.

Kaiser, W. & Bond, W.L. (1959). Nitrogen, a major impurity in common type I diamond. *Phys.Rev.*, **115**, 857-863.

Kennedy, C.S. & Kennedy, G.C. (1976). The equilibrium boundary between graphite and diamond. *J.Geophys.Res.*, **81**, 2467-2470.

Kesson, S.E. & Ringwood, A.E. (1989). Slab-mantle interactions, 2. The formation of diamonds. *Chem.Geol.*, **78**, 97-118.

Kinny, P.D. & Meyer, H.O.A. (1995). Zircon from the mantle: A new way to date old diamonds. *J.Geol.,* 102, 475-482.

Kirkley, M.B., Gurney, J.J., Otter, M.L., Hill, S.J., & Daniels, L.R.M. (1991). The application of C isotope measurments to the identification of the sources of C in diamonds. *Appl.Geochem.*, **6**, 447-494.

Klump, J. (1995). A pilot study of the Swartruggens kimberlite dyke swarm. B.Sc. Honours project, University of Cape Town, (unpublished).

Koons, P.O. (1984). Implications to garnet-clinopyroxene geothermometry of non-ideal solid solution in jadeitic pyroxenes. *Contrib.Mineral.Petrol.*, **88**, 340-347.

Kramers, J.D. (1979). Lead, uranium, strontium, potassium and rubidium in inclusion-bearing diamonds and mantle-derived xenoliths from southern Africa. *Earth Planet.Sci.Lett.*, **42**, 58-70.

Krogh, E.J. (1988). The garnet-clinopyroxene Fe-Mg geothermometer - a reinterpretation of existing experimental data. *Contrib.Mineral.Petrol.*, **99**, 44-48.

Lang, A.R. (1964). A proposed structure for nitrogen impurity platelets found in diamond. *Proc.Phys.Soc.Lond.*, **84**, 871-876.

Lang, A.R. (1974). On the growth-sectorial dependence of defects in natural diamonds. *Proc.R.Soc.Lond.*, **340**, 233-248.

Lappin, M.A. (1978). The evolution of a grospydite from the Roberts Victor mine, South Africa. *Contrib.Mineral.Petrol.*, **66**, 229-241.

Le Roex, A.P., Dick, H.J.B., Gulen, L., Reid, A.M. & Erlank, A.J. (1987). Local and regional heterogeneity in MORB from the Mid-Atlantic Ridge between 54.4°S and 51°S: Evidence for geochemical enrichment. *Geochim.Cosmochim.Acta,* **51,** 541-555.

Le Roex, A.P., Dick, H.J.B. & Fisher, R.L. (1989). Petrology and geochemistry of MORB from 25°E to 46°E along the Southwest Indian Ridge: Evidence for contrasting styles of mantle enrichment. *J. Petrol.,* **30,** 947-986.

Lorand, J.P. (1989). Mineralogy and chemistry of Cu-Fe-Ni sulfides in mantle-derived spinel peridotite bodies from Ariege (northeastern Pyrenees, France). *Contrib.Mineral.Petrol.*, **103**, 335-345.

Loubser, J.H.N. & van Wyk, J.A. (1981). *Diamond Conference Abstracts, Reading*, 35-40, (unpublished).

Loubser, J.H.N. & Wright, A.C.J. (1973). Discussion on the Endor and ESR spectra of diamonds with the N3 optical system. *Diamond Research, Industrial Diamond Information Bureau*, 16-20.

MacGregor, I.D. & Carter, J.L. (1970). The Chemistry of Clinopyroxenes and Garnets of Eclogite and Peridotite Xenoliths from the Roberts Victor Mine, South Africa. *Phys.Earth Planet Interiors*, **3**, 391-397.

MacGregor, I.D. & Manton, W.I. (1986). Roberts Victor eclogites: Ancient oceanic crust. *J.Geoph.Res.*, **91**, 14063-14079.

McCandless, T.E. & Gurney, J.J. (1989). Sodium in garnet and potassium in clinopyroxene: criteria for classifying mantle eclogites. In J. Ross (Ed.), *Kimberlites and Related Rocks, Vol. 2. Their Mantle/Crust Setting, Diamonds and Diamond Exploration,* (pp. 827-832). Blackwell Scientific.

Mendelssohn, M. J. (1971). The etching of diamond and the associated minerals garnet and olivine. Ph.D Thesis, University of London, (unpublished).

Mendelssohn, M. & Milledge, H.J. (1995). Geological significant information from routine analysis of the mid-infrared spectra of diamonds. *Int.Geol.Rev.*, **37**, 95-110.

Menzies, A.M. & Baumgartner, M.C. (1998). Application of garnet geothermobarometry to southern African kimberlites. *7th Int.Kimberlite Conf., Cape Town, (extended abstracts),* 570-572.

Menzies, A.H., Shirey, S.B., Carlson, R.W., & Gurney, J.J. (1998). Re-Os systematics of diamond-bearing eclogites and peridotites from Newlands kimberlite. *7th Int.Kimb.Conf., Cape Town, (extended abstracts)*, 579-581.

Meyer, H.O.A. (1985). Genesis of diamond: a mantle saga. *Am.Miner.*, **70**, 344-355.

Meyer, P.S., Dick, H.J.B. & Thompson, G. (1989). Cumulate gabbros from the Southwest Indian Ridge 54°S-71°6'E: Implications for magmatic processes at a slow spreading ridge. *Contrib.Mineral.Petrol.*, **103**, 44-63.

Milledge, H.J., Mendelssohn, M., Boyd, S.R., Pillinger, C.T., van Heerden, L.A., & Seal, M. (1989). I/R, C/L and MS data for Finsch diamonds and an Argyle stone exhibiting giant platelets. *Diamond Conference Abstracts, Bristol*, (unpublished).

Moore, R.O. & Gurney, J.J. (1985). Pyroxene solid solution in garnets included in diamond. *Nature*, **318** , 553-555.

Moore, R. O. and Gurney, J. J. (1989). Mineral inclusions in diamonds from the Monastery kimberlite, South Africa. In J. Ross (Ed.), *Kimberlites and Related Rocks, Vol. 2. Their Mantle/Crust Setting, Diamonds and Diamond Exploration, Geol.Soc.Aust., Spec.Publ. No.14,* (pp. 1029-1041). Blackwell Scientific.

Moore, R.O. & Gurney, J.J. (1991). Garnet megacrysts from Group II kimberlites in southern Africa. *5th Int.Kimberlite Conf., Brazil, (extended abstracts)*, 298-300.

Moore, R.O., Otter, M.L., Rickard, R.S., Harris, J.W., & Gurney, J.J. (1986). The occurrence of moissanite and ferro-periclase as inclusions in diamond. 4th Int.Kimberlite Conf., Perth, (extended abstracts), 409-411.

Moore, R.O., Griffin, W.L., Gurney, J.J., Ryan, C.G., Cousens, D.R., Sie, S.H., & Suter, G.F. (1992). Trace element geochemistry of ilmenite megacrysts from the Monastery kimberlite, South Africa. *Lithos*, **29**, 1-18.

Morgan, J.W. (1996). Ultramafic xenoliths: Clues to Earth's late accretionary history. *J.Geoph.Res.*, **91**, 12375-12387.

Mori, T. & Green, D.H. (1978). Laboratory duplication of phase equilibria observed in natural garnet lherzolites. *J.Geol.*, **86**, 83-97.

Myers, R.E., McCarthy, T.S., Bunyard, M., Cawthorne, R.G., Falatsa, T.M., Hewitt, T., Linton, P., Myers, J.M., Palmer, K.J., & Spencer, R. (1990). Geochemical stratigraphy of the Klipriviersberg group volcanic rocks. *S.Afr.J.Geol.*, **93**, 224-238.

Mysen, B. & Griffin, W.L. (1973). Pyroxene stoichiometry and the breakdown of omphacite. *Am.Miner.*, **53** , 60-63.

Navon, O. (1999). Diamond formation in the earth's mantle. In J.J. Gurney, J.L. Gurney, Pascoe M.D., & S.H. Richardson (Eds.), *Proc7th Int.Kimberlite Conf., Vol 2,* (pp. 584-604). Red Roof Design, Cape Town.

Nelson, D.R., Trendall, A.F., de Laeter, J.R., Grobler, N.J., & Fletcher, I.R. (1992). A comparative study of the geochemical and isotopic systematics of late Archaean flood basalts from the Pilbara and Kaapvaal cratons. *Prec.Res.*, **54**, 231-256.

Nielsen, H. (1978). Sulfur isotopes in nature. In K.H. Wedepohl (Ed.), *Handbook of geochemistry.* Springer-Verlag.

Ohmoto, H. & Rye, R.O. (1979). Isotopes of sulfur and carbon. In H.L. Barnes (Ed.), *Geochemistry of Hydrothermal Ore Depositis,* (pp. 509-567). John Wiley and Sons.

Orlov, Yu.I. (1977). *The mineralogy of the diamond.* John Wiley and Sons.

Otter, M. L. and Gurney, J. J. (1989). Mineral inclusions in diamonds from the Sloan diatremes of the Colorado-Wyoming state line kimberlite district, North America. In J. Ross (Ed.), *Kimberlites and Related Rocks, Vol. 2. Their Mantle/Crust Setting, Diamonds and Diamond Exploration, Geol.Soc.Aust., Spec.Publ. No.14,* (pp. 1042-1053). Blackwell Scientific.

Parman, S.W., Dann, J.C., Grove, T.L. & de Wit, M.J. (1997). Emplacement conditions of komatiite magmas from the 3.49 Ga Komati formation, Barberton greenstone belt, South Africa. *Earth Planet.Sci.Lett.*, **150,** 303-323.

Pattison, D.R.M. & Newton, R.C. (1989). Reversed experimental calibration of the garnet-clinopyroxene Fe-Mg exchange thermometer. *Contrib.Mineral.Petrol.*, **101**, 87-103.

Pearson, D.G. & Shirey, S.B. (1999). Isotope dating of diamonds. *Economic Geology special publication: Applications of radiogenic isotopes to ore deposit research,* 143-171.

Pearson, D.G., Shirey, S.B., Carlson, R.W., Boyd, F.R., Pokhilenko, N.P., & Shimizu, N. (1995a). Re-Os, Sm-Nd and Rb-Sr isotope evidence for thick Archaean lithospheric mantle beneath the Siberian craton modified by multistage metasomatism. *Geochim.Cosmochim. Acta,* **59**, 959-977.

Pearson, D.G., Snyder, G.A., Shirey, S.B., Taylor, L.A., Carlson, R.W., & Sobolev, N.V. (1995b). Archaean Re-Os age for Siberian eclogites and constraints on Archaean tectonics. *Nature*, **374**, 711-713.

Pearson, D.G., Shirey, S.B., Harris, J.W., & Carlson, R.W. (1998a). Sulfide inclusions in diamonds from the Koffiefontein kimberlite, S. Africa: constraints on diamond age and mantle Re-Os systematics. *Earth Planet.Sci.Lett.*, **160**, 311-326.

Pearson, D.G., Shirey, S.B., Bulanova, G.P., Carlson, R.W., & Milledge, H.J. (1998b). Dating diamonds using the Re-Os technique: A study of sulfide inclusions in Siberian diamonds. *7th Int.Kimberlite Conf., Cape Town, (extended abstracts)*, 661-663.

Pearson, D.G., Davies, R., Shirey, S.B., Carlson, R.W., & Griffin, W.L. (1998c). The age and origin of eastern Australian diamonds: Re-Os isotope evidence from sulfide inclusions in two diamonds from Wellington, New South Wales. *7th Int.Kimberlite Conf., Cape Town, (extended abstracts)*, 664-666.

Pearson, D.G., Shirey, S.B., Bulanova, G.P., Carlson, R.W., & Milledge, H.J. (1999a). Re-Os isotope measurements of single sulfide inclusions in a Siberian diamond and its nitrogen aggregation state. *Geochim.Cosmochim.Acta*, **63**, 703-711.

Pearson, D.G., Shirey, S.B., Bulanova, G.P., Carlson, R.W., & Milledge, H.J. (1999b). Dating and paragenetic distinction of diamonds using the Re-Os isotope system: application to some Siberian diamonds. In J.J. Gurney, J.L. Gurney, Pascoe M.D., & S.H. Richardson (Eds.), *Proc. 7th Int. Kimberlite Conf., Vol. 2* (pp. 637-643). Red Roof Design, Cape Town.

Phaal, C. (1965). Surface studies of diamond. *Ind.Diamond Rev.*, **25**, 486-489 and 591-595.

Phillips, D., Onstott, T.C., & Harris, J.W. (1989). $^{40}Ar/^{39}Ar$ laser-probe dating of diamond inclusions from the Premier kimberlite. *Nature*, **340**, 460-462.

Phillips, D., Harris, J.W., Kiviets, G.B., Burgess, R., & Fourie, L.F. (1998). $^{40}Ar/^{39}Ar$ laser probe analyses of clinopyroxene diamond inclusions from the Orapa and Mbuyi-Miya mines. *7th Int.Kimb.Conf., Cape Town, (extended abstracts)*, 687-689.

Pidgeon, R.T. (1989). Archaean diamond xenocrysts in kimberlites - how definitive is the evidence? In J. Ross (Ed.), *Kimberlites and Related rocks, Vol. 2. Their Mantle/Crust Setting, Diamonds and Diamond Exploration, Geol.Soc.Aust., Spec.Publ. No.14,* (pp. 1070-1074). Blackwell Scientific.

Polat, A., Kerrich, R. & Wyman, D.A. (1999). Geochemical diversity in oceanic komatiites and basalts from the late Archaean Wawa greenstone belt, Canada: Trace element and Nd isotope evidemce for a heterogeneous mantle. *Prec.Res.*, **94**, 139-173.

Pollack, H.N. & Chapman, D.S. (1977). On the regional variation of heat flow, geotherms and lithospheric thickness. *Tectonophysics*, **38**, 279-296.

Raheim, A. & Green, D.H. (1974). Experimental determination of the temperature and pressure dependence of the Fe-Mg partition coefficient for coexisting garnet and clinopyroxene. *Contrib.Mineral.Petrol.*, **48**, 179-203.

Reid, A.M., Brown, R.W., Dawson, J.B., Whitfield, G.G., & Siebert, J.C. (1976). Garnet and clinopyroxene compositions in some diamondiferous eclogites. *Contrib.Mineral.Petrol.*, **58**, 203-220.

Richardson, S.H. (1986). Latter-Day Origin of Diamonds of Eclogitic Paragenesis. *Nature*, **322**, 1-14.

Richardson, S. H. (1989). As definitive as ever: A reply to 'Archaean diamond xenocrysts in kimberlites - How definitive is the evidence? In J. Ross (Ed.), *Kimberlites and Related Rocks, Vol. 2. Their Mantle/Crust Setting, Diamonds and Diamond Exploration, Geol.Soc.Aust., Spec.Publ. No.14,* (pp. 1071-1072). Blackwell Scientific.

Richardson, S.H. & Harris, J.W. (1997). Antiquity of peridotic diamonds from the Siberian craton. *Earth Planet.Sci.Lett.*, **151**, 271-277.

Richardson, S.H., Gurney, J.J., Erlank, A.J., & Harris, J.W. (1984). Origin of diamonds in old enriched mantle. *Nature*, **310**, 198-202.

Richardson, S.H., Erlank, A.J., Harris, J.W., & Hart, S.R. (1990). Eclogitic diamonds of Proterozoic age from Cretaceous kimberlites. *Nature*, **346**, 54-56.

Richardson, S.H., Harris, J.W., & Gurney, J.J. (1993). Three generations of diamonds from old continental mantle. *Nature*, **366**, 256-257.

Richardson, S.H., Chinn, I.L. & Harris, J.W. (1999). Age and origin of eclogitic diamonds from the Jwaneng kimberlite, Botswana. In J.J. Gurney, J.L. Gurney, Pascoe M.D., & S.H. Richardson (Eds.), *Proc.7th Int.Kimberlite Conf., Vol. 2,* (pp. 709-713). Red Roof Design, Cape Town.

Righter, K. & Hauri, E.H. (1997). Rhenium is compatible in garnet during mantle melting and magma genesis. *LPI Contribution 921, Lunar and Planetary Institution, Houston*, 175.

Righter, K., Capobianco, C.J., & Drake, M.J. (1995). Experimental constraints on the partitioning of Re between augite, olivine, melilite and silicate liquid at high oxygen fugacities (>NNO). *EOS Trans.Am.Geophys.Union*, **76**, 698-698, (abstract).

Ringwood, A.E. (1982). Phase transformations and differentiation in subducted lithosphere: Implications for mantle dynamics, basalt genesis, and crustal evolution. *J.Geol.*, **90**, 611-643.

Robertson, R., Fox, J.J., & Martin, A.E. (1934). Two types of diamond. *Phil.Trans.R.Soc.Lond.*, **A232**, 463

Robinson, D. N. (1979). Surface textures and other features of diamonds. Ph.D. Thesis, University of Cape Town, (unpublished).

Robinson, D. N., Scott, J. A., Van Niekerk, A., and Anderson, V. G. (1989). The sequents of events reflected in the diamonds of some southern African kimberlites. In J. Ross (Ed.), *Kimberlites and Related rocks, Vol. 2. Their Mantle/Crust setting, Diamonds and Diamond exploration, Geol.Soc.Aust., Spec.Publ. No.14,* (pp. 990-1000). Blackwell Scientific.

Roy-Barman, M. & Allegre, C.J. (1995). $^{187}Os/^{186}Os$ in oceanic island basalts: tracing oceanic crust recycling in the mantle. *Geochim.Cosmochim.Acta*, **129**, 145-161.

Rudnick, R.L. (1995). Nature and composition of the continental crust: A lower crustal perspective. *Rev.Geophysics*, **33**, 267-309.

Sakai, H., Des Marais, D.J., Ueda, A., & Moore, J.G. (1984). Concentrations and isotope ratios of carbon, nitrogen and sulfur in ocean floor basalts. *Geochim.Cosmochim.Acta*, **48**, 2433-2441.

Salters, V.J.M. & Hart, S.R. (1989). The hafnium paradox and the role of garnet in the source of mid-ocean-ridge basalts. *Nature*, **342**, 4204-422.

Sautter, V. & Harte, B. (1986). Chemical disequilibrium and diffusion gradients in eclogite xenolith JJG 41. *4th Int.Kimberlite Conf., Perth, (extended abstracts)*.

Saxena, S.K. (1979). Garnet-clinopyroxene geothermometry. *Contrib.Mineral.Petrol.*, **70**, 229-235.

Saxena, S.K. (1989). Oxidation state of the mantle. *Geochim.Cosmochim.Acta*, **53**, 89-95.

Schrauder, M. & Navon, O. (1993). Solid carbon dioxide in a natural diamond. *Nature*, **365**, 42-44.

Schulze, D.J. (1986). Calcium anomalies in the mantle and subducted metaserpentinite origin for diamonds. *Nature*, **319**, 483-485.

Scott-Smith, B. H., Danchin, R. V., Harris, J. W, and Stracke, K. J. (1984). Kimberlites near Orroroo, south Australia. In J. Kornprobst (Ed.), *Kimberlites I: Kimberlites and Related Rocks*, (pp. 121-142). Elsevier.

Seal, M. (1963). The growth history of natural diamonds as revealed by etching experiments. *Proc.1st Int.Congr.on Diamonds in Industry., Paris*, 361-376.

Seal, M. (1965). Structure in diamonds as revealed by etching. *Am.Miner.*, **50**, 105-123.

Shee, S. R. (1978). The mineral chemistry of xenoliths from the Orapa pipe, Botswana. Ph.D. Thesis, University of Cape Town, (unpublished).

Shimizu, N. & Richardson, S.H. (1987). Trace element abundance patterns of garnet inclusions in peridotite-suite diamonds. *Geochim.Cosmochim.Acta*, **51**, 755-758.

Shimizu, N. & Sobolev, N.V. (1995). Young peridotitic diamonds from the Mir Kimberlite pipe. *Nature*, **375**, 394-397.

Shirey, S.B., Carlson, R.W., Gurney, J.J., & van Heerden, L.A. (1998). Re-Os systematics of eclogites from Roberts Victor: Implications for diamond growth and Archaean tectonic settings. *7th Int.Kimberlite Conf., Cape Town, (extended abstracts)*, 808-810.

Smith, C.B. (1983). Pb, Sr and Nd isotopic evidence for sources of southern African Cretaceous kimberlites. *Nature*, **304**, 51-54.

Smith, C.B., Gurney, J.J., Skinner, E.M.W., Clement, C.R., & Ebrahim, N. (1985a). Geochemical character of southern African kimberlites: A new approach based on isotopic constraints. *Trans.Geol.Soc.S.Afr.*, **88**, 267-280.

Smith, C.B., Allsopp, H.L., Kramers, J.D., Hutchinson, G., & Roddick, J.C. (1985b). Emplacement ages of Jurassic-Cretaceous South African kimberlites by the Rb-Sr method on phlogopite and whole-rock samples. *Trans.Geol.Soc.S.Afr.*, **88**, 246-266.

Smith, C.B., Gurney, J.J., Harris, J.W., Otter, M.L., Kirkley, M.B., & Jagoutz, E. (1991). Neodymium and strontium isotope systematics of eclogite and websterite paragenesis inclusions from single diamonds, Finch and Kimberley pool, RSA. *Geochim.Cosmochim.Acta*, **55**, 2579-2590.

Smith, C.B., Clark, T.C., Barton, E.S., & Bristow, J.W. (1994). Emplacement ages of kimberlite occurrences in the Prieska region, southwest border of the Kaapvaal craton, South Africa. *Chem.Geol.*, **113**, 149-169.

Smith, C.B., Schulze, D.J., Bell, D.R., & Viljoen, K.S. (1995). Bearing of the subcalcic, Cr-poor megacryst suite on kimberlite petrogenesis and lithospheric structure. *6th Int.Kimberlite.Conf., Novosibirsk, (extended abstracts)*, 546-548.

Smyth, J.R. (1977). Peraluminous omphacite: cation vacancies in mantle-derived pyroxene. *Trans.Am.Geophys.Union*, **55**, 523-523, (abstract).

Smyth, J.R. (1980). Cation vacancies and the crystal chemistry of breakdown reactions in kimberlitic omphacites. *Am.Miner.*, **65**, 1185-1191.

Smyth, J.R. & Hatton, C.J. (1977). A coesite-sanidine grospydite from the Roberts Victor eclogite. *Earth Planet.Sci.Lett.*, **34**, 284-288.

Smyth, J.R., Caporuscio, F.A., & McCormick, T.C. (1989). Mantle eclogites: Evidence for igneous fractionation in the mantle. *Earth Planet.Sci.Lett.*, **93**, 133-141.

Sobolev, N.V. (1983). Parageneses of the diamonds and the problems of mineral formation in deep seated conditions. *Zap.Vses.Mineral.Obsh.*, **112**, 389-397.

Sobolev, N.V., Yefimova, E.S., Lavret'yev, Yu.G., & Sobolev, E.V. (1984). Dominant calc-silicate association of crystalline inclusions in placer diamonds from southeastern Australia. *Dokl.Akad.Nauk.S.S.S.R.* , **247**, 148-153.

Sobolev, N.V., Kaminsky, F.V., Griffin, W.L., Yefimova, E.S., Win, T.T., Ryan, C.G., & Botkunov, A.I. (1997). Mineral inclusions in diamonds from the Sputnik kimberlite pipe, Yakutia. *Lithos*, **39**, 135-157.

Sobolev, E.V., Lisoivian, V.I., & Lenskaya, S.V. (1968). *Sov.Phys.Dokl.*, **12**, 665-668.

Stachel, T. & Harris, J.W. (1997). Diamond precipitation and mantle metasomatism-evidence from the trace element chemistry of silicate inclusions in diamonds from Akwatia, Ghana. *Contrib.Mineral.Petrol.*, **129**, 143-154.

Sunagwa, I. (1984a). Growth of crystals in nature. In I. Sunagwa (Ed.), *Materials Science of the Earths Interior, Terra Scientific, Tokyo,* 61-103.

Sunagwa, I. (1984b). Morphology of natural and synthetic diamonds. In I. Sunagwa (Ed.), *Materials Science of the Earths Interior, Terra Scientific, Tokyo,* 303-330.

Sutton, J.R. (1928). Kimberley diamonds: Especially cleavage diamonds. *Trans.Roy.Soc.S.Afr.*, **7**, 65-96.

Switzer, G. & Melson, W.G. (1969). Partially melted kyanite eclogite from the Roberts Victor mine, South Africa. *Smithson.Contrib.Earth Sci.*, **1**, 7.

Taylor, S.R. & McLennan, S.M. (1995). The geochemical evolution of the continental crust. *Rev.Geoph*, **33(2)**, 241-265.

Taylor, W. R. (1994). Report on nitrogen aggregation and other characteristics of diamonds from the Slave province, NWT, Canada. 1. Point Lake. (Internal BHP report, unpublished).

Taylor, W.R. & Milledge, H.J. (1995). Nitrogen aggregation character, thermal history, and stable isotope composition of some xenolith-derived diamonds from Roberts Victor and Finch. *6th Int.Kimberlite Conf., Novosibirsk, (extended abstracts),* 620-622.

Taylor, W.R., Jaque, A.L., & Ridd, M. (1990). Nitrogen-defect aggregation characteristics of some Australian diamonds: Time-temperature constraints on the source regions of pipe and alluvial diamonds. *Am.Miner.*, **75**, 1290-1310.

Taylor, W.R., Bulanova, G.P., & Milledge, H.J. (1995). Quantitative nitrogen aggregation study of some Yakutian diamonds: Constraints on the growth, thermal and deformation history of peridotitic and eclogitic diamonds. *6th Int.Kimberlite Conf., Novosibirsk, (extended abstracts)*, 608-610.

Thode, H.G., Monster, J., & Dunford, H.B. (1961). Sulfur isotope geochemistry. *Geochim.Cosmochim .Acta*, **25**, 159-174.

Tsai, H.-M., Shieh, Y.-N., & Meyer, H.O.A. (1979). Mineralogy and $^{34}S/^{32}S$ ratios of sulfides associated with kimberlite, xenoliths and diamonds. In F.R. Boyd & H.O.A. Meyer (Eds.), *The mantle sample: Inclusions in Kimberlites and Other Volcanic Rocks,* (pp. 87-103). A.G.U.

Ueda, A. & Sakai, H. (1984). Sulfur isotope study of Quaternary volcanic rocks from the Japanese arc islands. *Geochim.Cosmochim.Acta*, **48**, 1837-1848.

Urusovskaya, A.A. & Orlov, Yu.L. (1964). Nature of plastic deformation of diamond crystals. *Dokl.Akad.Nauk.S.S.S.R.*, **154**, 112-115.

van Heerden, L.A., Boyd, S.R., Milledge, H.J., & Pillinger, C.T. (1995). The carbon- and nitrogen-isotope characteristics of the Argyle and Ellendale diamonds, western Australia. *Int.Geol.Rev.*, **37**, 39-50.

Vance, E.R., Harris, J.W., & Milledge, H.J. (1973). Possible origins of α-damage in diamonds from kimberlite and alluvial sources. *Mineral. Mag.*, **39**, 349-360.

Vinnik, L.P., Green, R.W.E., & Nicolaysen, L.O. (1995). Recent deformations on the deep continental roots in Southern Africa. *Nature*, **375**, 50-52.

Wagner, P.A. (1914). The diamond fields of sothern Africa. *Transvaal Leader, Johannesburg*,

Walraven, F., Armstrong, R.A., & Kruger, F.J. (1989). A chronostratigraphic framework for the north-central Kaapvaal craton, the Bushveld complex and the Vredefort structure. *Tectonophysics*, **171**, 23-48.

Wilding, M. C. (1990). A study of diamonds with syngenetic inclusions. Ph.D. Thesis, University of Edinburgh, (unpublished).

Williams, A.F. (1932). *The genesis of diamond.* Ernest Benn, London.

Wood, B.J. (1976). Mixing properties of tschermakitic clinopyroxenes. *Am.Miner.*, **61**, 599-602.

Wood, B.J. & Henderson, C.M.B. (1978). Compositions and unit-cell parameters of synthetic non-stoichiometric tschermakitic clinopyroxenes. *Am.Miner.*, **63**, 66-72.

Woodhead, J.D., Harmon, R.S., & Fraser, D.G. (1978). O, S, Sr and Pb isotope variations in volcanic rocks from the Northern Mariana Islands: Implications for crustal recycling in intra-oceanic arcs. *Earth Planet.Sci.Lett.*, **83**, 39-52.

Woods, G.S. (1976). Electron microscopy of "giant" platelets on cube planes in diamond. *Phil.Mag.*, **34**, 993-1012.

Woods, G.S. (1986). Platelets and the infrared absorption of type Ia diamonds. *Proc.R.Soc.Lond.*, **407**, 219-238.

Woods, G.S. & Collins, A.T. (1983). Infrared absorption spectra of hydrogen complexes in type I diamonds. *J.Phys.C: Solid St.Phys*, **44**, 471-475.

Woods, G.S., Purser, G.C., Mtimkulu, A.S.S., & Collins, A.T. (1990). The Nitrogen Content of Type Ia Natural Diamonds. *J.Phys C:Solid St.Phys*, **51**, 1191-1197.

Wyllie, P.J. (1987). Metasomatism and fluid generation in mantle xenoliths. In P.H. Nixon (Ed.), *Mantle xenoliths,* (pp. 609-621). Wiley and Sons.

Wyllie, P.J. (1989). The genesis of kimberlites and some low-SiO_2, high-alkali magmas. In J. Ross (Ed.), *Kimberlites and Related Rocks: Their Composition, Occurence and Emplacement. Geol.Soc.Aus., Spec.Publ. No. 14, Vol. 1,* (pp. 603-615). Blackwell Scientific.

Yefimova, E.S., Sobolev, N.V., & Pospelova, L.N. (1983). Sulfide inclusions in diamond and specific features of their paragenesis. *Zap.Vses.Mineral.Obsh.*, **112**, 300-310, (in Russian).

York, D. (1969). Least squares fitting of a straight line with correlation errors. *Earth Planet.Sci.Lett.*, **5**, 320-324.

Zegers, T.E., de Wit, M.J., Dann, J., & White, S.H. (1998). Vaalbara, earth's oldest assembled continent? A combined structural, geochronological, and palaeomagnetic test. *Terra Nova*, **10**, 250-259.

Zezin, R.B., Saparin, G.V., Smirnova, E.P., Obyden, S.K., & Chukichev, M.V. (1990). Cathodoluminescence of natural diamonds from Jakutian deposits. *Scanning*, **12**, 326-333.

APPENDIX 1

RB-SR ISOTOPE ANALYSIS ON WHOLE-ROCK KIMBERLITES AND PHLOGOPITE CONCENTRATES

Kimberlite core samples were washed in water and visually inspected for xenoliths and carbonate veins before they were split in a hydraulic rock splitter. Pieces that were free of xenoliths and carbonate veins were then crushed in a steel jaw crusher. Whole-rock samples were obtained by grinding the samples in a pre-contaminated carbon steel Seib mill cleaned with water and acetone.

Crushed samples were further crushed by hand in a steel mortar and the samples were sieved in to different fractions. Larger sized phlogopite concentrates were prepared by hand-picking directly from the larger sieve fractions. Smaller fractions were "cleaned" in a magnetic separator before the phlogopite was hand-picked under binocular microscope. The phlogopites were as far as possible cleaned from other minerals (especially carbonates) attached to the rim of the grains by the use of two very fine tweezers.

Leaching of the phlogopites in HCl was performed to remove carbonate attached to the grains (see Section 3.2.1). The samples were added to ~ 10 ml of double distilled ~ 1 M HCl in a teflon beaker. Leaching was then performed for ten minutes with ultrasonic agitation during the first five minutes. The HCl was decanted and the samples were washed several times in double distilled water followed by rinsing with analytical grade acetone. The phlogopites were then inspected for any discoloration indicative of alteration.

The samples were weighed by difference on a Mettler AE 240. The sensitivity of the scale is 0.1 mg and since the sample weights range from about 7 to 23 mg, weighing errors introduced into the Rb and Sr abundances are negligible. Mixed Rb-Sr spikes were weighed separately in a teflon beaker and then added to the samples.

The samples were dissolved in double distilled 48 % HF in a 4:1 mixture with concentrated HNO_3. The latter serves as an oxidising agent to prevent the formation of insoluble fluorides. The beakers were covered with lids and put onto a hot-plate set at a temperature of about 100 °C over night. After complete dissolution, the lids were removed and excess HF was evaporated. To turn the salts into chloride, a couple of millilitres of 6.2 M HCl was then added to the samples and this procedure was repeated once after

evaporation of the HCl. Samples were then taken into solution with 1 ml 2.5 M HCL and centrifuged for 15 minutes at 4000 rpm.

500 µl of the sample was loaded onto a column with cation exchange resin and washes and collection of Rb and Sr were performed with 2.5 M HCl according to envisaged volumes from the calibration of the columns. After elution, a few drops of 20 % H_2SO_4 was added to the Rb fraction to turn the chloride into sulfate since the sulfate has a higher ionisation potential compared to the chloride and therefore will remain for a longer time on the filament and yield better analysis. Excess HCl was evaporated on hot-plate before excess H_2SO_4 was evaporated at higher temperatures. Two turns of 500 µl double distilled water were then added and evaporated on hot-plate before the Rb was loaded onto Ta filaments using double-distilled water.

To the Sr fraction, a few drops of HNO_3 was added and evaporated twice to turn the sample into nitrate. The samples were then loaded onto Ta filaments with a mixture of double distilled 2 % HNO_3 and 0.5 M H_3PO_4.

The samples were analyses on a VG Sector thermal ionisation mass spectrometer with a dynamic multi-collector system.

APPENDIX 2

ELECTRON MICROPROBE ANALYSIS OF CONCENTRATE GARNETS AND GARNET-CLINOPYROXENE NODULES

Mineral analyses were performed at the Department of Geology, University of Cape Town (UCT) and at the Department for Terrestrial Magnetism, Carnegie Institution of Washington (CIW). Analyses undertaken at UCT follow the method described in Appendix 5 for silicate diamond inclusions. Analyses undertaken at CIW also follow the method described in Appendix 5 with the exception for that the data were reduced according to the ZAF procedure and that other types of standards were used. The standards used at CIW were natural basalt for Na_2O, Al_2O_3 and TiO_2, synthetic olivine for MgO and SiO_2 and synthetic diopside for Cr_2O_3 and MnO.

Appendix 2.1 Chemical compositions of Main Fissure concentrate garnets.

	Main-1															
	1	2	3	4	5	6	7	8	9	10	11	12	13	14	15	16
SiO_2	42.2	41.8	41.8	41.8	41.7	41.5	41.3	42.2	41.5	41.7	41.4	41.9	41.6	42.0	41.9	41.4
TiO_2	0.05	0.05	0.02	0.03	0.11	0.08	0.03	0.02	0.08	0.00	0.12	0.02	0.06	0.05	0.02	0.19
Al_2O_3	21.4	20.6	20.4	20.4	20.6	19.6	19.6	22.3	21.5	20.6	18.4	19.0	19.5	21.6	20.5	20.5
Cr_2O_3	3.59	4.32	4.68	4.76	4.44	5.55	5.96	2.94	3.53	5.10	7.31	7.21	6.13	3.42	4.73	4.82
FeO	6.08	6.94	6.51	6.41	6.51	6.41	6.62	6.96	7.63	6.42	6.35	6.12	6.55	6.44	6.53	7.33
MnO	0.28	0.30	0.30	0.29	0.34	0.34	0.35	0.33	0.40	0.34	0.33	0.35	0.35	0.31	0.30	0.39
MgO	22.5	20.7	20.9	21.1	21.2	20.9	21.2	22.4	20.4	21.6	21.6	24.0	21.1	21.5	21.1	20.6
CaO	3.69	5.34	5.30	5.35	4.91	5.58	4.70	3.26	5.12	4.43	4.36	1.43	5.12	4.56	5.26	4.97
Na_2O	0.02	0.02	0.02	0.03	0.06	0.02	0.02	0.05	0.04	0.01	0.04	0.01	0.02	0.04	0.01	0.07
Total	99.84	100.06	100.00	100.10	99.90	99.99	99.92	100.45	100.23	100.13	99.87	100.11	100.43	99.97	100.30	100.23

				Main- 2												
	17	18	19	20	21	22	23	24	25	26	27	28	29	30	31	32
SiO_2	41.8	41.5	41.9	42.0	41.7	42.1	42.1	42.1	42.2	41.8	41.7	41.8	42.1	41.6	41.7	41.9
TiO_2	0.07	0.14	0.28	0.32	0.14	0.26	0.31	0.51	0.32	0.25	0.17	0.32	0.16	0.17	0.09	0.26
Al_2O_3	21.4	19.2	20.6	21.8	19.4	21.9	21.9	20.3	21.5	20.9	20.7	20.8	20.5	20.3	20.4	22.2
Cr_2O_3	3.77	6.24	4.69	2.86	5.82	2.71	2.83	4.14	3.31	4.15	4.58	4.48	4.38	4.94	5.01	2.57
FeO	7.34	7.06	6.62	6.53	6.23	6.77	7.00	6.25	6.86	6.80	6.72	6.56	6.39	7.53	6.37	6.88
MnO	0.38	0.35	0.30	0.28	0.25	0.31	0.31	0.26	0.32	0.34	0.31	0.31	0.27	0.35	0.27	0.35
MgO	20.6	20.4	21.4	21.6	21.5	22.1	21.6	22.0	22.0	21.4	21.3	21.8	21.6	20.5	21.1	21.6
CaO	5.14	5.62	4.87	4.89	5.15	4.17	4.47	4.83	4.28	4.86	5.09	4.49	4.96	5.13	5.44	4.86
Na_2O	0.03	0.03	0.04	0.05	0.04	0.07	0.06	0.05	0.06	0.06	0.02	0.08	0.04	0.05	0.03	0.04
Total	100.46	10.56	100.67	100.35	100.26	100.47	100.59	100.41	100.83	100.69	100.65	100.58	100.39	100.49	100.44	100.72

Appendix 2.1 continued

	Main-2						Main-3									
	33	34	35	36	37	38	1	2	7	8	10	13	14	17	19	20
SiO_2	42.2	42.2	42.1	42.2	42.2	42.3	41.7	39.4	42.0	41.0	42.3	41.9	42.2	42.0	41.6	41.4
TiO_2	0.28	0.26	0.34	0.53	0.19	0.44	0.40	0.38	0.45	0.31	0.42	0.30	0.37	0.34	0.49	0.39
Al_2O_3	21.3	22.1	21.6	21.5	21.0	21.5	23.8	22.9	23.5	23.1	23.5	24.1	23.8	23.9	23.0	23.2
Cr_2O_3	3.71	2.93	3.01	3.10	3.84	3.04	0.30	0.03	0.09	0.09	0.43	0.07	0.24	0.27	0.51	0.45
FeO	6.37	6.64	6.79	6.89	6.50	6.71	8.22	14.0	8.94	15.6	8.87	9.19	9.04	8.10	9.55	9.54
MnO	0.27	0.30	0.29	0.23	0.26	0.28	0.35	0.21	0.29	0.30	0.26	0.26	0.31	0.25	0.25	0.29
MgO	21.9	21.5	21.8	22.1	21.6	21.9	21.5	10.5	21.2	17.2	21.4	21.1	21.3	22.0	20.7	20.7
CaO	4.64	4.57	4.45	4.14	5.06	4.49	3.94	12.8	3.64	3.18	3.56	3.54	3.68	3.44	4.10	4.09
Na_2O	0.07	0.04	0.07	0.08	0.03	0.06	0.10	0.19	0.08	0.12	0.09	0.11	0.11	0.09	0.10	0.08
Total	100.63	100.52	100.47	100.80	100.61	100.73	100.26	100.44	100.20	100.90	100.78	100.53	101.07	100.36	100.36	100.11

	Main-3										Main-3b					
	22	24	26	28	31	32	35	37	38	41	42	3	5	6	11	13
SiO_2	40.2	40.2	42.3	41.4	41.9	40.5	42.1	41.6	41.2	41.8	41.5	42.2	41.7	41.6	41.8	42.0
TiO_2	0.08	0.09	0.20	0.38	0.31	0.26	0.27	0.54	0.30	0.40	0.64	0.19	0.14	0.34	0.28	0.23
Al_2O_3	23.1	23.5	24.0	23.8	23.9	23.2	23.9	23.5	23.2	23.4	22.9	23.7	23.1	23.3	22.6	22.8
Cr_2O_3	0.11	0.05	0.20	0.07	0.03	0.05	0.06	0.08	0.05	0.17	0.21	0.77	1.01	0.53	1.63	1.33
FeO	16.2	16.1	8.71	10.3	9.39	13.6	8.28	10.5	15.8	11.3	11.6	6.75	9.38	7.84	8.75	9.12
MnO	0.28	0.28	0.18	0.21	0.23	0.22	0.28	0.28	0.27	0.29	0.26	0.30	0.40	0.20	0.31	0.31
MgO	15.5	16.0	21.6	18.9	18.6	12.4	21.8	19.3	17.2	18.2	19.6	21.6	19.9	21.1	20.0	19.7
CaO	5.16	4.31	3.61	5.89	6.65	11.1	3.92	5.21	3.28	5.81	3.90	4.13	4.34	4.20	4.58	4.51
Na_2O	0.05	0.07	0.10	0.12	0.18	0.16	0.08	0.16	0.12	0.18	0.13	0.05	0.04	0.08	0.06	0.04
Total	100.69	100.58	100.97	101.00	101.21	101.54	100.65	101.18	101.38	101.58	100.80	99.62	99.99	99.07	99.96	100.02

Appendix 2.1 continued

	Main-3b															
	14	16	19	20	23	24	27	28	30	33	35	36	38	40	42	44
SiO_2	42.1	41.9	42.3	42.4	42.1	42.0	38.3	42.7	41.8	42.1	42.1	41.2	41.6	42.0	41.8	41.2
TiO_2	0.41	0.28	0.27	0.16	0.39	0.30	0.02	0.28	0.17	0.32	0.19	0.29	0.25	0.19	0.23	0.33
Al_2O_3	23.0	23.2	22.1	23.5	21.9	23.1	22.3	23.5	22.7	23.5	23.5	22.1	22.0	23.3	23.1	23.3
Cr_2O_3	0.90	1.59	2.51	1.12	2.70	1.23	0.04	1.28	1.53	0.68	0.80	1.56	2.28	0.77	1.18	0.33
FeO	9.02	7.94	6.60	7.60	6.93	8.64	28.2	7.15	9.62	8.09	8.22	11.0	8.66	8.11	8.85	11.7
MnO	0.34	0.28	0.32	0.29	0.25	0.35	0.74	0.27	0.28	0.32	0.23	0.37	0.31	0.30	0.30	0.36
MgO	20.0	20.5	22.0	21.0	21.5	20.0	8.4	21.1	19.4	21.1	20.6	18.5	20.0	20.7	19.9	18.4
CaO	4.21	4.47	3.73	4.34	4.35	4.35	2.47	4.48	4.35	4.05	4.20	4.83	4.75	4.45	4.48	4.15
Na_2O	0.08	0.04	0.06	0.04	0.08	0.07	0.00	0.05	0.04	0.07	0.03	0.04	0.04	0.02	0.05	0.07
Total	100.10	100.21	99.92	100.44	100.08	99.93	100.44	100.72	99.82	100.24	99.86	99.80	99.86	99.86	99.86	99.73

	Main-3b															
	46	48	51	52	54	56	58	61	63	65	67	68	71	72	75	76
SiO_2	42.4	41.5	40.7	41.0	42.3	42.2	41.5	41.8	42.3	42.5	42.0	41.5	41.7	41.4	41.6	41.9
TiO_2	0.51	0.19	0.59	0.35	0.36	0.30	0.47	0.37	0.39	0.38	0.34	0.13	0.33	0.18	0.33	0.13
Al_2O_3	23.4	23.4	22.5	22.9	23.8	23.5	23.3	22.1	22.2	22.2	21.5	20.2	20.2	19.7	19.2	19.1
Cr_2O_3	0.17	0.35	0.12	0.08	0.07	0.41	0.18	2.32	2.43	1.79	3.41	4.83	4.76	5.40	6.08	6.92
FeO	8.13	11.5	13.6	15.2	8.44	11.0	11.8	7.71	7.37	7.86	7.14	7.27	7.14	6.76	6.83	6.01
MnO	0.24	0.28	0.34	0.29	0.28	0.26	0.30	0.31	0.34	0.26	0.32	0.30	0.32	0.34	0.31	0.29
MgO	20.9	19.3	17.4	16.5	20.9	19.5	17.4	20.9	21.1	21.0	21.3	19.7	20.4	20.2	20.3	21.5
CaO	4.38	3.58	4.05	3.46	3.85	3.62	5.60	4.01	4.42	4.69	4.07	5.67	4.73	5.54	5.13	4.29
Na_2O	0.06	0.09	0.13	0.13	0.10	0.12	0.13	0.09	0.05	0.04	0.11	0.00	0.06	0.03	0.08	0.05
Total	100.09	100.17	99.56	99.88	100.10	100.85	100.68	99.63	100.54	100.67	100.18	99.62	99.68	99.53	99.92	100.17

Appendix 2.1 continued

	Main-3b															
	79	82	83	86	87	89	91	93	96	97	99	102	103	105	108	109
SiO_2	41.5	41.7	42.4	42.1	42.0	42.5	42.3	41.2	41.1	42.3	40.8	41.3	41.9	41.5	41.7	42.0
TiO_2	0.07	0.08	0.38	0.41	0.54	0.51	0.52	0.64	0.27	0.30	0.34	0.13	0.42	0.67	0.29	0.34
Al_2O_3	18.9	21.1	21.2	22.0	23.2	23.8	23.5	22.9	23.3	23.6	22.6	23.2	23.0	21.6	22.5	22.0
Cr_2O_3	6.79	4.20	3.27	2.69	0.37	0.06	0.11	0.16	0.12	0.45	0.43	0.31	1.38	2.31	1.79	2.23
FeO	7.33	7.69	6.87	7.13	9.98	9.83	8.76	13.5	16.0	9.94	15.0	15.1	8.37	8.89	8.90	7.35
MnO	0.37	0.37	0.29	0.31	0.26	0.28	0.25	0.27	0.32	0.28	0.36	0.33	0.32	0.29	0.37	0.24
MgO	19.7	19.8	21.6	21.3	20.0	20.2	20.5	18.3	16.8	20.5	16.6	17.3	20.5	19.9	19.8	20.8
CaO	5.81	5.38	4.36	4.59	4.03	4.12	4.24	3.38	3.08	3.27	4.15	2.65	4.28	4.73	4.48	4.58
Na_2O	0.04	0.03	0.10	0.05	0.09	0.07	0.12	0.13	0.12	0.05	0.09	0.10	0.08	0.08	0.08	0.06
Total	100.57	100.30	100.38	100.46	100.51	101.34	100.30	100.48	101.16	100.62	100.28	100.36	100.19	99.96	99.87	99.64

	Main-3b										Main-4					
	111	114	116	118	120	121	123	126	128	130	1	3	5	7	10	12
SiO_2	42.1	42.2	42.0	42.3	41.9	41.9	42.6	42.1	42.0	41.6	41.1	40.8	41.2	41.4	42.2	41.9
TiO_2	0.41	0.29	0.29	0.34	0.23	0.21	0.13	0.12	0.04	0.08	0.57	0.46	0.44	0.23	0.31	0.50
Al_2O_3	22.5	21.5	20.9	21.0	21.4	20.2	23.0	21.6	20.8	18.0	22.9	22.7	22.8	23.4	23.9	22.7
Cr_2O_3	1.73	3.38	3.97	3.78	3.72	4.93	1.99	3.53	4.20	7.76	0.07	0.14	0.14	0.06	0.08	0.56
FeO	8.29	6.78	6.73	6.59	7.06	6.76	7.10	7.66	6.85	5.83	13.1	13.7	13.6	11.7	7.90	9.13
MnO	0.26	0.25	0.27	0.31	0.34	0.31	0.33	0.30	0.32	0.22	0.29	0.37	0.39	0.28	0.24	0.29
MgO	20.3	20.9	21.1	20.9	20.4	20.5	20.9	19.9	20.4	21.7	17.7	17.8	17.8	18.8	20.7	20.5
CaO	4.40	4.71	4.73	4.48	5.04	4.90	4.45	4.99	5.25	3.66	4.09	3.52	3.46	3.64	4.59	4.27
Na_2O	0.07	0.06	0.05	0.07	0.05	0.07	0.06	0.05	0.02	0.02	0.17	0.10	0.09	0.13	0.07	0.07
Total	100.02	100.06	99.98	99.78	100.13	99.76	100.46	100.25	99.91	98.90	99.99	99.57	100.04	99.75	99.96	99.95

Appendix 2.1 continued

	Main-4															
	13	15	17	20	22	23	26	35	37	39	42	43	50	51	53	56
SiO_2	41.2	41.7	41.4	41.5	41.4	41.8	41.4	42.0	42.3	41.4	41.9	41.8	42.0	41.4	41.9	41.8
TiO_2	0.37	0.60	0.19	0.27	0.79	0.38	0.29	0.35	0.32	0.38	0.19	0.19	0.36	0.28	0.20	0.42
Al_2O_3	23.3	23.0	23.5	23.0	22.1	23.1	23.4	20.8	22.8	19.0	22.5	23.0	23.4	23.1	23.3	23.2
Cr_2O_3	0.06	0.03	0.06	0.41	0.82	0.96	0.02	3.47	1.73	5.61	1.92	1.18	0.51	0.07	0.71	0.65
FeO	11.7	10.5	8.55	13.0	11.3	8.26	12.6	6.38	6.49	6.44	7.59	7.59	9.54	14.9	9.02	8.71
MnO	0.24	0.31	0.22	0.27	0.25	0.33	0.29	0.29	0.33	0.31	0.29	0.32	0.32	0.34	0.36	0.28
MgO	17.6	19.8	18.9	18.9	19.3	20.7	16.7	21.7	22.1	21.2	21.0	21.0	20.0	17.1	20.4	21.3
CaO	5.26	3.98	6.63	2.76	3.62	4.07	5.56	4.50	3.98	5.20	4.48	4.46	4.14	3.23	4.09	3.34
Na_2O	0.15	0.10	0.05	0.11	0.15	0.08	0.14	0.08	0.08	0.05	0.04	0.06	0.08	0.13	0.05	0.13
Total	99.80	100.09	99.51	100.24	99.85	99.70	100.51	99.65	100.07	99.61	99.94	99.66	100.34	100.56	100.00	99.85

	Main-5						
	18	19	20	21	22	23	24
SiO_2	41.3	42.6	42.2	41.7	42.3	42.4	42.2
TiO_2	0.28	0.45	0.43	0.11	0.18	0.26	0.37
Al_2O_3	23.2	23.6	23.4	20.9	23.7	23.8	22.5
Cr_2O_3	0.10	0.32	0.46	4.28	0.65	0.37	1.76
FeO	15.1	7.55	8.58	7.01	9.08	9.04	7.38
MnO	0.30	0.27	0.31	0.30	0.29	0.25	0.26
MgO	17.1	22.0	21.0	20.8	20.7	20.8	21.6
CaO	3.35	3.89	4.37	5.28	4.28	4.01	4.15
Na_2O	0.14	0.09	0.06	0.03	0.06	0.07	0.07
Total	100.77	100.77	100.78	100.35	101.12	100.99	100.27

Appendix 2.2 Chemical compositions of Sugarbird Blow concentrate garnets.

	Blow-3										
	1	2	3	4	5	6	7	8	9	10	11
SiO_2	41.0	40.9	40.5	42.0	41.2	41.7	39.8	39.1	40.9	40.8	41.7
TiO_2	0.41	0.41	0.27	0.35	0.29	0.27	0.33	0.33	0.29	0.39	0.47
Al_2O_3	23.0	22.8	22.9	23.9	23.3	23.3	22.7	22.6	23.0	22.9	23.2
Cr_2O_3	0.25	0.27	0.20	0.07	0.08	0.23	0.04	0.04	0.10	0.05	0.55
FeO	11.8	11.4	15.9	8.28	11.4	9.93	17.4	17.5	15.2	16.5	10.3
MnO	0.26	0.36	0.30	0.22	0.26	0.37	0.28	0.28	0.34	0.33	0.30
MgO	19.3	19.7	17.2	21.4	19.4	20.5	14.3	9.57	17.5	16.3	20.2
CaO	3.78	3.93	3.16	4.14	3.98	4.32	5.11	11.0	3.21	4.00	4.15
Na_2O	0.12	0.12	0.15	0.07	0.11	0.07	0.18	0.19	0.13	0.16	0.10
Total	99.93	99.94	100.61	100.42	100.05	100.72	100.13	100.52	100.63	101.32	100.89

	Blow-3						Blow-4				
	12	13	14	15	16	17	1	2	3	4	5
SiO_2	42.1	40.8	41.1	41.1	39.4	40.7	41.8	41.9	41.9	42.0	42.0
TiO_2	0.48	0.41	0.70	0.73	0.43	0.45	0.05	0.02	0.02	0.08	0.00
Al_2O_3	23.3	23.1	22.5	22.5	22.3	23.1	20.5	20.6	21.1	18.7	20.6
Cr_2O_3	0.05	0.20	0.14	0.06	0.03	0.07	4.76	4.74	3.87	7.18	5.16
FeO	10.2	10.8	13.8	13.2	17.0	13.3	6.29	6.69	6.46	5.96	6.30
MnO	0.23	0.30	0.35	0.28	0.65	0.31	0.30	0.31	0.28	0.27	0.31
MgO	20.8	19.8	18.2	19.3	10.6	15.8	21.2	20.9	21.3	22.5	21.9
CaO	3.93	3.87	3.91	3.44	10.0	7.05	5.35	5.27	5.09	3.81	4.15
Na_2O	0.11	0.10	0.15	0.15	0.13	0.16	0.03	0.02	0.01	0.04	0.03
Total	101.17	99.49	100.91	100.66	100.47	100.94	100.27	100.52	100.08	100.49	100.46

Appendix 2.2 continued

	Blow-4										
	6	7	8	9	10	11	12	13	14	15	16
SiO_2	42.5	42.2	42.2	42.3	42.3	42.2	42.2	42.4	42.4	42.2	42.4
TiO_2	0.25	0.37	0.38	0.54	0.46	0.19	0.32	0.07	0.29	0.11	0.31
Al_2O_3	22.0	22.1	20.6	22.1	21.6	21.6	20.4	22.6	22.3	22.8	23.4
Cr_2O_3	2.38	2.58	4.04	2.10	2.31	3.53	4.45	2.31	2.41	1.87	1.07
FeO	6.49	7.11	6.40	6.86	7.41	7.10	6.51	6.46	6.36	6.84	6.99
MnO	0.29	0.28	0.27	0.26	0.30	0.34	0.27	0.30	0.28	0.29	0.30
MgO	22.8	21.9	21.6	21.7	21.3	21.6	21.6	21.9	22.3	21.6	22.2
CaO	3.49	4.03	4.62	4.58	4.82	4.26	4.96	4.62	4.06	4.64	3.99
Na_2O	0.09	0.07	0.06	0.07	0.05	0.07	0.04	0.02	0.05	0.02	0.07
Total	100.29	100.64	100.23	100.65	100.64	100.86	100.69	100.70	100.55	100.30	100.74

	Blow-4		
	17	18	19
SiO_2	42.6	42.6	42.9
TiO_2	0.29	0.32	0.26
Al_2O_3	23.8	23.3	23.3
Cr_2O_3	0.62	1.30	0.97
FeO	6.93	6.58	6.42
MnO	0.22	0.23	0.25
MgO	22.1	22.5	23.2
CaO	4.10	4.01	3.49
Na_2O	0.06	0.08	0.09
Total	100.70	100.90	100.86

Appendix 2.3 Chemical compositions for Marsfontein concentrate garnets.

	Mars-1															
	1	2	3	4	5	6	7	8	9	10	11	12	13	14	15	16
SiO_2	42.7	43.0	43.0	43.1	42.2	42.0	42.8	42.1	42.2	42.4	42.1	42.9	42.3	42.7	42.2	41.8
TiO_2	0.02	0.02	0.04	0.02	0.01	0.08	0.04	0.04	0.00	0.02	0.07	0.02	0.06	0.02	0.01	0.06
Al_2O_3	22.7	23.3	23.2	23.3	22.4	21.7	22.1	21.9	21.0	19.4	21.6	22.9	20.8	22.3	20.4	21.6
Cr_2O_3	2.86	2.14	2.18	2.06	2.77	3.65	3.07	3.39	4.30	6.86	3.70	2.38	4.31	3.09	5.52	3.29
FeO	4.90	4.93	4.90	4.96	6.21	6.71	5.29	6.79	6.47	5.22	6.64	5.08	6.02	5.20	6.39	7.79
MnO	0.22	0.22	0.22	0.20	0.28	0.35	0.21	0.33	0.33	0.24	0.34	0.25	0.26	0.24	0.33	0.34
MgO	25.3	25.5	25.5	25.6	22.9	21.7	24.2	21.4	21.3	24.7	21.8	24.8	22.6	23.7	24.2	20.6
CaO	1.68	1.60	1.41	1.43	3.20	4.31	2.98	4.82	5.26	1.71	4.13	2.15	4.09	3.32	1.01	4.82
Na_2O	0.01	0.01	0.03	0.02	0.02	0.05	0.02	0.04	0.01	0.02	0.03	0.01	0.03	0.01	0.00	0.04
Total	100.47	100.62	100.42	100.76	99.99	100.50	100.67	100.72	100.89	100.56	100.38	100.48	100.50	100.69	100.19	100.37

	Mars-1															
	17	18	19	20	21	22	23	24	25	26	27	28	29	30	31	32
SiO_2	41.6	42.1	41.8	42.3	42.4	42.2	42.2	42.2	42.3	42.2	42.6	42.2	42.1	41.7	42.2	42.6
TiO_2	0.07	0.07	0.04	0.28	0.35	0.22	0.39	0.45	0.20	0.38	0.36	0.34	0.11	0.19	0.08	0.12
Al_2O_3	17.8	21.8	20.9	22.1	21.5	21.9	22.3	21.6	21.2	22.5	22.1	21.2	21.7	20.7	20.8	22.7
Cr_2O_3	8.52	3.47	4.61	2.76	3.18	2.86	2.36	2.76	3.49	2.39	2.36	3.35	3.30	4.36	4.49	2.63
FeO	6.33	5.90	5.73	5.88	5.85	6.76	6.55	6.22	6.44	6.57	5.49	6.67	6.62	6.64	6.22	5.08
MnO	0.34	0.30	0.32	0.27	0.26	0.32	0.34	0.28	0.28	0.32	0.23	0.30	0.31	0.31	0.29	0.26
MgO	22.4	21.9	22.0	22.5	22.6	22.1	22.0	21.8	21.9	22.2	22.9	21.8	21.6	21.4	22.8	23.6
CaO	3.14	4.79	4.65	4.28	4.14	4.10	4.18	4.93	4.81	4.14	4.27	4.70	4.86	4.68	3.61	3.38
Na_2O	0.00	0.04	0.04	0.07	0.05	0.06	0.09	0.05	0.03	0.08	0.07	0.05	0.03	0.06	0.03	0.01
Total	100.22	100.33	100.18	100.39	100.33	100.49	100.46	100.29	100.63	100.70	100.35	100.62	100.63	100.06	100.55	100.38

Appendix 2.3 continued

	Mars-1											Mars-2				
	33	34	35	36	37	38	39	40	41	42	43	44	45	46	47	48
SiO_2	42.2	42.3	42.5	42.8	42.8	42.0	42.0	42.2	41.8	41.6	42.0	42.2	41.8	42.3	41.9	42.3
TiO_2	0.06	0.11	0.02	0.03	0.03	0.18	0.09	0.12	0.06	0.04	0.34	0.40	0.31	0.39	0.37	0.31
Al_2O_3	20.7	21.2	22.6	22.6	22.5	21.1	20.5	20.7	20.9	19.9	20.3	21.8	22.6	21.9	21.4	23.1
Cr_2O_3	4.57	3.97	2.10	2.39	2.36	3.95	4.70	4.55	4.28	5.55	4.82	1.94	1.75	2.10	2.20	1.29
FeO	5.93	6.26	5.51	5.65	5.62	6.66	6.38	6.18	6.32	6.69	6.59	8.75	9.04	7.14	8.61	7.32
MnO	0.26	0.28	0.22	0.21	0.23	0.26	0.30	0.28	0.26	0.33	0.30	0.31	0.31	0.27	0.34	0.34
MgO	22.1	21.8	23.1	22.7	22.9	22.0	21.5	21.7	21.4	20.7	21.8	20.3	20.3	21.6	20.5	21.5
CaO	4.68	4.83	4.13	4.35	4.32	4.34	4.94	4.84	5.15	5.44	4.11	5.15	4.48	4.78	5.10	4.30
Na_2O	0.03	0.03	0.01	0.03	0.02	0.03	0.04	0.03	0.02	0.03	0.06	0.03	0.05	0.07	0.03	0.02
Total	100.54	100.79	100.24	100.78	100.90	100.52	100.44	100.62	100.19	100.24	100.34	100.86	100.68	100.56	100.43	100.44

	Mars-2	Mars-3														
	49	1	2	3	4	5	6	7	8	9	10	11	12	13	14	15
SiO_2	41.9	41.7	42.5	41.6	41.8	42.6	41.5	41.8	41.7	42.4	42.1	41.5	42.3	41.9	42.3	41.1
TiO_2	0.30	0.38	0.45	0.30	0.36	0.29	0.22	0.31	0.23	0.51	0.46	0.24	0.46	0.33	0.45	0.28
Al_2O_3	23.1	23.4	23.8	23.3	23.2	24.1	23.5	23.4	23.6	22.8	23.5	23.7	23.2	23.7	23.6	23.4
Cr_2O_3	1.17	0.07	0.26	0.15	0.92	0.19	0.20	0.45	0.15	0.35	0.42	0.04	0.37	0.30	0.39	0.20
FeO	9.78	13.4	8.25	12.5	9.30	8.50	15.2	11.8	12.7	9.89	9.59	13.3	9.17	10.8	9.69	14.7
MnO	0.38	0.34	0.26	0.38	0.32	0.26	0.30	0.32	0.21	0.24	0.34	0.29	0.26	0.36	0.34	0.36
MgO	20.0	18.4	21.4	18.7	20.4	21.7	17.6	19.0	18.4	20.6	20.3	16.4	20.9	19.6	20.7	17.4
CaO	4.30	3.61	3.82	4.09	4.45	3.45	2.87	4.11	3.89	4.04	4.20	5.88	4.24	4.02	4.13	3.79
Na_2O	0.08	0.09	0.10	0.07	0.05	0.05	0.09	0.06	0.07	0.09	0.09	0.12	0.05	0.06	0.09	0.08
Total	100.96	101.41	100.88	101.11	100.89	101.31	101.49	101.30	100.96	100.90	100.99	101.45	100.94	100.99	101.30	101.27

Appendix 2.3 continued

	Mars-3															
	16	17	18	19	20	21	22	23	24	25	26	27	28	29	30	31
SiO_2	41.6	42.0	42.1	42.5	42.3	41.8	42.3	42.5	41.9	42.3	42.2	42.6	42.3	42.6	42.6	42.1
TiO_2	0.21	0.45	0.51	0.46	0.37	0.32	0.55	0.50	0.22	0.42	0.48	0.40	0.50	0.46	0.46	0.48
Al_2O_3	23.9	23.8	23.7	23.7	23.7	23.8	23.4	23.7	23.7	23.9	23.6	24.1	23.6	23.7	23.6	23.5
Cr_2O_3	0.08	0.06	0.04	0.18	0.12	0.05	0.18	0.11	0.15	0.11	0.04	0.01	0.09	0.13	0.06	0.08
FeO	13.8	10.3	8.32	8.86	10.1	11.5	9.43	8.71	12.0	9.57	8.57	7.32	9.73	8.54	8.44	9.81
MnO	0.33	0.29	0.22	0.25	0.30	0.24	0.23	0.27	0.28	0.27	0.28	0.27	0.27	0.23	0.25	0.29
MgO	17.7	20.5	20.1	20.8	20.2	19.1	21.0	20.7	19.4	20.7	20.5	21.5	19.5	20.6	21.5	19.3
CaO	3.75	3.31	5.82	4.51	3.93	4.19	4.02	4.56	3.30	3.38	5.20	4.75	5.25	4.67	3.75	5.21
Na_2O	0.09	0.11	0.07	0.07	0.08	0.10	0.07	0.08	0.06	0.11	0.07	0.08	0.09	0.08	0.09	0.09
Total	101.42	100.79	100.82	101.39	101.15	101.13	101.22	101.07	101.12	100.81	100.97	101.10	101.32	101.01	100.76	100.81

	Mars-3					Mars-4										
	32	33	34	35	36	1	2	6	7	11	14	16	17	3	4	5
SiO_2	42.7	41.9	42.5	42.8	41.3	42.0	42.3	42.2	42.4	42.0	42.0	42.4	42.2	41.0	41.1	41.2
TiO_2	0.19	0.09	0.55	0.36	0.29	0.06	0.20	0.22	0.44	0.44	0.35	0.53	0.50	0.08	0.29	0.29
Al_2O_3	24.2	23.9	23.5	24.0	23.6	24.1	24.1	23.8	23.8	23.4	23.1	22.0	21.7	23.2	23.3	23.3
Cr_2O_3	0.09	0.29	0.14	0.25	0.07	0.11	0.17	0.42	0.16	0.67	1.11	2.28	2.40	0.39	0.09	0.11
FeO	9.38	12.6	9.64	7.39	14.8	8.99	8.89	8.79	8.75	9.03	8.76	6.80	7.04	16.4	15.0	14.9
MnO	0.25	0.28	0.26	0.22	0.30	0.47	0.18	0.26	0.21	0.23	0.27	0.27	0.26	0.39	0.29	0.29
MgO	21.9	18.6	20.6	22.6	17.6	20.1	20.9	20.9	21.1	20.2	21.0	21.9	21.7	15.9	15.8	15.5
CaO	2.70	3.64	4.14	3.33	3.16	4.66	4.01	4.15	3.75	4.55	4.03	4.49	4.57	3.69	5.33	5.46
Na_2O	0.07	0.05	0.07	0.06	0.11	0.04	0.08	0.06	0.11	0.12	0.08	0.07	0.08	0.05	0.12	0.13
Total	101.48	101.44	101.37	101.02	101.22	100.53	100.86	100.82	100.68	100.63	100.73	100.68	100.40	101.12	101.22	101.12

Appendix 2.3 continued

	Mars-4									Misc-3			Misc-4			
	8	9	10	12	13	15	25	27	26	28	1	2	3	9	10	47
SiO_2	41.2	41.0	41.0	41.3	40.9	41.5	42.0	42.4	41.4	41.3	42.0	41.5	41.9	41.5	41.5	41.9
TiO_2	0.31	0.30	0.28	0.29	0.08	0.30	0.40	0.57	0.31	0.29	0.50	0.41	0.45	0.23	0.32	0.11
Al_2O_3	23.5	23.4	23.4	23.4	23.4	23.3	23.8	21.9	23.2	23.5	21.5	21.3	21.2	22.8	23.4	23.7
Cr_2O_3	0.06	0.09	0.08	0.08	0.18	0.07	0.05	2.30	0.07	0.06	2.19	2.99	2.48	1.00	0.30	0.54
FeO	14.8	15.0	14.8	15.0	16.2	13.3	10.5	7.38	13.2	14.9	7.06	7.47	7.01	9.74	11.7	10.2
MnO	0.25	0.27	0.28	0.28	0.36	0.30	0.30	0.24	0.32	0.28	0.25	0.29	0.26	0.29	0.26	0.32
MgO	15.9	15.6	15.6	15.4	15.6	17.6	19.8	21.5	17.4	15.8	21.4	20.7	21.4	20.0	19.4	19.2
CaO	5.35	5.46	5.27	5.39	4.14	4.03	3.99	4.32	4.84	5.10	4.69	4.60	4.92	4.35	3.50	4.31
Na_2O	0.11	0.12	0.10	0.11	0.03	0.05	0.15	0.10	0.06	0.13	0.08	0.06	0.05	0.04	0.11	0.03
Total	101.36	101.23	100.88	101.28	100.97	101.26	101.00	100.67	100.91	101.28	99.75	99.42	99.65	99.96	100.50	100.36

	Misc-4		
	48	49	50
SiO_2	42.3	41.6	41.1
TiO_2	0.34	0.06	0.30
Al_2O_3	23.5	23.9	23.7
Cr_2O_3	0.70	0.26	0.06
FeO	7.20	12.0	8.54
MnO	0.32	0.28	0.19
MgO	21.1	18.2	12.3
CaO	3.86	3.91	14.4
Na_2O	0.08	0.05	0.10
Total	99.47	100.28	100.65

Appendix 2.4a Chemical compositions for Klipspringer garnets from bimineralic garnet-clinopyroxene nodules. Cations were recalculated according to the formula unit of garnet, ie. 12 oxygens. Ferric iron was calculated according to Droop (1987). Samples with the same sample name are replicate analyses of one garnet.

Oxides	BM1	BM1	BM1	BM1	BM2	BM2	BM2	BM2	BM3	BM3	BM4	BM4	BM5
SiO_2	42.2	41.8	42.0	41.4	40.5	40.9	40.5	40.9	41.8	41.7	41.3	41.1	41.7
TiO_2	0.11	0.11	0.10	0.12	0.14	0.17	0.16	0.14	0.10	0.12	0.37	0.32	0.06
Al_2O_3	20.4	20.4	20.2	20.2	15.7	17.1	15.4	17.1	19.9	19.8	18.5	18.2	17.6
Cr_2O_3	5.03	4.99	5.03	5.01	10.55	8.89	10.53	8.61	5.34	5.29	6.78	6.87	8.63
FeO	6.70	6.54	6.48	6.60	6.38	6.35	6.52	6.37	7.65	7.40	6.84	6.82	6.68
MnO	0.41	0.39	0.43	0.38	0.38	0.36	0.40	0.31	0.39	0.34	0.32	0.38	0.40
MgO	20.3	20.6	20.6	20.7	18.9	19.5	18.9	19.6	19.9	19.9	19.9	19.7	20.7
CaO	5.02	4.96	5.02	4.99	6.75	6.25	6.69	6.10	5.12	5.08	5.85	5.85	4.63
Na_2O	0.03	0.03	0.08	0.04	0.07	0.04	0.07	0.08	0.06	0.06	0.07	0.08	0.01
Total	100.21	99.85	99.96	99.49	99.44	99.50	99.17	99.27	100.29	99.69	99.86	99.34	100.47
Cations													
Si	3.011	2.991	3.000	2.975	2.986	2.988	2.995	2.993	2.995	3.003	2.989	2.990	3.003
Ti	0.006	0.006	0.005	0.006	0.008	0.009	0.009	0.008	0.005	0.006	0.020	0.017	0.003
Al	1.719	1.721	1.703	1.715	1.364	1.472	1.344	1.476	1.685	1.682	1.574	1.565	1.497
Cr	0.284	0.282	0.284	0.285	0.614	0.514	0.616	0.498	0.303	0.301	0.388	0.395	0.491
Fe^{2+}	0.400	0.384	0.377	0.365	0.359	0.368	0.370	0.363	0.446	0.440	0.389	0.388	0.402
Fe^{3+}	0.000	0.007	0.010	0.032	0.034	0.020	0.032	0.026	0.013	0.005	0.025	0.027	0.000
Mn	0.025	0.023	0.026	0.023	0.024	0.023	0.025	0.019	0.024	0.021	0.020	0.024	0.024
Mg	2.160	2.203	2.201	2.220	2.081	2.120	2.080	2.136	2.132	2.142	2.141	2.135	2.222
Ca	0.384	0.381	0.384	0.384	0.533	0.489	0.530	0.478	0.393	0.392	0.454	0.456	0.357
Na	0.004	0.004	0.012	0.005	0.010	0.005	0.010	0.011	0.008	0.009	0.010	0.011	0.001
Total	7.992	8.002	8.003	8.011	8.011	8.007	8.011	8.009	8.004	8.002	8.008	8.009	8.000
Mg#	84	85	85	85	84	85	84	85	82	83	84	84	85

Appendix 2.4a continued

Oxides	BM5	BM6	BM6	BM7	BM7	BM8	BM8	BM8	BM9	BM10	BM10	BM11	BM11
SiO_2	41.5	42.2	42.4	41.1	41.2	41.3	41.6	41.5	41.8	41.9	41.7	40.4	40.5
TiO_2	0.08	0.04	0.04	0.30	0.31	0.38	0.35	0.34	0.28	0.30	0.32	0.34	0.33
Al_2O_3	17.7	22.6	22.4	20.9	21.1	22.7	22.7	23.1	22.6	23.3	23.2	22.6	22.6
Cr_2O_3	8.24	2.11	2.14	2.65	2.68	0.34	0.32	0.31	0.13	0.47	0.50	0.04	0.05
FeO	6.67	6.86	6.98	10.53	10.65	12.09	12.07	11.97	13.45	10.25	10.11	15.76	15.66
MnO	0.33	0.38	0.47	0.40	0.44	0.33	0.36	0.31	0.33	0.21	0.18	0.38	0.37
MgO	20.7	21.0	21.0	18.5	18.3	18.6	18.6	18.6	18.8	20.1	20.0	14.2	14.2
CaO	4.42	4.19	4.26	5.22	5.18	4.13	4.12	4.08	2.75	3.51	3.46	6.13	6.16
Na_2O	0.05	0.04	0.04	0.03	0.06	0.09	0.08	0.08	0.11	0.11	0.09	0.14	0.12
Total	99.67	99.45	99.70	99.71	99.79	99.94	100.22	100.28	100.26	100.18	99.50	99.91	100.07
Cations													
Si	3.004	2.998	3.009	2.983	2.985	2.978	2.988	2.978	3.002	2.977	2.986	2.977	2.981
Ti	0.004	0.002	0.002	0.016	0.017	0.021	0.019	0.019	0.015	0.016	0.017	0.019	0.018
Al	1.509	1.897	1.873	1.787	1.800	1.926	1.922	1.952	1.916	1.956	1.953	1.960	1.961
Cr	0.472	0.119	0.120	0.152	0.154	0.019	0.018	0.017	0.007	0.026	0.028	0.002	0.003
Fe^{2+}	0.398	0.408	0.414	0.589	0.608	0.676	0.683	0.681	0.765	0.575	0.587	0.922	0.923
Fe^{3+}	0.007	0.000	0.000	0.050	0.038	0.052	0.042	0.037	0.044	0.035	0.018	0.050	0.041
Mn	0.020	0.023	0.028	0.024	0.027	0.020	0.022	0.019	0.020	0.012	0.011	0.024	0.023
Mg	2.238	2.226	2.222	2.005	1.973	1.994	1.990	1.985	2.020	2.132	2.128	1.559	1.561
Ca	0.343	0.319	0.324	0.406	0.403	0.319	0.317	0.314	0.212	0.268	0.265	0.484	0.486
Na	0.007	0.006	0.006	0.004	0.008	0.012	0.012	0.011	0.015	0.015	0.012	0.021	0.017
Total	8.002	7.997	7.998	8.017	8.013	8.017	8.014	8.012	8.015	8.012	8.006	8.017	8.014
Mg#	85	85	84	76	75	73	73	73	71	78	78	62	62

Appendix 2.4a continued

Oxides	BM13	BM14	BM15	BM15	BM15	BM16	BM16	BM17	BM17	BM18	BM18	BM19	BM19
SiO_2	42.5	40.8	40.6	40.8	41.1	41.0	40.7	41.2	41.3	40.8	40.9	41.7	41.5
TiO_2	0.05	0.17	0.24	0.23	0.25	0.20	0.27	0.32	0.34	0.34	0.34	0.24	0.23
Al_2O_3	22.1	23.0	22.9	22.9	23.0	23.1	22.9	23.4	23.2	21.5	21.0	19.8	19.7
Cr_2O_3	2.63	0.15	0.37	0.36	0.31	0.16	0.21	0.06	0.08	1.90	1.85	5.05	4.92
FeO	7.33	13.29	13.96	13.72	14.17	13.90	13.86	12.03	12.07	12.52	12.48	6.76	7.00
MnO	0.37	0.46	0.41	0.34	0.39	0.41	0.39	0.39	0.38	0.36	0.30	0.26	0.30
MgO	22.4	17.0	17.2	17.0	17.3	17.2	17.2	18.1	18.2	17.5	17.3	20.1	20.3
CaO	2.59	4.51	3.59	3.66	3.64	3.67	3.98	4.23	4.19	4.85	4.88	5.31	5.29
Na_2O	0.04	0.10	0.09	0.11	0.08	0.07	0.06	0.06	0.07	0.04	0.06	0.04	0.05
Total	100.01	99.54	99.35	99.20	100.23	99.68	99.57	99.80	99.76	99.82	99.10	99.20	99.31
Cations													
Si	3.002	2.974	2.964	2.982	2.979	2.979	2.965	2.973	2.979	2.974	2.998	3.009	2.996
Ti	0.003	0.009	0.013	0.013	0.013	0.011	0.015	0.017	0.019	0.019	0.019	0.013	0.012
Al	1.840	1.977	1.972	1.974	1.962	1.976	1.971	1.991	1.969	1.842	1.814	1.687	1.679
Cr	0.147	0.008	0.022	0.021	0.018	0.009	0.012	0.004	0.005	0.110	0.108	0.288	0.281
Fe^{2+}	0.426	0.763	0.804	0.814	0.822	0.811	0.796	0.700	0.697	0.712	0.726	0.408	0.399
Fe^{3+}	0.007	0.046	0.049	0.024	0.036	0.034	0.049	0.025	0.031	0.051	0.040	0.000	0.023
Mn	0.022	0.028	0.025	0.021	0.024	0.025	0.024	0.024	0.023	0.022	0.019	0.016	0.018
Mg	2.353	1.844	1.873	1.857	1.864	1.869	1.866	1.940	1.954	1.903	1.898	2.160	2.183
Ca	0.196	0.352	0.281	0.286	0.282	0.286	0.311	0.327	0.324	0.379	0.384	0.411	0.409
Na	0.006	0.014	0.013	0.016	0.012	0.010	0.008	0.009	0.010	0.005	0.008	0.005	0.007
Total	8.002	8.015	8.016	8.008	8.012	8.011	8.016	8.008	8.010	8.017	8.013	7.997	8.008
Mg#	84	70	69	69	68	69	69	73	73	71	71	84	84

Appendix 2.4a continued

Oxides	BM20	BM20	BM21	BM22	BM22	BM23	BM23	BM23	BM24	BM24	BM25	BM25	BM26
SiO_2	41.8	41.6	42.4	42.0	41.6	42.5	42.3	42.4	41.4	41.4	40.9	41.7	42.4
TiO_2	0.33	0.34	0.27	0.33	0.30	0.39	0.39	0.38	0.33	0.31	0.36	0.35	0.38
Al_2O_3	23.3	23.4	24.2	22.8	22.7	23.6	23.3	23.2	21.9	21.6	22.3	22.5	22.4
Cr_2O_3	0.07	0.12	0.14	1.06	1.12	0.88	0.85	0.83	2.43	2.37	0.76	0.72	2.09
FeO	11.86	11.75	8.81	10.27	10.16	6.60	6.57	6.54	8.45	8.44	11.69	11.51	7.83
MnO	0.42	0.37	0.37	0.37	0.34	0.23	0.29	0.34	0.33	0.33	0.34	0.34	0.36
MgO	18.5	18.5	20.6	19.5	19.4	21.8	21.9	21.9	19.8	20.1	18.8	18.7	20.7
CaO	4.12	4.13	4.02	4.18	4.27	3.94	3.83	3.96	4.64	4.51	4.20	4.23	4.21
Na_2O	0.05	0.07	0.08	0.08	0.07	0.08	0.06	0.08	0.06	0.07	0.06	0.09	0.09
Total	100.38	100.20	100.84	100.58	99.99	100.02	99.45	99.68	99.31	99.08	99.40	100.15	100.45
Cations													
Si	2.991	2.979	2.977	2.986	2.980	2.986	2.989	2.992	2.977	2.981	2.963	2.994	2.998
Ti	0.018	0.018	0.014	0.018	0.016	0.020	0.021	0.020	0.018	0.017	0.019	0.019	0.020
Al	1.965	1.977	1.999	1.910	1.912	1.953	1.936	1.929	1.857	1.834	1.908	1.906	1.862
Cr	0.004	0.007	0.008	0.060	0.063	0.049	0.047	0.046	0.138	0.135	0.044	0.041	0.117
Fe^{2+}	0.693	0.680	0.502	0.586	0.578	0.388	0.383	0.377	0.491	0.476	0.639	0.661	0.463
Fe^{3+}	0.017	0.025	0.016	0.025	0.030	0.000	0.005	0.008	0.017	0.032	0.069	0.030	0.000
Mn	0.026	0.022	0.022	0.022	0.021	0.013	0.017	0.020	0.020	0.020	0.021	0.021	0.022
Mg	1.969	1.973	2.155	2.071	2.072	2.282	2.305	2.299	2.122	2.158	2.026	2.001	2.187
Ca	0.316	0.317	0.303	0.319	0.328	0.297	0.290	0.299	0.357	0.348	0.326	0.325	0.319
Na	0.007	0.010	0.010	0.011	0.009	0.010	0.009	0.011	0.008	0.009	0.009	0.012	0.012
Total	8.006	8.008	8.005	8.008	8.010	7.999	8.002	8.003	8.006	8.011	8.023	8.010	7.999
Mg#	74	74	81	77	77	85	86	86	81	81	74	74	83

Appendix 2.4a continued

Oxides	BM26	BM27	BM28	BM28	BM29	BM29	BM30	BM30	BM31	BM31	BM32	BM32	BM33
SiO_2	41.8	42.1	41.8	41.7	41.8	42.1	41.3	42.1	41.4	41.7	41.6	41.7	41.9
TiO_2	0.39	0.40	0.45	0.46	0.18	0.19	0.71	0.68	0.25	0.25	0.25	0.23	0.71
Al_2O_3	22.3	21.6	22.4	22.3	23.4	23.6	22.8	22.8	23.4	23.3	23.0	23.5	22.0
Cr_2O_3	1.93	2.38	0.66	0.65	0.31	0.31	0.12	0.14	0.08	0.12	0.08	0.09	1.24
FeO	7.94	7.47	10.43	9.76	8.48	8.39	11.05	11.28	12.53	12.72	12.79	12.63	8.65
MnO	0.31	0.29	0.29	0.27	0.31	0.31	0.27	0.29	0.30	0.31	0.30	0.34	0.27
MgO	20.9	20.9	19.7	20.0	20.8	20.9	19.7	19.7	18.5	18.5	18.5	18.4	20.2
CaO	4.14	4.72	4.20	4.19	4.16	4.04	3.26	3.27	3.41	3.41	3.35	3.38	3.95
Na_2O	0.08	0.06	0.05	0.07	0.03	0.05	0.16	0.13	0.10	0.09	0.08	0.09	0.12
Total	99.76	99.89	99.93	99.44	99.43	99.96	99.46	100.30	100.01	100.39	99.98	100.41	99.14
Cations													
Si	2.977	2.995	2.989	2.993	2.976	2.978	2.969	2.999	2.977	2.989	2.992	2.987	3.007
Ti	0.021	0.022	0.024	0.025	0.010	0.010	0.038	0.036	0.013	0.013	0.013	0.012	0.038
Al	1.867	1.812	1.890	1.888	1.960	1.970	1.935	1.912	1.984	1.971	1.953	1.987	1.864
Cr	0.108	0.134	0.038	0.037	0.018	0.017	0.007	0.008	0.005	0.007	0.005	0.005	0.070
Fe^{2+}	0.444	0.422	0.585	0.548	0.464	0.464	0.615	0.653	0.719	0.739	0.739	0.739	0.519
Fe^{3+}	0.029	0.022	0.039	0.037	0.041	0.032	0.049	0.020	0.035	0.023	0.031	0.017	0.000
Mn	0.019	0.017	0.017	0.016	0.019	0.019	0.017	0.018	0.019	0.019	0.018	0.020	0.016
Mg	2.217	2.215	2.101	2.135	2.206	2.207	2.113	2.092	1.983	1.973	1.989	1.965	2.164
Ca	0.316	0.360	0.322	0.322	0.317	0.306	0.251	0.250	0.263	0.262	0.258	0.259	0.303
Na	0.012	0.009	0.007	0.010	0.004	0.007	0.022	0.018	0.014	0.013	0.012	0.013	0.016
Total	8.010	8.007	8.013	8.012	8.014	8.011	8.016	8.007	8.012	8.008	8.010	8.006	7.998
Mg#	82	83	77	78	81	82	76	76	72	72	72	72	81

Appendix 2.4a continued

Oxides	BM33	BM34	BM34	BM35	BM35	BM36	BM37	BM37	BM38	BM38	BM39	BM39	BM40
SiO_2	41.8	41.9	42.1	42.2	41.6	41.6	41.9	41.9	40.8	40.5	41.3	41.9	42.2
TiO_2	0.57	0.24	0.18	0.73	0.50	0.40	0.47	0.39	0.26	0.26	0.47	0.18	0.33
Al_2O_3	22.1	23.0	22.9	22.3	22.8	22.5	23.1	22.9	21.3	20.8	18.9	19.4	23.4
Cr_2O_3	1.37	1.48	1.42	1.23	0.12	1.08	1.10	1.05	2.22	2.33	5.64	5.94	0.76
FeO	8.61	8.09	8.26	8.37	10.97	11.38	8.14	8.11	11.72	11.85	5.92	5.39	7.86
MnO	0.27	0.33	0.34	0.27	0.27	0.29	0.28	0.35	0.38	0.40	0.25	0.25	0.36
MgO	20.2	20.3	20.6	20.5	18.2	18.7	20.8	20.7	17.9	17.9	21.0	22.6	21.3
CaO	4.26	4.20	4.22	3.93	5.15	4.11	4.10	4.00	5.06	5.00	5.69	3.44	4.15
Na_2O	0.06	0.07	0.06	0.11	0.07	0.07	0.08	0.07	0.04	0.05	0.03	0.04	0.05
Total	99.28	99.66	100.07	99.59	99.72	100.19	99.97	99.38	99.67	99.17	99.21	99.15	100.31
Cations													
Si	2.999	2.987	2.983	3.009	2.997	2.990	2.972	2.985	2.970	2.969	2.984	2.997	2.971
Ti	0.031	0.013	0.010	0.039	0.027	0.022	0.025	0.021	0.014	0.014	0.025	0.009	0.017
Al	1.866	1.929	1.914	1.873	1.937	1.902	1.927	1.921	1.826	1.800	1.608	1.638	1.943
Cr	0.077	0.083	0.080	0.069	0.007	0.061	0.062	0.059	0.128	0.135	0.322	0.336	0.043
Fe^{2+}	0.512	0.482	0.469	0.499	0.646	0.664	0.463	0.470	0.653	0.647	0.316	0.310	0.430
Fe^{3+}	0.004	0.000	0.021	0.000	0.014	0.019	0.020	0.013	0.061	0.079	0.041	0.013	0.033
Mn	0.017	0.020	0.021	0.016	0.016	0.017	0.017	0.021	0.024	0.025	0.015	0.015	0.021
Mg	2.159	2.156	2.181	2.174	1.953	2.005	2.200	2.199	1.944	1.957	2.256	2.416	2.233
Ca	0.327	0.321	0.321	0.300	0.397	0.316	0.311	0.306	0.395	0.393	0.440	0.264	0.313
Na	0.009	0.010	0.008	0.014	0.010	0.010	0.010	0.009	0.005	0.007	0.005	0.006	0.007
Total	8.001	8.000	8.007	7.994	8.005	8.006	8.007	8.004	8.020	8.026	8.014	8.004	8.011
Mg#	81	82	82	81	75	75	82	82	73	73	86	88	83

Appendix 2.4a continued

Oxides	BM40	BM41	BM41	BM42	BM42	BM43	BM44	BM44	BM45	BM45	BM46	BM46	BM47
SiO_2	42.0	42.6	42.3	42.1	42.3	42.2	41.9	41.9	42.3	42.3	43.0	43.1	43.1
TiO_2	0.34	0.42	0.45	0.45	0.41	0.22	0.51	0.51	0.07	0.08	0.04	0.01	0.02
Al_2O_3	23.3	22.7	22.8	22.7	22.8	22.4	23.0	23.2	21.0	21.0	23.5	23.5	23.7
Cr_2O_3	0.81	1.18	1.19	1.34	1.39	2.00	0.34	0.33	4.56	4.45	1.94	1.95	1.56
FeO	7.63	7.33	7.05	8.44	8.55	8.23	12.24	12.02	6.56	6.53	5.13	4.96	4.90
MnO	0.36	0.32	0.27	0.34	0.28	0.38	0.23	0.29	0.33	0.40	0.22	0.27	0.22
MgO	21.0	21.5	21.4	20.7	20.7	20.7	18.8	18.8	21.2	21.4	24.7	24.5	24.5
CaO	4.40	4.24	4.24	4.21	4.13	4.39	3.86	3.76	4.38	4.35	1.66	1.62	1.76
Na_2O	0.06	0.04	0.06	0.08	0.07	0.07	0.13	0.11	0.05	0.05	0.01	0.00	0.03
Total	99.88	100.37	99.76	100.41	100.64	100.61	100.91	100.91	100.48	100.58	100.19	99.97	99.81
Cations													
Si	2.970	2.996	2.989	2.979	2.986	2.985	2.985	2.981	2.997	2.996	2.982	2.996	2.996
Ti	0.018	0.022	0.024	0.024	0.022	0.012	0.027	0.027	0.004	0.004	0.002	0.000	0.001
Al	1.948	1.885	1.900	1.897	1.900	1.866	1.929	1.951	1.754	1.752	1.923	1.927	1.943
Cr	0.045	0.066	0.067	0.075	0.077	0.112	0.019	0.019	0.255	0.249	0.106	0.107	0.085
Fe^{2+}	0.423	0.418	0.405	0.476	0.491	0.458	0.697	0.694	0.389	0.382	0.296	0.288	0.285
Fe^{3+}	0.029	0.013	0.012	0.023	0.014	0.029	0.033	0.022	0.000	0.005	0.002	0.000	0.000
Mn	0.021	0.019	0.016	0.020	0.017	0.023	0.014	0.018	0.020	0.024	0.013	0.016	0.013
Mg	2.213	2.259	2.261	2.182	2.176	2.183	1.993	1.994	2.241	2.255	2.551	2.539	2.537
Ca	0.334	0.320	0.321	0.319	0.312	0.333	0.295	0.287	0.333	0.330	0.123	0.120	0.131
Na	0.008	0.006	0.009	0.011	0.010	0.009	0.018	0.015	0.007	0.007	0.002	0.000	0.004
Total	8.010	8.004	8.004	8.008	8.005	8.010	8.011	8.007	7.999	8.002	8.001	7.993	7.995
Mg#	83	84	84	81	81	82	73	74	85	85	90	90	90

Appendix 2.4a continued

Oxides	BM47	BM48	BM48	BM49	BM49	BM50	BM50	BM51	BM51	BM52	BM52	BM53	BM53
SiO_2	42.9	42.8	42.2	42.0	42.0	42.2	42.0	42.2	41.8	41.6	41.4	42.2	42.1
TiO_2	0.02	0.03	0.02	0.34	0.39	0.37	0.34	0.09	0.10	0.06	0.08	0.65	0.67
Al_2O_3	23.5	21.5	21.5	21.9	21.6	22.0	22.1	22.4	22.5	17.9	17.5	22.4	22.5
Cr_2O_3	1.75	4.03	4.01	2.70	2.83	2.31	2.34	2.21	2.22	8.67	8.98	1.71	1.66
FeO	4.84	5.54	5.58	7.06	7.20	7.18	7.19	6.99	6.85	6.36	6.36	8.03	8.16
MnO	0.23	0.30	0.22	0.32	0.34	0.28	0.36	0.25	0.29	0.38	0.32	0.29	0.28
MgO	24.6	23.5	23.2	21.4	21.1	21.2	21.0	21.3	21.0	20.5	20.5	20.9	20.7
CaO	1.73	2.57	2.59	4.38	4.37	4.42	4.52	4.49	4.46	4.27	4.35	3.67	3.61
Na_2O	0.02	0.03	0.03	0.06	0.07	0.08	0.06	0.04	0.04	0.06	0.05	0.13	0.14
Total	99.66	100.29	99.33	100.12	99.87	100.05	99.90	99.97	99.25	99.76	99.50	99.89	99.81
Cations													
Si	2.987	3.000	2.992	2.975	2.987	2.992	2.983	2.991	2.979	3.008	3.004	2.996	2.995
Ti	0.001	0.002	0.001	0.018	0.021	0.020	0.018	0.005	0.005	0.003	0.004	0.035	0.036
Al	1.932	1.780	1.791	1.829	1.810	1.838	1.851	1.868	1.890	1.525	1.494	1.870	1.881
Cr	0.096	0.224	0.224	0.151	0.159	0.130	0.131	0.124	0.125	0.496	0.516	0.096	0.093
Fe^{2+}	0.282	0.325	0.329	0.387	0.409	0.410	0.409	0.397	0.394	0.385	0.386	0.477	0.485
Fe^{3+}	0.000	0.000	0.001	0.031	0.019	0.016	0.018	0.017	0.015	0.000	0.000	0.000	0.000
Mn	0.013	0.018	0.013	0.019	0.021	0.017	0.021	0.015	0.017	0.024	0.020	0.017	0.017
Mg	2.556	2.455	2.448	2.259	2.237	2.238	2.221	2.243	2.233	2.212	2.224	2.209	2.194
Ca	0.129	0.193	0.196	0.332	0.333	0.335	0.344	0.340	0.341	0.331	0.339	0.279	0.275
Na	0.002	0.004	0.004	0.008	0.010	0.011	0.008	0.006	0.005	0.009	0.008	0.018	0.020
Total	7.999	8.000	8.000	8.010	8.006	8.005	8.006	8.006	8.005	7.992	7.995	7.997	7.996
Mg#	90	88	88	84	84	84	84	84	85	85	85	82	82

Appendix 2.4a continued

Oxides	BM53	BM54	BM54	BM55	BM55	BM55	BM58	BM58	BM59	BM59	BM60	BM61	BM61
SiO_2	42.1	43.0	42.8	42.4	42.0	42.6	43.1	42.0	42.5	41.9	42.0	41.9	41.8
TiO_2	0.67	0.03	0.03	0.32	0.31	0.34	0.03	0.47	0.10	0.07	0.13	0.14	0.14
Al_2O_3	22.2	23.0	23.3	21.7	21.7	21.8	23.4	23.8	22.5	22.3	19.8	20.0	19.8
Cr_2O_3	1.89	2.41	2.22	2.95	3.01	2.95	1.92	0.17	2.37	2.24	6.13	6.01	5.98
FeO	8.21	5.25	5.23	6.96	6.89	7.09	5.67	11.10	6.73	6.90	6.14	6.20	5.95
MnO	0.23	0.25	0.24	0.29	0.22	0.30	0.25	0.27	0.29	0.32	0.38	0.35	0.34
MgO	20.9	24.1	23.9	20.8	20.7	21.1	22.8	18.5	20.9	21.2	20.3	20.2	20.5
CaO	3.75	1.80	1.84	4.38	4.34	4.46	2.87	4.48	4.54	4.46	5.11	5.21	5.11
Na_2O	0.13	0.00	0.02	0.06	0.05	0.06	0.03	0.11	0.04	0.05	0.06	0.05	0.03
Total	100.13	99.75	99.55	99.90	99.15	100.66	100.08	100.93	99.95	99.49	100.13	100.07	99.58
Cations													
Si	2.986	3.001	2.998	3.013	3.005	3.002	3.009	2.984	3.008	2.984	3.007	2.998	3.000
Ti	0.036	0.001	0.002	0.017	0.017	0.018	0.002	0.025	0.005	0.004	0.007	0.008	0.008
Al	1.857	1.893	1.918	1.820	1.827	1.812	1.931	1.991	1.878	1.873	1.672	1.691	1.674
Cr	0.106	0.133	0.123	0.166	0.170	0.165	0.106	0.010	0.133	0.126	0.347	0.340	0.340
Fe^{2+}	0.478	0.307	0.306	0.413	0.412	0.419	0.331	0.659	0.399	0.386	0.367	0.371	0.358
Fe^{3+}	0.009	0.000	0.000	0.000	0.000	0.000	0.000	0.000	0.000	0.024	0.000	0.000	0.000
Mn	0.014	0.015	0.014	0.018	0.013	0.018	0.015	0.016	0.017	0.019	0.023	0.021	0.021
Mg	2.215	2.508	2.489	2.202	2.208	2.220	2.374	1.958	2.204	2.245	2.167	2.156	2.196
Ca	0.285	0.135	0.138	0.333	0.332	0.337	0.215	0.341	0.345	0.340	0.392	0.399	0.394
Na	0.018	0.000	0.003	0.008	0.007	0.009	0.005	0.016	0.005	0.007	0.008	0.007	0.004
Total	8.003	7.992	7.991	7.991	7.992	7.998	7.986	7.999	7.992	8.008	7.990	7.991	7.994
Mg#	82	89	89	84	84	84	88	75	85	85	86	85	86

Appendix 2.4a continued

Oxides	BM61	BM62	BM62
SiO_2	42.0	42.0	41.5
TiO_2	0.07	0.37	0.47
Al_2O_3	21.4	23.4	23.3
Cr_2O_3	4.36	0.18	0.19
FeO	6.85	12.11	11.81
MnO	0.30	0.36	0.34
MgO	20.2	18.7	18.7
CaO	5.36	3.74	3.79
Na_2O	0.01	0.09	0.08
Total	100.61	100.92	100.24
Cations			
Si	2.984	2.987	2.974
Ti	0.004	0.020	0.026
Al	1.788	1.966	1.967
Cr	0.245	0.010	0.011
Fe^{2+}	0.407	0.702	0.682
Fe^{3+}	0.000	0.019	0.025
Mn	0.018	0.022	0.021
Mg	2.143	1.982	2.000
Ca	0.408	0.286	0.291
Na	0.002	0.013	0.011
Total	7.999	8.006	8.008
Mg#	84	73	74

Appendix 2.4b Chemical compositions for Klipspringer clinopyroxene from bimineralic garnet-clinopyroxene nodules. Cations recalculated according to the formulaunit of clinopyroxene, ie. 6 oxygens. Ferric iron was calculated according to Droop (1987). Samples with the same sample name are replicate analyses of one clinopyroxene.

Oxides	BM1	BM1	BM2	BM2	BM3	BM3	BM4	BM4	BM6	BM6	BM7	BM7	BM8
Na_2O	2.77	2.73	2.47	2.54	2.96	2.99	2.56	2.59	2.06	2.11	1.19	1.23	2.13
K_2O	0.01	0.01	0.02	0.02	0.01	0.01	0.01	0.02	0.01	0.02	0.02	0.03	0.04
SiO_2	54.6	54.2	54.2	54.3	54.4	54.6	54.6	54.4	55.2	55.0	54.1	54.4	54.2
TiO_2	0.12	0.13	0.11	0.09	0.13	0.16	0.28	0.25	0.01	0.04	0.19	0.16	0.29
Al_2O_3	2.81	2.83	2.12	2.16	3.20	3.15	2.40	2.37	2.63	2.75	1.42	1.48	2.91
Cr_2O_3	3.12	3.04	3.48	3.54	3.21	3.26	2.99	3.08	1.31	1.31	0.72	0.72	0.20
FeO	1.49	1.62	1.84	1.86	1.56	1.59	1.87	1.85	2.10	1.95	3.53	3.47	4.37
MnO	0.07	0.08	0.07	0.08	0.05	0.05	0.04	0.03	0.07	0.10	0.11	0.07	0.08
MgO	15.8	16.1	16.6	16.6	15.5	15.6	16.4	16.2	17.1	17.3	17.7	17.9	16.7
CaO	19.2	18.8	18.7	18.7	18.7	18.3	19.1	18.8	19.6	19.6	20.1	20.2	18.2
Total	100.00	99.48	99.71	99.94	99.69	99.73	100.30	99.62	100.01	100.15	99.11	99.70	99.14
Cations													
Na	0.194	0.191	0.173	0.178	0.207	0.209	0.178	0.182	0.143	0.146	0.084	0.086	0.150
K	0.001	0.000	0.001	0.001	0.001	0.001	0.000	0.001	0.001	0.001	0.001	0.002	0.002
Si	1.968	1.963	1.963	1.962	1.964	1.969	1.965	1.970	1.982	1.974	1.975	1.974	1.973
Ti	0.003	0.003	0.003	0.003	0.004	0.004	0.007	0.007	0.000	0.001	0.005	0.004	0.008
Al	0.119	0.121	0.090	0.092	0.136	0.134	0.102	0.101	0.112	0.116	0.061	0.063	0.125
Cr	0.089	0.087	0.100	0.101	0.092	0.093	0.085	0.088	0.037	0.037	0.021	0.021	0.006
Fe^{2+}	0.011	0.011	0.016	0.014	0.014	0.021	0.021	0.026	0.040	0.025	0.076	0.070	0.089
Fe^{3+}	0.034	0.038	0.039	0.043	0.034	0.027	0.035	0.030	0.023	0.033	0.032	0.036	0.044
Mn	0.002	0.002	0.002	0.002	0.002	0.002	0.001	0.001	0.002	0.003	0.004	0.002	0.002
Mg	0.849	0.867	0.898	0.894	0.836	0.840	0.881	0.874	0.915	0.922	0.964	0.970	0.908
Ca	0.742	0.728	0.727	0.726	0.724	0.710	0.735	0.731	0.753	0.752	0.788	0.786	0.708
Total	4.011	4.013	4.013	4.014	4.011	4.009	4.012	4.010	4.008	4.011	4.011	4.012	4.015
Mg#	95	95	94	94	95	95	94	94	94	94	90	90	87

Appendix 2.4b continued

Oxides	BM8	BM10	BM10	BM11	BM11	BM11	BM14	BM14	BM15	BM15	BM16	BM16	BM17
Na_2O	2.30	3.02	2.97	5.94	5.86	5.80	3.56	3.50	3.03	3.14	3.03	2.98	2.02
K_2O	0.03	0.12	0.12	0.15	0.14	0.14	0.03	0.03	0.02	0.03	0.02	0.03	0.01
SiO_2	54.5	55.0	55.7	55.1	55.2	55.6	55.1	54.4	55.0	54.9	54.7	54.6	54.2
TiO_2	0.31	0.34	0.35	0.52	0.52	0.55	0.27	0.25	0.36	0.32	0.34	0.31	0.32
Al_2O_3	2.96	5.01	4.99	11.11	11.01	11.21	5.32	5.29	4.18	4.15	4.37	4.19	2.91
Cr_2O_3	0.16	0.40	0.42	0.03	0.03	0.04	0.14	0.15	0.35	0.35	0.21	0.18	0.06
FeO	4.27	3.59	3.49	4.04	3.93	3.97	4.03	3.99	4.78	4.83	4.82	4.73	4.10
MnO	0.06	0.05	0.09	0.06	0.09	0.06	0.11	0.10	0.10	0.08	0.09	0.09	0.12
MgO	16.7	16.4	16.6	10.2	10.3	10.3	14.6	14.6	15.5	15.4	15.4	15.6	16.5
CaO	18.4	15.6	15.5	12.5	12.4	12.3	16.9	16.8	16.8	16.8	16.4	16.7	19.0
Total	99.60	99.48	100.11	99.62	99.53	100.02	100.06	99.10	100.12	100.06	99.47	99.37	99.25
Cations													
Na	0.161	0.210	0.205	0.410	0.405	0.399	0.248	0.246	0.211	0.219	0.213	0.209	0.143
K	0.002	0.006	0.006	0.007	0.007	0.006	0.001	0.002	0.001	0.002	0.001	0.001	0.000
Si	1.973	1.973	1.983	1.961	1.967	1.971	1.975	1.969	1.977	1.977	1.979	1.975	1.971
Ti	0.008	0.009	0.009	0.014	0.014	0.015	0.007	0.007	0.010	0.009	0.009	0.009	0.009
Al	0.127	0.212	0.209	0.466	0.462	0.468	0.225	0.226	0.177	0.176	0.186	0.179	0.125
Cr	0.005	0.011	0.012	0.001	0.001	0.001	0.004	0.004	0.010	0.010	0.006	0.005	0.002
Fe^{2+}	0.077	0.086	0.100	0.120	0.117	0.118	0.079	0.071	0.105	0.098	0.112	0.099	0.083
Fe^{3+}	0.052	0.022	0.004	0.000	0.000	0.000	0.041	0.050	0.038	0.048	0.034	0.044	0.042
Mn	0.002	0.002	0.003	0.002	0.003	0.002	0.003	0.003	0.003	0.002	0.003	0.003	0.004
Mg	0.900	0.879	0.880	0.542	0.547	0.545	0.780	0.789	0.833	0.828	0.833	0.844	0.895
Ca	0.712	0.599	0.590	0.477	0.475	0.468	0.650	0.651	0.646	0.649	0.637	0.647	0.742
Total	4.018	4.007	4.001	4.000	3.997	3.991	4.014	4.017	4.013	4.016	4.012	4.015	4.014
Mg#	87	89	89	82	82	82	87	87	85	85	85	86	88

Appendix 2.4b continued

Oxides	BM17	BM17	BM18	BM18	BM20	BM21	BM22	BM23	BM23	BM23	BM24	BM25	BM25
Na_2O	2.07	2.05	1.73	1.79	2.01	2.12	2.27	2.28	2.36	2.28	2.16	2.14	2.01
K_2O	0.02	0.02	0.02	0.02	0.02	0.02	0.01	0.03	0.03	0.03	0.02	0.03	0.03
SiO_2	54.6	54.7	54.1	54.4	55.0	54.7	55.1	55.5	55.2	55.1	55.3	55.2	54.8
TiO_2	0.33	0.31	0.20	0.17	0.32	0.43	0.37	0.44	0.46	0.44	0.27	0.33	0.34
Al_2O_3	2.96	2.96	2.03	2.07	3.05	3.29	3.01	3.44	3.47	3.47	2.55	2.85	2.80
Cr_2O_3	0.05	0.06	0.71	0.67	0.06	0.10	0.72	0.65	0.65	0.61	1.39	0.43	0.41
FeO	4.08	4.10	4.63	4.60	3.82	2.76	3.38	2.20	2.07	2.16	2.67	4.03	4.04
MnO	0.08	0.15	0.07	0.10	0.07	0.11	0.06	0.06	0.09	0.08	0.12	0.12	0.07
MgO	16.6	16.8	16.8	16.9	16.6	16.7	16.6	17.3	17.1	17.3	16.8	16.9	16.8
CaO	19.2	19.3	19.5	19.2	19.1	19.4	19.0	18.9	19.1	18.8	19.4	18.8	19.0
Total	99.94	100.35	99.77	99.96	100.07	99.74	100.63	100.80	100.53	100.34	100.69	100.84	100.31
Cations													
Na	0.145	0.143	0.122	0.126	0.141	0.148	0.158	0.157	0.163	0.158	0.150	0.148	0.140
K	0.001	0.001	0.001	0.001	0.001	0.001	0.001	0.001	0.001	0.001	0.001	0.002	0.002
Si	1.971	1.967	1.969	1.974	1.981	1.972	1.974	1.972	1.968	1.966	1.978	1.976	1.973
Ti	0.009	0.008	0.006	0.005	0.009	0.012	0.010	0.012	0.012	0.012	0.007	0.009	0.009
Al	0.126	0.126	0.087	0.088	0.129	0.140	0.127	0.144	0.146	0.146	0.107	0.120	0.119
Cr	0.001	0.002	0.021	0.019	0.002	0.003	0.020	0.018	0.018	0.017	0.039	0.012	0.012
Fe^{2+}	0.080	0.075	0.091	0.094	0.090	0.054	0.069	0.044	0.031	0.035	0.054	0.085	0.086
Fe^{3+}	0.044	0.049	0.050	0.045	0.025	0.030	0.032	0.022	0.030	0.030	0.025	0.036	0.036
Mn	0.002	0.005	0.002	0.003	0.002	0.003	0.002	0.002	0.003	0.003	0.004	0.004	0.002
Mg	0.895	0.899	0.910	0.912	0.893	0.899	0.887	0.916	0.909	0.923	0.898	0.902	0.903
Ca	0.742	0.743	0.758	0.747	0.737	0.750	0.731	0.720	0.728	0.719	0.744	0.719	0.731
Total	4.015	4.016	4.017	4.015	4.008	4.010	4.011	4.007	4.010	4.010	4.009	4.012	4.012
Mg#	88	88	87	87	89	92	90	93	94	93	92	88	88

Appendix 2.4b continued

Oxides	BM26	BM26	BM28	BM28	BM29	BM31	BM31	BM32	BM32	BM33	BM33	BM34	BM35
Na_2O	2.60	2.56	1.47	1.55	2.06	4.65	4.85	4.69	4.66	1.98	2.01	2.19	2.69
K_2O	0.03	0.02	0.06	0.06	0.02	0.03	0.03	0.03	0.03	0.05	0.05	0.02	0.07
SiO_2	54.9	54.9	55.1	55.3	55.1	55.6	55.7	55.9	55.8	55.4	55.2	55.7	55.3
TiO_2	0.41	0.41	0.18	0.18	0.20	0.42	0.46	0.41	0.45	0.35	0.34	0.18	0.32
Al_2O_3	3.26	3.20	2.17	2.26	3.30	7.10	7.21	7.16	6.89	2.51	2.60	3.02	4.13
Cr_2O_3	1.25	1.24	0.14	0.12	0.23	0.16	0.14	0.12	0.13	0.78	0.72	0.89	0.05
FeO	2.45	2.41	4.44	4.44	2.70	4.17	4.30	4.24	4.15	3.82	3.58	2.45	4.61
MnO	0.07	0.11	0.13	0.10	0.11	0.06	0.08	0.10	0.10	0.09	0.10	0.09	0.05
MgO	16.9	16.7	18.9	18.8	17.1	13.9	13.9	14.0	14.0	18.5	18.1	17.3	16.3
CaO	18.2	18.3	17.5	17.3	19.4	14.4	14.0	14.1	14.1	17.5	17.5	19.2	17.4
Total	100.12	99.85	100.11	100.06	100.19	100.51	100.65	100.70	100.31	100.98	100.23	100.99	100.85
Cations													
Na	0.181	0.179	0.102	0.108	0.143	0.319	0.333	0.322	0.321	0.137	0.139	0.151	0.186
K	0.001	0.001	0.003	0.003	0.001	0.001	0.001	0.002	0.001	0.002	0.002	0.001	0.003
Si	1.969	1.974	1.981	1.985	1.974	1.972	1.971	1.978	1.981	1.973	1.979	1.979	1.971
Ti	0.011	0.011	0.005	0.005	0.005	0.011	0.012	0.011	0.012	0.009	0.009	0.005	0.009
Al	0.138	0.136	0.092	0.096	0.139	0.297	0.301	0.298	0.289	0.105	0.110	0.127	0.174
Cr	0.036	0.035	0.004	0.004	0.006	0.005	0.004	0.004	0.004	0.022	0.020	0.025	0.001
Fe^{2+}	0.036	0.044	0.104	0.110	0.052	0.085	0.081	0.093	0.090	0.079	0.080	0.048	0.097
Fe^{3+}	0.037	0.029	0.029	0.024	0.029	0.039	0.046	0.033	0.033	0.035	0.027	0.025	0.040
Mn	0.002	0.003	0.004	0.003	0.003	0.002	0.002	0.003	0.003	0.003	0.003	0.003	0.002
Mg	0.903	0.895	1.013	1.005	0.912	0.736	0.733	0.736	0.740	0.979	0.967	0.916	0.867
Ca	0.700	0.703	0.673	0.666	0.745	0.546	0.530	0.532	0.538	0.667	0.672	0.729	0.664
Total	4.013	4.010	4.010	4.008	4.010	4.013	4.016	4.011	4.011	4.012	4.009	4.008	4.014
Mg#	92	92	88	88	92	86	85	85	86	90	90	93	86

Appendix 2.4b continued

Oxides	BM35	BM36	BM36	BM37	BM37	BM40	BM41	BM41	BM42	BM42	BM43	BM44	BM49
Na_2O	2.72	2.75	2.77	2.23	2.10	1.67	1.64	1.61	2.10	2.15	1.93	3.37	2.17
K_2O	0.07	0.03	0.03	0.03	0.02	0.03	0.04	0.05	0.04	0.06	0.04	0.08	0.09
SiO_2	55.0	55.4	55.1	54.9	55.1	55.3	55.3	55.5	55.0	55.1	55.4	55.7	55.2
TiO_2	0.35	0.43	0.41	0.42	0.38	0.28	0.18	0.20	0.43	0.43	0.22	0.44	0.19
Al_2O_3	4.21	3.51	3.45	3.20	3.06	2.41	2.21	2.26	2.98	2.87	2.40	5.14	2.48
Cr_2O_3	0.09	0.60	0.63	0.71	0.71	0.46	0.48	0.53	0.69	0.69	1.00	0.28	1.33
FeO	4.51	3.87	4.10	2.89	2.67	2.53	2.92	3.00	2.99	2.86	2.66	4.89	2.26
MnO	0.03	0.07	0.08	0.04	0.11	0.06	0.10	0.10	0.09	0.05	0.06	0.06	0.09
MgO	15.9	16.2	16.1	17.3	17.5	18.1	18.9	18.9	17.2	17.5	17.3	15.9	18.0
CaO	17.4	17.6	17.3	18.6	18.4	19.7	18.7	18.5	18.7	18.7	19.1	15.1	18.6
Total	100.20	100.38	100.05	100.34	100.01	100.51	100.46	100.69	100.19	100.40	100.14	100.91	100.43
Cations													
Na	0.189	0.191	0.193	0.155	0.146	0.116	0.114	0.111	0.146	0.149	0.134	0.232	0.150
K	0.003	0.001	0.001	0.001	0.001	0.002	0.002	0.002	0.002	0.003	0.002	0.004	0.004
Si	1.976	1.983	1.983	1.965	1.975	1.975	1.975	1.977	1.973	1.972	1.988	1.977	1.971
Ti	0.010	0.012	0.011	0.011	0.010	0.008	0.005	0.006	0.012	0.012	0.006	0.012	0.005
Al	0.178	0.148	0.146	0.135	0.129	0.102	0.093	0.095	0.126	0.121	0.102	0.215	0.104
Cr	0.003	0.017	0.018	0.020	0.020	0.013	0.014	0.015	0.020	0.020	0.029	0.008	0.038
Fe^{2+}	0.104	0.088	0.092	0.051	0.059	0.047	0.050	0.059	0.064	0.052	0.067	0.118	0.022
Fe^{3+}	0.031	0.028	0.032	0.036	0.021	0.028	0.037	0.030	0.025	0.034	0.013	0.027	0.046
Mn	0.001	0.002	0.002	0.001	0.003	0.002	0.003	0.003	0.003	0.001	0.002	0.002	0.003
Mg	0.849	0.863	0.866	0.921	0.936	0.964	1.006	1.006	0.920	0.932	0.927	0.841	0.959
Ca	0.668	0.676	0.667	0.715	0.707	0.754	0.715	0.707	0.718	0.717	0.735	0.573	0.714
Total	4.010	4.010	4.011	4.012	4.007	4.010	4.013	4.010	4.009	4.011	4.004	4.009	4.015
Mg#	86	88	88	91	92	93	92	92	91	92	92	85	93

Appendix 2.4b continued

Oxides	BM49	BM50	BM51	BM51	BM52	BM52	BM53	BM55	BM56	BM58	BM58	BM59	BM60
Na_2O	2.18	1.88	1.52	1.61	4.97	5.02	3.20	1.81	4.36	3.50	3.60	1.53	2.69
K_2O	0.06	0.03	0.07	0.07	0.02	0.03	0.07	0.10	0.03	0.02	0.03	0.07	0.02
SiO_2	55.0	55.3	54.9	54.7	55.1	55.0	55.5	55.3	55.4	55.2	55.2	54.7	55.2
TiO_2	0.19	0.22	0.03	0.03	0.06	0.04	0.53	0.11	0.34	0.67	0.67	0.03	0.08
Al_2O_3	2.61	2.27	2.18	2.18	3.87	4.02	3.98	2.43	6.82	5.45	5.49	2.15	2.58
Cr_2O_3	1.35	1.29	0.88	0.90	6.61	6.40	1.17	1.10	0.13	0.11	0.14	0.88	3.34
FeO	2.37	2.41	2.03	2.09	1.75	1.85	3.70	2.94	4.69	3.44	3.36	2.18	1.73
MnO	0.09	0.06	0.06	0.09	0.06	0.07	0.09	0.10	0.03	0.06	0.07	0.04	0.09
MgO	17.7	18.0	18.2	18.3	14.1	14.3	17.5	18.9	13.3	14.8	15.0	18.2	16.4
CaO	18.7	19.1	19.6	19.6	13.8	13.5	15.1	17.4	15.7	16.8	17.0	19.8	18.7
Total	100.33	100.65	99.54	99.55	100.39	100.23	100.77	100.12	100.80	100.04	100.50	99.59	100.76
Cations													
Na	0.152	0.130	0.107	0.113	0.345	0.349	0.220	0.126	0.301	0.242	0.248	0.107	0.187
K	0.003	0.001	0.003	0.003	0.001	0.001	0.003	0.004	0.001	0.001	0.001	0.003	0.001
Si	1.969	1.976	1.980	1.973	1.975	1.972	1.970	1.979	1.969	1.975	1.965	1.973	1.973
Ti	0.005	0.006	0.001	0.001	0.002	0.001	0.014	0.003	0.009	0.018	0.018	0.001	0.002
Al	0.110	0.096	0.093	0.093	0.163	0.170	0.166	0.102	0.286	0.230	0.230	0.091	0.109
Cr	0.038	0.036	0.025	0.026	0.187	0.181	0.033	0.031	0.004	0.003	0.004	0.025	0.094
Fe^{2+}	0.027	0.044	0.038	0.026	0.020	0.016	0.067	0.063	0.098	0.085	0.063	0.031	0.026
Fe^{3+}	0.044	0.027	0.024	0.037	0.032	0.040	0.042	0.025	0.042	0.018	0.037	0.034	0.026
Mn	0.003	0.002	0.002	0.003	0.002	0.002	0.003	0.003	0.001	0.002	0.002	0.001	0.003
Mg	0.946	0.959	0.980	0.983	0.752	0.763	0.924	1.006	0.706	0.787	0.794	0.981	0.874
Ca	0.719	0.732	0.757	0.756	0.531	0.518	0.572	0.666	0.598	0.645	0.650	0.764	0.715
Total	4.015	4.009	4.008	4.013	4.011	4.013	4.014	4.008	4.014	4.006	4.013	4.012	4.009
Mg#	93	93	94	94	93	93	89	92	84	88	89	94	94

Appendix 2.4b continued

Oxides	BM60	BM61	BM61	BM62
Na_2O	2.62	2.68	2.69	2.65
K_2O	0.02	0.02	0.02	0.04
SiO_2	54.9	54.8	54.7	55.4
TiO_2	0.08	0.08	0.11	0.39
Al_2O_3	2.56	2.58	2.48	3.84
Cr_2O_3	3.38	3.36	3.44	0.13
FeO	1.61	1.65	1.53	4.47
MnO	0.03	0.05	0.07	0.11
MgO	16.5	16.6	16.4	16.4
CaO	18.6	18.6	18.4	17.4
Total	100.31	100.41	99.84	100.87
Cations				
Na	0.183	0.187	0.188	0.184
K	0.001	0.001	0.001	0.002
Si	1.970	1.964	1.974	1.974
Ti	0.002	0.002	0.003	0.011
Al	0.108	0.109	0.106	0.162
Cr	0.096	0.095	0.098	0.004
Fe^{2+}	0.023	0.013	0.022	0.096
Fe^{3+}	0.025	0.037	0.025	0.038
Mn	0.001	0.002	0.002	0.003
Mg	0.882	0.888	0.880	0.874
Ca	0.717	0.715	0.711	0.667
Total	4.008	4.012	4.008	4.013
Mg#	95	95	95	87

APPENDIX 3

PHYSICAL CHARACTERISTICS OF THE DIAMONDS

Physical characteristics of the diamonds are described mainly according to the terminology used by Chinn (1995) and Robinson (1978). Abbreviations used in Appendix 3.1 are described below as well as explanations for some indices used.

COLOUR:	CL=colourless	P/B=pink-brown	LG=light green
	OW=off white	LY=light yellow	B/Y=brown-yellow
	LP=light pink		

MORPHOLOGY: (MORPH.)	THH=tetrahexahedroid
	THH/O(#)=partly resorbed octahedra with the percentage of the original diamond volume removed (see Section 5.3.2) indicated within the brackets.
	?=uncertain

CRYSTAL REGULATION: (CRYST.REG.)	R=regular (nearly equidimensional)
	E=elongate (2 dimensions<1/2 other dimension)
	F=flattened (1 dimension<1/2 other dimension)
	E/F=elongate and flattened
	ID=irregularly distorted
	?=uncertain

CRYSTAL STATE: (CR.ST.)	W=whole
	C=chipped (<10 % of original volume lost through breakage)
	B=broken (10-50 % of original volume lost through breakage)
	F=fragment (>50 % of original volume lost through breakage)
	?=uncertain

BREAKAGE SURFACE: (BREAK.)	LE=light etching	SC=subchoncoidal fracture
	RES=resorbed	ST=stepped fracture

RESORPTION SURFACE FEATURES: (RES.SURF.)	H=hillocks (elongate, pyramidoial or ellipsoid) MH=microhillocks T=terraces around 6-fold THH axis CS=corrosion sculpture ZZ=zig-zag patterns around 4-fold THH axis MP=circular micro-pits MD=circular micro-discs
OCTAHEDRAL SURFACE FEATURES: (OCTA.SURF.)	hexa=hexagonal etch pits -tri=negatively orientated trigonal etxh pits TP=triangular plates
DEFORMATION LAMINAE: (DEF.LAM.)	C=coarse (>100 μm separation between individual laminae) F=fine (>100 μm separation between individual laminae) C/F=coarse and fine laminae
RUTS:	Indicated if present

Appendix 3.1 Physical characteristics of Klipspringer diamonds

SAMPLE	COLOUR	MORPH.	CR. REG.	CR. ST.	BREAK				RES. SURF.							OCTA. SURF.	DEF.	LAM.	RUTS	COMMENTS
Main Fissure					LE	SCL	RES	ST	H	MH	T	CLS	ZZ	MP	MD					
1700-1	LG	THH	E	W					X		X		X				F			
1700-2	P/B	THH/O(65%)	R	W													F			
1700-3	CL	THH/O(60%)	R	F	X	X													X	
1700-4	P/B	THH	R	CL	X				X								F		X	Fract. ass. with incl. pit
1700-7	P/B	THH	F	B	X	X				X							F		X	Fract. ass. with ruts anc
1700-11	OW	THH	F	W						X							C			
1700-12	P/B	THH	E/F	W						X							F			
1700-13	LG	THH	E/F	W							X		X				F			
1700-14	CL	THH	E/F	W						X			X							
1700-15	CL	?	?	F	X	X	X			X					X*					*On resorbed fracture s
1700-17	P/B	THH	R	W					X	X							C			
1700-18	P/B	THH	E/F	W	X	X				X							F			
1700-19	CL	THH	E/F	W					X		X						F		X	
1700-20	CL	THH/O(65%)	F	W					X					X						
1700-21	LY	THH	F	B		X			X	X							C		X	
1700-24	CL	THH	?	F	X		X		X								F		X	Fract. ass. with ruts
1700-25	CL	THH	ID	W					X		X								X	
1700-26	P/B	THH	R	CL		X				X							F		X	
1700-28	LG	THH	F	W							X						C			
1700-30	CL	THH	ID	W						X			X							
1700-33	LG	THH	?	F	X	X	X								X					
1700-34	CL	THH	?	F	X				X	X							F			Fract. ass. with incl. pit
1700-35	OW	THH	E/F	W					X	X							C/F		X	Scotch-plaid texture
1700-43	Y/B	THH	ID	W					X	X							C		X	
P3-1	LG	THH	F	W					X		X						C			
P3-2	P/B	THH	ID	B		X			X	X							F		X	Fract. ass. with ruts
P4-1	CL	THH	ID	B	X				X										X	Fract. ass. with incl. pit
P4-9	CL	THH	E	W					X		X									
P5-1	CL	THH	E/F	W							X			X			F			
P5-2	CL	THH	F	B		X			X	X	X		X				F			
P5-3	CL	THH	E	CL		X			X	X	X		X	X			F			
P5-7	CL	?	ID	F		X	X	X		X									X	Fract. ass. with ruts
P5-8	CL	THH	E	W					X	X	X		X				F			
P5-9	P/B	THH	F	W					X	X	X	X		X			F		X	Parallell, linear narrow r
P6-1	P/B	THH	E/F	CL		X			X	X							C/F		X	
P6-2	LG	THH	F	CL				X	X		X						F		X	

Appendix 3.1 continued

SAMPLE	COLOUR	MORPH.	CR. REG.	CR. ST.	BREAK				RES. SURF.							OCTA. SURF.	DEF. LAM.	RUTS	COMMENTS
Main Fissure					LE	SCL	RES	ST	H	MH	T	CLS	ZZ	MP	MD				
P6-8	CL	THH	E/F	W							X		X						
P6-9	P/B	THH	E/F	W					X	X	X		X					X	
P7-3	CL	THH	VF	F		X				X									
P7-4	LG	THH	R	W							X		X						
P7-5	CL	THH	F	W							X		X						
P7-6	CL	THH	VF	B	X		X		X	X								X	
P7-8	CL	THH	E	B	X	X		X	X	X	X		X						
P7-9	CL	THH	ID	F		X				X	X		X				F		
P7-13	CL	THH	ID	F	X		X		X										Fract. ass. with incl. pit
P7-16	CL	THH	R	B	X		X				X		X					X	
P8-1	LG	THH	F	W							X							X	Ruts ass. with incl. pits
P8-2	CL	THH	F	W						X	X						C/F	X	
P8-3	CL	?	?	F		X		X	X										
P8-4	CL	THH	R	W					X				X					X	
P9-1	LY	THH	E	W					X		X								
P9-2	CL	THH	ID	B	X		X		X		X							X	Fracture ass. with ruts
P9-3	CL	THH	ID	W					X	X	X		X					X	
P9-4	CL	THH	ID	W					X		X							X	
P9-5	P/B	THH	F	W					X	X	X						C/F	X	
P9-6	CL	THH?	ID	B	X			X	X	X	X		X				F		
P9-7	CL	THH	E	B	X				X		X		X				C/F	X	Fracture ass. with ruts
P9-8	CL	THH	F	B	X						X			X				X	Fracture ass. with ruts
P9-9	CL	THH	R	W					X		X								
P9-10	CL	THH	R	B	X		X		X		X							X	Fracture ass. with ruts
P9-11	CL	THH	F	W					X				X					X	
P9-14	CL	THH	ID	W						X		X		X					
P10-1	CL	?	?	F	X	X				X								X	Fract. ass. with ruts anc
MDA-1	CL	THH	?	F	X	X			X										
MDA-3	OW	THH	ID	W					X		X		X					X	
MDA-8	CL	THH	F	B		X	X	X	X	X	X		X		X				
MDA-10	CL	THH?	?	?					X	X							F		Half the stone heavily e
MDA-12	CL	THH	E/F	W					X		X						F		
950W-1	CL	THH	VE/F	W							X		X				C	X	
950W-2	LY	THH?	VE/F	CL			X	X	X		X		X					X	
950W-3	B/Y	THH?	VF	W	X				X	X							F	X	
RUS-1	CL	THH	E/F	W					X		X		X						

Appendix 3.1 continued

SAMPLE	COLOUR	MORPH.	CR. REG.	CR. ST.	BREAK				RES. SURF.							OCTA. SURF.	DEF. LAM.	RUTS	COMMENTS
Sugarbird Blow					LE	SCL	RES	ST	H	MH	T	CLS	ZZ	MP	MD				
TB-5	CL	THH	E/F	W					X		X								
TB-10	P/B	THH	F	CL		X			X	X		X					C/F		
TB-14	Y/B	THH	ID	B			X			X							F	X	Heavily etched in ass. w
NFB-1	LG	THH	R	W					X		X		X						
BLO-3	P/B	THH/O(65%)	R	?					X	X							F		Half the stone heavily e
BLO-6	CL	THH	F	?								X	X					X	
SB-1	LY	THH/O(95%)	R	W												hexa/-tri		X	
SB-2	CL	TTH	ID	W					X		X	X	X						
SB-3	CL	THH	E	W						X	X	X		X					
SB-4	LY	THH	VF	W					X				X						
SB-5	CL	THH	F	W							X	X	X						
SB-6	CL	THH/O*	R	W						X		X				TP			* Pseudohemimorphic
SB-6(2)	CL	THH	F	CL	X						X	X							
SB-7	OW	THH	E	W							X	X							
SB-8	CL	THH	E	W					X		X	X	X						
SB-9	CL	THH	ID	W							X	X							
SB-10	OW	THH	VF	W					X		X		X	X				X	
SB-11	CL	THH	R	CL	X						X	X	X					X	Fracture ass. with ruts
SB-12	CL	THH	E/F	W							X	X						X	
SB-13	CL	THH	R	B			X				X	X							
SB-14	CL	THH	F	W					X	X			X		X			X	
SB-15	CL	THH	ID	W					X			X						X	
SB-16	CL	?	ID	B	X				X			X						X	
SB-17	CL	THH	R	W							X	X	X						
SB-18	CL	THH	R	W							X	X	X					X	
SB-18(2)	CL	THH	R	W							X	X							
SB-19	CL	THH	R	W						X	X	X							
SB-20	CL	THH	R	W							X	X	X						
SB-21	CL	THH	E	B	X					X	X							X	
SB-22	OW	THH	ID	W								X						X	
SB-23	CL	THH/O(65%)	R	CL	X						X	X				-tri		X	
SB-24	CL	THH	E	W						X								X	
SB-25	CL	?	E	B	X							X						X	
SB-26	CL	THH	R	W						X	X	X							
SB-27	CL	THH	F	W								X							
SB-28	CL	THH	ID	W						X	X				X		C	X	
SB-29	CL	THH	E	B	X		X					X	X						

Appendix 3.1 continued

SAMPLE	COLOUR	MORPH.	CR. REG.	CR. ST.	BREAK		RES. SURF.									OCTA. SURF.	DEF. LAM.	RUTS	COMMENTS
Sugarbird Blow					LE	SCL	RES	ST	H	MH	T	CLS	ZZ	MP	MD				
SB-30	CL	THH	F	W							X	X			X				
Marsfontein																			
MARS-3	LP	?	?	F	X	X						X				TP			
MARS-4	P/B	?	VF	F	X					X						TP		X	
MARS-5	P/B	?	?	F	X	X										TP		X	
MARS-8	OW	?	?	B	X	X	X		X	X							F	X	
MARS-9	OW	THH/O(95%)	?	F	X					X						TP		X	
MARS-10	CL	?	?	F	X	X			X									X	
MARS-11	CL	M	F	W												TP			Herringbone structure
MARS-12	CL	THH	VF	CL			X				X						F		
MARS-13	OW	M	F	B	X	X	X			X									
MARS-16	OW	?	?	F	X		X		X		X								
MARS-18	LY	THH	VF	W												TP			
MARS-22	LP	THH	VF	B	X		X								X		C/F	X	*Scotch-plaid texture
MARS-23	P/B	THH	VF	W						X							C	X	
MARS-24	CL	THH	?	F	X		X												
MARS-25	CL	THH	?	F		X			X										
MARS-26	CL	?	VF	CL			X		X										Fracture ass. with ruts
MARS-27	OW	?	?	F	X	X	X			X					X		C		
MARS-30	CL	?	VF	B			X												Fracture ass. with ruts
MARS-32	OW	?	?	F	X											TP			
MARS-33	CL	?	?	F	X	X			X										
MARS-34	CL	?	?	F	X	X										TP			
MARS-1	LG	THH	ID	W					X		X						F		
MARS-2	CL	THH	?	W					X		X						F		
MARS-3	CL	THH/Aggr*	R	W					X		X							X	*Aggregate of four diam
MARS-4	P/B	M	F	CL					X										
MARA-1	P/B	THH/O(65%)	ID	B		X				X						-ve tri.			Fract. ass. with incl. pit

APPENDIX 4

FOURIER TRANSFORM INFRA-RED AND CATHODOLUMINESCENCE ANALYSIS OF ROUGH DIAMONDS AND DIAMOND PLATES

FTIR ANALYSIS

Rough diamonds were mounted on sticky tape along the side of a glass slide, which provides a convenient and quick way to analyse a large number of samples. Spectra were measured with a Nicolette Magna-IR 760 spectrometer at Anglo American Research Laboratories (currently DeBeers Geoscience) in Johannesburg and at the Department of Geology, University of Cape Town using a Nicolette Magna-IR 560 spectrometer. Both spectrometers were attached to a KBr beam splitter and a MCT/A detector that was cooled with liquid nitrogen. During analyses at the University of Cape Town, nitrogen gas was purged over the sample to prevent a CO_2 build-up in the space around the sample. The resolution was set at 8 cm^{-1} and spectra were recorded over the range 4000-650 cm^{-1}. Background spectra were recorded with a few minute intervals and subtracted from the diamond spectra to correct for non-sample contributions. The spectra were background corrected on-line using the Nicolette OMNIC 5.0 and Bruker OPUS/3D softwares.

The estimation of nitrogen aggregation, especially at low nitrogen concentrations, is heavily dependent on the quality of the "raw" spectra and especially on a correct base-lining, which is particularly difficult for "low-quality" spectra. Therefore each spectrum has been inspected individually and only high quality "raw" spectra without significant fringing has been used.

Reference "thumb-nail" spectra for a semi-quantitative assessment of the level of nitrogen aggregation based on synthetic mixtures of different proportions of A and B aggregates and variable platelet peak intensity (Mendelssohn and Milledge, 1995) are shown in Appendix 4.1. These "thumb-nail" spectra are based on the examination of many thousands of spectra which has revealed that natural diamonds display a wide variability in platelet peak height (B') relative to the height of the 1282 cm^{-1} A-defect peak. Spectral types K, L, M and N have been arbitrarily assigned and represent ratios of the B' peak height and the 1282 cm^{-1} peak height of about 0, 1, 2 and 2.4 respectively. Thus, spectral types ranging from K to N display continuously lower degree of platelet peak degradation

and Type K and Type N would represent fully "irregular" and "regular" diamonds respectively (see Section 6.1).

The amount of aggregation was qualitatively estimated for each diamond through comparison with the "thumb-nail" spectra. This estimation was then used to assess which quantitative estimations based on different absorption peak ratios (see Section 6.2) were reasonable and should be used in the aggregation estimation.

CATHODOLUMINESCENCE ANALYSIS

Polished diamond plates were cleaned by ultrasonic agitation in dichloromethane followed by ethanol and mounted on aluminium plates with water-soluble carbon dag. Cl analysis was performed at the Electron Microscope Unit, University of Cape Town. CL images of the "front side" of the diamond plates were obtained with a Cambridge S200 scanning electron microscope running at 15 kV and an electron beam current of 1.1 nA. Images of the "rear sides" of the plates are photographs taken through an optical microscope attached to a Technosyn luminescence generator with an accelerating voltage of 12-15 kV and an electron beam current set at 0.8 mA.

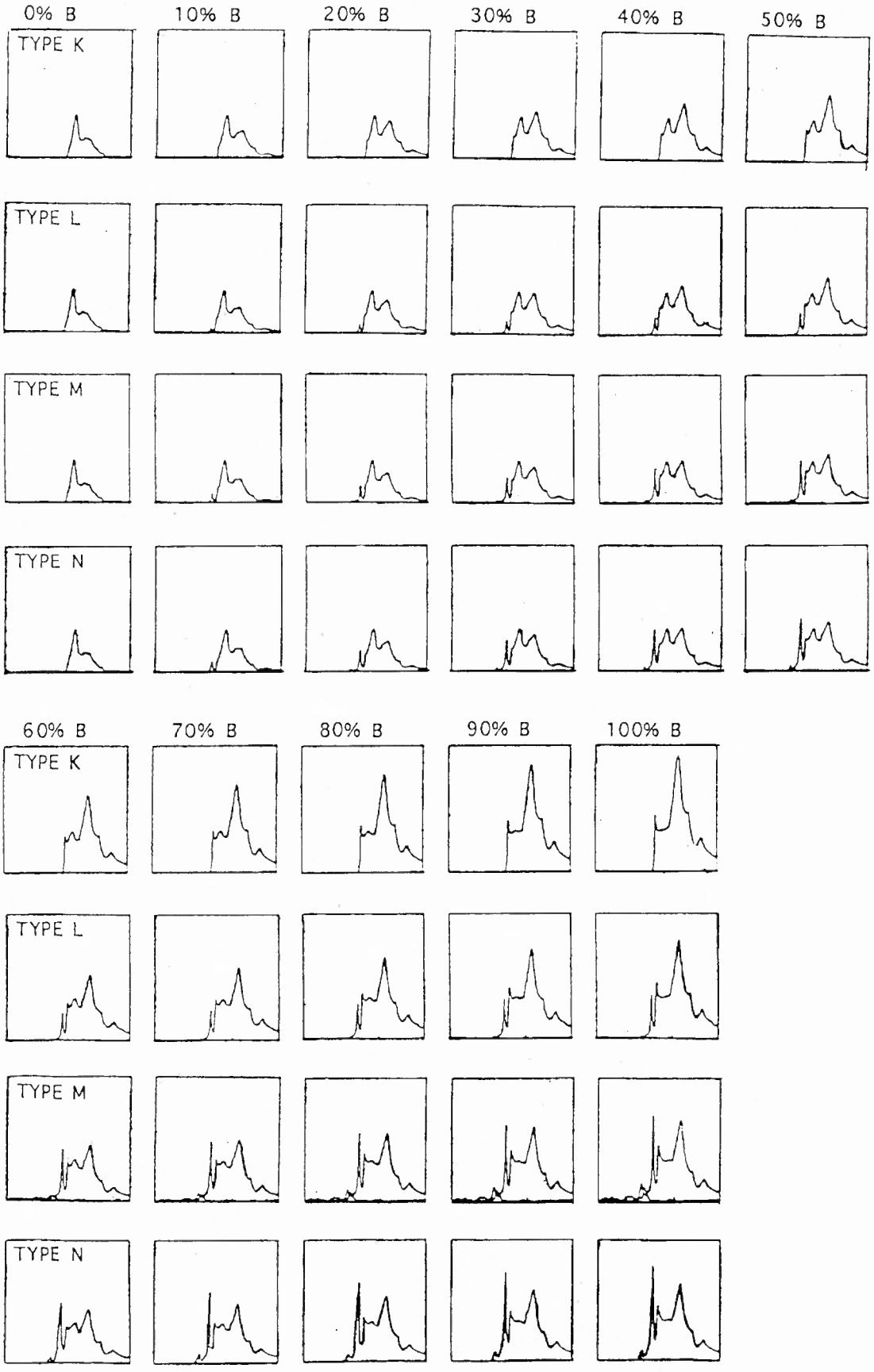

Appendix 4.1 Reference "thumb-nail" spectra for aggregation sequences K to N displaying different rates of platelet peak development. Vertical axis represents arbitrary absorption units and horisontal axis ranges from 1750 cm^{-1} to 900 cm^{-1} (from Chinn, 1995).

Appendix 4.2 IR properties for diamond plates

Analysis	T(cm^{-1})	mu(1365)	H(3107)	H(3237)	mu(1430)	mu(1282)	Nppm	Appm	Bppm	%NasB	T(°C)calc*
17-28A	1371.8	1.087	0.191	0.006	0.002	7.011	1370	1005.1	364.9	26.6	1088
17-28B	1371.5	1.16	0.102	0.003	0.007	6.638	1412	968.2	443.8	31.4	1093
17-28C	1371.7	1.153	0.175	0.008	0.004	6.793	1437	993	444	30.9	1092
17-28D	1371.8	1.22	0.14	0.005	0.005	6.92	1481	1007.6	473.4	32	1092
17-28E	1372.3	1.269	0.159	0.005	0.005	7.311	1505	1023.9	481.1	32	1092
17-30A	1377.9	0.095	1.963	0.06	0.029	3.787	816	548.4	267.6	32.7	1107
17-30B	1372.4	0.45	1.069	0.032	-0.007	5.207	1154	746.4	407.6	35.3	1102
17-30C	1370.8	0.718	0.484	0.014	0.016	4.687	1063	662.1	400.9	37.7	1106
17-30D	1371.6	0.335	1.145	0.025	0.041	4.546	985	657.4	327.6	33.3	1103
17-30E	1371.4	0.239	1.415	0.027	0.049	4.443	953	645.8	307.2	32.2	1103
17-30F	1377.7	0.145	1.589	0.033	0.047	4.374	924	638.5	285.5	30.9	1102
17-30G	1382.3	0.136	2.151	0.054	0.065	4.815	1012	702.4	309.6	30.6	1100
17-30H	1370.8	0.256	1.271	0.035	0.032	3.693	805	532.8	272.2	33.8	1109
17-30I	1370.8	0.237	1.463	0.038	0.05	3.906	856	562.2	293.8	34.3	1108
17-30J	1371.2	0.306	1.271	0.033	0.054	4.397	958	634.1	323.9	33.8	1104
17-30K	1371.5	0.339	1.016	0.019	0.042	4.51	977	649.6	327.4	33.5	1104
17-30L	1379.3	0.163	1.975	0.05	-0.07	4.734	1024	686.2	337.8	33	1102
17-30M	1376.2	0.184	1.464	0.046	0.052	3.636	799	523.2	275.8	34.6	1109
17-30N	1371.5	0.213	0.491	0.014	0.004	2.522	552	364	188	34	1118
A-3B	1365.8	0.512	0.007	0	-0.012	3.148	575	483.9	91.1	15.8	1093
A-3C	1366	0.474	0.012	0	-0.012	3.095	562	477.1	84.9	15.1	1092
A-3D	1366.4	0.385	0.059	0	-0.005	3.095	562	477.4	84.6	15.1	1092
A-3E	1366.6	0.375	0.078	0.002	-0.006	3.047	556	468.2	87.8	15.8	1094
A-3F	1367.5	0.285	0.153	0.005	0.003	2.82	514	434.5	79.5	15.4	1095
A-3G	1368.4	0.275	0.168	0.002	-0	2.825	520	433.9	86.1	16.5	1097
A-3J	1371.7	0.24	0.344	0.007	0.003	3.381	618	520.1	97.9	15.8	1091
A-3K	1371.6	0.291	0.369	0.007	0.005	3.739	682	574.4	107.6	15.8	1089
A-3L	1371.6	0.304	0.362	0.007	0.005	3.707	675	570.9	104.1	15.4	1089
A-3M	1371.2	0.324	0.37	0.007	0.004	3.822	703	587.1	115.9	16.5	1090
A-3N	1370.6	0.297	0.337	0.007	0.002	3.684	670	566.9	103.1	15.4	1089
A-3O	1369.6	0.231	0.34	0.009	0.002	3.298	587	511.5	75.5	12.8	1087

Appendix 4.2 continued

Analysis	T(cm^{-1})	mu(1365)	H(3107)	H(3237)	mu(1430)	mu(1282)	Nppm	Appm	Bppm	%NasB	T(°C)calc*
A-3R	1368.2	0.155	0.149	0.002	0.003	1.971	351	305	46	13.2	1099
A-3S	1366.6	0.295	0.113	0.002	0.003	2.513	465	385.2	79.8	17.3	1100
P6-8A	1369	0.505	0.059	0	0.003	3.571	692	537.9	154.1	22.3	1099
P6-8B	1370.3	0.339	0.147	0.002	0.004	3.389	638	514.8	123.2	19.3	1096
P6-8C	1371	0.656	0.145	0.004	0.007	4.213	871	621.5	249.5	28.7	1101
P6-8D	1367.9	0.73	0.042	0	0.005	3.912	764	589	175	23	1097
P6-8F	1370	0.417	0.597	0.011	0.017	4.529	868	685.6	182.4	21	1092
P6-8J	1367.6	0.776	0.039	0.002	0.002	3.993	788	594.7	193.3	24.5	1098
P6-8K	1368.9	0.651	0.1	0	0.006	3.981	773	600.2	172.8	22.3	1096
P6-8L	1369.2	0.459	0.393	0.006	0.006	4.165	795	630.7	164.3	20.7	1093
P6-8M	1370.5	0.507	0.409	0.009	0.008	4.598	875	691.1	183.9	21	1091
P6-8N	1369.9	0.448	0.368	0.007	0.001	4.187	775	636.2	138.8	17.9	1090
P6-8O	1367.3	0.632	0.054	0	0.006	3.667	692	556.3	135.7	19.7	1095
P6-9A	1373.1	0.365	0.48	0.014	0.001	3.621	683	551.2	131.8	19.3	1095
P6-9B	1369.7	0.177	0.092	0	0.002	2.071	373	319.8	53.2	14.3	1100
P6-9C	1372.3	0.187	0.245	0.004	0.001	2.455	482	368.2	113.8	23.6	1109
P6-9D	1375	0.31	0.87	0.023	0.002	4.326	814	659.2	154.8	19	1090
P6-9E	1369.9	0.679	0.331	0.007	0.002	4.617	900	693.8	206.2	23	1093
P6-9F	1369.6	0.382	0.411	0.009	0.003	4.163	777	629.7	147.3	19	1091
P6-9G	1372.8	0.359	0.552	0.016	0.002	3.617	696	547.2	148.8	21.3	1097
P6-9J	1374.6	0.337	0.526	0.012	-0.002	4.019	744	616	128	17.2	1089

*Temperature calculated for a mantle residence time of 2.5 Ga

Appendix 4.3 IR absorption characteristics for rough diamonds from Main Fissure, Sugarbird Blow and Marsfontein.

Sample/analysis	T(cm^{-1})	mu(1365)	H(3107)	H(3237)	mu(1430)	mu(1282)	Nppm	Appm	Bppm	%NasB	T(°C)calc*
Main Fissure											
P3-1a	1369.4	0.576	0.093	0	-0.013	4.019	778	604.7	173.3	22.3	1096
P3-1b	1367	1.039	0.008	0	-0.018	3.224	775	445.1	329.9	42.6	1118
P3-1c	1368.7	0.718	0.103	0.003	-0.002	3.536	771	510.6	260.4	33.8	1109
P3-3	1370.4	0.341	0.188	0.003	0.011	4.423	909	653.9	255.1	28.1	1099
P3-8b	1378.6	0.395	0.658	0.024	-0.09	6.091	1098	936.7	161.3	14.7	1076
P4-1a	1372.9	0.264	0.173	0.008	0.04	4.113	741	634.5	106.5	14.3	1085
P4-1b	1371.6	0.42	0.115	0	-0.007	4.177	738	646.6	91.4	12.4	1081
P4-4	1369.9	0.49	0.253	0.006	0.001	4.039	887	580.5	306.5	34.5	1107
P4-9c	1367.1	0.564	0	0	-0.042	3.946	699	612.3	86.7	12.4	1082
P5-1a	1369	1.042	0.076	0.004	-0.024	4.715	1076	665.4	410.6	38.2	1106
P5-2a	1362.5	0.188	0.011	0	0.005	0.316	92	39.6	52.4	56.4	1186
P5-2b	1361.9	0.885	0.018	0	0.003	0.84	365	73	292	79.9	1179
P5-3a	1369.2	0.974	0	0	0.002	4.812	974	703.3	270.7	27.8	1097
P5-3b	1368.7	0.991	0	0	0.004	4.661	951	686.3	264.7	27.8	1098
P5-3c	1365.9	0.221	0	0	0.001	1.503	266	232.7	33.3	12.4	1105
P5-8c	1368.4	0.456	0.062	0.009	0.011	3.468	609	538.5	70.5	11.7	1084
P5-9a	1361.5	0.145	0.068	0.005	0	0.25	74	31	43	57.8	1193
P5-9b	1364.1	1.032	0.094	0.004	0.017	1.026	427	93.4	333.6	78	1172
P5-9c	1361.5	0.061	0.039	0	0.005	0.151	35	21.2	13.8	40.3	1193
P5-9d	1361.9	0.373	0.07	0	-0.002	0.529	179	59.6	119.4	66.5	1179
P5-9e	1361.6	0.124	0.059	0	-0.011	0.218	62	27.5	34.5	56.4	1195
P5-9f	1363.8	3.442	0.01	0	0.063	1.891	935	134	801	85.6	1165
P6-1	1365.4	3.439	0.079	0.01	0.219	1.917	1131	86.8	1044.2	92.4	1178
P6-2a	1370.6	2.387	0.026	0	0.113	6.565	1701	874.3	826.7	48.6	1105
P6-2b	1369.7	2.279	0.04	0	0.074	6.169	1590	823.3	766.7	48.2	1107
P6-2c	1373.1	2.66	0.045	0	0.181	7.912	2163	1026.7	1136.3	52.5	1103
P7-3a	1362.9	2.015	0.049	0.002	0.033	0.837	479	41.2	437.8	91.4	1197
P7-4b	1368.3	0.64	0.057	0	-0.002	4.639	852	711.2	140.8	16.5	1085
P7-6a	1375.7	0.502	0.684	0.019	0.002	5.528	1025	841.1	183.9	17.9	1083
P7-6b	1372.2	1.02	0.469	0.016	0	7.295	1575	1030.6	544.4	34.5	1094

Appendix 4.3 continued

Sample/analysis	T(cm^{-1})	mu(1365)	H(3107)	H(3237)	mu(1430)	mu(1282)	Nppm	Appm	Bppm	%NasB	T(°C)calc*
P7-6c	1370.4	1.667	0.404	0.018	0.004	5.644	1497	742.9	754.1	50.3	1110
P7-8a	1364.7	0.687	0	0	-0.031	3.179	573	491.3	81.7	14.3	1090
P7-13a	1372.2	0.143	0.253	0.007	-0.012	3.651	754	537.6	216.4	28.6	1104
P7-13b	1366.7	0.261	0.035	0	0.007	2.584	523	383.3	139.7	26.6	1111
P7-13c	1382.1	0.038	0.523	0.015	0.016	4.398	926	642.4	283.6	30.6	1102
P7-16b	1377.2	0.214	1.406	0.037	-0.003	4.202	772	644	128	16.5	1088
P8-1b	1371.2	1.342	0.048	0	0.005	7.682	1655	1113.1	541.9	32.8	1091
P8-1f	1366.7	0.505	0.014	0	-0.002	3.837	743	579.5	163.5	22	1097
P8-1g	1371.5	1.58	0.008	0	0.018	8.676	1921	1243	678	35.3	1090
P8-1j	1371.2	1.556	0.017	0	0.006	8.232	1820	1181.9	638.1	35	1091
P8-1k	1371	1.329	0.031	0.006	0.003	7.598	1664	1093.6	570.4	34.3	1092
P8-2a	1362.5	1.904	0.066	0.004	0.02	1.364	703	89	614	87.3	1176
P8-2b	1364.5	2.848	0.025	0	0.098	1.796	957	108.1	848.9	88.7	1171
P8-2c	1361.7	2.133	0.008	0	0.009	1.439	722	99.2	622.8	86.2	1173
P8-3d	1367.8	0.226	0.08	0	0.002	2.83	549	426.2	122.8	22.3	1104
P9-1a	1371.5	1.532	0.03	0.004	0.096	6.437	1617	873.4	743.6	46	1104
P9-2b	1365.1	3.243	0.033	0	0.126	1.955	1034	118.2	915.8	88.6	1169
P9-2c	1363.7	1.961	0.066	0	0.021	1.41	695	100.4	594.6	85.6	1172
P9-2d	1367.4	0.504	0.02	0	-0.001	3.802	699	581.4	117.6	16.9	1090
P9-3	1373.6	0.265	0.471	0.019	0.014	4.502	860	682.6	177.4	20.7	1091
P9-4a	1365.4	2.296	0.046	0.004	0.028	3.199	1080	359	721	66.7	1134
P9-4b	1365.4	2.232	0.036	0.006	0.026	3.135	1079	346.4	732.6	67.9	1136
P9-4c	1365.4	2.609	0.057	0.006	0.035	3.254	1114	360.1	753.9	67.7	1135
P9-5b	1362.1	0.857	0.176	0.008	0.017	1.269	427	141.9	285.1	66.7	1157
P9-5c	1369.2	0.533	0.023	0	0.003	4.276	817	645.6	171.4	21	1093
P9-7a	1366.1	0.546	0.011	0	0.003	3.266	659	483.8	175.2	26.7	1105
P9-7b	1372	0.51	0.24	0.009	0.013	4.898	966	732.4	233.6	24.2	1093
P9-7c	1375.2	0.4	0.447	0.014	-0.059	5.607	1070	848.5	221.5	20.7	1086
P9-8a	1367.7	0.426	0.123	0.003	0.008	3.716	813	534.3	278.7	34.3	1109
P9-8b	1369.2	0.656	0.065	0	0.005	4.179	980	583.9	396.1	40.4	1111
P9-9	1369.7	0.474	0.068	0	0.009	3.601	818	509.9	308.1	37.7	1112

Appendix 4.3 continued

Sample/analysis	T(cm^{-1})	mu(1365)	H(3107)	H(3237)	mu(1430)	mu(1282)	Nppm	Appm	Bppm	%NasB	T(°C)calc*
P9-10a	1368.3	0.757	0	0	0.005	4.052	807	604	203	25.1	1099
P9-10c	1366.1	0.595	0.032	0	0.009	3.28	734	466.3	267.7	36.5	1113
P9-11a	1371.2	0.193	0.172	0.007	-0.005	4.113	725	637.5	87.5	12	1081
P9-11b	1369.6	0.279	0.03	0	-0.006	3.016	584	453.8	130.2	22.3	1103
P9-11c	1389	0.007	0.726	0.015	-0.036	4.496	819	689.7	129.3	15.8	1085
P9-11d	1372	0.515	0.152	0.008	0.007	4.135	812	620.2	191.8	23.6	1097
P9-14	1361.5	1.261	0.016	0	0.002	1.512	553	158.3	394.7	71.3	1156
P10-2	1373.2	0.302	0.254	0	-0.025	4.193	751	646.4	104.6	14	1084
17-1	1365.5	2.628	0.142	0.01	0.142	3.029	1117	316	801	71.7	1139
17-2a	1363.4	1.298	0.195	0.006	0.049	0.884	426	65.5	360.5	84.7	1183
17-2b	1361.5	0.997	0.095	0.002	0.005	0.918	444	67.1	376.9	85	1183
17-2c	1360.3	0.081	0.027	0	0.009	0.461	101	66.4	34.6	34.7	1160
17-3	1364.2	3.245	0.033	0.011	0.043	1.83	884	135.3	748.7	84.6	1165
17-3b	1364	2.184	0.015	0	0.035	1.682	778	133.5	644.5	82.8	1164
17-4	1366.3	0.754	0.193	0.013	0.002	0.83	340	77	263	77.3	1177
17-4b	1365	0.736	0.149	0.009	0.005	2.505	629	339.9	289.1	46	1127
17-6	1365.4	4.515	0.403	0.029	0.352	2.343	1307	126.3	1180.7	90.3	1168
17-8	1362	1.41	0.128	0.004	0	1.168	452	115.9	336.1	74.3	1165
17-9	1366.9	1.979	0.017	0	-0	4.531	1290	574.2	715.8	55.5	1118
17-11	1361.5	0.837	0.046	0	0.004	0.839	332	81.6	250.4	75.3	1175
17-12	1375	0.153	3.083	0.043	-0.055	4.298	945	618.5	326.5	34.5	1106
17-13a	1368.8	1.52	0.098	0.007	0.003	4.731	1263	620.5	642.5	50.9	1115
17-13c	1369.2	2.22	0.01	0	0.039	5.651	1637	706.7	930.3	56.8	1114
17-14	1373.8	0.286	2.288	0.097	0.072	4.534	997	652.9	344.1	34.6	1104
17-15	1371.9	0.572	0.396	0.012	0.006	4.917	1040	719.1	320.9	30.9	1099
17-17	1363.3	2.047	0.119	0.007	0.014	1.56	675	136.3	538.7	79.7	1163
17-18	1362.6	1.359	0.151	0.013	0.004	0.964	436	77.1	358.9	82.3	1178
17-19	1369.4	0.809	0.058	0.006	0.003	5.514	1006	689.6	316.4	31.4	1101
17-20a	1370	0.604	1.026	0.023	0.178	4.753	956	707	249	26	1096
17-20b	1370.1	0.475	1.083	0.02	0.046	4.347	917	636.4	280.6	30.6	1102
17-21	1380.8	-0.01	0.108	0	-0.008	0.305	50	48.6	1.4	1.9	1106

Appendix 4.3 continued

Sample/analysis	T(cm^{-1})	mu(1365)	H(3107)	H(3237)	mu(1430)	mu(1282)	Nppm	Appm	Bppm	%NasB	T(°C)calc*
17-24	1364.3	3.423	0.034	0.002	0.101	2.455	1072	211.2	860.8	80.3	1152
17-25	1367.1	0.521	0.119	0.002	0.001	3.469	719	510.9	208.1	29	1106
17-26	1363.9	4.17	0.1	0.009	0.115	2.065	1070	132.7	937.3	87.6	1166
17-33	1367.3	6.684	0.443	0.051	0.583	3.583	1960	203.5	1756.5	89.6	1156
17-34	1364	0.876	0.115	0	-0.008	0.963	364	96.2	267.8	73.7	1170
17-35	1363.4	1.949	0.117	0.01	0.018	0.966	536	52.9	483.1	90.1	1190
17-43	1369.5	0.419	0.273	0.007	0.001	3.509	732	508.2	223.8	30.6	1107
17-45	1365.1	1.642	0.376	0.024	0.131	1.752	716	163.4	552.6	77.2	1157
950W-1a	1365.5	0.359	0.004	0	0.001	1.848	411	264.9	146.1	35.5	1126
950W-1b	1366.1	0.838	0	0	0.004	3.131	746	434.6	311.4	41.7	1118
950W-1c	1366.2	1.162	0	0	0.002	4.27	1029	589	440	42.8	1112
950W-2a	1365.4	0.125	0.006	0	-0.001	0.781	178	110.4	67.6	37.9	1149
950W-2b	1368.7	0.875	0.092	0.008	0.002	3.547	813	500.6	312.4	38.4	1113
950W-2c	1369.2	0.9	0.117	0.005	0.005	3.437	817	477.9	339.1	41.5	1116
A-1b	1367.2	0.574	0.029	0	-0.058	2.946	550	449.4	100.6	18.3	1098
A-10a	1360	0.075	0.008	0	-0	0.255	62	34.3	27.7	45.2	1183
A-10b	1361.2	0.242	0.053	0	-0.011	0.358	119	40.8	78.2	65.8	1189
Sugarbird Blow											
SB-1a	1368.3	6.2	0.026	0.004	0.581	3.377	1983	155.6	1827.4	92.2	1163
SB-1b	1365.4	4.355	0.02	0.005	0.229	2.538	1382	145.8	1236.2	89.5	1164
SB-1c	1365.4	1.733	0.37	0.024	0.067	3.327	1030	398.6	631.4	61.3	1130
SB-1d	1366.8	3.691	0.031	0.004	0.325	2.324	1274	131.3	1142.7	89.7	1167
SB-2a	1373.1	0.501	0.314	0.015	0.055	6.017	1308	869.1	438.9	33.5	1097
SB-2b	1371.5	0.471	0.071	0	-0.016	4.78	1027	693.3	333.7	32.5	1101
SB-2c	1363.7	2.639	0.053	0.006	0.099	1.786	922	116	806	87.4	1169
SB-2d	1364.4	3.189	0.008	0	0.107	1.941	1030	118.6	911.4	88.5	1169
SB-3a	1367	0.516	0.022	0	0.006	3.753	786	549.5	236.5	30.1	1105
SB-3b	1365.6	0.604	0.006	0	0.006	3.351	709	488.2	220.8	31.2	1109
SB-4a	1365.7	0.421	0.108	0	0.002	2.667	539	390.5	148.5	27.5	1111
SB-4b	1369.2	0.447	0.028	0	-0.038	4.288	972	607.7	364.3	37.5	1108
SB-5a	1366	3.74	0.008	0	0.298	2.246	1220	129.7	1090.3	89.4	1167

Appendix 4.3 continued

Sample/analysis	T(cm^{-1})	mu(1365)	H(3107)	H(3237)	mu(1430)	mu(1282)	Nppm	Appm	Bppm	%NasB	T(°C)calc*
SB-5b	1365.8	3.108	0.133	0.011	0.066	1.993	1039	126.9	912.1	87.8	1167
SB-5c	1365.4	1.851	0.037	0.005	0.057	1.367	649	104.1	544.9	83.9	1171
SB-5d	1366.1	4.414	0.011	0	0.376	2.562	1426	139	1287	90.3	1165
SB-6a	1370.2	0.413	0.102	0.007	0	3.25	713	467	246	34.6	1112
SB-6b	1371	1.072	0.068	0	0.002	5.953	1410	827.5	582.5	41.3	1103
SB-6c	1365.5	0.621	0.006	0	0	3.556	761	515.9	245.1	32.2	1108
SB-6d	1369.4	0.326	0.104	0.004	0.001	4.092	786	618.3	167.7	21.3	1094
SB-7a	1365.9	0.494	0.023	0	0.007	3.457	720	505.9	214.1	29.8	1107
SB-7b	1365.4	0.594	0	0	-0.001	3.594	754	525.4	228.6	30.4	1106
SB-8a	1369.2	0.376	0.059	0.002	0.007	3.618	723	539.1	183.9	25.4	1102
SB-8b	1365.3	0.458	0	0	-0.001	2.711	532	406.2	125.8	23.6	1106
SB-8c	1365.5	0.569	0	0	-0.023	3.259	713	468.5	244.5	34.3	1112
SB-8d	1370.7	0.732	0.074	0	0.004	4.756	1033	686.8	346.2	33.5	1102
SB-9a	1366	0.719	0	0	-0.004	3.793	810	551	259	32	1106
SB-9b	1373.1	0.73	0.343	0.014	0.057	5.935	1278	859.3	418.7	32.7	1097
SB-9c	1369.2	0.688	0.051	0	-0.008	4.572	955	670.7	284.3	29.8	1100
SB-9d	1372.2	0.699	0.137	0.004	0.016	6.55	1369	954	415	30.4	1092
SB-9e	1365.9	0.687	0.005	0	-0.006	3.411	729	495.9	233.1	32	1109
SB-10b	1365.4	0.558	0	0	-0.008	3.162	670	461.3	208.7	31.2	1110
SB-10c	1365.4	0.461	0	0	-0	2.781	610	399.5	210.5	34.6	1116
SB-10d	1365.4	0.538	0	0	-0.005	3.024	652	438.1	213.9	32.7	1112
SB-11a	1370.1	0.274	0.243	0.005	-0.001	4.126	720	642.3	77.7	10.9	1078
SB-11b	1378.3	0.121	0.261	0.005	-0.008	3.287	590	507.8	82.2	14	1089
SB-11c	1378.7	0.142	0.445	0.011	-0.024	4.005	706	621.3	84.7	12	1081
SB-11d	1365.4	0.613	0	0	0.003	3.11	574	475.3	98.7	17.2	1095
SB-12a	1367.9	0.393	0.019	0	0.002	3.181	679	462.1	216.9	32	1111
SB-12b	1366.7	0.81	0.009	0	0.003	4.059	864	590.2	273.8	31.7	1105
SB-12c	1368.7	0.327	0.026	0	0	3.375	679	501.8	177.2	26	1104
SB-12d	1371	0.617	0.253	0.01	0.025	5.162	1142	738.7	403.3	35.3	1102
SB-12e	1372.2	0.546	0.405	0.015	0.019	5.203	1123	752.1	370.9	33	1100
SB-13a	1374.4	0.682	0.751	0.035	0.014	7.106	1542	1025.2	516.8	33.5	1093

Appendix 4.3 continued

Sample/analysis	T(cm^{-1})	mu(1365)	H(3107)	H(3237)	mu(1430)	mu(1282)	Nppm	Appm	Bppm	%NasB	T(°C)calc*
SB-13b	1372.7	0.665	0.46	0.022	0.013	5.888	1274	850.1	423.9	33.3	1097
SB-13c	1369.2	0.175	0.033	0	-0.004	1.559	307	234	73	23.9	1120
SB-13d	1365.4	0.704	0	0	0.001	3.51	712	520	192	26.9	1104
SB-14a	1372.8	0.105	0.08	0	0.002	2.707	468	422.5	45.5	9.6	1085
SB-14b	1368	0.138	0.013	0	-0.003	1.778	311	276.9	34.1	10.8	1098
SB-14c	1369.2	0.204	0.063	0	-0.003	3.122	551	484.6	66.4	12	1087
SB-14d	1378.3	0.094	0.204	0.005	-0.006	4.072	724	631	93	12.8	1082
SB-14e	1369.2	0.327	0.037	0	0.003	3.353	584	522.7	61.3	10.5	1082
SB-14f	1372.8	0.141	0.101	0	-0.003	3.255	582	503.4	78.6	13.6	1089
SB-15a	1366.2	0.724	0	0	0.003	3.637	794	523.9	270.1	34.1	1109
SB-15b	1367.3	0.267	0.149	0	-0.001	3.28	626	496.4	129.6	20.7	1099
SB-16a	1368.1	0.267	0.004	0	-0.004	3.119	602	469.7	132.3	22	1101
SB-16b	1369.2	0.278	0.018	0	-0.004	3.598	671	548.4	122.6	18.3	1094
SB-17a	1369.2	0.675	0.054	0.005	0.004	5.503	1159	804	355	30.6	1097
SB-17b	1370.1	0.304	0.129	0.006	0.003	2.868	621	414.4	206.6	33.3	1114
SB-17c	1371.2	0.317	0.727	0.014	0.026	5.051	1154	713.4	440.6	38.2	1105
SB-18a	1368.5	0.452	0.079	0	-0.001	3.543	716	525	191	26.6	1103
SB-18b	1369.2	0.541	0.04	0	0.007	3.789	773	560.3	212.7	27.5	1103
SB-18c	1365.4	0.491	0.008	0	-0.003	3.101	692	442.6	249.4	36	1114
SB-18d	1365.3	0.391	0	0	-0.004	2.595	501	390.7	110.3	22	1106
SB-18e	1368.9	0.297	0.02	0	0.002	2.716	541	405.1	135.9	25.1	1108
SB-18f	1368.1	0.375	0.018	0	-0.007	3.024	595	452.6	142.4	23.9	1104
SB-19a	1372.1	0.288	0.234	0.007	-0.019	3.94	874	563.4	310.6	35.5	1108
SB-19b	1374	0.429	0.424	0.014	0.015	5.459	1224	777.1	446.9	36.5	1101
SB-20a	1367.5	0.553	0.023	0	0.003	3.539	763	512.9	250.1	32.7	1109
SB-20b	1371.7	0.425	0.226	0.007	-0.005	4.676	953	690.9	262.1	27.5	1098
SB-22a	1369.7	0.265	0.029	0	0.007	4.37	859	654	205	23.9	1096
SB-22b	1362	0.623	0.104	0.005	0.011	0.802	281	86.6	194.4	69.2	1171
SB-23a	1365.7	0.56	0.009	0	0.005	2.93	636	423.1	212.9	33.6	1114
SB-23b	1368.9	0.911	0.027	0	-0	4.634	1048	657.9	390.1	37.2	1106
SB-24a	1370.6	0.675	0.144	0.007	0.002	4.775	1049	686.7	362.3	34.6	1103

Appendix 4.3 continued

Sample/analysis	T(cm^{-1})	mu(1365)	H(3107)	H(3237)	mu(1430)	mu(1282)	Nppm	Appm	Bppm	%NasB	T(°C)calc*
SB-24b	1367.8	1.754	0.01	0	0.006	5.052	1451	634.9	816.1	56.3	1116
SB-25a	1363.9	2.191	0.056	0.006	0.064	1.419	742	89.7	652.3	87.9	1176
SB-25b	1364.3	1.786	0.011	0	0.058	1.136	581	74.1	506.9	87.2	1181
SB-26a	1365.7	0.428	0.013	0	0.001	2.987	629	436.4	192.6	30.6	1111
SB-26b	1367.9	0.558	0.041	0	0.005	3.755	809	543.9	265.1	32.7	1107
SB-26c	1368.5	0.696	0.058	0	0.003	4.154	912	597	315	34.6	1106
SB-27a	1363.9	2.564	0.043	0.003	0.067	1.976	967	142.6	824.4	85.3	1163
SB-27b	1363.8	2.548	0.081	0.005	0.03	1.93	910	147.5	762.5	83.8	1162
SB-27c	1365.4	5.034	0.02	0	0.239	2.804	1515	164.2	1350.8	89.2	1161
SB-28a	1364	2.365	0.019	0	0.092	1.49	781	93.7	687.3	88	1175
SB-28b	1364.1	2.306	0.026	0	0.073	1.394	756	81	675	89.3	1179
SB-28c	1367.1	0.687	0.022	0	-0.011	3.858	840	556.4	283.6	33.8	1107
SB-28d	1363.4	2.005	0.027	0	0.086	1.386	727	86.9	640.1	88.1	1177
SB-29a	1369.2	0.539	0.018	0	0.002	4.21	852	624.7	227.3	26.6	1099
SB-29b	1365.4	0.574	0	0	0.004	3.011	709	419.5	289.5	40.9	1119
SB-29c	1369.6	0.417	0.078	0	-0.002	3.985	826	584.8	241.2	29.2	1103
SB-29d	1371.6	0.406	0.109	0	-0.002	4.13	852	607.9	244.1	28.7	1102
SB-30	1370.2	0.156	0.052	0	0	2.112	397	322	75	19	1107
SB-32a	1368.2	0.697	0	0	-0.006	4.808	998	706.4	291.6	29.2	1099
SB-32b	1368.1	0.739	0	0	0.001	4.847	1044	702.4	341.6	32.8	1101
BLO-1a	1371.2	0.617	0.023	0	0.008	6.11	1153	926.2	226.8	19.7	1083
BLO-1b	1370.4	0.438	0.013	0.013	0.003	4.892	921	745.9	175.1	19	1087
BLO-3	1371.4	0.876	0.026	0.026	0.006	4.306	922	746.9	123.5	20	1088
BLO-4a	1369.2	0.692	0	0	0.002	4.531	860	685	175	20.3	1091
BLO-4b	1369.4	0.804	0.011	0	0.006	5.127	988	771.1	216.9	22	1090
BLO-4c	1366.4	0.686	0	0	-0.004	3.778	739	566.9	172.1	23.3	1098
BLO-4d	1367.2	0.714	0	0	0.003	3.957	774	593.6	180.4	23.3	1097
BLO-6	1372	0.739	0.215	0.014	0.01	5.428	1084	808.2	275.8	25.4	1092
TB-10	1363.1	2.524	0.087	0	0.009	1.363	659	100.5	558.5	84.7	1172
TB-3	1364.9	0.142	0	0	0.003	1.829	328	283.3	44.7	13.6	1102
TB-4	1364.8	0.479	0.006	0	-0.009	1.999	416	294.3	121.7	29.2	1119

Appendix 4.3 continued

Sample/analysis	T(cm^{-1})	mu(1365)	H(3107)	H(3237)	mu(1430)	mu(1282)	Nppm	Appm	Bppm	%NasB	T(°C)calc*
TB-5	1365.4	0.91	0.011	0	0.003	3.347	728	484.1	243.9	33.5	1111
TB-6	1373.5	1.941	0.353	0	0.113	7.981	1883	1113.5	769.5	40.9	1096
NFB	1371.1	0.211	0.548	0	0.008	4.058	912	579.2	332.8	36.5	1108
TB-14a	1362.7	1.653	0.038	0.004	0.002	1.726	677	169.3	507.7	75	1156
TB-14b	1363.7	1.963	0.013	0	0.032	1.834	756	168.7	587.3	77.7	1157
Marsfontein											
MARS-3	1367.6	0.266	0	0	-0.006	2.634	539	389.4	149.6	27.8	1111
MARS-4a	1367.1	0.298	0.026	0	0.004	1.92	415	278.3	136.7	33.1	1123
MARS-4b	1367.1	0.421	0.071	0	0.003	3.163	662	463.2	198.8	30.1	1109
MARS-5a	1365.4	1.14	0	0	0.008	3.514	832	490.3	341.7	41.1	1115
MARS-5b	1365.4	1.119	0	0	0.007	3.5	860	479.9	380.1	44.2	1117
MARS-8a	1372.6	0.231	0.07	0	0.009	5.344	1033	806.3	226.7	22	1089
MARS-8b	1372.5	0.169	0.028	0	0.003	5.7	1088	862.9	225.1	20.7	1086
MARS-8c	1372.1	0.213	0.035	0	0.005	5.443	1051	820	231	22	1089
MARS-8d	1374.4	0.167	0.023	0	0.004	6.316	1133	970.6	162.4	14.3	1075
MARS-9a	1375.2	0.162	0.134	0.005	0	5.66	952	892.1	59.9	6.3	1059
MARS-9b	1375	0.196	0.082	0	-0.003	5.938	973	941	32	3.2	1044
MARS-9c	1375.3	0.181	0.136	0.005	-0.001	5.875	965	929.6	35.4	3.7	1046
MARS-10a	1367.4	0.653	0.015	0.003	-0.004	4.231	772	647.3	124.7	16.2	1087
MARS-10b	1366.7	0.474	0.015	0	-0.002	3.637	691	550.4	140.6	20.3	1096
MARS-11a	1363.7	0.008	0.032	0	0.003	5.294	974	812.7	161.3	16.5	1082
MARS-11b	1363.8	0.01	0.037	0	0	5.044	891	783.7	107.3	12	1076
MARS-11c	1363.9	0.012	0.069	0.006	0.003	4.617	765	730.1	34.9	4.6	1056
MARS-11d	1364	-0.006	0.059	0.003	-0.006	4.999	901	771.9	129.1	14.3	1080
MARS-11e	1363.6	0.01	0.03	0	0.003	5.32	950	824.8	125.2	13.2	1077
MARS-11f	1375.4	0.007	0.029	0	-0.008	4.744	802	747.7	54.3	6.7	1064
MARS-11g	1375.4	-0.012	0.035	0	-0.009	5.186	832	828.1	3.9	0.5	1006
MARS-12a	1368.7	0.786	0.028	0.003	-0.003	5.379	1099	797	302	27.5	1094
MARS-12b	1369.8	1.01	0.032	0.004	0.007	6.19	1317	902.8	414.2	31.4	1095
MARS-13a	1365.2	5.501	0.073	0.003	0.437	2.256	1351	93.1	1257.9	93.1	1177
MARS-13b	1364.3	4.677	0.061	0.006	0.356	2.027	1188	92.8	1095.2	92.2	1176

Appendix 4.3 continued

Sample/analysis	T(cm^{-1})	mu(1365)	H(3107)	H(3237)	mu(1430)	mu(1282)	Nppm	Appm	Bppm	%NasB	T(°C)calc*
MARS-13c	1364.6	5.369	0.046	0	0.479	2.395	1468	92.9	1375.1	93.7	1177
MARS-13d	1363.4	3.921	0.062	0.004	0.158	1.657	991	71.6	919.4	92.8	1183
MARS-16	1367.3	0.272	0.006	0.006	-0.034	3.665	678	560.9	117.1	17.2	1092
MARS-18	1365.7	0.399	0.101	0	-0.021	2.57	549	372	177	32.2	1116
MARS-22	1377.6	-0.027	0.941	0.015	-0.02	4.556	744	719.9	24.1	3.2	1049
MARS-22	1380.8	-0.016	0.72	0.016	-0.025	4.439	764	693.8	70.2	9.3	1073
MARS-23a	1363.4	1.203	0.797	0.043	-0.008	3.53	1002	447.3	554.7	55.3	1124
MARS-23b	1379.6	0.039	1.269	0.064	-0.027	6.343	1219	951.4	267.6	22	1085
MARS-24	1366.5	0.783	0.027	0	-0.002	3.905	790	577.1	212.9	26.9	1101
MARS-24	1366.4	0.741	0.027	0.003	-0.001	3.783	780	553.9	226.1	28.9	1104
MARS-25	1376.8	0.019	0.047	0	-0.021	4.904	792	781.3	10.7	1.4	1029
MARS-26	1378.1	0.094	0.453	0.016	-0.007	5.993	1095	921.7	173.3	15.8	1078
MARS-27a	1362.2	3.096	0.012	0.006	0.016	1.332	740	72.7	667.3	90.2	1182
MARS-27b	1368.1	0.48	0.037	0.012	-0.065	4.427	886	660.9	225.1	25.4	1097
MARS-30a	1376.9	0.008	0.34	0.016	0.004	4.022	653	640.3	12.7	1.9	1041
MARS-30b	1365.9	1.378	0.036	0.003	0.007	3.913	996	526.4	469.6	47.1	1117
MARS-30c	1366.1	0.378	0.004	0	0.007	2.133	437	315.7	121.3	27.8	1116
MARS-30d	1366.3	0.379	0	0.004	-0.001	2.159	462	314.4	147.6	32	1120
MARS-32a	1368.1	3.635	0.045	0.015	0.106	5.412	1783	620.1	1162.9	65.2	1121
MARS-32b	1367.3	3.288	0.028	0.007	0.018	4.691	1491	553.2	937.8	62.9	1122
MARS-32c	1366.9	3.035	0.035	0	0.024	4.348	1429	500.2	928.8	65	1126
MARS33	1362.5	1.233	0.062	0	0	1.548	454	192.7	261.3	57.5	1146
MARS-34	1362.7	1.686	0.039	0.008	-0.01	1.772	576	205.6	370.4	64.3	1147
M1-1a	1366.2	2.504	0.448	0.026	0.185	2.219	987	186.4	800.6	81.2	1155
M1-1b	1364.3	2.705	0.082	0.006	0.064	1.883	826	161.5	664.5	80.4	1159
M1-1c	1364.9	4.533	0.077	0	0.165	2.558	1195	199.7	995.3	83.3	1154
M1-1d	1366.6	4.323	0.443	0.029	0.35	2.832	1330	219.3	1110.7	83.5	1152
M1-4	1376.5	0.105	0.038	0	-0.028	6.825	1182	1068	114	9.7	1064
MAR-1	1364.2	0.469	0.091	0.006	-0.026	3.043	611	453.8	157.2	25.7	1106
M1-2	1369.2	0.154	0.119	0	-0.011	3.267	632	490.8	141.2	22.3	1101

* Temperature calculated for a mantle residence time of 2.5 Ga

APPENDIX 5

ELECTRON MICROPROBE ANALYSIS OF DIAMOND INCLUSION MINERALS

Diamond samples were treated in concentrated hydrochloric acid for 5 hours and then wiped off with ethanol. The stones were carefully examined visually for any cracks connecting the inclusions to the exterior of the diamonds and then described in detail before they were cracked in a steel diamond cracker designed by S. H. Richardson. Liberated inclusions were mounted individually on frosted glass slides in Petropox epoxy and cured for at least two hours before they were polished first with silica-carbon abrasive paper and then with 3 and 1 μm diamond paste.

Silicate inclusions were analysed at the University of Cape Town using a Cameca Camebax electron microprobe running with an operating voltage of 15 kV and a secondary current of ~40 nA. Natural pyrope, diopside, and olivine were used as standards and the data was reduced according to the PAP procedure. Counting times were 10 seconds for peaks and background except for sodium in garnet and potassium in omphacite for which peaks were measured for 30 seconds.

Sulfide inclusion analysis was performed at the Carnegie Institution of Washington using a Jeol Superprobe electron microprobe. The sulfides were analysed with an operating voltage and a secondary current of 15 kV and ~20 nA respectively. Counting times were 30 seconds for peaks and 10 seconds for background and concentrations were determined relative to standards of pyrite for iron and sulfur, chalcopyrite for copper and synthetic nickel and cobolt sulfides.

Appendix 5.1 Chemical compositions of Klipspringer garnet diamond inclusions. Sample notations: a, b, c etc. indicates multiple inclusions from an individual diamond; /2 indicates replicate analysis close to same spot as the first analysis; (e) indicates replicate analysis close to the edge of the grain. Cations were recalculated according to the formula unit of garnet, ie. 12 oxygen.

	Main Fissure												
Oxides	P3-1	P3/1-2	P3-2	P5-1a	P5-1a/2	P5-2a	P5-2a(e)	P5-2b	P5-2c	P5-2d	P5-2d/2	P5-2e	P5-2e(e)
SiO_2	38.8	38.7	40.5	39.7	39.6	39.3	39.1	39.0	39.0	39.4	39.3	39.7	39.1
TiO_2	0.59	0.60	0.13	0.45	0.44	0.40	0.37	0.41	0.59	0.46	0.44	0.43	0.44
Al_2O_3	22.3	22.3	14.1	22.9	22.9	22.2	21.8	22.2	22.1	22.4	22.3	22.8	22.6
Cr_2O_3	0.01	0.02	12.5	0.04	0.05	0.06	0.04	0.05	0.04	0.05	0.03	0.03	0.07
FeO	8.71	8.68	5.60	17.1	17.1	16.2	16.2	16.3	15.8	16.2	16.3	15.9	16.3
MnO	0.10	0.13	0.26	0.29	0.25	0.30	0.30	0.30	0.22	0.30	0.32	0.29	0.28
MgO	5.44	5.54	24.6	9.88	9.86	11.7	11.7	11.9	8.79	11.7	11.7	11.1	11.2
CaO	22.4	22.5	1.72	9.97	9.87	9.27	9.29	9.16	12.9	9.44	9.41	9.15	9.46
Na_2O	0.21	0.20	0.02	0.20	0.20	0.17	0.16	0.16	0.22	0.17	0.17	0.16	0.19
Total	98.55	98.64	99.49	100.60	100.26	99.61	99.07	99.52	99.64	100.12	99.98	99.54	99.52
Cations													
Si	2.950	2.941	2.945	2.961	2.959	2.941	2.945	2.925	2.949	2.935	2.930	2.968	2.930
Ti	0.034	0.034	0.007	0.025	0.025	0.022	0.021	0.023	0.033	0.026	0.024	0.024	0.025
Al	1.999	1.996	1.210	2.014	2.021	1.956	1.939	1.959	1.966	1.964	1.965	2.005	1.993
Cr	0.001	0.001	0.718	0.003	0.003	0.004	0.003	0.003	0.002	0.003	0.002	0.002	0.004
Fe	0.554	0.551	0.340	1.067	1.068	1.017	1.022	1.021	0.997	1.009	1.014	0.997	1.020
Mn	0.006	0.009	0.016	0.018	0.016	0.019	0.019	0.019	0.014	0.019	0.021	0.018	0.018
Mg	0.617	0.627	2.669	1.098	1.098	1.307	1.316	1.331	0.989	1.301	1.305	1.236	1.253
Ca	1.824	1.832	0.134	0.796	0.791	0.744	0.749	0.736	1.041	0.753	0.752	0.734	0.760
Na	0.032	0.029	0.003	0.028	0.029	0.025	0.023	0.023	0.032	0.024	0.025	0.023	0.027
Total	8.016	8.020	8.043	8.010	8.010	8.035	8.037	8.040	8.024	8.034	8.037	8.008	8.030
Mg#	53	53	89	51	51	56	56	57	50	56	56	55	55

Appendix 5.1 continued

	Main Fissure												
Oxides	P5-2f	P5-2f(e)	P5-2g	P5-2g(e)	P5-2h	P5-2h/2	P5-2i	P5-2i(e)	P5-2j	P5-2j/2	P5-3a	P5-3b	P5-3d
SiO_2	39.7	39.2	39.9	39.6	39.4	40.0	40.7	40.4	38.8	39.1	38.5	39.1	38.4
TiO_2	0.46	0.42	0.46	0.44	0.33	0.36	0.32	0.35	0.44	0.46	0.52	0.50	0.50
Al_2O_3	22.8	22.8	23.2	22.9	23.0	22.9	23.1	23.2	22.4	22.6	21.6	22.0	21.5
Cr_2O_3	0.06	0.06	0.03	0.08	0.05	0.04	0.04	0.04	0.03	0.06	0.04	0.01	0.03
FeO	15.8	16.2	15.8	15.9	14.7	14.9	15.0	15.1	15.7	16.2	21.2	20.8	20.6
MnO	0.25	0.35	0.26	0.23	0.34	0.32	0.32	0.28	0.28	0.29	0.37	0.30	0.40
MgO	11.0	11.0	11.1	11.0	13.6	13.7	14.0	14.1	11.0	11.2	8.34	8.54	8.27
CaO	9.50	9.52	9.57	9.52	6.77	6.76	6.71	6.83	9.42	9.49	9.40	9.34	8.92
Na_2O	0.18	0.19	0.15	0.19	0.16	0.15	0.14	0.21	0.16	0.19	0.25	0.24	0.28
Total	99.80	99.77	100.50	99.86	98.31	99.16	100.21	100.64	98.20	99.57	100.30	100.77	98.86
Cations													
Si	2.962	2.933	2.956	2.952	2.946	2.964	2.981	2.954	2.948	2.930	2.935	2.956	2.960
Ti	0.026	0.024	0.026	0.025	0.019	0.020	0.018	0.019	0.025	0.026	0.030	0.028	0.029
Al	2.007	2.011	2.022	2.011	2.027	2.006	1.997	2.000	1.999	1.997	1.945	1.956	1.951
Cr	0.003	0.004	0.002	0.005	0.003	0.003	0.002	0.002	0.002	0.004	0.003	0.001	0.002
Fe	0.982	1.013	0.976	0.993	0.921	0.927	0.917	0.925	0.996	1.016	1.352	1.312	1.330
Mn	0.016	0.022	0.017	0.015	0.022	0.020	0.020	0.018	0.018	0.019	0.024	0.019	0.026
Mg	1.228	1.228	1.230	1.226	1.514	1.514	1.525	1.537	1.242	1.248	0.948	0.962	0.951
Ca	0.759	0.763	0.759	0.761	0.543	0.537	0.527	0.535	0.766	0.762	0.767	0.756	0.737
Na	0.026	0.028	0.021	0.027	0.023	0.021	0.020	0.029	0.023	0.027	0.037	0.036	0.042
Total	8.010	8.025	8.008	8.015	8.016	8.011	8.006	8.020	8.019	8.028	8.040	8.027	8.028
Mg#	56	55	56	55	62	62	62	62	55	55	41	42	42

Appendix 5.1 continued

	Main Fissure												
Oxides	P5-3d/2	P5-3e	P5-3e/2	P6-1a	P6-1a/2	P6-1b	P6-1c	P6-1d	P6-1d/2	P7-4	P7-4/2	P7-13a	P7-13a/2
SiO_2	37.8	38.4	39.2	38.5	38.8	39.3	39.5	39.9	39.9	39.6	38.2	37.4	38.9
TiO_2	0.47	0.49	0.47	0.61	0.63	0.63	0.63	0.42	0.43	0.55	0.50	0.44	0.47
Al_2O_3	21.0	21.5	21.9	21.6	21.9	21.9	22.1	23.0	23.3	23.0	21.7	21.3	21.9
Cr_2O_3	0.01	0.02	0.06	0.05	0.03	0.03	0.04	0.05	0.04	0.02	0.03	0.00	0.01
FeO	20.8	21.0	20.7	9.12	8.77	8.85	8.95	16.8	16.9	15.4	15.0	17.7	17.5
MnO	0.29	0.35	0.42	0.12	0.15	0.13	0.14	0.28	0.28	0.25	0.23	0.24	0.23
MgO	8.15	8.36	8.43	5.61	5.83	5.84	5.81	10.2	9.54	9.00	9.62	6.60	7.02
CaO	9.01	9.30	9.04	22.5	22.2	22.5	22.2	10.2	10.1	12.7	12.4	13.8	13.9
Na_2O	0.28	0.27	0.25	0.23	0.25	0.27	0.23	0.18	0.18	0.22	0.20	0.18	0.24
Total	97.80	99.65	100.39	98.34	98.53	99.48	99.64	100.95	100.78	100.73	97.93	97.70	100.19
Cations													
Si	2.952	2.942	2.970	2.940	2.950	2.960	2.970	2.959	2.968	2.926	2.988	2.925	2.956
Ti	0.028	0.028	0.027	0.035	0.036	0.036	0.035	0.024	0.024	0.028	0.025	0.026	0.027
Al	1.935	1.940	1.954	1.946	1.963	1.949	1.960	2.009	2.044	1.963	2.026	1.966	1.962
Cr	0.001	0.001	0.003	0.003	0.002	0.002	0.002	0.003	0.002	0.002	0.002	0.000	0.001
Fe	1.356	1.346	1.315	0.583	0.558	0.558	0.563	1.041	1.054	0.961	0.820	1.157	1.108
Mn	0.019	0.023	0.027	0.008	0.010	0.008	0.009	0.017	0.017	0.015	0.014	0.016	0.015
Mg	0.949	0.955	0.953	0.640	0.661	0.656	0.651	1.125	1.058	1.098	1.131	0.769	0.794
Ca	0.754	0.764	0.735	1.846	1.809	1.817	1.792	0.808	0.806	1.016	0.956	1.153	1.129
Na	0.043	0.040	0.037	0.034	0.036	0.039	0.033	0.026	0.026	0.029	0.031	0.028	0.035
Total	8.037	8.039	8.021	8.034	8.025	8.024	8.015	8.012	7.999	8.039	7.994	8.040	8.027
Mg#	41	41	42	52	54	54	54	52	50	53	58	40	42

Appendix 5.1 continued

Oxides	P7-13b	P7-13b/2	P8-2a	P8-2a/2	P8-2c	P8-2c/2	P8-2f	P8-2f/2	17-2a	17-2b	17-3	17-3/2	17-13a
SiO_2	38.1	38.0	41.3	40.5	38.3	39.7	39.7	41.2	39.1	39.1	39.5	39.5	38.2
TiO_2	0.46	0.48	0.40	0.39	0.67	0.68	0.40	0.38	0.46	0.45	0.64	0.62	0.55
Al_2O_3	21.1	21.4	22.9	22.8	21.4	22.3	22.8	23.3	22.4	22.2	22.4	22.5	21.7
Cr_2O_3	0.03	0.06	0.05	0.04	0.05	0.07	0.06	0.06	0.02	0.02	0.08	0.09	0.03
FeO	17.5	17.5	15.2	15.0	15.1	15.3	15.0	15.0	11.5	11.5	16.5	16.8	16.5
MnO	0.26	0.22	0.30	0.27	0.22	0.30	0.28	0.32	0.15	0.11	0.28	0.33	0.23
MgO	6.80	6.94	15.4	15.6	10.6	10.7	15.1	15.3	9.03	9.00	11.3	11.3	6.68
CaO	13.6	13.7	6.59	6.42	10.9	10.8	6.42	6.29	16.6	16.2	8.09	8.04	14.7
Na_2O	0.26	0.26	0.17	0.18	0.22	0.27	0.18	0.19	0.17	0.19	0.20	0.20	0.21
Total	98.11	98.59	102.37	101.16	97.33	100.06	100.00	102.06	99.39	98.73	99.02	99.45	98.78
Cations													
Si	2.960	2.937	2.960	2.933	2.938	2.958	2.919	2.959	2.931	2.948	2.973	2.965	2.940
Ti	0.027	0.028	0.021	0.021	0.038	0.038	0.022	0.021	0.026	0.025	0.036	0.035	0.032
Al	1.935	1.952	1.938	1.947	1.932	1.956	1.971	1.969	1.979	1.977	1.989	1.989	1.967
Cr	0.002	0.004	0.003	0.002	0.003	0.004	0.003	0.004	0.001	0.001	0.005	0.005	0.002
Fe	1.134	1.129	0.912	0.909	0.968	0.954	0.924	0.904	0.720	0.724	1.035	1.053	1.061
Mn	0.017	0.014	0.019	0.017	0.014	0.019	0.017	0.019	0.009	0.007	0.018	0.021	0.015
Mg	0.788	0.800	1.648	1.690	1.216	1.194	1.655	1.637	1.009	1.012	1.267	1.264	0.767
Ca	1.130	1.135	0.506	0.499	0.894	0.861	0.505	0.484	1.333	1.305	0.652	0.646	1.214
Na	0.040	0.040	0.023	0.025	0.032	0.039	0.025	0.026	0.024	0.027	0.029	0.029	0.031
Total	8.032	8.038	8.030	8.042	8.036	8.022	8.042	8.023	8.032	8.026	8.004	8.009	8.030
Mg#	41	41	64	65	56	56	64	64	58	58	55	55	42

Appendix 5.1 continued

	Main Fissure											Sugarbird Blow	
Oxides	17-13a/2	A-10b	A-10b/2	MDA-1a	MDA-1b	MDA-1b/2	MDA-1c	MDA-1c/2	950W-2b	950W-2c	950W-2c/2	SB-2a	SB-2g
SiO_2	38.4	39.9	39.5	39.2	39.6	39.5	38.1	38.7	38.8	38.4	38.9	39.7	39.8
TiO_2	0.48	0.73	0.74	0.43	0.41	0.38	0.41	0.45	0.44	0.43	0.44	0.42	0.50
Al_2O_3	21.5	22.2	22.4	22.5	22.7	22.3	21.8	22.2	21.9	21.9	21.8	22.3	21.9
Cr_2O_3	0.06	0.07	0.12	0.02	0.05	0.06	0.06	0.06	0.07	0.06	0.05	0.12	0.12
FeO	16.4	17.5	17.4	15.9	15.8	15.5	15.9	16.0	15.2	15.3	15.2	15.5	15.0
MnO	0.27	0.33	0.30	0.22	0.25	0.26	0.27	0.29	0.24	0.24	0.15	0.34	0.30
MgO	6.71	11.1	11.3	9.72	10.2	10.2	9.82	10.0	9.33	8.91	9.13	16.7	16.3
CaO	14.8	8.87	8.87	12.0	11.8	11.8	11.8	11.8	13.3	13.4	13.3	4.18	4.13
Na_2O	0.20	0.29	0.23	0.21	0.18	0.17	0.21	0.22	0.21	0.18	0.17	0.14	0.20
Total	98.80	101.04	100.84	100.30	101.02	100.18	98.52	99.81	99.39	98.87	99.14	99.41	98.31
Cations													
Si	2.954	2.961	2.934	2.933	2.934	2.948	2.910	2.913	2.931	2.925	2.946	2.925	2.960
Ti	0.028	0.041	0.041	0.024	0.023	0.021	0.024	0.025	0.025	0.024	0.025	0.023	0.028
Al	1.949	1.941	1.962	1.986	1.986	1.959	1.963	1.969	1.949	1.968	1.950	1.932	1.917
Cr	0.004	0.004	0.007	0.001	0.003	0.003	0.003	0.003	0.004	0.003	0.003	0.007	0.007
Fe	1.058	1.083	1.081	0.996	0.978	0.970	1.017	1.007	0.961	0.976	0.963	0.954	0.932
Mn	0.017	0.021	0.019	0.014	0.015	0.016	0.017	0.018	0.015	0.015	0.010	0.021	0.019
Mg	0.770	1.227	1.247	1.084	1.125	1.140	1.117	1.123	1.052	1.011	1.031	1.833	1.811
Ca	1.219	0.705	0.705	0.963	0.940	0.946	0.967	0.954	1.073	1.089	1.080	0.330	0.329
Na	0.030	0.042	0.032	0.030	0.026	0.025	0.031	0.032	0.030	0.026	0.024	0.020	0.029
Total	8.029	8.024	8.028	8.032	8.031	8.031	8.049	8.046	8.041	8.039	8.032	8.046	8.032
Mg#	42	53	54	52	53	54	52	53	52	51	52	66	66

Appendix 5.1 continued

	Sugarbird Blow							Marsfontein					
Oxides	SB-2g/2	Blow-3b	Blow-3b/2	Blow-6	TB-5	TB-14a	TB-14b	M1-1	M1-1/2	M1-2a	M1-2a(e)	M1-2b	M1-2c
SiO_2	40.3	39.4	39.4	40.5	39.4	39.6	39.9	38.4	37.9	38.5	39.0	39.1	38.9
TiO_2	0.46	0.46	0.46	0.37	0.52	0.49	0.46	0.62	0.68	0.43	0.43	0.48	0.43
Al_2O_3	22.1	22.5	22.1	23.0	22.2	22.0	22.3	21.8	21.7	22.2	22.6	22.5	22.5
Cr_2O_3	0.13	0.01	0.03	0.16	0.04	0.05	0.05	0.02	0.00	0.04	0.04	0.02	0.00
FeO	15.2	11.6	12.1	13.5	16.2	16.2	16.4	17.9	17.8	15.6	15.6	15.8	15.9
MnO	0.30	0.19	0.18	0.18	0.27	0.28	0.30	0.30	0.26	0.29	0.28	0.23	0.27
MgO	16.7	11.7	12.0	19.1	10.8	12.0	11.8	8.03	8.06	9.17	9.26	9.30	9.27
CaO	4.18	12.6	12.6	3.17	10.5	8.98	8.79	12.4	12.4	12.8	12.8	12.5	12.5
Na_2O	0.20	0.20	0.18	0.15	0.17	0.14	0.16	0.23	0.25	0.28	0.19	0.00	0.23
Total	99.55	98.60	99.01	100.11	100.07	99.73	100.14	99.72	99.08	99.26	100.15	99.95	99.96
Cations													
Si	2.957	2.943	2.938	2.920	2.944	2.958	2.969	2.928	2.908	2.916	2.928	2.941	2.927
Ti	0.025	0.026	0.026	0.020	0.029	0.027	0.026	0.036	0.039	0.024	0.024	0.027	0.024
Al	1.909	1.981	1.945	1.955	1.952	1.934	1.952	1.958	1.963	1.982	1.994	1.995	1.990
Cr	0.008	0.000	0.002	0.009	0.003	0.003	0.003	0.001	0.000	0.003	0.003	0.001	0.000
Fe	0.933	0.724	0.752	0.816	1.014	1.014	1.022	1.140	1.142	0.988	0.977	0.992	1.000
Mn	0.019	0.012	0.012	0.011	0.017	0.018	0.019	0.020	0.017	0.018	0.018	0.015	0.017
Mg	1.830	1.301	1.330	2.048	1.201	1.335	1.305	0.912	0.922	1.036	1.035	1.042	1.039
Ca	0.328	1.010	1.009	0.245	0.845	0.719	0.701	1.009	1.019	1.036	1.026	1.003	1.004
Na	0.028	0.029	0.026	0.020	0.025	0.020	0.023	0.034	0.036	0.042	0.028	0.000	0.034
Total	8.037	8.028	8.038	8.044	8.031	8.028	8.019	8.037	8.045	8.044	8.032	8.017	8.035
Mg#	66	64	64	72	54	57	56	44	45	51	51	51	51

Appendix 5.1 continued

	Marsfontein		
Oxides	M1-2d	M1-2d/2	M1-2e
SiO_2	39.3	39.5	38.8
TiO_2	0.42	0.43	0.41
Al_2O_3	22.6	22.8	22.2
Cr_2O_3	0.04	0.02	0.03
FeO	15.7	15.6	15.9
MnO	0.25	0.26	0.29
MgO	8.78	8.81	9.23
CaO	12.3	12.6	12.7
Na_2O	0.22	0.21	0.21
Total	99.63	100.29	99.78
Cations			
Si	2.960	2.959	2.924
Ti	0.024	0.024	0.023
Al	2.005	2.011	1.977
Cr	0.003	0.001	0.002
Fe	0.992	0.978	1.003
Mn	0.016	0.017	0.018
Mg	0.987	0.982	1.037
Ca	0.997	1.010	1.024
Na	0.032	0.031	0.031
Total	8.014	8.013	8.040
Mg#	50	50	51

Appendix 5.2 Chemical compositions of Klipspringer clinopyroxene diamond inclusions. Sample notations: a, b, c etc. indicates multiple inclusions from an individual diamond; /2 indicates replicate analysis close to same spot as the first analysis; (e) indicates replicate analysis close to the edge of the grain. Cations were recalculated according to the formula unit of pyroxene, ie. 6 oxygen.

	Main Fissure												
Oxides	P7-3	P7-3(e)	P8-1b	P8-1b/2	P8-2b	P8-2d	P8-2d/2	P8-2e	P8-2e/2	P9-1	P9-1/2	P9-2a	P9-2b
Na_2O	7.49	7.45	5.53	5.38	6.15	5.97	6.05	6.26	6.31	5.20	5.09	6.29	6.18
K_2O	0.22	0.21	0.34	0.34	0.18	0.15	0.15	0.16	0.16	0.23	0.22	0.29	0.31
SiO_2	55.5	55.7	54.8	54.4	54.8	55.0	55.4	54.3	55.2	55.7	55.9	55.6	54.6
TiO_2	0.67	0.65	0.57	0.55	0.42	0.34	0.36	0.41	0.39	0.50	0.53	0.30	0.30
Al_2O_3	19.2	19.1	11.1	10.9	12.0	11.3	11.5	11.9	12.4	8.14	8.11	17.9	17.3
Cr_2O_3	0.04	0.05	0.05	0.05	0.09	0.07	0.05	0.05	0.05	0.10	0.11	0.04	0.05
FeO	2.60	2.51	4.43	4.40	4.33	4.62	4.67	4.42	4.34	6.81	6.91	1.86	1.83
MnO	0.05	0.03	0.08	0.04	0.05	0.05	0.07	0.07	0.02	0.14	0.14	0.00	0.03
MgO	4.99	5.00	9.66	9.66	9.76	10.7	10.7	9.64	9.94	14.5	14.0	6.53	6.54
CaO	10.1	9.89	14.5	14.2	12.0	11.4	11.2	12.0	11.7	9.83	9.62	12.8	12.6
Total	100.79	100.62	101.08	99.92	99.66	99.62	100.10	99.18	100.50	101.10	100.62	101.64	99.83
Cations													
Na	0.505	0.503	0.379	0.373	0.424	0.412	0.415	0.435	0.431	0.355	0.350	0.422	0.422
K	0.010	0.009	0.015	0.016	0.008	0.007	0.007	0.008	0.007	0.010	0.010	0.013	0.014
Si	1.929	1.938	1.940	1.945	1.949	1.958	1.959	1.944	1.945	1.963	1.979	1.921	1.923
Ti	0.018	0.017	0.015	0.015	0.011	0.009	0.010	0.011	0.010	0.013	0.014	0.008	0.008
Al	0.785	0.784	0.461	0.461	0.502	0.474	0.478	0.500	0.515	0.338	0.338	0.731	0.719
Cr	0.001	0.002	0.001	0.001	0.003	0.002	0.001	0.002	0.001	0.003	0.003	0.001	0.001
Fe	0.076	0.073	0.131	0.132	0.129	0.138	0.138	0.132	0.128	0.201	0.205	0.054	0.054
Mn	0.001	0.001	0.002	0.001	0.001	0.001	0.002	0.002	0.001	0.004	0.004	0.000	0.001
Mg	0.259	0.259	0.509	0.515	0.518	0.566	0.566	0.514	0.523	0.759	0.741	0.337	0.343
Ca	0.376	0.369	0.551	0.543	0.457	0.434	0.425	0.459	0.442	0.371	0.365	0.476	0.477
Total	3.959	3.954	4.006	4.002	4.002	4.002	4.001	4.007	4.003	4.018	4.008	3.961	3.963

Appendix 5.2 continued

	Main Fissure												
Oxides	P9-2b(e)	P9-2c	P9-2c/2	P9-2d	P9-2e	P9-2f	P9-6a	P9-6b	P9-6b/2	P9-6c	P9-6d	P9-14	P9-14/2
Na_2O	6.26	5.97	5.92	6.00	2.97	6.08	7.24	7.06	7.03	7.43	7.32	4.54	4.50
K_2O	0.30	0.31	0.30	0.30	0.17	0.30	0.18	0.17	0.17	0.18	0.17	0.42	0.43
SiO_2	54.6	54.9	54.3	54.2	53.6	54.1	53.7	54.1	54.2	53.9	54.5	55.2	55.1
TiO_2	0.27	0.31	0.27	0.31	0.35	0.29	0.49	0.51	0.47	0.45	0.50	0.53	0.55
Al_2O_3	17.6	17.7	17.7	17.8	17.4	17.8	14.3	14.4	14.7	14.5	14.4	8.40	8.25
Cr_2O_3	0.06	0.04	0.07	0.05	0.07	0.06	0.04	0.03	0.04	0.03	0.06	0.04	0.04
FeO	1.72	1.94	2.02	2.03	2.21	1.84	2.64	2.59	2.64	2.63	2.54	5.68	5.88
MnO	0.03	0.05	0.02	0.01	0.00	0.00	0.05	0.02	0.04	0.03	0.04	0.11	0.08
MgO	6.62	6.53	6.63	6.54	8.52	6.70	8.32	8.37	8.48	8.70	8.31	11.1	11.0
CaO	12.4	13.1	12.9	13.0	16.3	13.1	12.6	12.8	12.7	12.7	12.5	15.1	15.1
Total	99.81	100.85	100.17	100.22	101.63	100.26	99.63	99.97	100.45	100.53	100.30	101.15	100.97
Cations													
Na	0.427	0.404	0.403	0.409	0.201	0.414	0.497	0.483	0.479	0.506	0.499	0.313	0.311
K	0.014	0.014	0.013	0.014	0.007	0.014	0.008	0.007	0.008	0.008	0.007	0.019	0.020
Si	1.921	1.918	1.910	1.904	1.875	1.899	1.902	1.910	1.905	1.892	1.915	1.964	1.968
Ti	0.007	0.008	0.007	0.008	0.009	0.008	0.013	0.013	0.013	0.012	0.013	0.014	0.015
Al	0.728	0.727	0.733	0.737	0.716	0.738	0.599	0.597	0.608	0.598	0.596	0.353	0.347
Cr	0.002	0.001	0.002	0.001	0.002	0.002	0.001	0.001	0.001	0.001	0.002	0.001	0.001
Fe	0.051	0.057	0.059	0.060	0.065	0.054	0.078	0.077	0.078	0.077	0.075	0.169	0.176
Mn	0.001	0.002	0.001	0.000	0.000	0.000	0.001	0.001	0.001	0.001	0.001	0.003	0.003
Mg	0.347	0.340	0.348	0.343	0.444	0.350	0.440	0.440	0.444	0.455	0.435	0.592	0.587
Ca	0.467	0.490	0.486	0.490	0.611	0.491	0.480	0.483	0.476	0.477	0.470	0.577	0.578
Total	3.964	3.959	3.962	3.965	3.931	3.969	4.019	4.011	4.011	4.027	4.013	4.006	4.005

Appendix 5.2 continued

	Main Fissure										Sugarbird Blow		
Oxides	17-4	17-7c	17-7c(e)	17-21a	17-21b	17-21b/2	17-21c	950W-1c	950W-2a	950W-2a/2	SB-2c	SB-2d	SB-2e
Na_2O	6.76	0.78	0.85	6.92	6.72	6.94	6.96	6.94	7.33	7.41	4.64	4.87	4.85
K_2O	0.30	0.05	0.05	0.22	0.23	0.24	0.24	0.25	0.24	0.24	0.14	0.13	0.14
SiO_2	55.3	53.3	54.3	54.7	50.5	54.5	54.4	52.8	54.6	54.4	54.0	55.4	54.7
TiO_2	0.48	0.06	0.07	0.41	0.39	0.41	0.42	0.54	0.45	0.44	0.50	0.48	0.48
Al_2O_3	18.2	1.92	2.01	13.3	13.8	13.3	13.4	16.8	16.1	16.0	7.98	8.10	8.19
Cr_2O_3	0.04	0.17	0.16	0.07	0.04	0.03	0.05	0.07	0.05	0.10	0.10	0.12	0.10
FeO	1.95	4.30	4.13	2.42	2.37	2.35	2.34	2.14	2.85	2.75	5.77	5.87	5.94
MnO	0.03	0.08	0.12	0.02	0.04	0.00	0.00	0.05	0.02	0.01	0.11	0.10	0.11
MgO	5.82	17.9	18.1	9.20	8.67	8.91	8.80	6.19	6.17	6.31	12.9	13.4	13.2
CaO	11.6	20.9	20.7	13.4	12.4	13.0	12.9	11.2	10.9	10.8	12.9	12.6	12.6
Total	100.50	99.51	100.47	100.56	95.10	99.68	99.44	96.85	98.73	98.47	99.02	101.09	100.34
Cations													
Na	0.458	0.055	0.059	0.471	0.484	0.476	0.478	0.488	0.506	0.513	0.325	0.334	0.335
K	0.014	0.002	0.002	0.010	0.011	0.011	0.011	0.012	0.011	0.011	0.006	0.006	0.007
Si	1.929	1.947	1.958	1.919	1.873	1.928	1.929	1.914	1.945	1.943	1.953	1.960	1.951
Ti	0.013	0.002	0.002	0.011	0.011	0.011	0.011	0.015	0.012	0.012	0.014	0.013	0.013
Al	0.750	0.083	0.086	0.549	0.603	0.556	0.558	0.716	0.675	0.673	0.340	0.338	0.344
Cr	0.001	0.005	0.005	0.002	0.001	0.001	0.001	0.002	0.001	0.003	0.003	0.003	0.003
Fe	0.057	0.131	0.124	0.071	0.074	0.069	0.069	0.065	0.085	0.082	0.175	0.174	0.177
Mn	0.001	0.003	0.004	0.001	0.001	0.000	0.000	0.002	0.001	0.000	0.003	0.003	0.003
Mg	0.303	0.972	0.976	0.481	0.480	0.470	0.465	0.335	0.328	0.336	0.693	0.707	0.701
Ca	0.435	0.819	0.798	0.503	0.494	0.491	0.490	0.434	0.418	0.413	0.501	0.476	0.482
Total	3.959	4.018	4.013	4.018	4.031	4.013	4.013	3.981	3.982	3.985	4.014	4.013	4.017

Appendix 5.2 continued

Oxides	SB-2f	SB-2g	SB-2h	SB-2h(e)	TB-10a	TB-10a/2	TB-10b	NFB
Na_2O	4.72	4.67	4.51	4.92	5.91	6.01	5.81	6.92
K_2O	0.14	0.13	0.21	0.22	0.10	0.11	0.12	0.34
SiO_2	54.2	54.6	54.0	54.6	55.5	55.6	55.7	55.1
TiO_2	0.51	0.50	0.53	0.51	0.38	0.36	0.38	0.48
Al_2O_3	7.59	7.49	7.48	7.60	11.1	11.0	10.5	14.1
Cr_2O_3	0.11	0.09	0.11	0.08	0.06	0.02	0.03	0.07
FeO	5.87	5.82	5.96	5.88	4.73	4.54	4.62	3.06
MnO	0.09	0.11	0.10	0.12	0.09	0.08	0.08	0.01
MgO	13.1	13.0	12.8	13.3	11.6	11.6	12.3	7.84
CaO	13.1	12.8	13.5	13.1	10.7	10.7	10.5	11.9
Total	99.44	99.25	99.11	100.36	100.11	100.05	100.04	99.76
Cations								
Na	0.330	0.327	0.317	0.340	0.405	0.412	0.398	0.475
K	0.006	0.006	0.010	0.010	0.005	0.005	0.005	0.015
Si	1.955	1.970	1.955	1.950	1.960	1.964	1.966	1.947
Ti	0.014	0.014	0.014	0.014	0.010	0.010	0.010	0.013
Al	0.322	0.318	0.319	0.320	0.461	0.460	0.439	0.590
Cr	0.003	0.003	0.003	0.002	0.002	0.001	0.001	0.002
Fe	0.177	0.176	0.181	0.176	0.140	0.134	0.136	0.091
Mn	0.003	0.003	0.003	0.004	0.003	0.002	0.003	0.000
Mg	0.704	0.700	0.691	0.708	0.610	0.608	0.647	0.413
Ca	0.505	0.494	0.523	0.503	0.407	0.407	0.398	0.449
Total	4.018	4.011	4.016	4.025	4.002	4.002	4.003	3.995

Appendix 5.3 Chemical analyses for kyanite, coesite and rutile diamond inclusions. Sample notations as indicated in Appendix 5.1.

	Kyanite		*Coesite*			*Rutile*					
Oxide	SB-1a	SB-1b	P9-3	17-7a	17-7b	P5-1b	A-10a	A-10c	A-10c/2	A-10d	A-10d(e)
SiO_2	36.7	18.4	99.5	99.7	99.3	0.01	0.00	0.00	0.01	0.06	0.53
TiO_2	0.15	0.08	0.01	0.01	0.02	98.3	98.7	96.8	97.2	98.1	96.8
Al_2O_3	63.5	31.8	0.00	0.01	0.00	0.91	0.05	0.89	0.85	0.59	0.66
Cr_2O_3	0.01	0.01	0.01	0.00	0.01	0.11	0.09	0.12	0.09	0.11	0.11
FeO	0.27	0.14	0.00	0.01	0.00	0.43	0.49	0.38	0.33	0.42	0.40
MnO	0.00	0.00	0.01	0.00	0.02	0.00	0.01	0.00	0.00	0.00	0.00
MgO	0.10	0.05	0.00	0.00	0.00	0.02	0.02	0.00	0.01	0.00	0.07
CaO	0.00	0.00	0.00	0.01	0.00	0.01	0.01	0.04	0.04	0.03	0.05
Na_2O	0.03	0.02	0.01	0.00	0.01	-	-	-	-	-	-
K_2O	0.01	0.01	0.01	0.00	0.01	-	-	-	-	-	-
Total	100.70	50.39	99.59	99.72	99.50	99.79	99.37	98.27	98.54	99.35	98.63

Appendix 5.4 Chemical analyses for pyrope, olivine and orthopyroxene diamond inclusions. Sample notations as indicated in Appendix 5.1.

	Pyrope	*Olivine*								*Orthopyroxene*		
Oxide	P3-2	P5-9b	P5-9c	950W-3a	950W-3a/2	950W-3b	950W-3d	950W-3e	950W-3f	P9-4	P9-4(e)	950W-3c
SiO_2	40.5	41.5	41.4	41.1	41.2	40.1	41.2	40.9	40.7	57.1	57.4	57.3
TiO_2	0.13	0.00	0.01	0.00	0.00	0.00	0.04	0.02	0.00	0.04	0.01	0.00
Al_2O_3	14.1	0.02	0.00	0.01	0.00	0.00	0.03	0.00	0.02	0.44	0.38	0.61
Cr_2O_3	12.5	0.03	0.04	0.10	0.07	0.08	0.10	0.07	0.11	0.02	0.03	0.45
FeO	5.60	6.93	6.60	6.73	7.03	6.86	7.28	7.02	6.95	6.72	6.89	4.33
MnO	0.26	0.06	0.08	0.13	0.10	0.10	0.09	0.13	0.05	0.18	0.13	0.12
MgO	24.6	51.8	51.8	52.1	52.1	52.4	51.5	51.1	51.0	34.8	35.1	37.4
CaO	1.72	0.03	0.03	0.02	0.04	0.05	0.01	0.04	0.05	0.77	0.80	0.47
Na_2O	0.02	-	-	-	-	-	-	-	-	0.27	0.27	0.11
K_2O	-	-	-	-	-	-	-	-	-	0.00	0.00	0.00
NiO	-	0.30	0.23	0.27	0.27	0.24	0.28	0.26	0.28	-	-	-
Total	99.50	100.63	100.17	100.50	100.85	99.87	100.55	99.57	99.15	100.31	100.96	100.83
Mg#	88.7	93.0	93.3	93.2	93.0	93.2	92.7	92.9	92.9	90.2	90.1	93.9

Appendix 5.5 Chemical compositions for the different phases present in the sulfide diamond inclusions.

Phyrrotite

	Main Fissure															Sugarbird Blow		
	P5-7	P5-8f	P7-5a	P7-6b	P7-9	P8-4	P9-6	P9-7a	P9-8a	P9-8c	P9-8e	P9-10	P9-11a	A-8a	A-8b	A-12	RUS-1	SB-3.1	SB-3.2
Ni	1.32	0.25	1.37	2.24	2.44	0.21	1.32	1.11	0.19	0.20	0.29	0.40	2.13	0.97	0.20	0.20	1.11	0.23	0.28
Fe	57.0	58.2	57.7	56.2	56.1	58.4	56.6	58.3	59.3	57.9	58.7	57.6	55.8	58.6	58.6	58.5	57.7	57.5	57.9
S	39.2	38.0	38.9	39.3	39.3	39.4	38.7	39.1	38.9	39.0	39.5	38.7	38.8	39.2	39.2	39.0	39.0	39.0	38.6
Cu	0.00	0.00	0.02	0.12	0.03	0.02	1.63	0.08	0.03	0.03	0.03	0.09	0.07	0.02	0.13	0.03	1.34	0.03	0.13
Co	0.15	0.05	0.23	0.13	0.14	0.05	0.31	0.31	0.08	0.08	0.10	0.06	0.39	0.23	0.06	0.07	0.33	0.13	0.13
Total	97.62	96.52	98.20	98.01	97.97	98.04	98.57	98.97	98.50	97.19	98.65	96.86	97.17	99.09	98.13	97.79	99.60	96.93	97.07

Phyrrotite

	Sugarbird Blow cont.																	
	SB-6	SB-6a	SB-6b	SB-7	SB-8a	SB-8b	SB-9a	SB-9b	SB-10	SB-10	SB-10c	SB-11	SB-11	B-12.	SB-12.	SB-12.	SB-12.4	B-12.	SB-13
Ni	0.35	1.06	0.23	0.27	0.22	0.33	0.41	0.19	0.73	0.55	0.49	0.47	0.56	0.38	0.44	0.60	0.45	0.42	0.57
Fe	57.9	56.6	58.9	58.9	58.7	58.4	57.6	57.9	58.2	56.9	58.2	58.2	58.0	59.0	58.7	59.1	59.0	58.8	58.2
S	39.4	39.0	39.2	39.0	39.6	38.9	38.9	39.1	39.3	38.7	39.2	38.9	39.1	39.4	39.1	38.6	39.0	39.4	39.6
Cu	0.04	0.01	0.00	0.00	0.17	0.07	0.04	0.00	0.00	0.54	0.00	0.08	0.03	0.00	0.01	0.03	0.00	0.10	0.02
Co	0.12	0.11	0.07	0.10	0.06	0.11	0.06	0.09	0.12	0.11	0.06	0.07	0.15	0.08	0.05	0.11	0.12	0.11	0.13
Total	97.82	96.82	98.44	98.33	98.82	97.74	97.06	97.29	98.32	96.80	98.03	97.72	97.77	98.86	98.25	98.40	98.56	98.81	98.46

Phyrrotite

	Sugarbird Blow cont.															Marsfontein		
	SB-15	SB-16	SB-17	SB-18	SB-19	SB-20	SB-21	SB-22	SB-23	SB-24	SB-25	SB-26	SB-27	SB-28	SB-30	M1/A-1	MARS-3	M1-4
Ni	0.27	0.81	0.38	4.20	2.00	0.28	0.40	1.67	0.28	4.69	1.17	0.54	3.11	1.45	0.34	4.82	1.80	2.38
Fe	58.5	59.4	58.2	55.8	56.5	59.9	60.1	58.6	59.6	55.7	57.4	59.4	56.1	57.2	59.9	52.4	57.1	56.4
S	38.7	39.7	38.1	39.2	39.2	39.6	39.2	39.1	38.5	38.9	39.4	39.8	38.0	39.6	39.1	38.2	39.1	39.5
Cu	0.02	0.05	0.03	0.00	0.00	0.02	0.01	0.00	0.03	0.20	0.15	0.00	0.00	0.12	0.02	1.99	0.00	0.00
Co	0.08	0.12	0.09	0.37	0.08	0.13	0.10	0.13	0.02	0.15	0.09	0.04	0.21	0.03	0.13	0.26	0.06	0.25
Total	97.62	100.05	96.87	99.57	97.73	99.84	99.87	99.43	98.50	99.68	98.24	99.77	97.45	98.33	99.47	97.71	98.09	98.44

Appendix 5.5 continued

Pentlandite

	Main Fissure			Sugarbird Blow													
	P7-9	P7-5a	P7-6b	P8-4	P9-7a	P9-8a	P9-10	A-8a	SB-3.1	SB-3.2	SB-6	SB-6a	SB-6b	SB-7	SB-8a	SB-8b	SB-9a	SB-9b
Ni	37.0	33.2	37.7	27.2	25.2	29.2	25.5	29.6	29.3	31.5	31.6	31.2	29.2	31.2	26.9	25.2	30.8	30.6
Fe	26.3	29.0	27.4	32.7	36.8	28.7	36.2	31.6	29.6	28.3	27.4	30.1	33.9	28.2	29.7	30.9	29.5	29.5
S	32.8	33.3	33.5	34.1	34.8	33.4	35.4	33.5	33.6	33.3	32.9	33.2	34.1	32.0	33.5	33.9	33.7	33.1
Cu	0.00	0.02	0.05	0.00	0.00	0.00	0.00	0.00	0.02	0.00	0.06	0.00	0.00	0.00	0.00	0.00	0.00	0.00
Co	1.07	3.90	0.59	5.36	3.65	7.68	3.44	4.76	5.59	5.51	7.49	3.19	2.34	6.41	8.03	8.53	5.16	4.92
Total	97.24	99.40	99.23	99.32	100.49	98.93	100.46	99.55	98.21	98.69	99.38	97.71	99.53	97.78	98.12	98.49	99.08	98.12

Pentlandite

	Sugarbird Blow cont.													
	SB-10a	SB-10b	SB-10c	SB-11a	SB-11b	B-12.	B-12.	B-12.	B-12.	B-12.	SB-13	SB-16	SB-18	SB-22	SB-24
Ni	27.7	31.3	33.1	32.9	33.2	33.0	32.2	33.5	31.7	31.7	33.1	29.1	36.4	37.8	33.3
Fe	33.6	29.2	27.1	28.3	27.4	29.4	29.8	29.0	28.5	30.9	27.9	34.5	30.2	29.0	23.7
S	33.4	34.3	32.1	33.2	32.9	32.7	31.9	32.9	32.0	33.4	33.0	34.9	34.0	32.9	37.9
Cu	0.00	0.00	0.00	0.00	0.00	0.00	0.00	0.00	0.00	0.02	0.05	0.00	0.06	0.00	0.00
Co	4.27	4.24	5.02	4.29	4.38	3.37	3.81	3.85	3.46	3.87	4.96	2.75	0.62	0.79	3.50
Total	99.02	99.04	97.35	98.72	97.76	98.45	97.74	99.17	95.71	99.91	99.03	101.33	101.26	100.50	98.45

Chalcopyrite

	Main Fissure			Sugarbird Blow												Marsfontein
	P7-6b	P9-8b	P9-8c	P9-11a	SB-3.2	SB-6a	SB-7	SB-8a	SB-8b	SB-10c	SB-11a	SB-21	SB-22	SB-23	SB-24	SB-25	MARS-3
Ni	0.35	0.05	0.56	0.05	0.03	0.14	0.01	0.08	0.10	0.07	0.15	0.03	2.07	0.12	0.00	1.83	2.69
Fe	29.9	30.2	30.7	29.8	28.9	29.9	30.1	33.1	29.8	31.2	30.9	30.3	31.0	30.4	30.3	30.6	30.7
S	34.6	34.7	35.2	3.6	34.0	35.0	35.2	35.6	34.7	34.4	35.0	35.4	34.8	34.3	35.0	34.6	36.0
Cu	33.2	35.6	31.2	32.7	33.6	32.9	33.7	31.4	33.0	33.5	34.2	34.9	33.3	34.5	34.9	31.7	29.0
Co	0.02	0.06	0.17	0.05	0.05	0.05	0.01	0.06	0.09	0.01	0.06	0.01	0.08	0.10	0.09	0.09	1.17
Total	98.06	100.55	97.93	66.22	96.03	97.97	99.08	100.19	97.73	99.15	100.34	100.60	101.15	99.50	100.69	98.87	99.56

APPENDIX 6

SULFUR ISOTOPE ANALYSIS ON SULFIDE DIAMOND INCLUSIONS

Prior to sulfur isotope analysis, the samples were analysed with the electron microprobe (EMP) and the procedure for preparation of the polished sulfide sections was described in Appendix 5. After the EMP analysis, the carbon coating was removed and the samples were coated with gold of a thickness of about 400 A to minimise charging of the sample.

The sulfides were analysed using a Cameca IMS 6f ion microprobe at the Department of Terrestrial Magnetism, Carnegie Institution of Washington. Secondary ions were generated with a primary beam of Cs^+ ions set at 1.2 V which yielded a current of about 0.55 nA and generated a beam size of about 30 μm. Secondary ions were accelerated at –4.650 kV. In comparison to a duoplasmatron source, Cs^+ ions are very efficient in generating negative secondary ions for highly electronegative elements such as P and Se, and other elements such as H, O, S, C, F and Cl. The samples were analysed with a very low mass resolution of 300, which is not capable of discriminating between ^{32}S ions and $^{16}O_2$ ions. However, since a duoplasmatron source is not used, the generation of $^{16}O_2$ ions is minimised. Further, the samples were analysed with an extreme energy filtering which was set at +250±50 eV. At this extreme off-set, interference from $^{16}O_2$ ions possibly generated in the sample is avoided since the intensity of $^{16}O_2$ ions has a narrow energy distribution compared to ^{32}S ions. At an energy off-set of +250±50 eV, the intensity from $^{16}O_2$ ions is negligible. The window of ±50 eV in the energy filtering and the low mass resolution compensate for the intensity lost by the extreme energy filtering. If samples are analysed without energy filtering, the measured intensity will be dominantly produced by ions with low energies around 50 mV. At these low energies, the fractionation factor varies substantially with the energy of the secondary ions which is very sensitive to possible charging of the sample (pers. comm. Eric Hauri). The main advantage with the current set-up is that instrumental fractionation is better controlled through extreme energy filtering through which intensities at low energies are avoided.

Peaks were measured with an electron multiplier working in a direct pulse counting mode. Secondary ^{32}S ions were measured dynamically in 10 blocks of 10 cycles with counting times of 1 second for ^{32}S and 5 seconds for ^{34}S. Count rates with the current set-up

was about 10^6 cps for ^{32}S and 50000 cps for ^{34}S which yielded 2σ errors in $^{34}S/^{32}S$ ranging from ±0.15 ‰ to ±0.40 ‰.

As shown by Eldridge et al. (1987), there is a substantial difference in $^{34}S/^{32}S$ instrumental fractionation when different sulfide species are analysed due to matrix effects. As described in Chapter 7, the sulfides consisted of homogeneous, low-Ni pyrrhotite with flame-like pentlandite exsolution that was avoided during sulfur isotope analysis. This was confirmed after analysis by observation in a petrographic microscope. The maximum Ni content measured for pyrrhotite in any of the samples was 2.4 wt.%. If this amount of Ni was accounted for, the corrected $^{34}S/^{32}S$ would differ less than 0.1 ‰ from that of a $^{34}S/^{32}S$ ratio corrected to pure pyrrhotite free of Ni. Therefore all samples were corrected for instrumental mass fractionation by comparison to the "Anderson pyrrhotite" with a known $^{34}S/^{32}S$ (ΔS_T) of 0.0450615. Six standard measurements were performed during analysis (Appendix 6.1) which gave a measured mean value (ΔS_M) of 0.043043. $^{34}S/^{32}S$ for the analysed samples were corrected for instrumental mass fractionation by dividing the measured ratio with the estimated correction factor ($\Delta S_M/\Delta S_T$) of 0.9552123. The corrected ratios (ΔS_C) were then compared to the $^{34}S/^{32}S$ of the Canyon Diablo Troilite (ΔS_{CDT}) as follows: $[(\Delta S_C-\Delta S_{CDT})/\Delta S_{CDT}]$ x 1000 and the results are thus given as per mil difference in $^{34}S/^{32}S$ to the $^{34}S/^{32}S$ of the Canyon Diablo Troilite which is 0.0450045. The variability of the standard measurements must be accounted for in the estimation of a "total" analytical error. The 2σ standard deviation around the mean value of the standard measurements (Appendix 6.1) is about ±0.5 ‰. Adding this uncertainty to the highest analytical error due to counting statistics presented above (±0.4 ‰) yields a total error of 0.9 ‰. A total 2σ error of 1 ‰ has been adopted for all the data. However, for samples with "better" counting statistics the error would be lower and if the accuracy of the $^{34}S/^{32}S$ estimated for the standard is somewhat over estimated the error would be slightly worse.

APPENDIX 6.1 Analysis of the "Anderson pyrrhotite" standard

Analysis	$^{34}S/^{32}S$
A	0.04305
B	0.04302
C	0.04304
D	0.04302
E	0.04306
F	0.04307
Mean (±2σ error)	0.04304±0.000021

APPENDIX 7

RE-OS ISOTOPE ANALYSIS ON SULFIDE DIAMOND INCLUSIONS

The sulfides were recovered as described in Section 9.2 and weighed by difference in a small aluminium tray using a Mettler UMT2 microbalance. Spikes were weighed by difference into the indented centre of an inverted cap to a 7ml PFA beaker using the same balance. Before adding the spike, the cap was wrapped in aluminium foil to minimize static charging. A mixed, extremely diluted Re-Os spike was used with ^{187}Re and ^{190}Os concentrations of 8.51938 x 10^{-13} m/g and 2.4557 x 10^{-13} m/g respectively. The samples were then transferred to the spike under binocular microscope by the use of a non-magnetic pair of tweezers followed by 15 µl 12 N H_2SO_4 and 15 µl 0.10 g/g CrO_3 solution in 12 N H_2SO_4. 15 µl 9 N HBr was put in the apex of the beaker. The threads of the beaker were wrapped with PTFE tape before it was gently turned around and tightened to the cap. Keeping the beaker inverted, it was covered with aluminium foil, leaving only the "back fins" uncovered. The beaker (still inverted) was then put onto a hot plate at 80 ° C for about 2.5 hours for dissolution of the sulfide and distillation of the Os into the HBr "trap". Thereafter the beaker was unscrewed, gently turned around and the Os fraction was concentrated by evaporating the HBr under a warm lamp and in flowing air. The Re fraction in the cap was investigated for any undissolved sulfide. In all samples the sulfides were completely digested. The Re fraction was then transferred to a 15 ml Savillex teflon beaker with the aid of a couple of drops of 5 N H_2SO_4 when necessary.

In preparation for the Re extraction, 1 ml 5 N H_2SO_4 was added to the Re fraction followed by concentrated H_2O_2 in 5 µl steps until the chrome was reduced. The Re was extracted using 0.25 ml teflon microcolumns and AG-1x8 resin.

The column chemistry procedure was as follows:

Column preparation

3 ml QD H_2O

6 ml 8 N HNO_3

2 ml 5 N H_2SO_4

Sample

in 1 ml 5 N H_2SO_4 and H_2O_2 (as described above)

Washes

2 times 1 ml 5 N H_2SO_4

2 times 1 ml 1 N HCl

1 ml 0.8 N HNO_3

Re collection

4 ml 4 N HNO_3

The Re was then dried down under warm lamp and in flowing air.

Re and Os was loaded onto platinum filaments using 0.5 M HBr and $Ba(NO_3)$ (20 μg Ba/μl) respectively and the samples were metallised before analysis.

The samples were run on a modified 15'' radius N-TIMS and the Os is analysed as OsO_3^- and the Re is analysed as ReO_4^-.